NUREG/CR-0840
TREE-1281
for U.S. Nuclear Regulatory Commission

FRAP-T5
A COMPUTER CODE FOR THE TRANSIENT ANALYSIS OF OXIDE FUEL RODS

L. J. SIEFKEN M.P. BOHN
S.O. PECK J.A. DEARIEN

June 1979

EG&G Idaho, Inc.

IDAHO NATIONAL ENGINEERING LABORATORY

DEPARTMENT OF ENERGY

IDAHO OPERATIONS OFFICE UNDER CONTRACT DE-AC07-76IDO1570

Available from
National Technical Information Service
Springfield, Virginia 22161
Price: Printed Copy A16; Microfiche $3.00

The price of this document for requesters outside the North American continent can be obtained from the National Technical Information Service.

NUREG/CR-0840
TREE-1281
R4

FRAP-T5

A COMPUTER CODE FOR THE TRANSIENT ANALYSIS OF OXIDE FUEL RODS

L. J. Siefken
M. P. Bohn
S. O. Peck
J. A. Dearien

EG&G Idaho, Inc.
Idaho Falls, Idaho 83401

Published June 1979

PREPARED FOR THE
U.S. NUCLEAR REGULATORY COMMISSION
AND THE U.S. DEPARMENT OF ENERGY
IDAHO OPERATIONS OFFICE
UNDER CONTRACT NO. DE-AC07-76ID01570
NRC FIN NO. A6050

ABSTRACT

The Fuel Rod Analysis Program - Transient (FRAP-T5) is a FORTRAN IV computer code that calculates the transient response of light water reactor fuel rods during hypothesized accidents such as a loss-of-coolant accident or a power-cooling mismatch. The code calculates the temperature, pressure, deformation, and failure histories of a fuel rod as functions of time-dependent fuel rod power and coolant boundary conditions. The phenomena modeled by the code include: (a) heat conduction, (b) elastic-plastic fuel and cladding deformation, (c) fuel-cladding mechanical interaction, (d) fission gas release, (e) transient fuel rod gas pressure, (f) heat transfer between fuel and cladding, (g) cladding oxidation, (h) cladding annealing, and (i) heat transfer from cladding to coolant. The code contains all the needed material properties, water properties, and heat transfer correlations.

The code includes a user's option that automatically provides a detailed uncertainty analysis of code calculated response parameters.

FRAP-T5 is programmed on the CDC 7600 computer and is structured to enable direct linkage to a thermal-hydraulic code for transient analysis.

CONTENTS

FIGURES

TABLES

FRAP-T5
A COMPUTER CODE FOR THE TRANSIENT ANALYSIS OF OXIDE FUEL RODS

I. INTRODUCTION

The ability to accurately predict the performance of light water reactors (LWRs) under hypothesized accident conditions is a major objective of the Reactor Safety Research Program being conducted by the U.S. Nuclear Regulatory Commission (NRC). To achieve this objective, the NRC has sponsored an extensive program of analytical computer code development as well as both in-pile and out-of-pile experiments against which to benchmark and assess the analytical code capabilities. The computer code being developed for the prediction of the transient response of a single fuel rod under hypothesized accident conditions is the Fuel Rod Analysis Program - Transient (FRAP-T) code. This report describes FRAP-T5, which is the fifth in a series of code versions released at approximately one-year intervals.

FRAP-T5 predicts the transient behavior of LWR fuel rods during any hypothesized accident ranging from mild operational transients to design basis accidents such as the loss-of-coolant accident (LOCA) and the reactivity initiated accident (RIA). The code calculates the variation with time of all significant fuel rod variables, including fuel and cladding temperature, cladding hoop strain, cladding oxidation, and internal pressure. No restrictions are placed on the power or coolant boundary condition histories of the fuel rods being analyzed.

As a user-specified option, FRAP-T5 calculates the uncertainties in the predicted fuel rod variables due to uncertainties in fuel rod fabrication variables, material properties, power, and cooling. The uncertainty analysis calculations are based on the response surface method. No additional analysis is required on the part of the code user to use this option, and only minimal additional input is required.

The coolant conditions needed as input by FRAP-T5 consist of the coolant pressure, flow, and enthalpy histories. These variables can be taken from the output of a thermal-hydraulic code such as RELAP4[1]. The data can be input either on cards or magnetic tape.

Since a number of the fuel rod variables that must be specified at the start of a transient are burnup dependent, a steady state fuel rod analysis must be performed if the fuel rod to be analyzed has undergone significant prior irradiation. The FRAPCON-1[a] code has been developed at EG&G Idaho, Inc., to generate initial conditions for FRAP-T5. FRAPCON calculates such burnup-dependent variables as fission gas inventory, fuel densification and swelling, and cladding creep strain, which are passed to FRAP-T5 by means of a restart tape. (If the transient event is occurring at beginning-of-life, FRAP-T5 can determine the initial conditions of the fuel rod, so that a restart tape is not needed.)

The accurate prediction of fuel rod behavior during a transient also requires access to accurate material properties over a broad range of temperatures. To meet this requirement, FRAP-T5 is linked with the MATPRO-11[2] subcode so that the user is not required to provide any material property input. This subcode is composed of modular subroutines that define material properties over temperatures varying from room temperature to temperatures above the melting temperature. Each subroutine defines only one material property. For example, MATPRO contains subroutines which define fuel thermal conductivity as a function of temperature and fuel density; fuel thermal expansion as a function of temperature; and the cladding stress-strain relation as a function of temperature, strain rate, cold work, and fast neutron damage.

The FRAP-T5 development process includes two separate assessment efforts designed both to provide configuration control and to test the

---

a. FRAPCON MOD 001, MATPRO Version 10A, EG&G Idaho Code Configuration Control Number H00730IB.

analytical capabilities of the code. In each assessment effort, experimental data on fuel rod response parameters, such as centerline temperature and cladding deformation, are compared with FRAP-T5 calculated values. The first effort, Developmental Assessment, is an ongoing assessment process whereby model additions are checked for correctness, and the performance of the code is checked for any unanticipated perturbations. This effort is completed before the code is released for general use. Independent Assessment is the second assessment process that takes place after a code version has been frozen to further changes and involves comparisons with a much larger fuel rod response data base. The results of this comparison will be presented in the FRAP-T5 Independent Assessment report to be released at a later date.

This report serves as both a model description document and a user input manual. An overview of FRAP-T5 is given in Section II, which is designed to give a general description of the code structure, input, output, and solution scheme. A detailed description of each analytical model in the code is given in Section III. The uncertainty analysis option is described in Section IV. A complete description of the required control and input data cards for FRAP-T5 is given in Appendix A. A sample problem solution which illustrates the code input and output is given in Appendix B. Appendices C and D provide additional details for the heat transfer calculations. Appendix E describes the passive link between FRAP-T5 and any thermal-hydraulic systems code. Appendix F outlines the configuration control procedure that assures the reproducibility of succeeding versions of the FRAP-T code. Appendix G presents the numerical scheme used in obtaining the plenum temperature solution, and Appendix H describes two schemes that have been used to link FRAP-T5 actively with a thermal-hydraulic systems code.

II. GENERAL CODE DESCRIPTION

In this section, the code structure and computation scheme are outlined and the input data requirements and output information of FRAP-T5 are summarized. The link with the FRAPCON-1 code, which can be used to provide initial conditions, is also described. Finally, the code user's means of controlling computation accuracy and computer running time are outlined.

1. CODE STRUCTURE AND CALCULATION PROCEDURE

FRAP-T5 is a modular code composed of several subcodes that iteratively calculate the interrelated effects of fuel and cladding temperature, fuel rod plenum temperature, fuel and cladding deformation, rod internal pressure, and fission gas release.

The calculation procedure is illustrated in Figure 1, which shows a simplified flow chart of FRAP-T5. The calculations begin by the code processing the input information. If the fuel rod has an irradiation history, a tape created by the FRAPCON-1 code is also read. Next the fuel rod state at the start of the transient is determined through a self-initialization (steady state) calculation. Then time is advanced according to the input-specified time step, a transient solution is performed, and the fuel rod state at the new time is determined. The new fuel rod state then provides the initial conditions for the next time step. The calculations are cycled in this manner until a complete solution for the user-specified transient has been obtained.

The complete solution at each time step consists of (a) the temperature distribution throughout the fuel and the cladding, (b) the temperature in the fuel rod plenum, (c) the deformation of the fuel and cladding, (d) the pressure inside the fuel rod, and (e) the release of fission products inside the fuel rod. Each of these calculations is made in separate modular subcodes. These subcodes are called iteratively, so that all significant interactions are taken

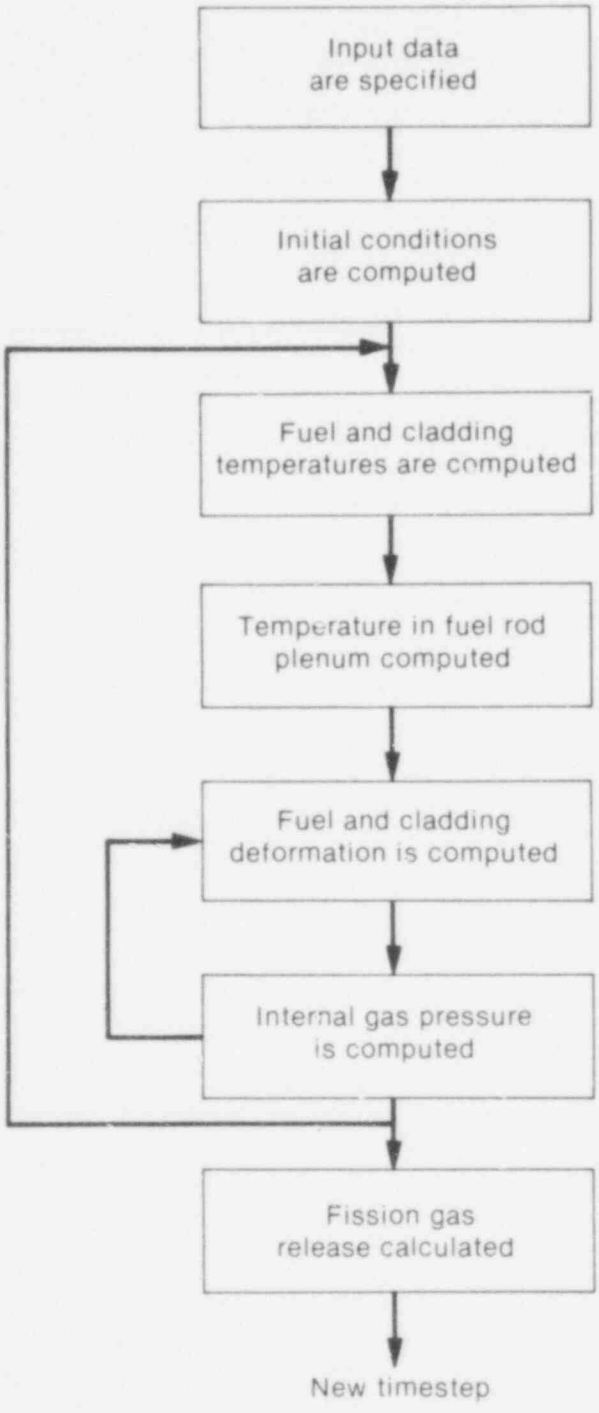

Fig. 1 Simplified FRAP-T5 flow chart.

573 032

into account. For example, the deformation of the fuel affects the fuel rod gas pressure since the internal volume of the rod is changed. The deformation of the fuel also affects the temperature in the fuel and cladding because the flow of heat from the fuel to the cladding is critically dependent on the gap size between the fuel and cladding. These and all other interactions are taken into account by the solution procedure described subsequently.

As shown in Figure 1, the transient fuel rod response is determined by repeated cycling through two nested loops of calculations until convergence occurs. In the outside loop, the fuel rod temperature and deformation are alternately calculated. On the first cycle through this loop, the gap conductance is computed using the gas gap size from the past time step. Then the fuel rod temperature distribution is computed. This temperature distribution then feeds into the deformation calculations and influences such variables as the fuel and cladding thermal expansions and the cladding stress-strain relation. A new gas gap is computed, which is used in the gap conductance calculation on the next cycle of calculations. The calculations are cycled until two successive cycles compute the same temperature distribution.

The inner loop of calculations shown in Figure 1 is cycled through in a manner similar to that used for the outer loop, but with the internal gas pressure being the variable determined by iteration. The fuel rod deformation and gas pressure are alternately determined. The temperature distribution remains the same. On the first cycle through this loop, the deformation is computed using the past time step pressure. Variables that influence the pressure solution, such as gas gap and plenum volume, are computed. Then the pressure calculation is made and an updated cladding pressure is fed back to the deformation calculations. The calculations are cycled until two successive cycles compute the same pressure.

After the two loops of calculations have converged, fission gas release is determined. The fission gas release is determined only once per time step.

A complete description of the five major calculations is presented in Section III.

2. INPUT REQUIREMENTS

The required input information for FRAP-T5 consists of data describing fuel rod design, burnup effects, fuel rod power, and boundary conditions. Also needed is specification of model options and accuracy of the numerical solution. The input information is completely described in Appendix A.

The fuel rod design is described by input data cards that specify the fuel pellet geometry, fuel density, cladding geometry and cold work, and the amount and type of fill gas. More detailed data, such as the fuel sintering temperature and plenum spring dimensions, are also required.

As a fuel rod undergoes burnup in a reactor, significant changes occur to the fuel and cladding dimensions, cladding ductility, and gas inventory. These changes greatly affect the response of a fuel rod during an accident. To account for these changes, FRAPCON-1[a] which calculates steady state fuel rod response, can be linked to FRAP-T5 by magnetic tape. The data transferred by means of the tape link are shown in Table I. Except for the fission gas inventory, the data are supplied as functions of fuel rod elevation. If significant fuel rod burnup has not occurred, this link with FRAPCON-1 is not needed.

Coolant conditions are usually obtained from the output of a thermal-hydraulic systems analysis code such as RELAP4[1]. The coolant conditions are input to FRAP-T5 either by input data cards or by a magnetic tape. If the coolant conditions change significantly with time, however, input by tape is less cumbersome. The required

---

a. FRAPCON MOD 001, MATPRO Version 10A, EG&G Idaho Code Configuration Control Number H00730IB.

TABLE I

BURNUP DEPENDENT DATA REQUIRED TO INITIATE FRAP-T5

(1)	Gas pressure
(2)	Radial gap thickness
(3)	Interfacial pressure
(4)	Fission gas inventory
(5)	Temperature distribution
(6)	Axial node elevation
(7)	Fuel surface displacement due to densification and swelling
(8)	Fuel burnup
(9)	Peak average cladding temperature attained
(10)	Permanent cladding strains
(11)	Volume fraction of open porosity
(12)	Zircaloy oxide thickness

tape content and format for the coolant condition data are shown in Appendix E. An auxiliary subcode to FRAP-T5 can be used to convert a RELAP4 plot tape into a coolant condition data tape of the proper content and format. Instructions for the use of this subcode are also given in Appendix E. If the coolant flow and pressure are only slowly varying or constant, boundary conditions from a thermal-hydraulic code are not needed. In this case, steady state thermal-hydraulic calculations internal to FRAP-T5 can be used to calculate the coolant conditions as a user option.

The fuel rod power history is input to FRAP-T5 by data cards, which requires that the fuel rod power distribution and power history be determined by a reactor physics code prior to FRAP-T5 calculations. The radial power profile, axial power profile, and history of linearly

averaged rod power must be input. The radial power profile is assumed not to change with elevation or time, and the axial power profile is assumed not to change with time.

3. OUTPUT INFORMATION

The FRAP-T5 output gives a complete description of the fuel rod response to the user-specified transient. This output includes, for example, the fuel and cladding temperature histories, internal pressure history, and cladding deformation history, all of which are both printed and plotted. Quantities such as peak cladding temperature and time and location of cladding failure are readily determined from the code output. If the uncertainty analysis option is used, the uncertainties of the code outputs are also given.

A complete list of the FRAP-T5 output information is given in Table II. An example of the code output is given in Appendix B, where both the printed and plotted output for the solution of a simplified LOCA problem are shown.

4. NODALIZATION, ACCURACY, AND COMPUTATION TIME CONSIDERATIONS

The code user has four means of controlling accuracy and computer running time. These are through input specifications of (a) nodalization, (b) temperature accuracy, (c) pressure accuracy, and (d) time-step size. The nodalization input data specify the points at which variables such as temperature, stress, and strain are to be computed. Increasing the number of node points provides greater spatial detail at the cost of computer running time. The nodalization data consist of three types: (a) axial nodalization, (b) radial nodalization, and (c) azimuthal nodalization. If the azimuthal temperature distribution is not computed, the azimuthal nodalization data are not required.

The axial nodalization data specify the elevations at which the radial distribution of the fuel rod temperature and deformation are to

TABLE II

FRAP-T5 OUTPUT

(1)	Fuel rod radial temperature distribution at an arbitrary number of elevations
(2)	Fuel diameter, gas gap thickness, and cladding outer diameter at an arbitrary number of elevations
(3)	Length change of fuel stack and cladding
(4)	Pressure of internal fuel rod gas
(5)	Time and location of cladding rupture
(6)	Cladding surface heat transfer coefficients
(7)	Critical heat flux at fuel rod surface
(8)	Gas gap heat transfer coefficients
(9)	Plastic strains in cladding
(10)	Radial stress at fuel-cladding interface
(11)	Elastic and permanent strains in fuel
(12)	Stress distribution in fuel
(13)	Void volume
(14)	Probability of fuel rod failure
(15)	Cladding oxide thickness
(16)	Energy generated by cladding oxidation
(17)	Stored energy in fuel
(18)	Radial extent of fuel melting
(19)	Plenum gas temperature
(20)	Coolant conditions

be computed. Each of these elevations is defined as an axial node. In particular, the axial nodes are considered to be points on the longitudinal axis of the fuel rod. A minimum of one and a maximum of 20 axial nodes may be defined. Unequal spacing of the axial nodes is permitted.

The radial nodes lie in planes that pass through the axial nodes and are perpendicular to the fuel rod axis, that is, the centerline of the fuel rod. The first radial node is the point at the intersection of the plane and axis. Other radial nodes are placed at the fuel pellet surface and at the cladding inside and outside surfaces. In addition, up to 16 more radial nodes can be placed within the fuel and cladding.

An example of fuel rod nodalization is shown in Figure 2. The axial nodes are numbered from bottom to top. The radial nodes are numbered from the fuel rod centerline to the cladding outside surface.

The computer running time is directly proportional to the number of axial nodes but not as sensitive to the number of radial nodes. If the number of axial nodes is doubled, the computer running time is doubled. if the number of radial nodes is doubled, the running time is increased about 15%. In general, about ten axial nodes and eight radial nodes are recommended. If cladding ballooning can occur, and an accurate calculation of the ballooning length is wanted, a closely spaced axial nodalization is required in the region of anticipated cladding ballooning. In this region, the axial nodes should not be spaced farther apart than a distance equal to ten cladding diameters.

The temperature accuracy is specified by inputting a single parameter. This parameter is the maximum permissible fractional difference[a] in temperature calculated by two successive cycles

---

a. Fractional difference: $(T^n - T^{n-1})/T^{n-1}$, where T^n = temperature computed by n-th cycle through the temperature-deformation loop, and T^{n-1} = temperature computed by the previous cycle.

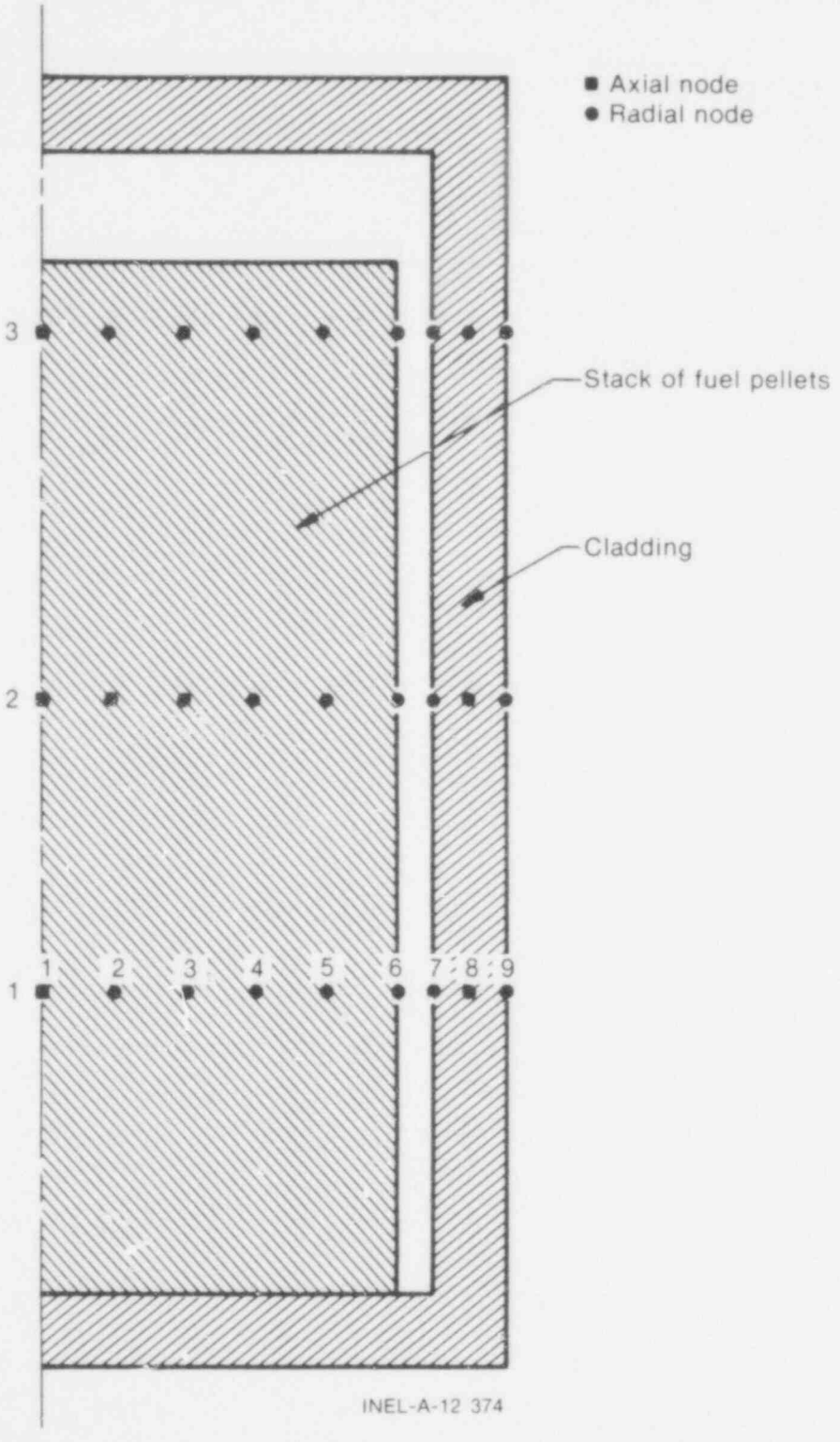

Fig. 2 Example of fuel rod nodalization.

through the temperature-deformation loop, as shown in Figure 1. If the temperature difference between the two successive cycles at any point in the fuel rod is greater than the value of this parameter, another cycle of calculations occurs. The temperature calculations, however, are not repeated at the axial nodes at which the temperature differences at all radial nodes were less than this value.

The pressure accuracy is similarly specified by one parameter. This parameter is defined as the maximum permissible fractional difference in the internal fuel rod pressure calculated by two successive cycles through the deformation-pressure loop of calculations. If the pressure difference between two successive cycles is greater than this number, another cycle of calculation occurs.

By making the temperature and pressure accuracies large (>1), each loop is cycled through only once, which results in an explicit solution of the transient. This approach reduces computer running time and precludes convergence problems. If sufficiently small time steps are specified, adequate calculational accuracies can be assured. In general, the explicit solution is recommended. If an accurate prediction of the onset of cladding ballooning is needed, however, an implicit solution should be used. In this case, the temperature and pressure accuracies parameters should each be set equal to 0.001.

The time step input is a table of time-step versus time data. If a constant time step is desired, only the value of the time step is input. Otherwise, a different time step can be specified for a maximum of ten intervals of problem time. This permits a large time step to be used when coolant conditions and power are changing slowly with time, and a small time step to be used when either the power or coolant conditions are changing rapidly. In general, the time step should not exceed 0.1 seconds during the time span in which boiling at the cladding surface changes from the nucleate to the film boiling mode.

573

For a LOCA, time steps in the range of 0.05 to 0.2 seconds are adequate. For an RIA, time steps in the range of 0.001 to 0.01 seconds are required. If the convergence criteria are small ($\leq$0.001), the upper range of the time step is permissible. If the input temperature and pressure accuracies are large ($>$0.05), the lower range of the time step is required.

The code has the capability of restarting and continuing calculations from a previously terminated job. This capability is useful in case of computer failure or underestimation of the end time of transient behavior. The restart process is simple, requiring only two additional cards to be added to the normal deck of control cards.

III. DESCRIPTION OF MODELS

As outlined in the general code description (Section II), the calculation of the transient fuel rod response has been separated into five essentially independent analyses. In this section, the individual models that constitute the five areas of analysis are described in detail. The models and their subcodes are described in the order in which they occur in the calculational scheme, as was shown in Figure 1.

Thus, the analysis of the temperature distribution in the fuel and cladding is described in Section 1. This analysis involves models for gap conductance between the fuel and the cladding, models for determination of the appropriate heat transfer coefficients at the outside of the fuel rod, and finally models for the calculation of the temperature distribution in the fuel and cladding.

The analysis of the temperature in the fuel rod plenum is described in Section 2. The basic model used is a lumped mass thermal model including the effects of radiation heat transfer and gamma heating of the plenum region.

The analysis of the deformation of the fuel and cladding is described in Section 3. The deformation of the fuel may be modeled as either due to thermal expansion alone (as in the FRACAS-1 subcode) or due to both thermal expansion and stress-induced deformation (as in the FRACAS-2 subcode).

The analysis of the fuel rod internal pressure is presented in Section 4. The fuel rod pressure may be modeled as either a static or transient response at the option of the code user.

Finally, the production of fission gas and its release is described in Section 5. The calculation of fission gas production and release in FRAP-T5 is based on the GRASS[3] subcode developed at the Argonne National Laboratory.

1. FUEL AND CLADDING TEMPERATURE

The temperature distribution throughout the fuel and the cladding is calculated at each axial node. Either a one-dimensional (radial) or two-dimensional (radial plus circumferential) temperature distribution solution can be specified by the user. In either case, the models and sequence of calculations are essentially the same. A flow chart of the temperature distribution solution is shown in Figure 3.

First, the local coolant conditions (pressure, quality, and enthalpy) are determined, either from a steady state enthalpy rise calculation or from an input coolant boundary condition tape. Then the distribution of heat generated in the fuel pellet is found from the user-input average fuel rod power history. Through use of the most recently computed gap size, a value of the gap conductance across the fuel-to-cladding gap is computed. This calculation requires that the gap gas material properties be obtained from the MATPRO subcode. In addition, values of the fuel conductivity are also obtained from MATPRO and are modified to account for the effects of fuel cracking. Finally, the surface temperature of the cladding is found from the coolant boundary conditions (that is, the appropriate regime of heat transfer on the outside surface of the cladding) and the complete temperature distribution throughout the fuel and cladding is found.

The models used in the temperature calculations involve a number of assumptions and limitations, the most important of which are:

(1) No heat conduction in the longitudinal direction

(2) Steady state critical heat flux correlations are assumed to be valid during transient conditions

(3) Steady state cladding surface heat transfer correlations are assumed to be valid during transient conditions

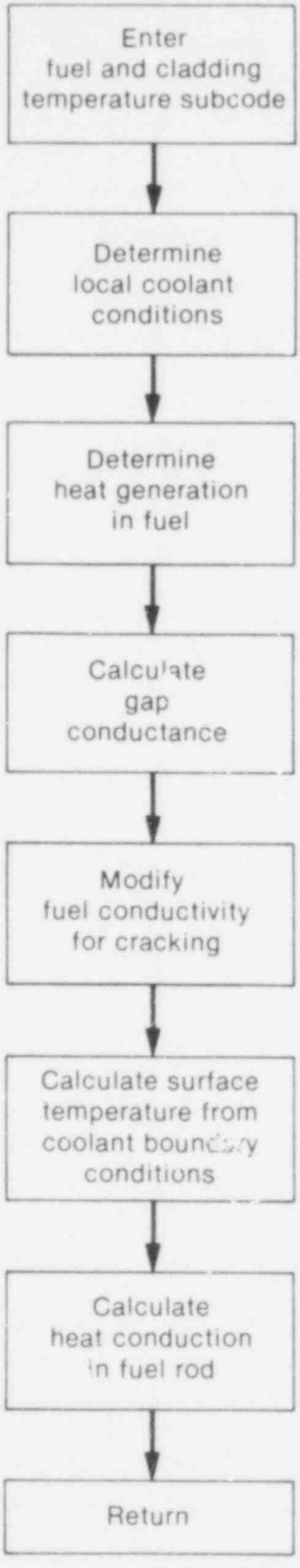

Fig. 3 Flow chart of fuel and cladding temperature calculations.

573 014

(4) No convective mode of heat transfer occurs across the gas gap

(5) Cladding oxidation does not influence the cladding thermal properties.

Nonetheless, extensive code assessment and benchmarking have demonstrated the appropriateness of the models chosen for the thermal calculations. These models are described in detail in the following.

1.1 Local Coolant Conditions

The pressure, mass flux, and enthalpy of the coolant specify the conditions of the coolant and are needed to calculate fuel rod cooling. The pressure is also needed to calculate the cladding deformation. In general, the coolant conditions must be computed by a thermal-hydraulic code and input to FRAP-T. The coolant pressure and mass flux must always be specified by user input. Depending upon the option selected by the code user, the coolant enthalpy either can be specified by user input or calculated by energy balance, as described in Appendix D.

The coolant condition input is either on cards or magnetic tape. If the input is on tape, the tape is read as the problem time advances to find the two times on the tape that bracket the current problem time. The coolant conditions at the current time are then determined by interpolation. The coolant conditions must be stored on the tape according to the format shown in Appendix E.

1.2 Heat Generation in the Fuel Pellet

Heat is generated in the fuel by fission of uranium or plutonium atoms and by radioactive decay of fission products. The heat generation must be determined by a reactor physics code and input to FRAP-T5 by cards. Alternatively, only the heat generation due to fission is prescribed by card input, and that due to radioactive decay

is calculated by the ANS Standard formula[4]. If the reactor is scrammed at initiation of an accident, so that no heat is generated by fission during the accident, the last option is preferable.

The heat generation input consists of three sets of tables: (a) linearly averaged rod power versus time, (b) power versus elevation, and (c) power versus radius. The tables are input on cards. The power versus elevation table, which prescribes the axial power profile, is assumed not to change with time. The power versus radius table, which prescribes the radial power profile, is assumed not to change with elevation or time.

1.3 Gap Conductance

The heat transfer coefficient across the gap between the fuel pellets and the cladding (usually called the gap conductance) plays a critical role in determining the transient temperature response of the fuel rod. In general, the gap conductance has different forms depending on whether the gap is open or closed. The model used in FRAP-T5 is basically a modification of the formulation due to Ross and Stoute[5], and is based on the assumptions that:

(1) The gap between fuel and cladding is axisymmetric. If the gap is closed, the interface pressure is axisymmetric.

(2) Elastic cladding deformation occurs at the points of fuel and cladding contact after the gap is closed.

The models for the open and closed gap cases are described separately in the following paragraphs.

1.3.1 Open Gap. If the fuel and cladding are not in contact, heat is transferred across the gas gap by conduction through the gas and by radiation. The heat transfer coefficient across the gas gap is determined by the equation

$$h_g = \frac{K_g}{t_g + (g_1 + g_2)} + h_r \qquad (1\text{-}1)$$

where

h_g = gap conductance

K_g = conductivity of gas in gas gap

t_g = gap thickness

g_1 = temperature jump distance at cladding inside surface

g_2 = temperature jump distance at fuel outside surface

h_r = radiant heat transfer conductance.

The radiant heat transfer coefficient is computed using the following equation

$$h_r = \sigma F_e (T_f^2 + T_c^2)(T_f + T_c) \qquad (1\text{-}2)$$

where

h_r = radiant heat transfer conductance

σ = Stefan-Boltzmann constant

F_e = emissivity factor

T_f = temperature of outside surface of fuel

T_c = temperature of inside surface of cladding.

The emissivity factor is computed by the equation

$$F_e = \left[\frac{1}{e_f} + \frac{r_f}{r_c}\left(\frac{1}{e_c} - 1\right)\right]^{-1} \quad (1\text{-}3)$$

where

F_e = emissivity factor

e_f = emissivity of fuel surface

e_c = emissivity of cladding inside surface

r_f = outside radius of fuel

r_c = inside radius of cladding.

The temperature jump distance term $(g_1 + g_2)$ is computed by an empirically derived equation presented in the GAPCON-THERMAL-1 code report[6]. The equation is

$$g_1 + g_2 = 5.448 \frac{\mu}{P}\left(\frac{T}{M}\right)^{1/2} \quad (1\text{-}4)$$

where

$(g_1 + g_2)$ = jump distance (cm)

μ = viscosity of gas (g/cm·s)

P = pressure of gas (psi)

T = temperature of gas (K)

M = molecular weight of gas.

1.3.2 Closed Gap. If the fuel and cladding are in contact, the equation for contact conductance used in the GAPCON-THERMAL-1 code[6]

is used. This equation agrees with the gap conductance data presented by Ross and Stoute[5]. The equation is

$$h_g = \frac{K_m P_i}{a_o R^{0.5} H} + \frac{K_g}{c(R_f + R_c) + (g_1 + g_2)} + h_r \qquad (1\text{-}5)$$

where

h_g = gap conductance (cal/s cm^2 ^oC)

$K_m = \frac{2K_fK_c}{K_f + K_c}$

K_f = fuel conductivity (cal/s·cm·^oC)

K_c = cladding conductivity (cal/s·cm·^oC)

P_i = interfacial pressure between fuel and cladding (psi)

a_o = a constant, 0.5 $cm^{1/2}$

$R = \frac{(R_f^2 + R_c^2)^{1/2}}{2}$

R_c = arithmetic mean roughness height of cladding (cm)

R_f = arithmetic mean roughness height of fuel (cm)

H = Meyer-Hardness of cladding (psi)

K_g = thermal conductivity of gas (cal/s·cm·^oC).

The coefficient, c, in Equation (1-5) is computed by the empirical equation

$$c = 1.98\, e^{-0.00125\, P_i} \qquad (1\text{-}6)$$

where

P_i = interfacial pressure between fuel and cladding (kg/cm^2).

1.4 Thermal Conductivity of Cracked Fuel

The fourth calculation shown in Figure 3 is performed by the cracked fuel conductivity model. This model calculates the increased resistance to heat flow that occurs when fuel relocates and forms circumferential cracks. The cracks are a resistance to the flow of heat from the center to the outside surface of the fuel. To account for this resistance, the thermal conductivity of fuel computed by MATPRO is modified by the equation

$$K_{eff} = R\,K_f \qquad (1\text{-}7)$$

where

K_{eff} = effective thermal conductivity of relocated fuel

K_f = fuel thermal conductivity computed by MATPRO, which assumes no cracks exist in the fuel

R = correction factor to account for cracks formed by fuel relocation.

The correction factor R is computed by the following equations:

$$\begin{cases} R = 1 - 25.1\,C_{REL}\,(\delta/r_f)(1 - K_{g\infty}/K_f) & (T_f < T_{SINT}) \\ R = 1 & (T_f \geq T_{SINT}) \\ R \geq 0.45 & \text{(lower limit)} \end{cases}$$

where

R = correction factor to MATPRO fuel thermal conductivity

δ = as-fabricated radial gap between fuel and cladding (m)

r_f = as-fabricated outside radius of fuel pellets (m)

$K_{g\infty}$ = thermal conductivity of gas in cracks, not including Knudsen domain effect (W/m·K)

K_f = fuel thermal conductivity determined by MATPRO (W/m·K)

T_f = fuel temperature (K)

T_{SINT} = fuel sintering temperature (K), assumed to be 1773 K.

The coefficient C_{REL} is computed by the equation

$$\begin{cases} C_{REL} = U_c/(\delta - 0.005\ r_f) \\ C_{REL} \geq 0.25 \qquad \text{(lower limit)} \end{cases}$$

where

U_c = radial displacement of fuel surface due to relocation.

The empirical factor R was derived from centerline and off-center thermocouple data taken on fuel rods irradiated in the Power Burst Facility at the Idaho National Engineering Laboratory.

1.5 Fuel Rod Surface Heat Transfer

The fifth model shown in the flow chart, Figure 3, determines the fuel rod cooling. This model calculates the heat transfer coefficient, heat flux, and temperature at the cladding surface. A fuel rod is cooled by the transfer of heat from the cladding outside surface to the surrounding fluid. To calculate the amount of heat transfer, two independent equations are simultaneously solved for cladding surface heat flux and surface temperature.

One of the equations is the appropriate correlation for convective heat transfer from the fuel rod surface. This correlation relates surface heat flux to surface temperature and coolant conditions. Different correlations are required for different heat transfer modes. The surface heat flux given by the various heat transfer modes is shown in Figure 4. Logic for selecting the appropriate mode and the correlations available for each mode are shown in Table III. The correlations are described in detail in Appendix D.

The second independent equation containing surface temperature and surface heat flux as the only unknown quantities is derived from the finite difference equation for heat conduction at the mesh bordering the fuel rod surface. A typical plot of this equation for the nucleate boiling mode of heat transfer is also shown in Figure 4. The intersection of the plot of this equation and that of the heat transfer correlations determines the surface heat flux and temperature. The derivation of this equation and the simultaneous solution for surface temperature and surface heat flux are described in Appendix C. Neither of the two equations solved simultaneously contains past iteration values so that numerical instabilities at the onset of nucleate boiling are avoided.

A separate set of heat transfer correlations[7] is used to calculate fuel rod cooling during the reflooding period of a LOCA. During this period, liquid cooling water is injected into the lower plenum and the

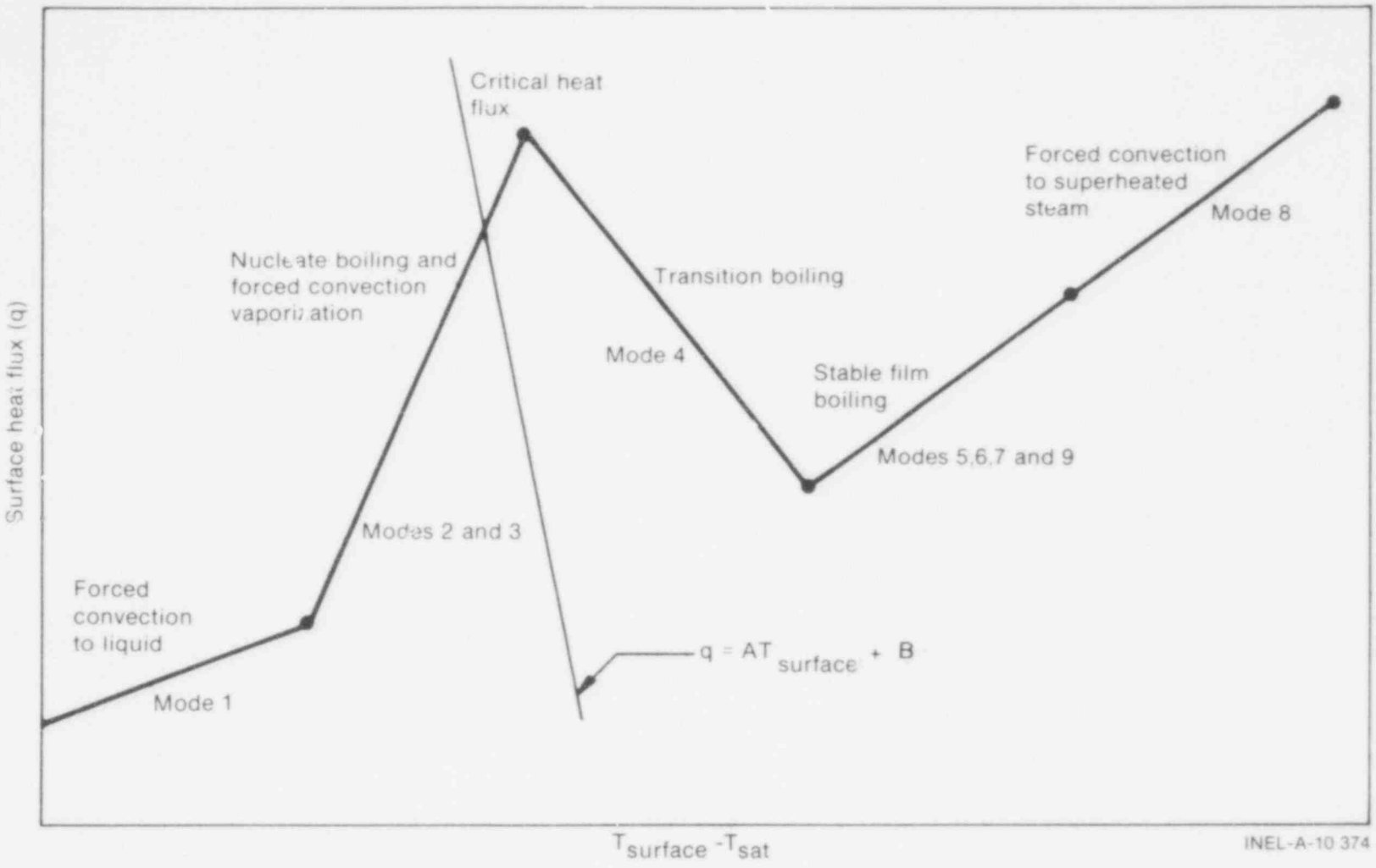

Fig. 4 Heat transfer modes considered in FRAP-T.

TABLE III

HEAT TRANSFER MODE SELECTION AND CORRELATIONS

Heat Transfer Mode	Range[a]	Heat Transfer Correlation[b]
1. Forced convection to liquid	$T_w < T_{sat}$ or $Q_2 < Q_1 < Q_{crit}$	Dittus-Boelter[8]
2. Nucleate boiling	$Q_1 < Q_2 < Q_{crit}$; $T_w > T_{sat}$; $\alpha < 0.9$	Thom[9]
3. Forced convection vaporization	$Q < Q_{crit}$; $\alpha \geq 0.9$	Shrock-Grossman[10]
4. Flow transition boiling	Q_2 or $Q_3 > Q_{crit}$; $Q_4 > Q_5$; $G > 200{,}000$; $P > 500$ or $Q_4 < Q_9$	McDonough, Milich, and King[11] Tong-Young[12] Condie-Bengston[13]
5. Flow film boiling	Q_2 or $Q_3 > Q_{crit}$; $Q_5 > Q_4$ $G > 200{,}000$ or $Q_5 > Q_6$ ($\alpha \leq 0.6$) or Q_7 ($\alpha > 0.6$)	Groeneveld[14] Dougall-Rohsenow[15] Tong-Young[12] Condie-Bengston[13]
6. Pool film boiling	Q_2 or $Q_3 > Q_{crit}$; $G < 200{,}000$ $Q_6 > Q_5$; $\alpha \leq 0.3$	Modified Bromley[d]
7. Free convection	Q_2 or $Q_3 > Q_{crit}$; $G < 200{,}000$ and $Q_7 > Q_5$; $\alpha > 0.3$	Free convection[d]

TABLE III (continued)

Heat Transfer Mode	Range[a]	Heat Transfer Correlation[b]
8. Forced convection to gas	$X \geq 1$	Dittus-Boelter[8]
9. Low pressure film boiling[c]	$P < 500$ and range of mode 5	Dougall-Rohsenow[15]

a. The symbols used are:

Q_i = surface heat flux for i-th heat transfer mode
Q_{crit} = critical heat flux
T_W = cladding surface temperature
T_{sat} = saturation temperature of coolant
α = coolant void fraction
X = coolant quality
G = mass flux ($lbm/hr\text{-}ft^2$)
P = coolant pressure (psia)

b. For each heat transfer mode shown, only one of the listed correlations next to the parameter limits describing the range of the heat transfer mode is used. The correlation to be used is specified on the card input.

c. If a flow film boiling correlation other than Groeneveld is specified, mode 9 is not considered.

d. Correlation generated at INEL.

liquid level rises up along the length of the fuel rods. The complex heat transfer conditions which exist in the reactor core during reflooding are modeled by a set of empirical relations derived from experiments performed in the FLECHT facility. A full description of these models is presented in Reference 7. These models replace the previously described heat transfer correlations at the user-specified time of initiation of core reflooding.

1.6 Heat Conduction

Once values for the gap conductance, modified fuel conductivities, and surface temperature have been obtained, the complete temperature distribution in the fuel and cladding can be obtained from the heat conduction equations, in either one or two dimensions as specified by the code user.

1.6.1 Radial Heat Conduction. Heat conduction in the radial direction in both the fuel and the cladding is described by the equation

$$\frac{1}{r}\frac{\partial}{\partial r}\left(kr\frac{\partial T_n(r)}{\partial r}\right) + q_n(r) = \rho C_p \frac{\partial T_n(r)}{\partial t} \qquad (1\text{-}8)$$

where

$T_n(r)$ = temperature at axial node n and radial coordinate r

t = time

r = radius

$q_n(r)$ = heat generation rate per unit volume at axial node n and radius r

C_p = specific heat

573 056

ρ = density

k = thermal conductivity.

The parameters C_p and k are temperature-dependent. The following boundary conditions are used with Equation (1-8)

$$\left.\frac{\partial T_n}{\partial r}\right|_{r = 0} = 0 \qquad (1\text{-}9)$$

$$\left.T_n\right|_{r = r_o} = T_s \qquad (1\text{-}10)$$

where

r_o = outer radius of fuel rod

T_s = fuel rod surface temperature.

The numerical solution to Equation (1-8) is performed by a modularized version of the HEAT-1 code[16]. The solution is obtained using an implicit finite difference approximation. The solution accounts for temperature- and time-dependent thermal properties and boundary conditions as well as a transient, spatially varying heat source. Phase changes are handled by iteratively computing the fictitious negative heat source required to keep the temperature equal to the value of the phase change temperature. The source is removed when the heat subtracted sums to the heat of fusion.

With Figure 5 as a reference for geometry terms, the finite difference approximation for heat conduction used by the HEAT-1 subcode is

$$\frac{(T_n^{m+1} - T_n^{m})\,(c_{\ell n}\, h^{v}_{\ell n} + c_{rn}\, h^{v}_{rn})}{\Delta t} = -(T_n - T_{n-1})\, k_{\ell n}\, h^{s}_{\ell n}$$

$$+ (T_{n+1} - T_n)\, k_{rn}\, h^{s}_{rn} + Q_{\ell n}\, h^{v}_{\ell n} + Q_{rn}\, h^{v}_{rn} \qquad (1\text{-}11)$$

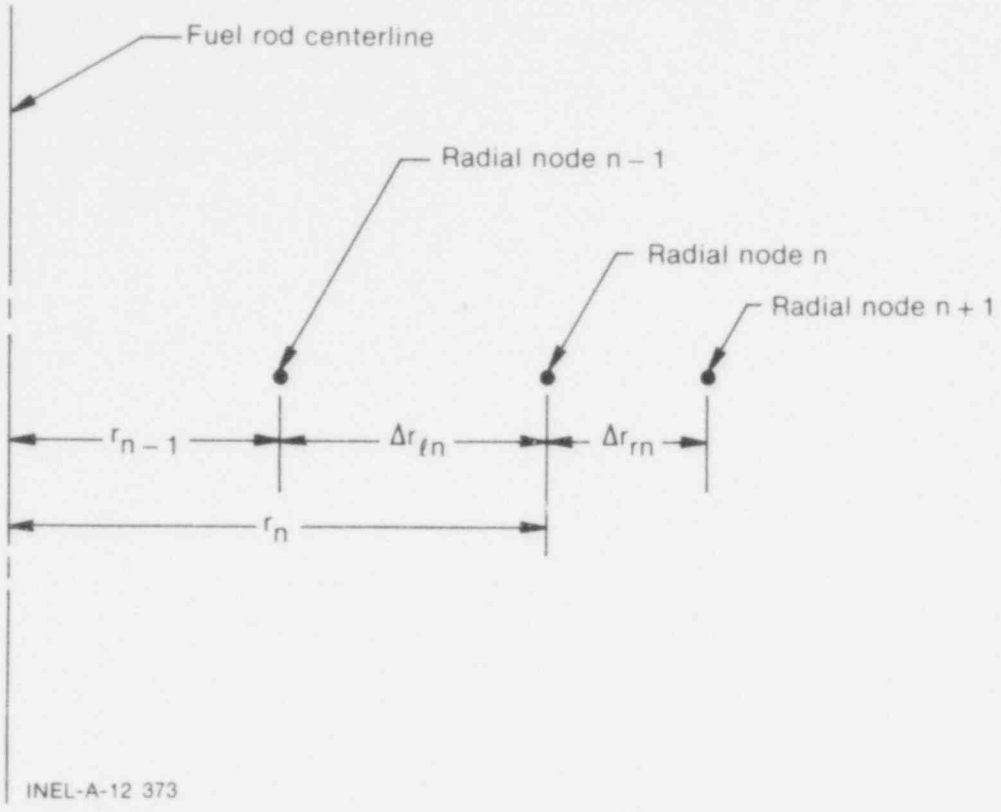

Fig. 5 Geometry terms in finite difference equation for heat conduction.

where

T_n^{m+1} = temperature at radial node n and time point m+1

Δt = time step

$c_{\ell n}$ = volumetric heat capacity on left side of node n

c_{rn} = volumetric heat capacity on right side of node n

k_{rn} = thermal conductivity at right side of node n

$k_{\ell n}$ = thermal conductivity at left side of node n

$h^v_{\ell n}$ = volume weight of mesh spacing on left side of radial node n = $\pi \Delta r_{\ell n} \left(r_n - \frac{\Delta r_{\ell n}}{4}\right)$

h^V_{rn} = volume weight on right side of node n

$$= \pi \Delta r_{rn} \left(r_n + \frac{\Delta r_{rn}}{4}\right)$$

$h^S_{\ell n}$ = surface weight on right side of node n

$$= \frac{2\pi}{\Delta r_{\ell n}} \left(r_n - \frac{\Delta r_{rn}}{2}\right)$$

h^S_{rn} = surface weight on right side of node n

$$= \frac{2\pi}{\Delta r_{rn}} \left(r_n + \frac{\Delta r_{rn}}{2}\right)$$

$Q_{\ell n}$ = heat generation per unit volume.

The finite difference approximations at each radial node can be combined together to form one tridiagonal matrix equation. The equation has the form

$$\begin{vmatrix} b_1 & c_1 & 0 & 0 & & \\ a_2 & b_2 & c_2 & 0 & & 0's \\ 0 & a_3 & b_3 & c_3 & & \\ & \cdot & \cdot & \cdot & & \\ & & \cdot & \cdot & & \\ & & \cdot & \cdot & \cdot & \\ & 0's & a_{N-1} & b_{N-1} & c_{N-1} & \\ & & 0 & a_N & b_N & \end{vmatrix} \begin{vmatrix} T_1^{m+1} \\ T_2^{m+1} \\ T_3^{m+1} \\ \cdot \\ \cdot \\ \cdot \\ T_{N-1}^{m+1} \\ T_N^{m+1} \end{vmatrix} = \begin{vmatrix} d_1 \\ d_2 \\ d_3 \\ \cdot \\ \cdot \\ \cdot \\ d_{N-1} \\ d_N \end{vmatrix} \tag{1-12}$$

Equation (1-12) is solved by Gaussian elimination for the radial node temperatures. Since the off-diagonal elements are negative and the sum of the diagonal elements is greater than the sum of the off-diagonal elements, little roundoff error occurs.

When the forward reduction step of Gaussian elimination has been applied to matrix Equation (1-12), the last equation in the transformed matrix equation is

$$A\ T_N^{m+1} + B = q_N^{m+1} \qquad (1\text{-}18)$$

where

T_N^{m+1} = cladding surface temperature

q_N^{m+1} = cladding surface heat flux

A,B = coefficients that are completely defined in Appendix C.

Equation (1-13) is plotted in Figure 4.

1.6.2 Radial and Azimuthal Heat Conduction. Optionally, heat conduction in both the radial and azimuthal (circumferential) directions is modeled. Two dimensional heat conduction is necessary in cases of skewed fuel rod power or offset fuel pellets. Azimuthal heat conduction due to azimuthally varying coolant conditions cannot be modeled in FRAP-T5, however. For the two-dimensional calculations, the one-dimensional (radial) HEAT-1 subcode is still used to determine the fuel rod temperature distribution. The heat generation rate for each HEAT-1 mesh is modified to account for heat addition (or loss) due to azimuthal heat conduction. The HEAT-1 subcode then determines the radial temperature distribution in each azimuthal sector.

The mesh configuration used for the calculation of two dimensional heat conduction is shown in Figure 6. The user specifies the number of angular sectors to be used. The dashed lines denote the boundaries of control volumes. The radial control volume boundaries lie midway between the radial nodes. One radial node is used for each control volume. The temperatures of the radial nodes along a ray are

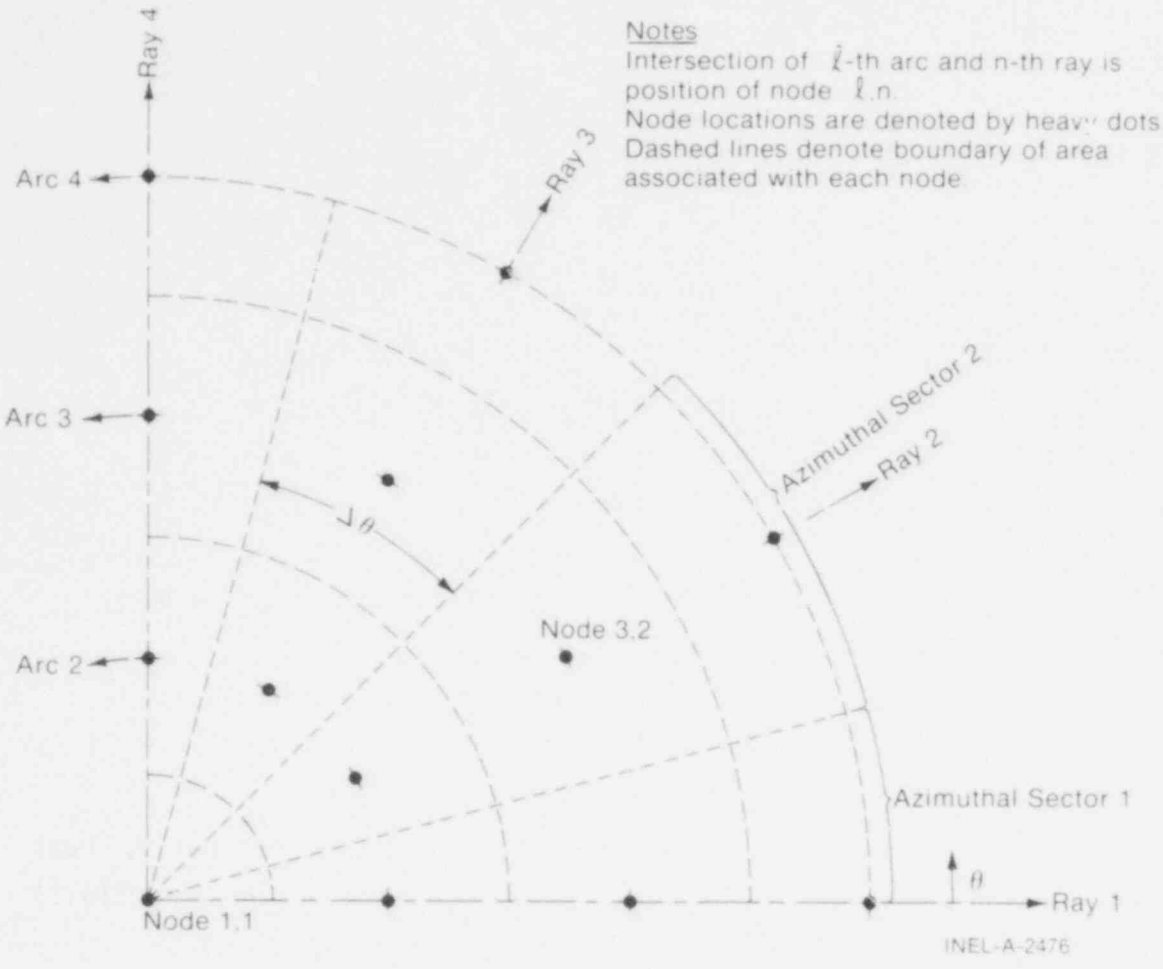

Fig. 6 Mesh configuration for R-θ heat conduction.

determined in the HEAT-1 subcode by simultaneous solution of the set of equations describing radial heat conduction for the sector.

The only new equations required to model two-dimensional (R,θ) heat conduction are those that compute the heat added (or subtracted) from each HEAT-1 subcode control volume by azimuthal heat conduction. In continuous form, azimuthal heat conduction is computed by the equation

$$q(r,\theta) = \frac{1}{r}\frac{\partial kT}{\partial \theta} \qquad (1\text{-}14)$$

573 061

where

$q(r,\theta)$ = rate of azimuthal heat conduction at radial coordinate r and azimuthal coordinate θ (W/m·unit length)

k = thermal conductivity (W/m·K)

T = temperature (K).

Referring to the mesh configuration shown in Figure 6 the finite difference form of Equation (1-14) is

$$q_{\ell,n+1/2} = \frac{k_{\ell,n+1/2}}{r_\ell} \frac{(T_{\ell,n+1} - T_{\ell,n})}{\Delta\theta} \qquad (1\text{-}15)$$

where

$q_{\ell,n+1/2}$ = rate at which heat is conducted in azimuthal direction across the common boundary of the control volumes centered about nodes ℓ,n and $\ell,n+1$.

$k_{\ell,n+1/2}$ = thermal conductivity = $0.5\ (k_{\ell,n} + K_{\ell,n+1})$

r_ℓ = radial coordinate of radial node ℓ

$T_{\ell,n}$ = temperature at radial coordinate ℓ and azimuthal coordinate n

$\Delta\theta$ = azimuthal span between ray n and ray n+1 (radians).

The volumetric rate at which heat is added (or subtracted) by azimuthal heat conduction into the control volume centered about the node ℓ,n with corners at nodes ℓ-1/2, n-1/2; ℓ+1/2, n-1/2; ℓ+1/2, n+1/2; and ℓ-1/2, n+1/2 is

$$q_{\ell,n} = -\frac{0.5(r_{\ell+1,n} - r_{\ell-1,n})}{r_{\ell,n}\Delta\theta\, A}\left[k_{\ell,n+1/2}\,(T_{\ell,n+1} - T_{\ell,n}) + k_{\ell,n-1/2}(T_{\ell,n-1} - T_{\ell,n})\right] \quad (1\text{-}16)$$

where

$q_{\ell,n}$ = rate at which heat is added by azimuthal heat conduction to control volume centered about node ℓ,n (W/m^3) (height of control volume assumed to be one unit)

A = area of mesh

$$= (\Delta\theta/2)\left\{\left[0.5(r_{\ell,n} + r_{\ell+1,n})\right]^2 - \left[0.5(r_{\ell,n} + r_{\ell-1,n})\right]^2\right\}$$

The quantity $q_{\ell,n}$ is added to the heat generation term at the ℓ^{th} radial node in the HEAT-1 subcode equations to account for azimuthal heat conduction. This equation is used for all radial nodes except the center node.

For the control volume associated with the center node, the heat generation term in the HEAT-1 subcode is modified in a different manner. The first radial node of each azimuthal sector must be at the same temperature. To force this condition, the azimuthal heat conduction is set equal to the heat generation required to bring the temperature of the first radial node of each azimuthal sector to the average center node temperature at the end of the past time step. This heat generation is computed according to the equation

$$q_{1n} = \rho C_p\,(T_{avg} - T_{1n})/\Delta T \quad (1\text{-}17)$$

where

ρ = fuel density

C_p = fuel specific heat at temperature T_{avg}

Δt = time step

T_{1n} = temperature at first radial node of n^{th} azimuthal sector at the end of the last time step

$T_{avg} = (1/N) \sum_{n=1}^{N} T_{1n}$

N = number of azimuthal sectors.

The description of the calculations for the temperature distribution in the fuel and cladding is complete at this point. The calculation of the temperature of the gas in the fuel rod plenum is then needed to complete the solution for the fuel rod temperature distribution. This calculation is performed by a separate subcode and is described in the following section.

2. TRANSIENT PLENUM TEMPERATURE

To calculate the internal fuel rod pressure, the temperature for all gas volumes in the fuel rod must be calculated. Under steady state and transient reactor conditions, approximately 40 to 50% of the gas in a fuel rod is located in the fuel pellet expansion chamber (plenum) provided at the top of the fuel rod. The plenum temperature model (subcode PLNT) computes the temperature of this gas. This model includes all thermal interactions between the plenum gas and the top pellet surface, hold-down spring, and cladding wall.

The transient plenum temperature model is based on three assumptions:

(1) The temperature of the top surface of the fuel stack is independent of the plenum gas temperature

(2) The plenum gas is well mixed by natural convection

(3) Temperature gradients in the spring and cladding are small.

The first assumption allows the end pellet temperature to be treated as an independent variable. The second assumption permits the gas to be modeled by one lumped mass with average properties. The third assumption allows the temperature response of the cladding and spring to be represented by a small number of lumped masses.

The plenum temperature model consists of a set of six simultaneous first order differential equations that model the heat transfer between the plenum gas and the structural components of the plenum. These equations involve heat transfer coefficients between the various components. The heat transfer equations for the plenum temperature are described in Section 2.1, the required heat transfer coefficients are described in Section 2.2, and finally, the calculation of the gamma heating of the plenum hold-down spring and cladding is described in Section 2.3. A flow chart of the calculations is shown in Figure 7.

2.1 Plenum Temperature Equations

The plenum thermal model calculates the energy exchange between the plenum gas and structural components. The structural components consist of the hold-down spring, end pellet, and cladding. Energy exchange between the gas and structural components occurs by natural convection, conduction, and radiation. A schematic of these energy exchange mechanisms is shown in Figure 8. The spring is modeled by two nodes of equal mass (a center node and a surface node) as shown in Figure 9. The cladding is modeled by three nodes (two surface nodes and one center node) as shown in Figure 10. The center node has twice the mass of the surface nodes. This nodalization scheme results in a set of six energy equations from which the plenum thermal response can be calculated. The transient energy equations for the gas, spring, and cladding are as follows (Table IV defines the nomenclature used in the equations):

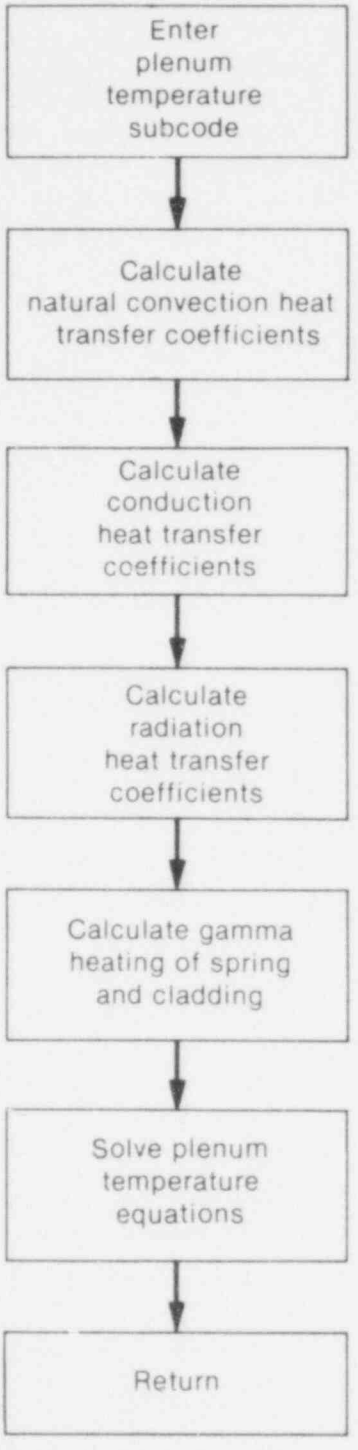

Fig. 7 Flow chart of plenum temperature calculations.

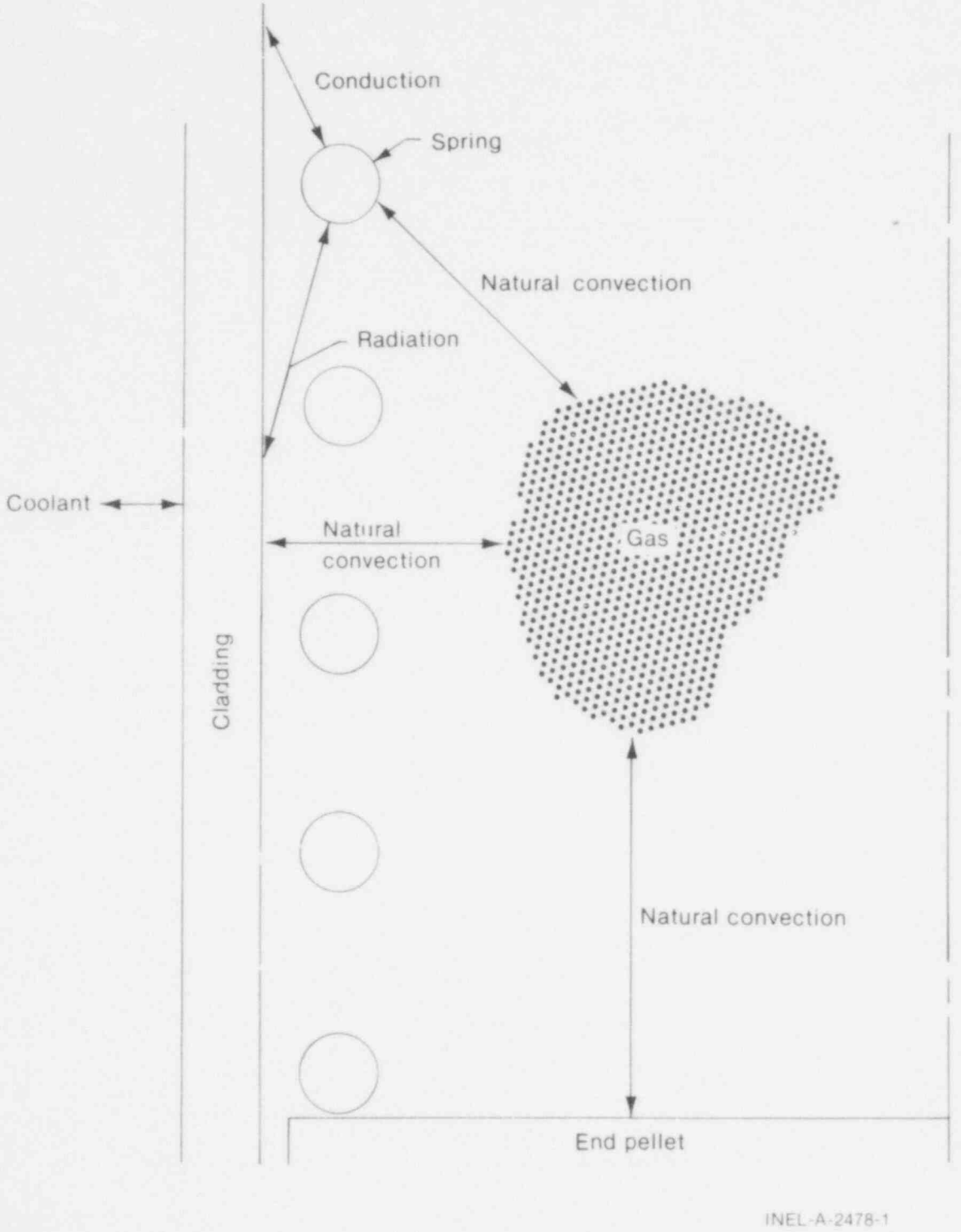

Fig. 8 Plenum energy flow model.

(1) Plenum gas:

$$\rho_g V_g C_g \frac{\partial T_g}{\partial t} = A_{ep} h_{ep} (T_{ep} - T_g) + A_{cl} h_{cl} (T_{cli} - T_g) + A_{ss} h_s (T_{ss} - T_g). \quad (2\text{-}1)$$

(2) Spring center node:

$$V_{sc} C_s \rho_s \frac{\partial T_{sc}}{\partial t} = \bar{q} V_{sc} + \frac{A_{sc} K_s (T_{ss} - T_{sc})}{R_{ss}} \quad (2\text{-}2)$$

(3) Spring surface node:

$$V_{ss} C_s \rho_s \frac{\partial T_{ss}}{\partial t} = \bar{q} V_{ss} + A_{sc} K_s (T_{sc} - T_{ss}) + A_{ss} h_{rads} (T_{cli} - T_{ss}) + A_{ss} h_s (T_g - T_{ss}) + A_{ss} h_{cons} (T_{cli} - T_{ss}) \quad (2\text{-}3)$$

where h_{cons} is the conductance between the spring and cladding. The conductance, h_{cons}, is used only when a stagnant gas condition exists; that is, when the natural convection heat transfer coefficient for the spring (h_s) is zero.

(4) Cladding interior node:

$$\rho_{cl} C_{cl} V_{cli} \frac{\partial T_{cli}}{\partial t} = A_{cl} h_{radc} (T_{ss} - T_{cli}) + A_{cl} h_{cl} (T_g - T_{cli}) + A_{cl} h_{conc} (T_{ss} - T_{cli}) + \frac{A_{cl} K_{cl}}{\Delta r/2} (T_{clc} - T_{cli}) + \bar{q} V_{cli} . \quad (2\text{-}4)$$

573 068

R_{ss} = radius of spring

$$R_{sc} = \frac{R_{ss}}{\sqrt{2}}$$

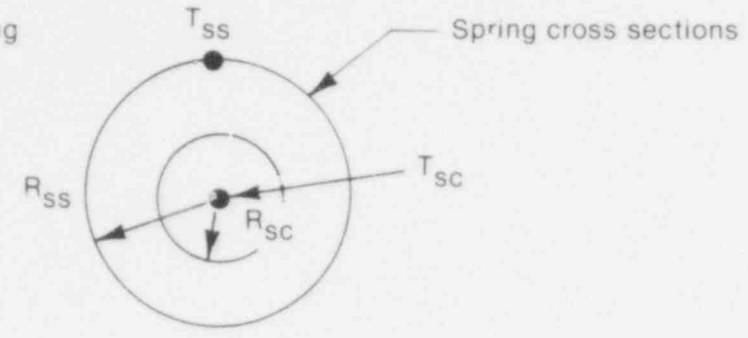

INEL-A-2480-1

Fig. 9 Spring noding.

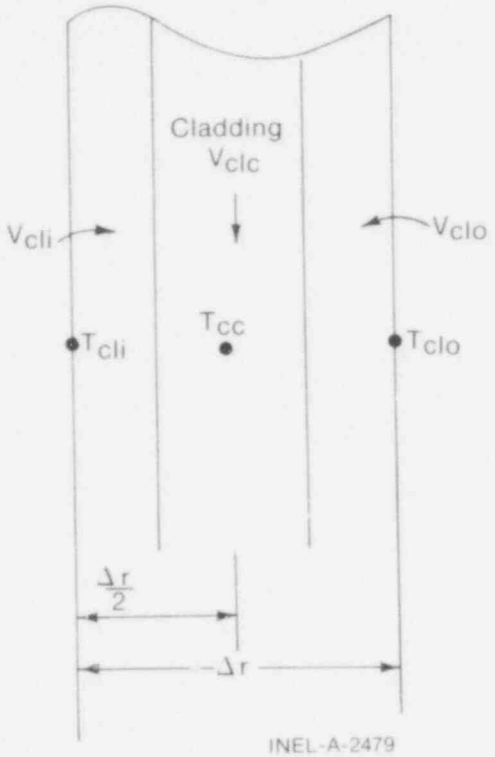

INEL-A-2479

Fig. 10 Cladding noding.

(5) Cladding central node:

$$\rho_{cl} C_{cl} V_{clc} \frac{\partial \bar{T}_{clc}}{\partial t} = \bar{q} \quad V_{clc} + \frac{A_{cl} K_{cl}}{\Delta r/2} \quad (T_{cli} - T_{clc})$$

$$+ \frac{A_{cl} K_{cl}}{\Delta r/2} \quad (T_{clo} - T_{clc}) \quad . \qquad (2\text{-}5)$$

TABLE IV

NOMENCLATURE FOR PLENUM THERMAL MODEL

Quantities		
A	=	surface area
C	=	heat capacitance
DIAC	=	diameter of the spring coil
DIAS	=	diameter of the spring wire
$\bar{F}_{1-2}$	=	gray-body shape factor from body 1 to body 2
F_{1-2}	=	view factor from body 1 to body 2
Gr	=	Grashof number
h	=	surface heat transfer coefficient
I	=	radiation flux
ID	=	inside diameter of the cladding
K	=	thermal conductivity
L	=	length
OD	=	outside diameter of the cladding
Pr	=	Prandtl number
q	=	energy
$\dot{\bar{q}}''$	=	surface heat flux
$\dot{\bar{q}}'''$	=	volumetric heat generation
R	=	radius
Δr	=	thickness of the cladding (OD-ID)/2.0
T	=	temperature
V	=	volume
σ	=	Stefan-Boltzmann constant
C_g	=	heat capacitance of gas, set equal to the value of 1.24 Btu/lb-^{o}F, which is the heat capacitance of helium.

TABLE IV (continued)

Quantities		
ρ	=	density
Σ	=	absorption coefficient
ε	=	emissivity
δ	=	spring to cladding spacing (ID-DIAC)/2.0
t	=	time

Subscripts		
cl	=	cladding
clc	=	cladding center node
cli	=	cladding interior node
clo	=	cladding outside node
cool	=	coolant
conc and cons	=	conduction between the spring and cladding
conv	=	convective heat transfer to coolant
ep	=	end pellet
g	=	gas
p	=	plenum
sc	=	spring center node
ss	=	spring surface node
s	=	spring
rads and radc	=	radiation heat transfer between the spring and cladding
m,m+1	=	old and new time step

(6) Cladding exterior node:

$$T_{clo} = T_{cool}. \tag{2-6}$$

For steady state, the time derivatives of temperature on the left side of Equations (2-1) through (2-5) are set to zero, and the temperature distribution in the spring and cladding is assumed to be uniform.

To obtain a set of algebraic equations, Equations (2-1) through (2-6) are rewritten in the Crank-Nicolson[17] implicit finite difference form. This formulation results in a set of six equations and six unknowns.

The details of the difference formulation of Equations (2-1) through (2-5) and the programming logic of subcode PLNT are given in Appendix G.

2.2 Heat Conduction Coefficients

Heat transfer between the plenum gas and the structural components occurs by natural convection, conduction, and radiation. The required heat transfer coefficients for these three modes are described in the following three subsections.

2.2.1 Natural Convection Heat Transfer Coefficients. Energy exchange by natural convection occurs between the top of the fuel pellet stack and the plenum gas, spring and plenum gas, and cladding and plenum gas. Heat transfer coefficients, h_{ep}, h_s, and h_{cl}, in the equations described above, model this energy exchange. To calculate these heat transfer coefficients, the top of the fuel stack is considered to be a flat plate, the spring a horizontal cylinder, and the cladding a vertical surface. Both laminar and turbulent natural convection are assumed to occur. Correlations for the heat transfer coefficients for these types of heat transfer are obtained from Kreith[18] and McAdams[19].

The flat plate natural convection coefficients used for the end pellet surface heat transfer are:

(1) For laminar conditions on a heated surface,

$$h_{ep} = 0.54\ K_g\ (Gr \times Pr)^{0.25}/ID \qquad (2\text{-}7)$$

(2) For turbulent conditions, Grashof number (Gr) greater than 2.0×10^7, on a heated surface,

$$h_{ep} = 0.14\ K_g\ (Gr \times Pr)^{0.33}/ID \qquad (2\text{-}8)$$

(3) For laminar conditions on a cooled surface,

$$h_{ep} = 0.27\ K_g\ (Gr \times Pr)^{0.25}/ID \qquad (2\text{-}9)$$

The following natural convection coefficients for horizontal cylinders are used for the film coefficient for the spring:

(1) For laminar conditions,

$$h_s = 0.53\ K_g\ (Gr \times Pr)^{0.25}/DIAS \qquad (2\text{-}10)$$

(2) For turbulent conditions, Gr from 10^9 to 10^{12},

$$h_s = 0.18\ (T_g - T_{ss})^{0.33} \qquad (2\text{-}11)$$

The vertical surface natural convection coefficients used for the cladding interior surface are given by:

(1) For laminar conditions,

$$h_{cl} = 0.55\ K_g\ (Gr \times Pr)^{0.25}/L_p. \qquad (2\text{-}12)$$

(2) For turbulent conditions, Gr greater than 10^9,

$$h_{cl} = 0.021\ K_g\ (Gr \times Pr)^{0.4}/L_p \qquad (2\text{-}13)$$

These natural convection correlations were derived for flat plates, horizontal cylinders, and vertical surfaces in an infinite gas volume. Heat transfer coefficients calculated using these correlations are expected to be higher than those actually existing within the confined space of the plenum. However, until plenum temperature experimental data are available, these coefficients are believed to provide a good estimate of the true values.

2.2.2 Conduction Heat Transfer Coefficients. Conduction of energy between the spring and cladding is represented by the heat transfer coefficients, h_{cons} and h_{conc}, in Equations (2-3) and (2-4). These coefficients are both calculated in subcode PLNT when stagnant gas conditions exist. The conduction coefficients are calculated on the basis of the spring and cladding geometries shown in Figure 10, and the assumptions that:

(1) The cladding and spring surface temperatures are uniform

(2) Energy is conducted only in the direction perpendicular to the cladding wall (heat flow is one-dimensional).

On the basis of these assumptions and the geometry given in Figure 11, the energy (q) conducted from an elemental surface area of the spring ($L_s R_s d\theta$) to the cladding is

$$dq = \frac{K_g(T_{ss} - T_{cli})\ (L_s\ R_s\ \sin(\theta)\ d\theta)}{(d + R_s - R_s \sin\theta)} \qquad (2\text{-}14)$$

where

= the azimuthal coordinate.

573 074

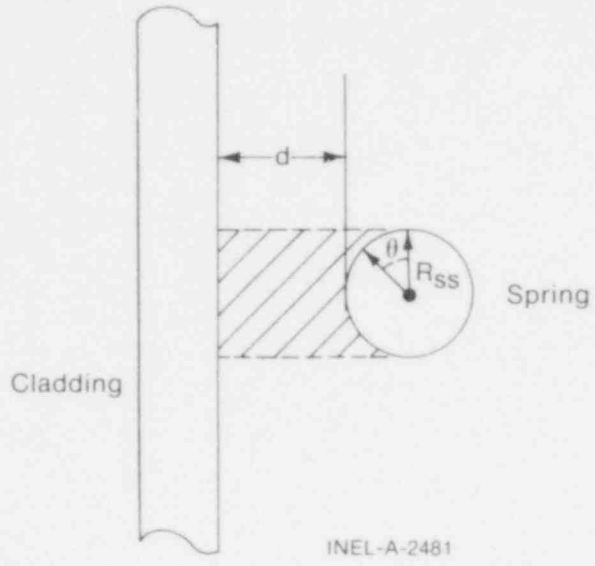

Fig. 11 Geometrical relationship between the cladding and spring.

By integration of Equation (2-14) over the surface area of the spring facing the cladding, the total flow of energy is given by

$$q = \frac{k_g A_{ss}}{\pi} (T_{ss} - T_{cli}) \left[-\frac{\pi}{2R_s} + \frac{2}{R_s} \left\{ \frac{1}{\frac{1-R_s^2}{(\delta+2R_s)^2}} + \mathrm{Tan}^{-1} \left[\left(\mathrm{Tan}\left(\frac{\theta}{2}\right) - \frac{R_s}{(\delta+2R_s)} \right) \Big/ \left(1 - \frac{R_s^2}{(\delta+2R_s)^2} \right) \right] \right\} \right]_{\theta=0}^{\theta=\frac{\pi}{2}} \quad (2\text{-}15)$$

The two conduction heat transfer coefficients are given by

$$h_{cons} = q/A_{ss} (T_{ss} - T_{cli}) \quad (2\text{-}16)$$

and

$$h_{conc} = h_{cons} A_{ss}/A_{cl} \quad (2\text{-}17)$$

When natural convection heat transfer exists, h_{cl} or $h_s > 0.0$, energy is assumed to flow to the gas from the spring and then from the gas to the cladding wall, or vice versa. Under these conditions,

h_{cons} and h_{conc} are set to zero. Therefore, in the current version of PLNT h_{cons} and h_{conc} are used only when the temperature is uniform throughout the plenum. Future plenum data or analytical analysis may indicate that natural convection flow between the spring and the cladding does not exist, in which case non-zero conduction coefficients will be used at all times.

2.2.3 Radiation Heat Transfer Coefficients. Transport of energy by radiation between the spring and cladding is included in the plenum model by use of the heat transfer coefficients, h_{rads} and h_{radc}, in Equations (2-3) and (2-4). These coefficients are calculated in subcode PLNT and are derived from the radiant energy exchange equation for two gray bodies in thermal equilibrium[18] as follows:

$$q_{1-2} = A_1 \bar{F}_{1-2} \sigma (T_1^4 - T_2^4) \qquad (2\text{-}18)$$

where q_{1-2} is the net rate of heat flow by radiation between bodies 1 and 2.

The gray-body factor ($\bar{F}_{1-2}$) is related to the geometrical view factor (F_{1-2}) from body 1 to body 2 by

$$A_1\bar{F}_{1-2} = \frac{1}{(1-\varepsilon_1)/A_1\varepsilon_1 + 1/A_1F_{1-2} + (1-\varepsilon_2)/A_2\ 2} \qquad (2\text{-}19)$$

Using Equations (2-18) and (2-19) and approximating the geometric view factor from the cladding to the spring (F_{cl-s}) by

$$F_{cl-s} = \frac{A_{ss}}{2\ A_{cl}} + \frac{(2A_{cl} - A_{ss})\ A_{ss}}{4A_{cl}^{\ 2}} \qquad (2\text{-}20)$$

the net radiant energy exchange between the cladding and spring may be written as

$$q_{cl-s} = A_{cl} \bar{F}_{cl-s} (T_{cli}^4 - T_{ss}^4) \qquad (2\text{-}21)$$

The radiation heat transfer coefficients, h_{radc} and h_{rads}, are calculated by

$$h_{radc} = q_{cl-s}/A_{cl} * (T_{cli} - T_{ss}) \quad (2\text{-}22)$$

and

$$h_{rads} = (h_{radc} * A_{cl})/A_{ss}. \quad (2\text{-}23)$$

2.3 Gamma Heating of the Spring and Cladding

The volumetric power generation term, $\bar{q}$, shown in Equations (2-2) through (2-5) represents the gamma radiation heating of the spring and cladding. A simple relationship is used to calculate $\bar{q}$ in subroutine PLNT. The relationship used is derived from the gamma flux attenuation equation

$$-dI(x) = \Sigma_\gamma \; I(x)\, dx \quad (2\text{-}24)$$

where $I(x)$ is the gamma flux, Σ_γ is the gamma ray absorption coefficient, and x is the spatial dimension of the solid on which the gamma radiation is incident. Since the cladding and spring are thin in cross section, the gamma ray flux can be assumed constant throughout the volume. Of the gamma flux (I) incident on the spring and cladding, the portion absorbed (ΔI) can be described by

$$-\Delta I = \Sigma_\gamma \; I\bar{x} \quad (2\text{-}25)$$

where $\bar{x}$ is the thickness of the spring or cladding. Therefore, the volumetric gamma ray absorption rate is given by

$$-\frac{\Delta I}{\bar{x}} = \Sigma_\gamma \; I. \quad (2\text{-}26)$$

Equation (2-26) can also represent gamma volumetric energy deposition by letting I represent the energy flux associated with the gamma radiation. Approximately 10% of the energy released in the fissioning of uranium is in the form of high energy gamma radiation. Therefore,

the gamma energy flux leaving the fuel rod would be approximately equal to 10% of the thermal flux. The gamma energy flux throughout the reactor can then be estimated by

$$I = 0.10\ \bar{q}_{rod} \tag{2-27}$$

where $\bar{q}_{rod}$ is the average fuel rod power. For zirconium, Σ_γ is approximately 11.0 ft^{-1}. Therefore, the gamma energy deposition rate is given by

$$-\frac{\Delta I}{\bar{X}} = \bar{q} = 1.1\ \bar{q}_{rod} \tag{2-28}$$

Equation (2-28) is an estimate of the gamma heating rate for the spring and cladding.

3. FUEL ROD DEFORMATION AND FAILURE

An accurate analysis of the fuel and cladding deformation is necessary in any fuel rod response analysis because of the fact that the heat transfer coefficient across the fuel-to-cladding gap is a strong function of the gap size. In addition, an accurate calculation of stresses in the cladding is needed so that an accurate prediction of the onset of cladding failure (and subsequent release of fission products) can be made.

In analyzing the deformation of fuel rods, four physical situations are encountered. The first situation occurs when the fuel pellets and cladding are not in contact. Here, the problem of a cylindrical shell (the cladding) with specified internal and external pressures and a specified cladding temperature distribution must be solved. This situation is called the "open gap" regime.

Second, the situation is encountered in which the fuel pellets (which are considerably hotter than the cladding) have expanded so as to be in contact with the cladding. Further heating of the fuel results in "driving" the cladding outward. This situation is called

the "closed gap" regime. Alternatively, this closed gap regime can occur due to the collapse of the cladding onto the fuel pellets due to elevated cladding temperatures and a high coolant pressure.

A third situation occurs in which a number of pellets not in contact with the cladding are trapped between the lower end of the fuel rod and a fuel pellet which is in firm contact with the cladding. Then, the axial expansion of the stack of trapped fuel pellets is imparted to the cladding. Here, the problem of a thin cylindrical shell, with not only prescribed internal and external pressures but also a prescribed total change in length, must be solved. This situation is called the "trapped stack" regime.

The preceding three regimes of fuel rod deformation are characterized by small cladding strains, and by the cladding retaining its essentially cylindrical shape. By contrast, a short region of cladding might swell locally when a net outward pressure differential exists and the cladding temperature is elevated. This so-called "ballooning" regime is often predicted and observed during LOCA type transients. This regime of deformation is essentially different from the first three regimes described, and requires a completely different type of analytical model because of the large displacement nature of the deformation.

As shown in Figure 12, the deformation analysis in FRAP-T5 consists of three parts: (a) a small deformation analysis, (b) a large deformation (ballooning) analysis, and (c) a cladding failure analysis. First, a small deformation analysis of the stresses, strains, and displacements in the fuel and cladding is performed for the entire fuel rod. This analysis is based on the assumption that the cladding retains its cylindrical character, and includes the effects of:

(1) Fuel thermal expansion, creep, swelling, densification, and relocation

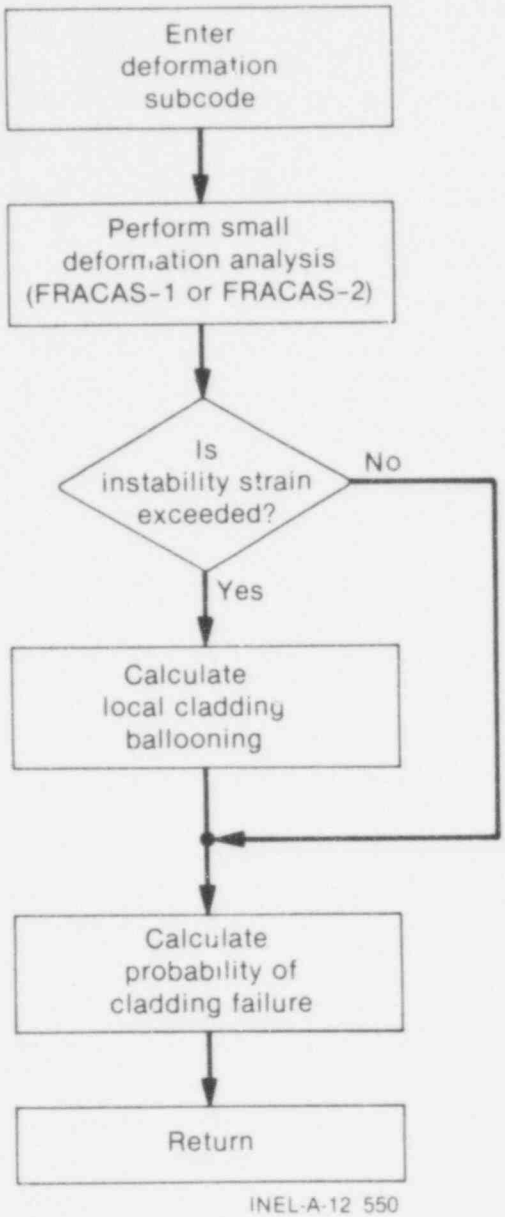

Fig. 12 Flow chart of deformation subcode.

(2) Cladding thermal expansion, creep, and plasticity

(3) Fission gas and external coolant pressures.

As part of the small displacement analysis, the correct regime of deformation (open gap, closed gap, or trapped stack) is determined.

573 080

Two models are available for the calculation of the small displacement deformation of the fuel and cladding. The more simplified model neglects the stress-induced deformation of the fuel, and is called the rigid pellet model (FRACAS-1). The second option includes the stress-induced fuel pellet deformation, and is called the deformable pellet model (FRACAS-2).

After the small strain analysis has been performed for the entire fuel rod, the cladding strains are compared with the value of an instability strain obtained from MATPRO. If, at any point along the rod, the instability strain has been exceeded, then the cladding cannot maintain a cylindrical shape and local ballooning has occurred. For the local region at which instability is predicted, a large deformation ballooning analysis is performed using subcode BALLOON. This analysis allows for nonaxisymmetric large deformation of the cladding, and can take into account local axial and circumferential temperature variations. Modification of local heat transfer coefficients is calculated as the ballooning progresses and additional surface area is presented to the coolant.

The last step in the deformation anaysis is the cladding failure calculation. Computed stresses and strains in the cladding are passed into the FRAIL failure analysis subcode, and a statistical prediction of fuel rod failure is made.

In both the small deformation analysis (rigid or deformable pellet models) and the large deformation ballooning analysis, plastic behavior of the cladding must be considered. The plasticity equations used in the two small deformation models are the same, and are based on the general theory of multiaxial plasticity. A more simplified plastic analysis is used in the ballooning model.

In Section 3.1, the general theory of plastic analysis is outlined and the method of solution used in FRAP-T5 is presented. This method of solution is used in both the rigid pellet and deformable pellet models. In Section 3.2, the equations and subroutines for the

rigid pellet model and deformable pellet model are described. Section 3.3 describes the large deformation analysis model (BALLOON) and, finally, Section 3.4 describes the cladding failure analysis package, FRAIL.

3.1 General Considerations in Elastic-Plastic Analysis

Problems involving elastic-plastic deformation and multiaxial states of stress involve a number of aspects that do not require consideration in a uniaxial problem. In the following, an attempt is made to briefly outline the structure of incremental plasticity, and to outline the Method of Successive Substitutions (also called the Method of Successive Elastic Solutions), which has been used successfully in treating multiaxial elastic-plastic problems[20]. The method can be used for any problem for which a solution based on elasticity can be obtained, and this method is used in both the rigid pellet and deformable pellet models.

In a problem involving only uniaxial stress, σ_1, the strain, ε_1, is related to the stress by an experimentally determined stress-strain curve, as shown in Figure 13, and Hookes's law is taken as

$$\varepsilon_1 = \frac{\sigma_1}{E} + \varepsilon_1^p + \int \alpha \, dT \tag{3-1}$$

where ε_1^p is the plastic strain and E is the modulus of elasticity. The onset of yielding occurs at the yield stress, which can be determined directly from Figure 13. Given a load (stress) history, the resulting deformation can be determined in a simple fashion. Increase of yield stress with work-hardening is easily computed directly from Figure 13.

In a problem involving multiaxial states of stress, however, the situation is not so clear. In such a problem, a method of relating the onset of plastic deformation to the results of a uniaxial test is

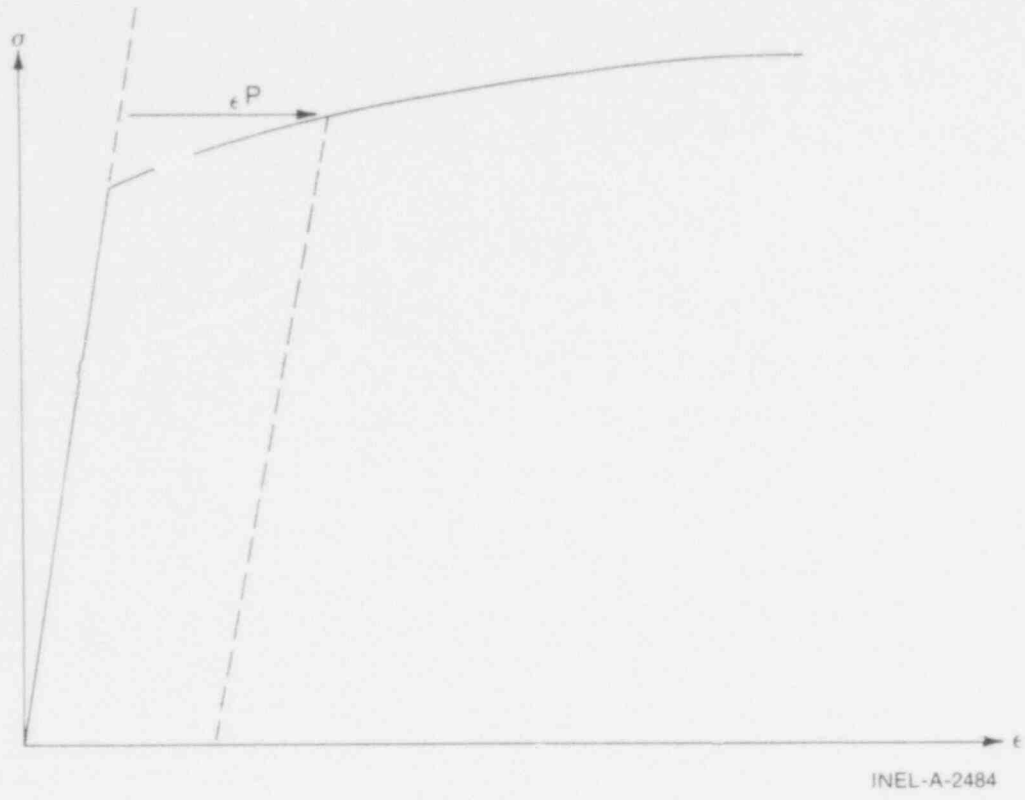

Fig. 13 Typical isothermal stress-strain curve.

required, and further, when plastic deformation occurs, some means is needed for determining how much plastic deformation has occurred and how that deformation is distributed among the individual components of strain. These two complications are taken into account by use of the so-called "yield function" and "flow rule," respectively.

A considerable wealth of experimental evidence exists on the onset of yielding in a multiaxial stress state. The bulk of this evidence supports the von Mises yield criterion, which asserts that yielding occurs when the stress state is such that

$$0.5\,[(\sigma_1 - \sigma_2)^2 + (\sigma_2 - \sigma_3)^2 + (\sigma_3 - \sigma_1)^2] = \sigma_y^2 \qquad (3\text{-}2)$$

where the σ_i values are the principal stresses, and σ_y is the yield stress as determined in a uniaxial stress-strain test. The square root of the left side of this equation is referred to as the "effective stress", σ_e, and this effective stress is one commonly used type of yield function.

To determine how the yield stress changes with permanent deformation, the yield stress is hypothesized to be a function of the equivalent plastic strain, ε^P. An increment of equivalent plastic strain is determined at each load step, and ε^P is defined as the sum of all increments incurred:

$$\varepsilon^P \triangleq \sum d\varepsilon^P . \tag{3-3}$$

Each increment of effective plastic strain is related to the individual plastic strain components by

$$d\varepsilon^P = \frac{2}{3}[(d\varepsilon_1^P - d\varepsilon_2^P)^2 + (d\varepsilon_2^P - d\varepsilon_3^P)^2 + (d\varepsilon_3^P - d\varepsilon_1^P)^2]^{1/2} \tag{3-4}$$

where the $d\varepsilon_i^P$ are the plastic strain components in principal coordinates. Well-known experimental results indicate that at pressures on the order of the yield stress, plastic deformation occurs with no change in volume, which implies that

$$d\varepsilon_1^P + d\varepsilon_2^P + d\varepsilon_3^P = 0 \tag{3-5}$$

and hence, in a uniaxial test with $\sigma_1 = \sigma$, $\sigma_2 = \sigma_2 = 0$, the plastic strain increments are

$$d\varepsilon_2^P = d\varepsilon_3^P = -1/2\ d\varepsilon_1^P .$$

Hence, in a uniaxial test, Equations (3-2) and (3-4) reduce to

$$\sigma_e = \sigma$$
$$d\varepsilon^P = d\varepsilon_1^P \tag{3-6}$$

Thus, when the assumption is made that the yield stress is a function of the total effective plastic strain (called the Strain Hardening

Hypothesis), the functional relationship between yield stress and plastic strain can be taken directly from a uniaxial stress-strain curve by virtue of Equation (3-6).

The relationship between the magnitudes of the plastic strain increments and the effective plastic strain increment is provided by the Prandtl-Reuss Flow Rule:

$$d\varepsilon_i^P = \frac{3\, d\varepsilon^P}{2\, \sigma_e} S_i \qquad i = 1, 3 \tag{3-7}$$

where the S_i values are the deviatoric stress components (in principal coordinates) defined by

$$S_i = \sigma_i - \frac{1}{3}(\sigma_1 + \sigma_2 + \sigma_3) \qquad i = 1, 3 \tag{3-8}$$

Equation (3-7) embodies the fundamental observation of plastic deformation: plastic strain increments are proportional to the deviatoric stresses. The constant of proportionality is determined by the choice of the yield function[20]. Direct substitution shows that Equations (3-2), (3-3), (3-4), (3-7), and (3-8) are consistent with one another.

Once the plastic strain increments have been determined for a given load step, the total strains are determined from a generalized form of Hooke's law given by

$$\left.\begin{aligned}
\varepsilon_1 &= \frac{1}{E}\{\sigma_1 - \nu(\sigma_2 + \sigma_3)\} + \varepsilon_1^P + d\varepsilon_1^P + \int \alpha dT \\
\varepsilon_2 &= \frac{1}{E}\{\sigma_2 - \nu(\sigma_1 + \sigma_3)\} + \varepsilon_2^P + d\varepsilon_2^P + \int \alpha dT \\
\varepsilon_3 &= \frac{1}{E}\{\sigma_3 - \nu(\sigma_2 + \sigma_1)\} + \varepsilon_3^P + d\varepsilon_3^P + \int \alpha dT
\end{aligned}\right\} \tag{3-9}$$

in which ε_1^P, ε_2^P, and ε_3^P are the total plastic strain components at the end of the previous load increment.

573 085

The remaining continuum field equations of equilibrium, strain displacement, and strain compatibility are unchanged. The complete set of governing equations is presented in Table V, written in terms of rectangular Cartesian coordinates and employing the usual indicial notation in which a repeated Latin index implies summation. This set of equations is augmented by experimentally determined uniaxial stress-strain relation.

3.1.1 The Method of Solution. When the problem under consideration is statically determinate, so that stresses can be found from equilibrium conditions alone, the resulting plastic deformation can be determined directly. However, when the problem is statically indeterminate, and the stresses and deformation must be found simultaneously, then the full set of plasticity equations proves to be quite formidable, even in the case of simple loadings and geometries.

One numerical procedure which has been used with considerable success is the Method of Successive Substitutions. This method can be applied to any problem for which an elastic solution can be obtained, either in closed form or numerically. A full discussion of this technique, including a number of technologically useful examples is contained in Reference 20.

Briefly, the method involves breaking the loading path up into a number of small increments. For example, in the present application, the loads are external pressure, temperature, and either internal pressure or prescribed displacement of the inside surface of the cladding. These loads all vary during the operating history of the fuel rod. For each new increment of the loading, the solution to all the plasticity equations listed in Table V is obtained as follows.

First, an initial estimate of the plastic strain increments, $d\varepsilon^{P}_{ij}$, is made. On the basis of these values, the equations of equilibrium, Hooke's Law, and strain-displacement and compatibility are solved as for any elastic problem. From the stresses so obtained, the

TABLE V

ELASTIC-PLASTIC GOVERNING EQUATIONS

Equilibrium

$$\sigma_{ji,j} + \rho f_i = 0$$

where σ_{ji} = stress tensor

ρ = mass density

f_i = components of body force per unit mass

Stress Strain

$$\varepsilon_{ij} = \frac{1+\nu}{E}\sigma_{ij} - \delta_{ij}\left(\frac{\nu}{E}\sigma_{kk} - \int \alpha dT\right) + \varepsilon^P_{ij} + d\varepsilon^P_{ij}$$

Compatibility

$$\varepsilon_{ij,k\ell} + \varepsilon_{k\ell,ij} - \varepsilon_{ik,j\ell} - \varepsilon_{j\ell,ik} = 0$$

Definitions Used in Plasticity

$$\sigma_e \triangleq \sqrt{\frac{3}{2} S_{ij} S_{ij}}$$

$$S_{ij} \triangleq \sigma_{ij} - \frac{1}{3}\sigma_{kk}$$

$$d\varepsilon^P \triangleq \sqrt{\frac{2}{3} d\varepsilon^P_{ij} \; d\varepsilon^P_{ij}}$$

Prandtl-Reuss Flow Rule

$$d\varepsilon^P_{ij} = \frac{3}{2}\frac{d\varepsilon^P}{\sigma_e} S_{ij}$$

deviatoric stresses, S_{ij}, may be computed. This "pseudo-elastic" solution represents one path in the computational scheme.

Independently, through use of the assumed $d\varepsilon^P_{ij}$ values, the increment of effective plastic strain, $d\varepsilon^P$, may be computed, and from this result and the stress-strain curve, a value of the effective stress, σ_e, is obtained.

Finally, a new estimate of the plastic strain increments is obtained from the Prandtl-Reuss flow rule

$$d\varepsilon^P_{ij} = \frac{3}{2} \frac{d\varepsilon^P}{\sigma_e} S_{ij} \qquad (3\text{-}10)$$

and the entire process is continued until the $d\varepsilon^P_{ij}$ converge. A schematic of the iteration scheme is shown in Figure 14.

The mechanism by which improved estimates of $d\varepsilon^P_{ij}$ are obtained results from the fact that the effective stress obtained from $d\varepsilon^P$ and the stress-strain curve will not be equal to the effective stress that would be obtained with the stresses from the elastic solution. The effective stresses will only agree when convergence is obtained.

The question of convergence is one that cannot, in general, be answered a priori. However, convergence can be shown[20] to be obtained for sufficiently small load increments. Experience has shown that this technique is suitable for both steady state and transient fuel rod analyses.

3.1.2 Extension to Creep and Hot Pressing. The method of solution described for the time-independent plasticity calculations can also be used for time-dependent creep and hot pressing calculations. In this context, the term creep refers to any time-dependent constant volume permanent deformation, whereas the term hot pressing refers to any time-dependent process which results in a permanent change in volume. Both creep and hot pressing are stress-driven processes, and are usually highly dependent on temperature.

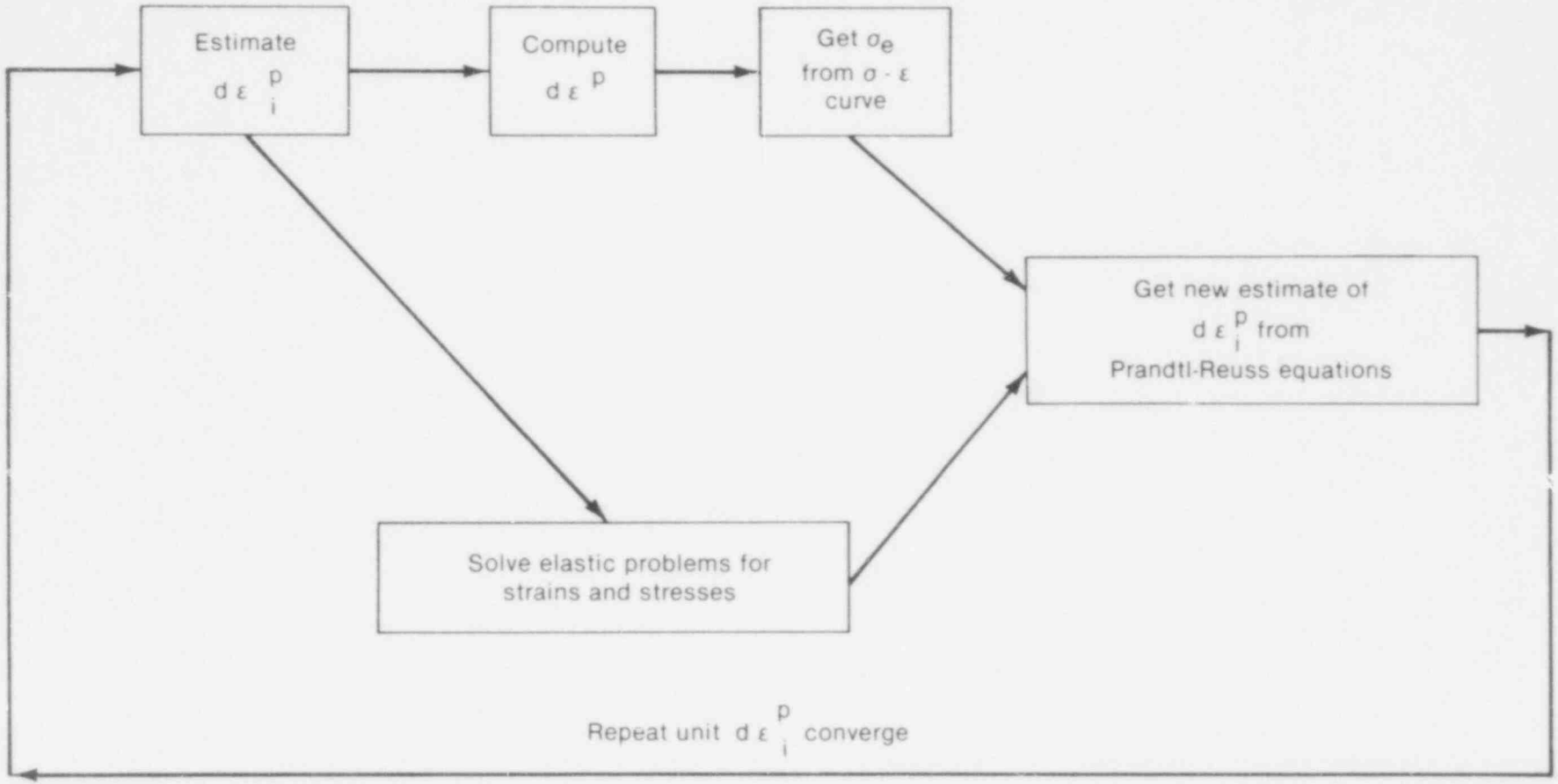

Fig. 14 Schematic of the Method of Successive Elastic Solutions.

The only change required to extend the Method of Successive Elastic Solutions to allow consideration of creep and hot pressing is to rewrite the Prandtl-Reuss flow rule, Equation (3-7), as

$$d\varepsilon_1^c = 1.5 \frac{\dot{\varepsilon}^c \Delta t}{\sigma_e} S_1 + \frac{\dot{V}^c \Delta t}{9} \frac{(\sigma_1 + \sigma_2 + \sigma_3)}{\sigma_m}$$

$$d\varepsilon_2^c = 1.5 \frac{\dot{\varepsilon}^c \Delta t}{\sigma_e} S_2 + \frac{\dot{V}^c \Delta t}{9} \frac{(\sigma_1 + \sigma_2 + \sigma_3)}{\sigma_m}$$

$$d\varepsilon_3^c = 1.5 \frac{\dot{\varepsilon}^c \Delta t}{\sigma_e} S_3 + \frac{\dot{V}^c \Delta t}{9} \frac{(\sigma_1 + \sigma_2 + \sigma_3)}{\sigma_m} .$$

The first term on the right hand side of each of these equations computes the constant volume creep strain, whereas the second term in each equation computes the permanent change in volume. To use this form of the flow rule, two additional material property correlations must be available. The first is a correlation for constant volume creep strain ε^c(taken in a uniaxial test) as a function of stress, time, temperature, and neutron flux; that is,

$$\varepsilon^c = f(\sigma, T, t, \dot{F})$$

where

σ_e = uniaxial stress

T = temperature

t = time

$\dot{F}$ = neutron flux.

In FRAP-T5, the strain hardening hypothesis[20] is assumed, which implies that the creep strain correlation can be differentiated and solved for creep strain rate in the form

$$\dot{\varepsilon}^c = h(\sigma, \varepsilon^c, T, \dot{F})$$

which is no longer an explicit function of time. This equation is obtained from the MATPRO subcode during the creep calculations.

The second additional correlation required is a relationship between the rate of permanent volumetric strain and the applied loads, that is,

$$\dot{V}^c = g(\sigma_m, T, t, V_{avail})$$

where

σ_m = $\sigma_1 + \sigma_2 + \sigma_3$ is the mean stress

T = temperature

t = time

V_{avail} = measure of maximum permanent volume change possible.

The permanent volumetric strain increment dV^c is related to the plastic strain increments by the equation

$$dV^c = d\varepsilon_1^c + d\varepsilon_2^c + d\varepsilon_3^c.$$

In FRAP-T5, hot pressing is considered only in the fuel. The source of the permanent volume change is assumed to be the closing of cracks in the relocated fuel. The maximum amount of volume available for permanent volume change is thus the amount of volume generated by fuel relocation. The equation for the permanent volume change was generated by comparing FRAP-T5 calculated and measured length changes for experimental fuel rods irradiated in the Power Burst Facility and the Halden Test Reactor. The correlation which resulted in the best agreement with measured fuel rod length changes was found to be

573 091

$$\dot{V}^c = -A\sigma_m^{4.5} (V^c + V_{reloc}) \exp(-15800/T)$$

where

$\dot{V}^c$ = rate of volumetric strain (1/s)

A = 3.64×10^{-18}

σ_m = mean stress (N/m^2)

V^c = volumetric strain

T = temperature (K)

V_{reloc} = $2U_r / r_p$ in which U_r is the relocation displacement and r_p is the cold pellet radius.

The relocation displacement for the deformable pellet model (FRACAS-2) is computed by the equation

$$U_r = (2/3)\delta$$

where

δ = as-fabricated radial gap between fuel pellets and cladding.

This equation for relocation displacement is based on the assumption that the fuel has not been subjected to repeated power cycles, as does the equation for relocation displacement shown in Subsection 3.2.1(2). No permanent volume change is permitted if σ_m is positive, and as the volumetric strain V^c approaches the volume available from relocation (V_{reloc}), the permanent volumetric strain rate goes to zero. This hot pressing correlation has been incorporated in FRAP-T5 in subroutine FPRESS, and is called only when the deformable pellet option is specified.

573 092

3.2 Small Deformation Fuel Rod Models

Two models are available for analyzing the small deformation of the fuel and cladding. The first model considers the fuel pellets to be essentially rigid, and to deform due to thermal expansion and relocation only. Thus, in the rigid pellet model, the displacement of the fuel is calculated independently of the deformation of the cladding. This rigid pellet analysis is performed in the FRACAS-1 subcode.

The second model available for the small deformation analysis is a more general analysis in which the fuel is assumed to deform due to stress, and in this case the deformation of the fuel and cladding must be determined simultaneously. This deformable pellet analysis is performed in the FRACAS-2 subcode.

The code user has the option of choosing either the rigid pellet or deformable pellet model. In general, the rigid pellet model (FRACAS-1) is less time-consuming, and has proven to be quite adequate for a wide variety of reactor transients in which pellet-cladding interaction is not the dominant failure mechanism. When failure due to pellet-cladding mechanical interaction is anticipated, however, the deformable pellet model (FRACAS-2) gives a more accurate calculation. Guidance for choosing between these two models is given in Appendix A.

3.2.1 Rigid Pellet Cladding Model. The cladding deformation model in FRACAS-1 is described in Subsection (1). The fuel deformation model is described in Subsection (2). If the fuel and cladding gas gap is closed, the fuel deformation model will apply a driving force to the cladding deformation model. The cladding deformation model, however, never influences the fuel deformation model.

The cladding deformation model in FRACAS-1 is based on the following assumptions:

- Incremental theory of plasticity
- Prandtl-Reuss flow rule
- Isotropic work-hardening
- No creep deformation of cladding
- Thin wall cladding (stress, strain, and temperature uniform through cladding thickness)
- If fuel and cladding are in contact, no axial slippage occurs at fuel cladding interface
- Bending strains and stresses in cladding are negligible
- Axisymmetric loading and deformation of cladding.

The fuel deformation in FRACAS-1 is based on the following assumptions:

- Thermal expansion and fuel relocation are the only sources for fuel deformation
- No resistance to thermal expansion of fuel
- Axial thermal expansion of fuel stack is equal to thermal expansion of a line projected through the dish shoulder of the fuel pellets
- No creep deformation of fuel
- Isotropic fuel properties.

(1) Cladding Deformation Model. The rigid pellet (FRACAS-1) cladding deformation subcode consists of six individual

subroutines, each of which is independent of the others. Hence, the model contained in each subroutine can be modified or replaced without requiring changes in any part of the subcode.

Deformation and stresses in the cladding in the open gap regime are computed in subroutine CLADF. The model considered is a thin cylindrical shell with specified internal and external pressures and a prescribed uniform temperature.

Calculations for the closed gap regime are made in subroutine COUPLE. The model considered is a thin cylindrical shell with prescribed external pressure and a prescribed radial displacement of its inside surface. The prescribed displacement is obtained from the fuel thermal expansion models described in Subsection (2). Further, since no slip is assumed to take place when the fuel and cladding are in contact, the axial expansion of the fuel is transmitted directly to the cladding, and hence, the change in axial strain in the shell is also prescribed.

Calculations for the trapped stack regime are made in subroutine STACK. The model considered is a thin cylindrical shell with prescribed internal and external pressures and a prescribed total change in length of the cylinder. In contrast to CLADF and COUPLE, which solve for the stresses and strains at only one axial location at a time, subroutine STACK simultaneously solves for the stresses and strains in all axial nodes which are being strained axially by the trapped stack of fuel pellets.

The decision whether the gap is open or closed, and whether to call COUPLE, STACK, or CLADF is made in the executive subroutine FCMI (Fuel Cladding Mechanical Interaction), which is the only subroutine that must be called by FRAP-T to initiate the fuel-cladding interaction analysis. At the completion of this analysis, FCMI returns either a new gap size or a new interface pressure between the fuel and cladding for use in the next iteration of the thermal calculations.

In each of COUPLE, STACK, and CLADF, an elastic-plastic solution is obtained. Two additional subroutines, STRAIN and STRESS, compute changes in yield stress with work-hardening, given a uniaxial stress-strain curve. This stress-strain curve is obtained from the MATPRO[2] subcode. Subroutine STRAIN computes the effective total strain and new effective plastic strain, given a value of effective stress and the effective plastic strain at the end of the last loading increment. Subroutine STRESS computes the effective stress, given an increment of plastic strain and the effective plastic strain at the end of the last loading increment. Depending on the work-hardened value of yield stress, loading can be either elastic or plastic, and unloading is constrained to occur elastically. (Isotropic work-hardening is assumed in these calculations.) These six subroutines are described in detail in the following.

(a) Subroutine FCMI. Subroutine FCMI performs the basic function of determining whether or not the fuel pellets and the cladding are in contact. The decision as to whether or not the fuel is in contact with the cladding is made by comparing the radial displacement of the fuel with the radial displacement that would occur in the cladding due to the prescribed external (coolant) pressure and the prescribed internal (fission and fill gas) pressure. Both of these values are passed to FCMI through the calling sequence. This cladding free radial displacement is obtained in CLADF. Then, if

$$u_r^{fuel} \geq u_r^{clad} + \delta \qquad (3\text{-}11)$$

where δ is the initial (as-fabricated) gap between the fuel and the cladding, the fuel is determined to be in contact with the cladding. The as-fabricated gap, δ, is a constant that does not change throughout the loading history of the rod. The loading history enters into this decision by virtue of the permanent plastic cladding strains which are used in the CLADF solution, and which are updated at each call to CLADF or COUPLE. These plastic strains (and total effective plastic strain, ε^P) are stored in the main calling program, and are passed to FCMI through the calling sequence.

If the fuel and cladding displacements are such that Equation (3-11) is not satisfied, the gap has not closed during the current load step, and the solution obtained by CLADF is the appropriate solution. The current value of the gap is computed and passed back to the main calling program. The plastic strain values may be changed in the solution obtained by CLADF if additional plastic straining has occurred.

If Equation (3-11) is satisfied, however, the fuel and the cladding have come into contact during the current loading increment. At the contact interface, radial continuity requires that

$$u_r^{clad} = u_r^{fuel} - \delta \qquad (3\text{-}12)$$

while in the axial direction the assumption is made that no slip occurs between the fuel and the cladding.

Note that only the additional strain which occurs in the fuel after "lock-up" has occurred is transferred to the cladding. Thus, if $\varepsilon_{z,o}^{clad}$ is the axial strain in the cladding just prior to contact, and $\varepsilon_{z,o}^{fuel}$ is the corresponding axial strain in the fuel, then the no-slip condition in the axial direction becomes

$$\varepsilon_z^{clad} - \varepsilon_{z,o}^{clad} = \varepsilon_z^{fuel} - \varepsilon_{z,o}^{fuel}. \qquad (3\text{-}13)$$

The values of the "prestrains," $\varepsilon_{z,o}^{fuel}$ and $\varepsilon_{z,o}^{clad}$, are set equal to the values of the strains that existed in the fuel and cladding at the time of gap closure and are stored in the main calling program and passed to FCMI in the calling sequence. The values are updated at the end of any load increment during which the gap closed.

After u_r^{clad} and ε_z^{clad} have been computed in FCMI, they are passed to subroutine COUPLE, which considers a thin cylindrical shell with prescribed axial strain, external pressure, and prescribed radial displacement of the inside surface. After the solution to this

problem is obtained in COUPLE, subroutine FCMI passes a value of the interface pressure back to the main calling program, along with new plastic strains and stresses.

(b) Subroutine CLADF. This subroutine considers a thin cylindrical shell loaded by both internal and external pressures. Axisymmetric loading and deformation are assumed. Loading is also restricted to being uniform in the axial direction, and no bending is considered. The geometry and coordinates are shown in Figure 15. The displacements of the midplane of the shell are u and w in the radial and axial directions, respectively.

For this case, the equilibrium equations are identically satisfied by

$$\sigma_\theta = \frac{r_i P_i - r_o P_o}{t} \tag{3-14}$$

$$\sigma_z = \frac{\pi r_i^2 P_i - \pi r_o^2 P_o}{\pi(r_o^2 - r_i^2)} \tag{3-15}$$

where

σ_θ = hoop stress

σ_z = axial stress

r_i = inside radius of cladding

r_o = outside radius of cladding

P_i = internal pressure of fuel rod

P_o = coolant pressure

t = cladding thickness.

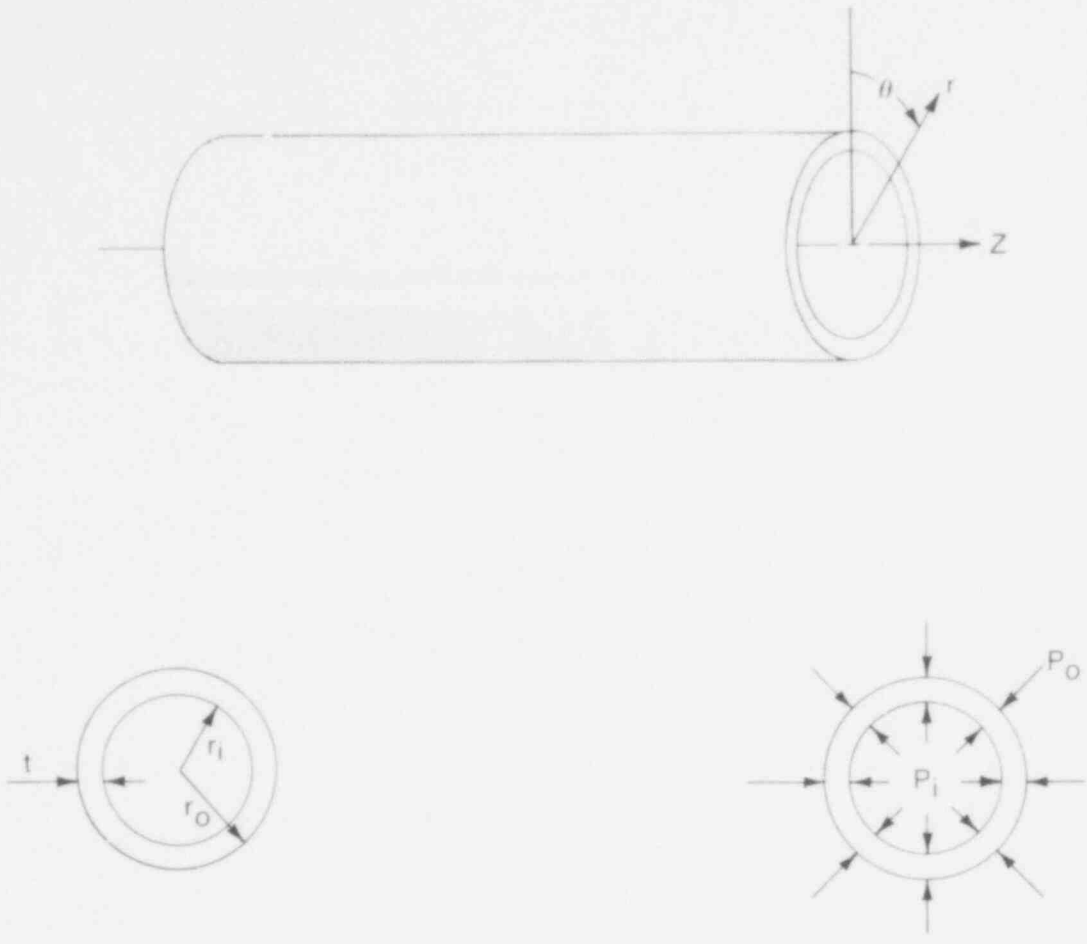

Fig. 15 Fuel rod geometry and coordinates.

For a membrane shell theory[21], the strains are related to the midplane displacements by

$$\varepsilon_z = \frac{\partial w}{\partial z} \tag{3-16}$$

$$\varepsilon_\theta = \frac{u}{\bar{r}} \tag{3-17}$$

where $\bar{r}$ is the radius of the midplane. Strain across the thickness of the shell is allowed. In shell theory, since the radial stress can be neglected, and since the hoop stress, σ_θ, and axial stress, σ_z, are uniform across the thickness when bending is not considered, the radial strain is due only to the Poisson's effect, and is uniform across the thickness. (Normally, radial strains are not considered in a shell theory, but when plastic deformations are considered, plastic radial strains must be included.)

The stress-strain relations are written in the incremental form

$$\varepsilon_\theta = \frac{1}{E}\{\sigma_\theta - \nu\,\sigma_z\} + \varepsilon_\theta^P + d\varepsilon_\theta^P + \int_{T_o}^{T} \alpha\, dT \tag{3-18}$$

$$\varepsilon_z = \frac{1}{E}\{\sigma_z - \nu\,\sigma_\theta\} + \varepsilon_z^P + d\varepsilon_z^P + \int_{T_o}^{T} \alpha\, dT \tag{3-19}$$

$$\varepsilon_r = -\frac{\nu}{E}\{\sigma_\theta + \sigma_z\} + \varepsilon_r^P + d\varepsilon_r^P + \int_{T_o}^{T} \alpha\, dT \tag{3-20}$$

in which T_o is the strain-free reference temperature, α is the coefficient of thermal expansion, T is the current average cladding temperature, E is the modulus of elasticity, and ν is Poisson's ratio. The terms ε_θ^P, ε_z^P, and ε_r^P are the plastic strains at the end of the last load increment, and $d\varepsilon_\theta^P$, $d\varepsilon_r^P$, and $d\varepsilon_z^P$ are the additional plastic strain increments which occur due to the new load increment.

The magnitudes of the additional plastic strain increments are determined by the effective stress and the Prandtl-Reuss flow rule, expressed as

$$\sigma_e = \frac{1}{\sqrt{2}} \left\{ (\sigma_\theta - \sigma_z)^2 + (\sigma_z)^2 + (\sigma_\theta)^2 \right\}^{1/2} \qquad (3\text{-}21)$$

$$d\varepsilon_i^P = \frac{3}{2} \frac{d\varepsilon^P}{\sigma_e} S_i \quad \text{for} \quad i = r,\theta,z \qquad (3\text{-}22)$$

$$S_i = \sigma_i - \frac{1}{3} (\sigma_\theta + \sigma_z) \quad \text{for} \quad i = r,\theta,z \qquad (3\text{-}23)$$

The solution in CLADF proceeds as follows. At the end of the last load increment the plastic strain components, ε_r^P, ε_θ^P, and ε_z^P are known, and also the total effective plastic strain, ε^P, is known.

The loading is now incremented with the prescribed values of P_i, P_o, and T. The new stresses can be determined from Equations (3-14) and (3-15), and a new value of effective stress is obtained from Equation (3-21).

The increment of effective plastic strain, $d\varepsilon^P$, which results from the current increment of loading, can now be determined from the uniaxial stress-strain curve at the new value of σ_e, as shown in Figure 16. (The new elastic loading curve depends on the value of ε^P.) This computation is performed by subroutine STRAIN.

Once $d\varepsilon^P$ is determined, the individual plastic strain components are found from Equation (3-22), and the total strain components are obtained from Equations (3-18) through (3-20).

573 101

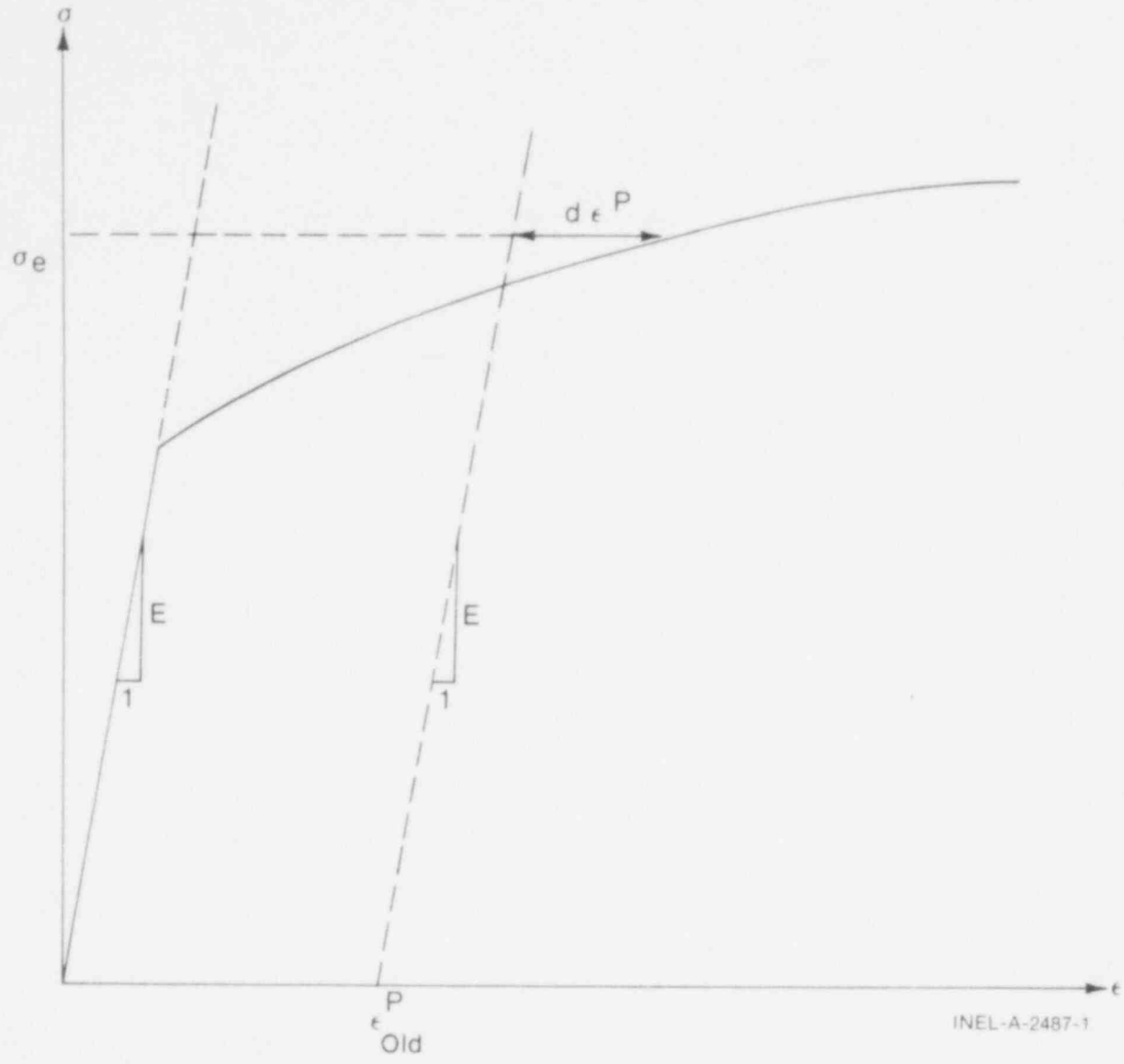

Fig. 16 Calculation of effective stress σ_e from $d\varepsilon^P$.

The displacement of the inside surface of the shell must be determined so that a new gap width can be computed. The radial displacement of the inside surface is given by

$$u(r_i) = \bar{r}\,\varepsilon_\theta - \frac{t}{2}\,\varepsilon_r \qquad (3\text{-}24)$$

where the first term is the radial displacement of the midplane (from Equation (3-17)) and ε_r is the uniform strain across the thickness, t.

The cladding thickness, t, is computed by the equation

$$t = (1 + \varepsilon_r)\, t_o$$

t_o = cold state, unstressed thickness of cladding. (3-25)

The final step performed by CLADF prior to returning control to FCMI is to add the plastic strain increments to the previous plastic strain values, that is,

$$(\varepsilon_\theta^P)_{new} = (\varepsilon_\theta^P)_{old} + d\varepsilon_\theta^P$$

$$(\varepsilon_z^P)_{new} = (\varepsilon_z^P)_{old} + d\varepsilon_z^P$$

$$(\varepsilon_r^P)_{new} = (\varepsilon_r^P)_{old} + d\varepsilon_r^P$$

$$(\varepsilon^P)_{new} = (\varepsilon^P)_{old} + d\varepsilon^P \qquad (3\text{-}26)$$

and these values are returned to FCMI for use at the next load increment.

Thus, all the stresses and strains can be computed directly since, in this case, the stresses are determinate. In the case of the driven cladding displacement, the stresses depend on the displacement, and such a straightforward solution is not possible.

(c) Subroutine COUPLE. This subroutine considers the problem of a cylindrical shell for which the radial displacement of the inside surface and axial strain are prescribed. Here the stresses cannot be computed directly since the pressure at the inside surface (the interface pressure) must be determined as part of the solution.

As in CLADF, the displacement at the inside surface is given by

$$u(r_i) = u - \frac{t}{2}\varepsilon_r \qquad (3\text{-}27)$$

573 103

where u is the radial displacement of the midplane. From Equation (3-18), $u = r\varepsilon_\theta$ and

$$u(r_i) = \bar{r}\,\varepsilon_\theta - \frac{t}{2}\,\varepsilon_r. \tag{3-28}$$

Thus, prescribing the displacement of the inside surface of the shell is equivalent to a constraining relation between ε_θ and ε_r. As before, Hooke's law is taken in the form

$$\varepsilon_\theta = \frac{1}{E}(\sigma_\theta - \nu\,\sigma_z) + \varepsilon_\theta^p + d\varepsilon_\theta^p + \int_{T_o}^{T} \alpha\,dT \tag{3-29}$$

$$\varepsilon_z = \frac{1}{E}(\sigma_z - \nu\,\sigma_\theta) + \varepsilon_z^p + d\varepsilon_z^p \int_{T_o}^{T} \alpha\,dT \tag{3-30}$$

$$\varepsilon_r = -\frac{\nu}{E}(\sigma_\theta + \sigma_z) + \varepsilon_r^p + d\varepsilon_r^p + \int_{T_o}^{T} \alpha\,dT\ . \tag{3-31}$$

Use of Equations (3-28) and (3-31) in Equation (3-29) results in a relation between the stresses σ_θ, σ_z and the prescribed displacement $u(r_i)$:

$$\frac{u(r_i)}{\bar{r}} + \frac{1}{2}\left(\frac{t}{\bar{r}}\right)\left\{\varepsilon_r^p + d\varepsilon_r^p + \int_{T_o}^{T} \alpha\,dT\right\}$$

$$-\left\{\varepsilon_\theta^p + d\varepsilon_\theta^p + \int_{T_o}^{T} \alpha\,dT\right\} = \frac{1}{E}\left[\left(1 + \frac{\nu}{2}\,\frac{t}{\bar{r}}\right)\sigma_\theta\right.$$

$$\left. + \nu\left(\frac{1}{2}\,\frac{t}{\bar{r}} - 1\right)\sigma_z\right]. \tag{3-32}$$

Equations (3-30) and (3-32) are now a pair of simultaneous algebraic equations for the stresses σ_θ and σ_z, which may be written as

$$\begin{bmatrix} A_{11} & A_{12} \\ A_{21} & A_{22} \end{bmatrix} \begin{bmatrix} \sigma_\theta \\ \sigma_z \end{bmatrix} = \begin{bmatrix} B_1 \\ B_2 \end{bmatrix}$$

where

$$A_{11} = 1 + \frac{\nu}{2} \frac{t}{\bar{r}}$$

$$A_{12} = \nu \left(\frac{1}{2} \frac{t}{\bar{r}} - 1\right)$$

$$A_{21} = -\nu$$

$$A_{22} = 1$$

$$B_1 = E \frac{u(r_i)}{\bar{r}} + \frac{E}{2} \left(\frac{t}{\bar{r}}\right) \{e_r^P + d\varepsilon_r^P + \int_{T_o}^{T} \alpha dT\}$$

$$-E \{\varepsilon_\theta^P + d\varepsilon_\theta^P + \int_{T_o}^{T} \alpha dT\}$$

$$B_2 = E \varepsilon_z - E\{\varepsilon_z^P + d\varepsilon_z^P + \int_{T_o}^{T} \alpha dT\}.$$

Then the stresses can be written explicitly as

$$\sigma_\theta = \frac{B_1 A_{22} - B_2 A_{12}}{A_{11} A_{22} - A_{12} A_{21}} \qquad (3\text{-}33)$$

$$\sigma_z = \frac{B_2 A_{11} - B_1 A_{21}}{A_{11} A_{22} - A_{12} A_{21}} \qquad (3\text{-}34)$$

These equations relate the stresses to $u(r_i)$ and ε_z, which are prescribed, and to $d\varepsilon_\theta^P$, $d\varepsilon_z^P$, and $d\varepsilon_r^P$, which are to be determined. The remaining equations which must be satisfied are

$$\sigma_e = \frac{1}{\sqrt{2}} \{(\sigma_\theta - \sigma_z)^2 + (\sigma_\theta)^2 + (\sigma_z)^2\}^{1/2} \qquad (3\text{-}35)$$

$$d\varepsilon^P = \frac{2}{3} \{(d\varepsilon_r^P - d\varepsilon_\theta^P)^2 + (d\varepsilon_\theta^P - d\varepsilon_z^P)^2 + (d\varepsilon_z^P - d\varepsilon_r^P)^2\}^{1/2} \qquad (3\text{-}36)$$

and the Prandtl-Reuss flow equations [defined in Equation (3-22)]

$$d\varepsilon_\theta^P = \frac{3}{2} \frac{d\varepsilon^P}{\sigma_e} [\sigma_\theta - \frac{1}{3} (\sigma_\theta + \sigma_z)]$$

$$d\varepsilon_z^P = \frac{3}{2} \frac{d\varepsilon^P}{\sigma_e} [\sigma_z - \frac{1}{3} (\sigma_\theta + \sigma_z)]$$

$$d\varepsilon_r^P = - d\varepsilon_\theta^P - d\varepsilon_z^P \; . \qquad (3\text{-}37)$$

The effective stress, σ_e, and the plastic strain increment, $d\varepsilon^P$, must, of course, be related by the uniaxial stress-strain law. Equations (3-33) through (3-37) must be simultaneously satisfied for each loading increment.

As discussed in Section 3.1, a straightforward numerical solution to these equations can be obtained by means of the Method of Successive Elastic Solutions. By this method, arbitrary values are initially assumed for the increments of plastic strain, and Equations (3-33) through (3-37) are used to obtain improved estimates of the plastic strain components. The steps performed by COUPLE are as follows for each increment of load:

(1) Values of $d\varepsilon_\theta^P$, $d\varepsilon_z^P$, and $d\varepsilon_r^P$ are assumed. Then, $d\varepsilon^P$ is computed from Equation (3-28) and the effective stress is obtained from the stress-strain curve at the value of ε^P by calling subroutine STRESS.

(2) From Hooke's law, still using the assumed plastic strain increments and the prescribed values of $u(r_i)$ and ε_z, values for the stresses can be obtained from Equations (3-33) and (3-34).

(3) New values for $d\varepsilon_\theta^P$, $d\varepsilon_z^P$, and $d\varepsilon_r^P$ are now computed from the Prandtl-Reuss relations,

$$d\varepsilon_i^P = \frac{3}{2}\frac{d\varepsilon^P}{\sigma_e}\left[\sigma_i - \frac{1}{3}(\sigma_\theta + \sigma_z)\right] \qquad i = r,\theta,z$$

using σ_e as computed in Step (1), and σ_i as computed in Step (2).

(4) The old and new values of $d\varepsilon_\theta^P$, $d\varepsilon_z^P$, and $d\varepsilon_r^P$ are compared and the process continued until convergence is obtained.

(5) Once convergence has been obtained, the interface pressure is computed from Equation (3-14)

$$P_{int} = \frac{t\,\sigma_\theta + r_o\,P_o}{r_i} . \qquad (3\text{-}38)$$

When Steps (1) through (5) have been accomplished, the solution is complete, provided that the interface pressure is not less than the local gas pressure.

Due to unequal amounts of plastic straining in the hoop and axial directions, however, upon unloading, the interface pressure as obtained in Step (5) is often less than the gas pressure, even though the gap has not opened. When this situation occurs, the frictional "locking" mechanism (which is assumed to constrain the cladding axial deformation to equal the fuel axial deformation) can no longer act. The axial strain and stress adjust themselves so that the interface pressure just equals the gas pressure, at which point the axial strain is again "locked." Thus, upon further unloading, the axial strain and

the hoop and axial stresses continually readjust themselves to maintain the interface pressure equal to the gas pressure until the gap opens. Since the unloading occurs elastically, a solution for this portion of the fuel-cladding interaction problem can be obtained directly as follows.

Since the external pressure and the interface pressure are known, the hoop stress is obtained from Equation (3-7) as

$$\sigma_\theta = \frac{r_i P_{int} - r_o P_o}{t} \tag{3-39}$$

From Equation (3-28), the following expression can be written

$$\varepsilon_\theta = \frac{u_r^{fuel} - \delta + t/2\ \varepsilon_r}{\bar{r}} \tag{3-40}$$

Substitution of ε_θ and ε_r, as given by Equations (3-29) and (3-31), into Equation (3-40) results in an explicit equation for σ_z:

$$\nu r_i \sigma_z = (\bar{r} + \nu\, t/2)\, \sigma_\theta + \bar{r} E \left(\int \alpha dT + \varepsilon_\theta^P \right) - \frac{t}{2} E \left(\int \alpha dT + \varepsilon_r^P \right) - E\, u(r_i) \tag{3-41}$$

in which σ_θ is known from Equation (3-39). With σ_z and σ_θ known, the strains may be computed from Hooke's law, Equations (3-29) through (3-31). This set of equations is included in subroutine COUPLE and is automatically invoked when a value of P_{int} less than the local gas pressure is computed.

As in CLADF, the last step performed by COUPLE before returning control to FCMI is to set the plastic strain components and total effective strain equal to their new values by adding in the computed increments $d\varepsilon_i^P$ and $d\varepsilon^P$.

(d) Subroutine STACK. Subroutine STACK is called when one or more fuel pellets are trapped between the lower end of the cladding and a pellet in firm contact with the cladding, as shown in Figure 17. In this case, the axial expansion of the fuel will be imparted to the cladding even though the cladding and fuel are not in contact.

The total change in length of the trapped cladding is computed in FCMI, and passed to STACK in the calling sequence. For each axial node in the trapped cladding, the axial strain is given by

$$\varepsilon_z(i) = \frac{1}{E(i)} \left[\sigma_z - \nu(i)\, \sigma_\theta(i)\right] + \varepsilon_z^P(i) + d\varepsilon_z^P(i) + \int_{T_o}^{T(i)} \alpha dT \qquad (3\text{-}42)$$

in which i denotes the axial node number. Axial force equilibrium requires that σ_z be the same in each node. Since the total length change is prescribed, the following expression can be written.

$$\Delta\ell = \sum_{i=1}^{n} \left[\left(\varepsilon_z(i) - \varepsilon_z^o(i)\right)\, dz(i)\right] \qquad (3\text{-}43)$$

in which dz(i) are the cladding axial node lengths, and ε_z^o are the axial strains in the cladding at the end of the last load step. Insertion of Equation (3-42) in the preceding equation yields

$$\sigma_z = \left[\sum_{i=1}^{N} \frac{E(i)}{dz(i)}\right] \left\{ \Delta\ell + \sum_{i=1}^{N} dz(i) \left[\frac{\nu(i)\, \sigma_\theta(i)}{E(i)} + \varepsilon_z^o(i) - \varepsilon_z^P(i) - d\varepsilon_z^P(i) - \int_{T_o}^{T(i)} \alpha dT\right]\right\} . \qquad (3\text{-}44)$$

The equation for the effective cladding stress [defined in Equation (3-21)] is

$$\sigma_e(t) = \left[\sigma_z^2 + \sigma_\theta^2(i) - \sigma_z\, \sigma_\theta(i)\right]^{1/2} \qquad (3\text{-}45)$$

The equation for the increment of effective plastic strain defined in Equation (3-4) is

573 109

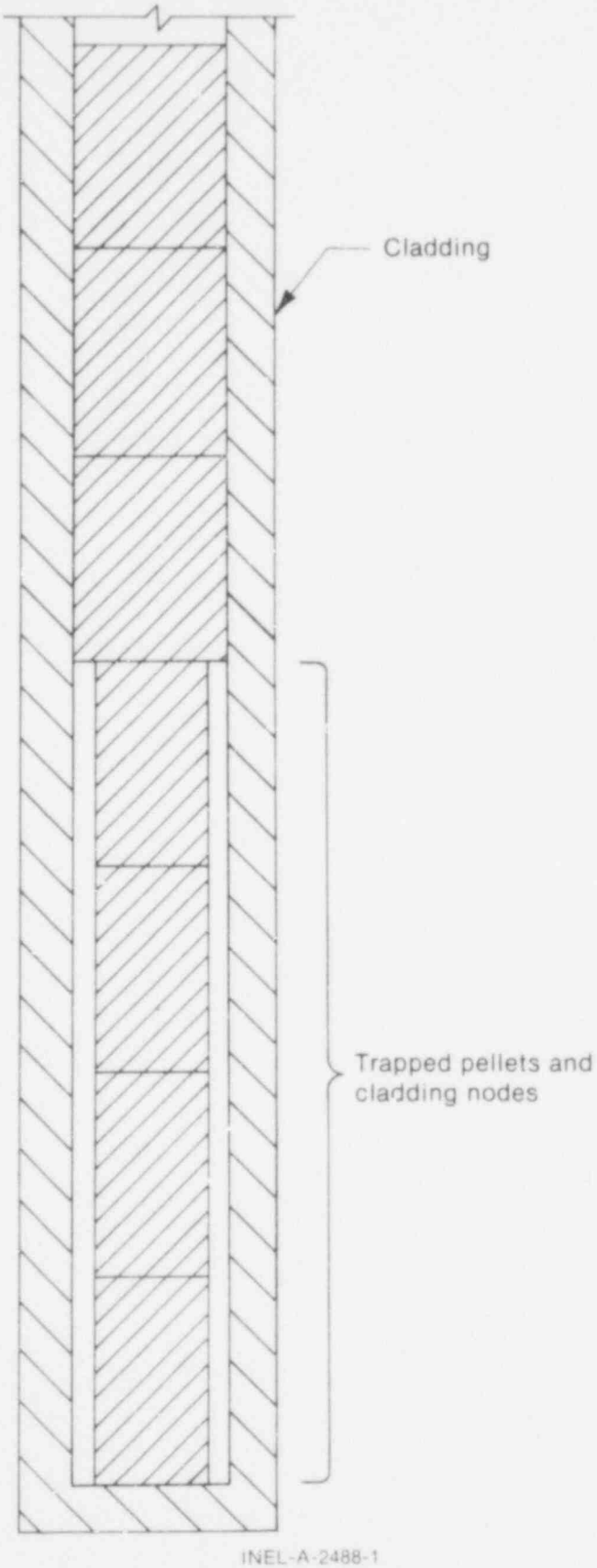

Fig. 17 Schematic of trapped stack.

573 110

$$d\varepsilon^P(i) = \sqrt{\frac{2}{3}} \left\{ \left[d\varepsilon_z^P(i) - d\varepsilon_r^P(i) \right]^2 + \left[d\varepsilon_z^P(i) - d\varepsilon_\Theta^P(i) \right]^2 \right.$$

$$\left. + \left[d\varepsilon_r^P(i) - d\varepsilon_\Theta^P(i) \right]^2 \right\}^{1/2} . \qquad (3\text{-}46)$$

As defined in Equation (3-22), the equations for the components of the plastic strain increment are

$$d\varepsilon_z^P(i) = \frac{3}{2} \frac{d\varepsilon^P(i)}{\sigma_e(i)} \left\{ \sigma_z - \frac{1}{3} \left[\sigma_z + \sigma_\Theta(i) \right] \right\}$$

$$d\varepsilon_\Theta^P(i) = \frac{3}{2} \frac{d\varepsilon^P(i)}{\sigma_e(i)} \left\{ \sigma_\Theta - \frac{1}{3} \left[\sigma_z + \sigma_\Theta(i) \right] \right\}$$

$$d\varepsilon_r^P(i) = - d\varepsilon_\Theta^P(i) - d\varepsilon_z^P(i) . \qquad (3\text{-}47)$$

Equations (3-44) through (3-47) must be simultaneously satisfied for all the trapped cladding axial nodes. Since the nodes may have different temperatures, different stress-strain curves are used at different nodes.

As before, the Method of Successive Elastic Solutions is used. In contrast to subroutine COUPLE, however, the method is applied simultaneously to several axial nodes. Because more than one node is being considered, two additional possibilities arise.

The first is the possibility that, due to the axial stretching and Poisson's effect, some (or all) of the cladding nodes may come into contact with the fuel pellets, although contact would not occur due to internal and external pressure alone. In this case, the hoop stress in Equation (3-44) is no longer given by Equation (3-14), but now depends on σ_z and the radial displacement of the fuel. While contact occurs, however, radial compatibility as expressed in Equation (3-28) requires that

$$\bar{r}\,\varepsilon_\theta(i) - 0.5\,t\,\varepsilon_r(i) = u_r^{fuel}(i) - \delta. \qquad (3\text{-}48)$$

Through the substitution for $\varepsilon_\theta(i)$ and $\varepsilon_r(i)$ from Hooke's law, Equations (3-18) and (3-20), a single equation is produced which relates $\sigma_\theta(i)$ at each node to the axial stress σ_z. This equation can be solved for $\sigma_\theta(i)$ explicitly to obtain

$$\left[\frac{\bar{r}}{E(i)} + \frac{0.5\nu(i)\,t}{E(i)}\right]\sigma_\theta(i) = u_r^{fuel}(i) - \delta - \bar{r}\left[\frac{-\nu(I)}{E(i)}\,\sigma_z + \varepsilon_\theta^P(i) + d\varepsilon_\theta^P(i) + \int_{T_o}^{T(i)} \alpha_\theta dT\right] + \frac{t}{2}\left[\frac{-\nu(i)}{E(i)}\,\sigma_z + \varepsilon_r^P(i) + d\varepsilon_r^P(i) + \int_{To}^{T(i)} \alpha_r dT\right] \qquad (3\text{-}49)$$

which applies at each node where contact has occurred. Finally, Equation (3-49) is used to eliminate $\sigma_\theta(i)$ from Equation (3-44) for those nodes at which contact has occurred. Thus, an equation is obtained for σ_z involving summations over all nodes not in contact plus summations over all nodes, denoted j*, where contact has occurred. This equation, solved explicitly for σ_z, is

$$\left\{\sum_i \frac{dz(i)}{E(i)} - \sum_{i=j^*} \frac{dz(i)\,\nu(i)}{E(i)}\left[\frac{(\bar{r}-0.5t)\,\nu(i)}{(\bar{r}+0.5t)\,\nu(i)}\right]\right\}\sigma_z = \Delta\ell + \sum_i \varepsilon_z^0(i)\,dz(i) - \sum_i\left[\varepsilon_z^P(i) + d\varepsilon_z^P(i) + \int_{T_o}^{T(i)} \alpha_z dT\right] dz(i) + \sum_{i\neq j^*} \frac{\nu(i)}{E(i)}\left[\frac{P_i(i)\,r_i - P_o(i)\,r_o}{r_o - r_i}\right] dz(i)$$

$$+\sum_{i=j^*} \frac{\nu(i)dz(i)}{(r+0.5t)\nu(i)} \left\{ u_r^{fuel}(i) - \delta - \bar{r}\left[\varepsilon_\theta^P(i) + d\varepsilon_\theta^P(i) + \int_{T_o}^{T(i)} \alpha_\theta dT\right] \right.$$

$$\left. + 0.5t\left[\varepsilon_r^P(i) + d\varepsilon_r^P(i) + \int_{T_o}^{T(i)} \alpha_r dT\right]\right\} . \qquad (3\text{-}50)$$

This modified equation for σ_z allows for an arbitrary number of contacting nodes, and is solved for σ_z at each step in the iteration for the plastic strain increments. Locations of nodes that may be in contact are not known a priori. However, for given values of the plastic strain increments (the iterates in the Method of Successive Elastic Solutions), the equations are linear. Thus, a feasible approach is to solve for σ_z, assuming no pellets are in contact, then compute the gaps, and if any negative gaps are found, recompute σ_z with those nodes now assumed to be in contact. This process is repeated until all calculated gaps are either positive or zero. At most, N steps are required where N is the number of nodes in the stack, since the equations are linear.

The second possibility to be considered is that in the iteration for the plastic strain increments, some of the nodes may only be strained elastically. Here, the plastic strain increments for these nodes approach zero, which causes difficulty when a check for convergence is made. This difficulty is circumvented by checking the absolute values of the plastic strain increments at each iteration, and when they become smaller than some predetermined value, those nodes are deleted from the iteration scheme.

Thus, in this application, the Method of Successive Elastic Solutions becomes an iteration within an iteration, and one in which the set of variables iterated upon is determined as the solution progresses.

573 113

(e) Subroutines STRAIN and STRESS. These two subroutines are called by COUPLE and CLADF to relate stress and plastic strain, taking into consideration the direction of loading and the previous plastic deformation. A typical stress-strain curve is shown in Figure 18. This curve represents the results of a uniaxial stress strain experiment, and may be interpreted (beyond initial yield) as the locus of work-hardened yield stresses. The equation of the curve is provided by the MATPRO subcode at each temperature.

To utilize this information, the usual idealizations of the mechanical behavior of metals are made. Thus, linear elastic behavior is assumed until a sharply defined yield stress is reached, after which plastic (irrecoverable) deformation occurs. Unloading from a

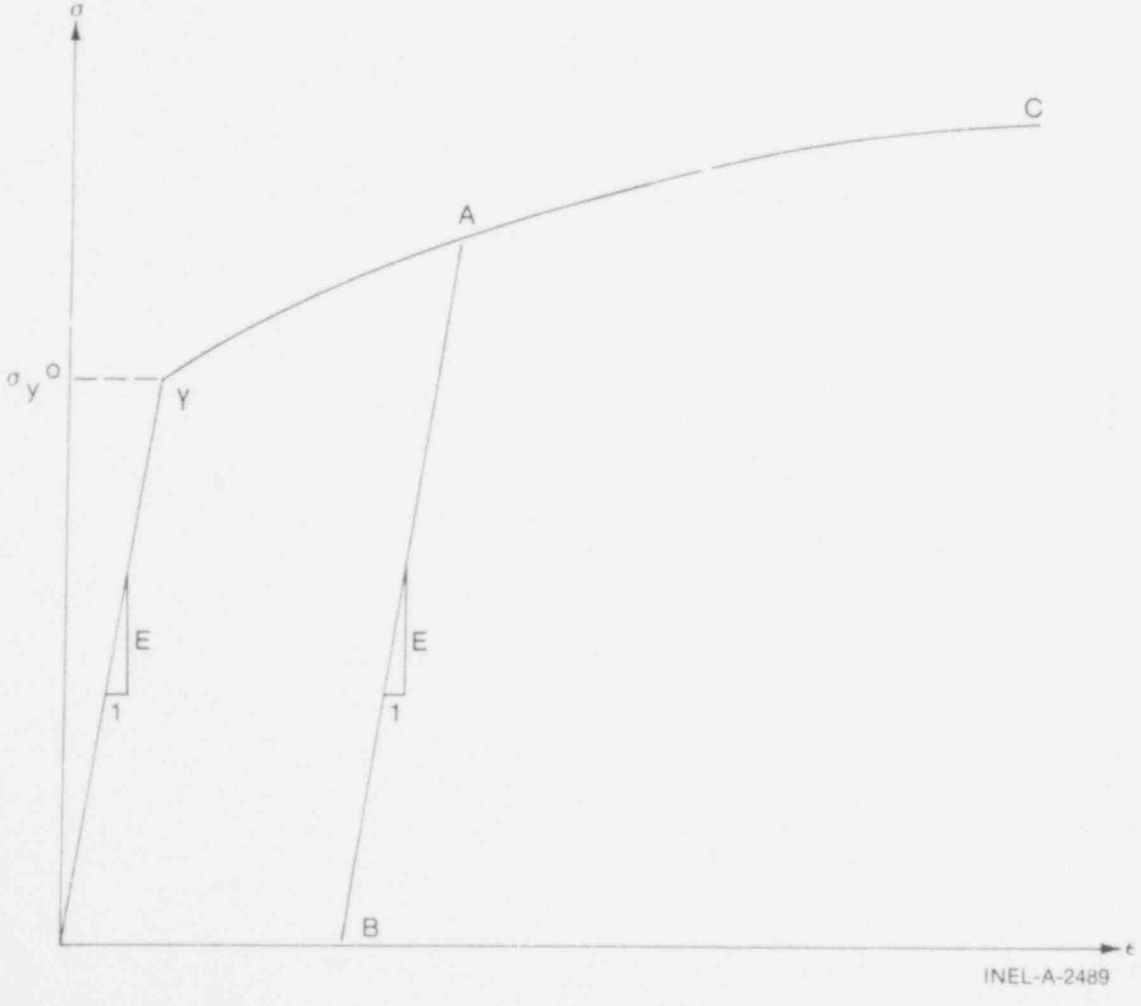

Fig. 18 Typical isothermal stress-strain curve.

state of stress beyond the initial yield stress, σ_y^o, is assumed to occur along a straight line having the elastic modulus for its slope. When the (uniaxial) stress is removed completely, a residual plastic strain remains, and this completely determines the subsequent yield stress. That is, when the specimen is loaded again, loading will occur along line BA, and no additional plastic deformation will occur until point A is again reached. Point A is the subsequent yield stress. If $\sigma = f(\varepsilon)$ is the equation of the plastic portion of the stress-strain curve (YAC), then for a given value of plastic strain, the subsequent yield stress is found by simultaneously solving the pair of equations:

$$\begin{cases} \sigma = f(\varepsilon) \\ \sigma = E(\varepsilon - \varepsilon^P) \end{cases} \qquad (3\text{-}51)$$

which may be written as

$$\sigma = f\left(\frac{\sigma}{E} + \varepsilon^P\right). \qquad (3\text{-}52)$$

The solution to this nonlinear equation may be computed very efficiently by Newton's iteration scheme:

$$\sigma^{(m+1)} = f\left[\frac{\sigma^{(m)}}{E} + \varepsilon^P\right] \quad m = 0, 1, 2, \ldots \qquad (3\text{-}53)$$

The initial iterate, $\sigma^{(o)}$, is arbitrary, and, without loss of generality, is taken as 5000 psi. For any monotonically increasing stress-plastic strain relation, the iteration scheme in Equation (3-53) can be proven to converge uniformly and absolutely.

The computations in STRAIN and STRESS are described in the following. Note that STRESS is called only when additional plastic deformation has occurred.

(i) Subroutine STRAIN. Values of plastic strain, ε^P, temperature and stress are passed to STRAIN through the calling sequence.

- For a given temperature, $\sigma = f(\varepsilon)$ is obtained from MATPRO function CSIGMA

- The yield stress σ_y for given ε^P is obtained from Equation (3-53)

- For a given value of stress, σ,

$$\text{if } \sigma \leq \sigma_y, \quad \varepsilon = \frac{\sigma}{E} + \varepsilon^P$$

$$\varepsilon^P_{new} = \varepsilon^P_{old}$$

where E is computed by MATPRO function CELMØD.

$$\text{if } \sigma > \sigma_y, \quad \varepsilon = f(\sigma)$$

$$\varepsilon^P_{new} = \varepsilon - \sigma/E$$

$$d\varepsilon^P = \varepsilon^P_{new} - \varepsilon^P_{old} .$$

(ii) Subroutine STRESS. Values of plastic strain, ε^P, temperature, and plastic strain increment, $d\varepsilon^P$, are passed to STRESS through the calling sequence.

- For a given temperature, $\sigma = f(\varepsilon)$ is obtained from MATPRO function CSIGMA

- The yield stress σ_y for given ε^P is obtained from Equation (3-53)

- Given $d\varepsilon^P$ (see Figure 19),

$$\varepsilon^P_{new} = \varepsilon^P_{old} + d\varepsilon^P$$

Since $d\varepsilon^P > 0$, the new value of stress and strain must lie on the plastic portion of the

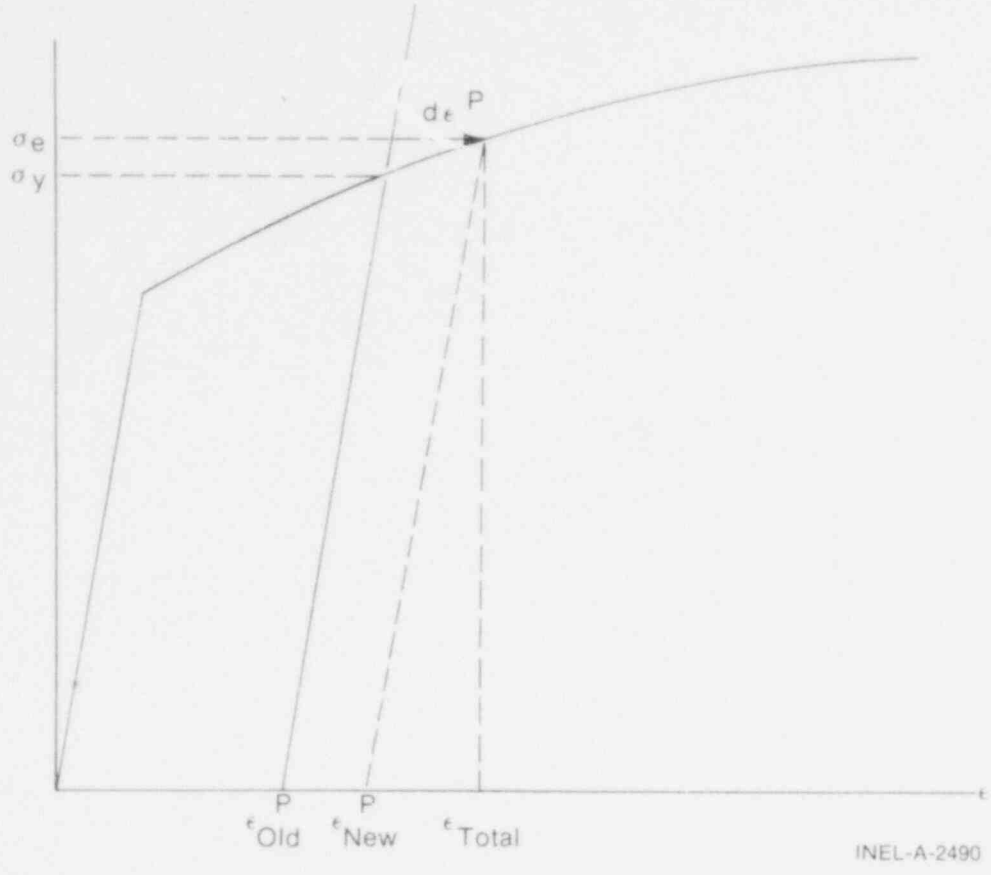

Fig. 19 Computations in subroutine STRESS.

stress-strain curve $\sigma = f(\epsilon)$. So, σ and ϵ are obtained by simultaneously solving, as before,

$$\begin{cases} \sigma = f(\epsilon) \\ \sigma = E(\epsilon - \epsilon^P_{new}). \end{cases}$$

(2) Rigid Pellet Fuel Deformation in FRACAS-1. The analytical models used to compute fuel deformation in FRACAS-1 are next described. Models are available to calculate fuel stack length change, fuel radial displacement, fuel crack volume, and fuel open porosity.

(a) Fuel Stack Length Change. The length change of the fuel pellet stack is assumed equal to the thermal expansion of the line projected through the shoulders of the fuel pellet dishes, as illustrated in Figure 20. The length change is given by the equation

573 117

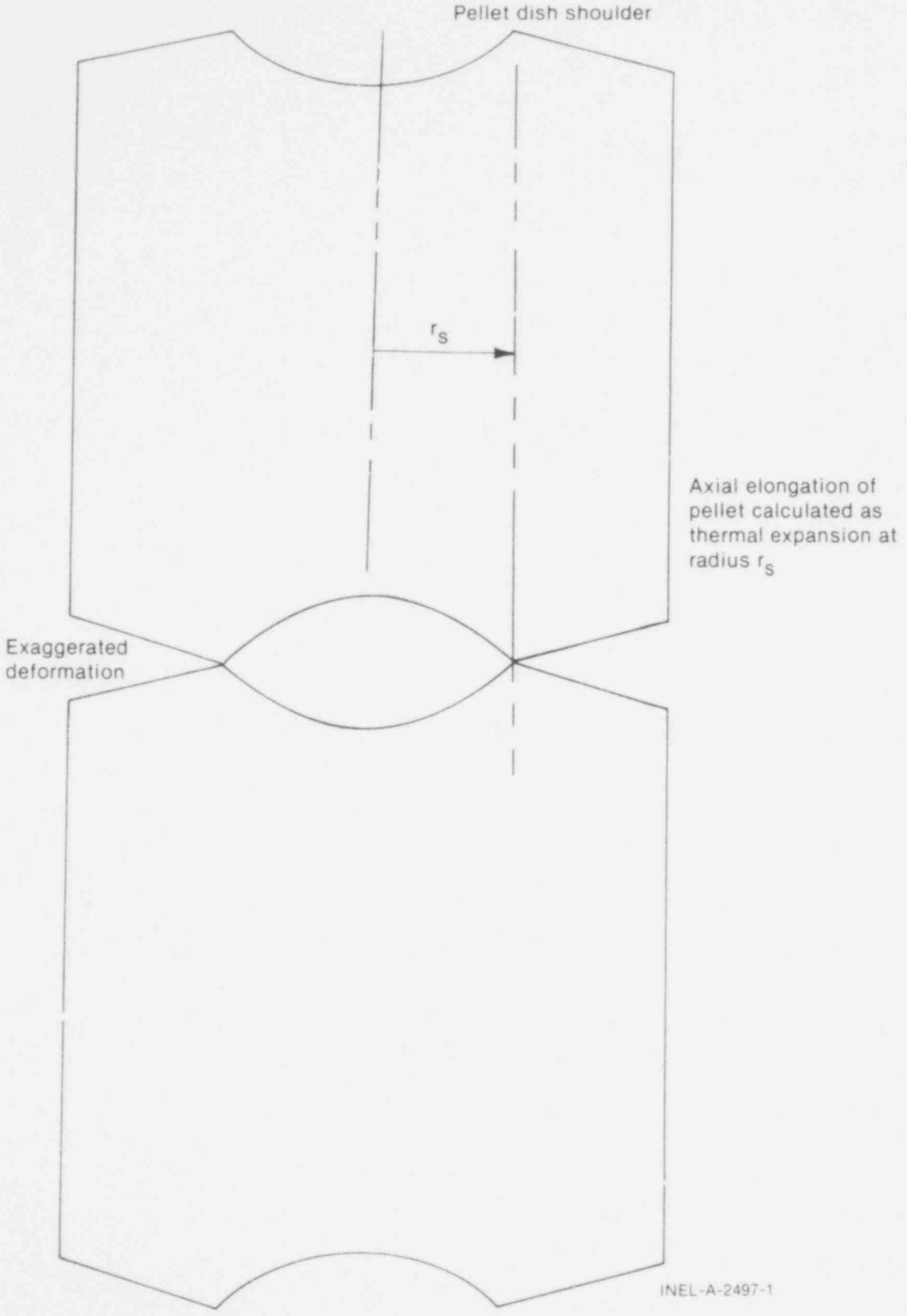

Fig. 20 Axial thermal expansion using FRACAS-1.

573 118

$$\Delta L_f = \sum_{n=1}^{N} [\varepsilon_T(T_{sn}) - \varepsilon_T(T_o)] \Delta Z_n \qquad (3\text{-}54)$$

where

ΔL_f = fuel stack length change

$\varepsilon_T(T)$ = thermal expansion of fuel at temperature T (obtained from the MATPRO subcode)

T_{sn} = fuel temperature at pellet shoulder at axial node n

T_o = strain free fuel reference temperature

ΔZ_n = fuel stack length associated with axial node n.

(b) Fuel Radial Displacement. Fuel radial displacement is caused by thermal expansion and relocation, and is computed by the equation

$$U_F = U_T + U_C \qquad (3\text{-}55)$$

where

U_F = radial displacement of fuel pellet outer surface (m)

U_T = radial displacement of fuel due to thermal expansion (m)

$$= \int_o^{r_f} \varepsilon_T [T(r)] dr$$

ε_T = thermal expansion of fuel

r_f = as fabricated fuel pellet outer radius (m)

$T(r)$ = fuel temperature at radial coordinate r (K)

U_c = radial displacement of fuel due to relocation (m).

The relocation displacement is computed by two different equations, as a user option. The first model (the variable relocation model) allows the relocation displacement to vary with the cold gap size, whereas in the second model (the constant relocation model) the relocation does not vary. With reference to Figure 21, the equation for the variable relocation model displacement is

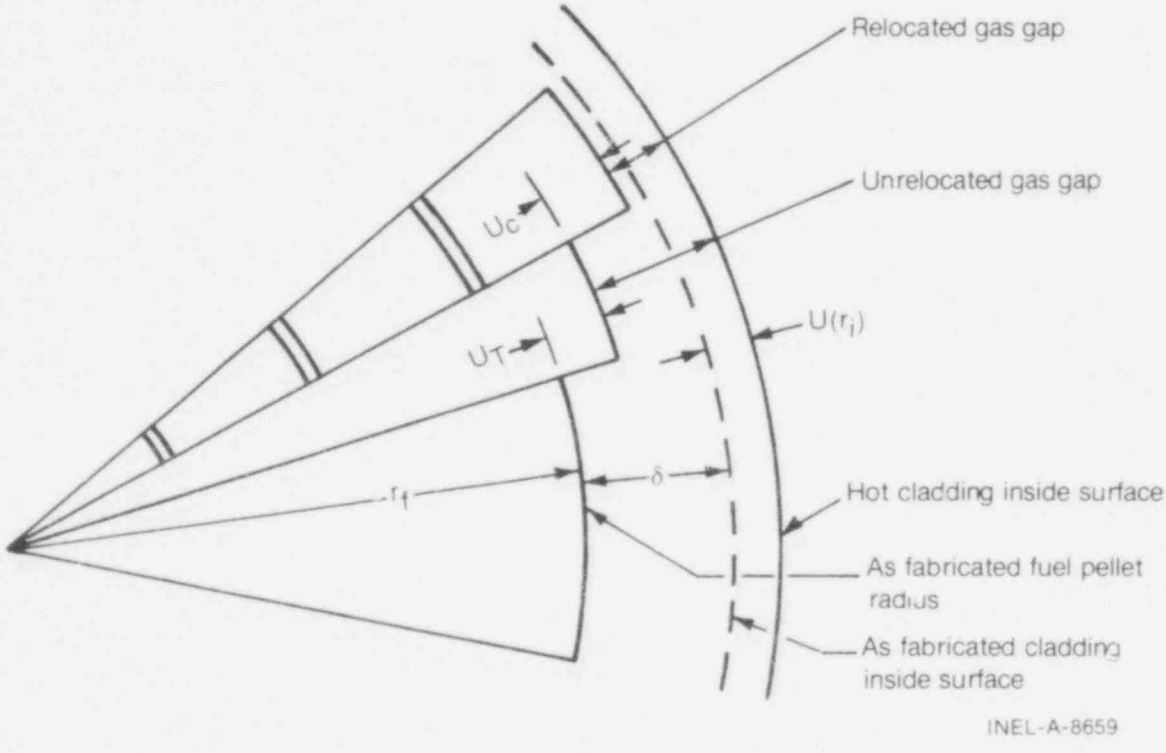

Fig. 21 Fuel relocation.

1. Open Gap Case

$$U_c = \delta - 0.005 r_f$$

2. Closed Gap Case

$$U_c = \delta - U_T - U(r_i)$$

573 120

where

δ = as-fabricated radial gap between fuel pellets and cladding

$U(r_i)$ = radial displacement of inside surface of cladding [given by Equation (3-24)].

If the user specifies the preceding relocation model, the gas gap used in thermal and internal pressure calculations includes the fuel relocation, while the gap used in the structural calculations does not. The fuel conductivity is modified according to Equation (1-7) to account for the cracks formed by fuel relocation.

Alternatively, fuel relocation can be specified according to the constant relocation model, which is

$$\begin{cases} U_c = 0.0025\, r_f & P_I = 0 \\ U_c = 0.0025\, r_f\, (1 - P_I/5000) & 0 < P_I < 5000 \\ U_c = 0 & P_I \geq 5000 \end{cases} \qquad (3\text{-}56)$$

where

P_I = fuel-cladding interface pressure (psi).

If this relocation option is used, the gas gap in structural calculations accounts for fuel relocation, whereas the gap used in thermal and internal pressure calculations does not.

(c) Fuel Crack Volume. The fuel crack volume is the sum of the volume of the fuel radial cracks and void volume generated by fuel relocation. The cracks create space which is occupied by the fuel rod internal gas. Axial cracks are not considered. Closed radial cracks are assumed to exist in the fuel even in the cold state. As the fuel rises in temperature, the cracks open, with the crack width increasing

with radius. The width of the radial cracks is the difference between circumference change caused by radial displacement and circumferential thermal expansion. The total width is independent of the number of cracks, and is computed by the equation

$$\Delta c(r) = 2\pi \left(\int_0^r \varepsilon_T[T(r)]\, dr - r\, \varepsilon_T[T(r)] \right)$$

where

$\Delta c(r)$ = sum of widths of all radial cracks at radius r.

The first term in the parentheses is the circumference change at cold state radius r due to radial displacement. The second term is the circumference change due to circumferential thermal expansion.

The volume of the radial cracks is

$$V_{CR} = \int_0^{r_f} \Delta c(r)\, dr$$

The total crack volume is then computed by the equation

$$V_{cn} = V_{CR} + \pi[(r_f + U_c)^2 - r_f^2] \quad \text{(variable relocation)} \qquad (3\text{-}57)$$

or, $$V_{cn} = V_{CR} \quad \text{(constant relocation)}$$

where

V_{cn} = volume of cracks per unit length at axial node n

U_c = radial displacement of the fuel pellet outer surface due to fuel relocation.

(d) Fuel Open Porosity. The open porosity of the fuel is empirically correlated with fuel density. The open porosity is multiplied by the fuel volume to determine the volume of gas in the

fuel pores that is connected to the fuel rod gas gap. This quantity is used in the calculation of fuel rod internal pressure.

Depending on fuel density, one of the following correlations is used to compute fuel open porosity.

$$\left.\begin{aligned} P &= 16.9297 - 0.232855\,(D-1.25) \\ &\quad - 8.71836 \times 10^{-4}\,(D-125)^2 \\ &\quad + 1.52442\ 10^{-5}\,(D-1.25)^3 \qquad (D < 92.5) \\ P &= 1.20196 \times 10^{-3}\,(95.25-D) \qquad (92.5 \leq D \leq 95.25) \\ P &= 0 \qquad (D > 95.25) \end{aligned}\right\} \quad (3\text{-}58)$$

where

P = open porosity of fuel (fraction of theoretical volume)

D = fuel density (percentage of theoretical maximum density).

3.2.2 Deformable Pellet Deformation Model The deformable pellet deformation model (FRACAS-2 subcode) is used to calculate the fuel rod deformation when stress effects on fuel deformation become important. This model computes the stress and strain distributions in both the fuel and cladding. Elastic and plastic strains in both the fuel and cladding are considered. The stresses and strains in the fuel and cladding are obtained by the transfer matrix approach. The plastic strains are obtained by the Method of Successive Substitutions, which was outlined in Section 3.1.

A transfer matrix approach is used for determining pellet stresses and strains. The following paragraphs describe the method of obtaining the "pseudo-elastic" solution for fuel rod stresses and strains required at each plastic strain iteration in the Method of Successive Substitutions.

The geometric model is a right circular cylinder (either solid or hollow) in a state of generalized plane strain. The applied loads are external pressure, internal pressure (if the cylinder is hollow), and axial force. The cylinder may be made of a single material, or may be a composite cylinder consisting of two layers of different materials. An arbitrary radial temperature distribution may be prescribed, and all material properties may be arbitrary functions of temperature.

The case of the single layer (homogeneous) cylinder is used to analyze the fuel pellets and the cladding separately before they have come into contact. The case of the two-layered (composite) cylinder is used to analyze the fuel and cladding after the fuel has expanded out so as to be in firm contact with the cladding[a]. For the composite cylinder case, the stress and strain distributions are permitted to be discontinuous at the interface between the layers, and the discontinuity in radial displacement and axial strain must be determined. (The discontinuity values are obtained from the displacements which existed in the fuel and cladding at the instant of contact.)

The method used to solve for the stresses, strains and displacements in the composite cylinder is the transfer matrix approach, as described in Reference 20, and modified to consider the state of generalized plane strain. In addition, the technique has been extended to consider displacement discontinuities and both axial and radial cracks in the cylinder. This solution is obtained in a subroutine called TRANSF.

First, a complete homogeneous cylinder with no discontinuities, but variable E, ν, and α (modulus of elasticity, Poisson's ratio, and coefficient of thermal expansion, respectively) is considered. Only radial variations in temperature T and material properties are considered. Generalized plane strain deformation is assumed, so that for all r,

---

a. The trapped stack regime is not considered in FRACAS-2.

$$\varepsilon_z = \text{constant}. \tag{3-59}$$

The value of the constant axial strain ε_z will be determined from the condition of axial force equilibrium,

$$\iint \sigma_z dA = F_z \tag{3-60}$$

where F_z is the axial force resultant. F_z is determined from the known internal and external pressures.

The governing equations of equilibrium and compatibility in the absence of any dislocations (displacement discontinuities) are given by

$$\frac{d\sigma_r}{dr} + \frac{\sigma_r - \sigma_\theta}{r} = 0 \tag{3-61}$$

$$\frac{d\varepsilon_\theta}{dr} + \frac{\varepsilon_\theta - \varepsilon_r}{r} = 0 \tag{3-62}$$

The elastic-plastic stress-strain relations are

$$\varepsilon_r = \frac{1}{E}\left[\sigma_r - \nu(\sigma_\theta + \sigma_z)\right] + \alpha_r T + \varepsilon_r^p + d\varepsilon_r^p \tag{3-63}$$

$$\varepsilon_\theta = \frac{1}{E}\left[\sigma_\theta - \nu(\sigma_r + \sigma_z)\right] + \alpha_\theta T + \varepsilon_\theta^p + d\varepsilon_\theta^p \tag{3-64}$$

$$\varepsilon_z = \frac{1}{E}\left[\sigma_z - (\sigma_r + \sigma_\theta)\right] + \alpha_z T + \varepsilon_z^p + d\varepsilon_z^p \tag{3-65}$$

Substitution of Equations (3-63) and (3-64) into Equation (3-62) results in

$$\frac{d}{dr}\left\{\frac{\sigma_\theta}{E} - \frac{\nu}{E}(\sigma_r + \sigma_z) + \alpha_\theta T + \varepsilon_\theta^p + d\varepsilon_\theta^p\right\}$$

$$+ \frac{1+\nu}{E}\,\frac{(\sigma_\theta - \sigma_r)}{r} + \frac{\alpha_\theta T - \alpha_r T}{r} + \frac{\varepsilon_\theta^p - \varepsilon_r^p}{r}$$

$$+ \frac{d\varepsilon_\theta^p - d\varepsilon_r^p}{r} = 0 \tag{3-66}$$

Equations (3-59), (3-61), and (3-66) relate the stresses as they vary across the cylinder. A number of node points are introduced along the radius of the cylinder, and the stresses are evaluated only at the nodes. Thus Equations (3-59), (3-61), and (3-66) can be written in finite difference form, and a set of recursion relations

$$\begin{Bmatrix} \sigma_r \\ \sigma_\theta \\ \sigma_z \end{Bmatrix}_{i+1} = \begin{bmatrix} L(i) \end{bmatrix} \begin{Bmatrix} \sigma_r \\ \sigma_\theta \\ \sigma_z \end{Bmatrix}_i + \begin{Bmatrix} M(i) \end{Bmatrix} \tag{3-67}$$

are obtained. This matrix equation relates the stresses at node i+1 to those at node i. The matrices $[L(i)]$ and $\{M(i)\}$ depend on the material properties, geometry, and plastic strains only.

By successive application of Equation (3-67), a relation between the stresses at any node and the stresses at node 1, the node at the inside of the cylinder, can be obtained. This relation takes the form

$$\{\sigma\}_{i+1} = \left[A(i)\right] \{\sigma\}_1 + \{B(i)\} \tag{3-68}$$

where

$$\{\sigma\} = \{\sigma_r, \sigma_\theta, \sigma_z\} .$$

The matrices $[A(i)]$ and $\{B(i)\}$ may be determined from $[L(i)]$ and $\{M(i)\}$, the result being

$$\left[A(i)\right] = \left[L(i)\right] \left[A(i-1)\right] \tag{3-69}$$

$$\{B(i)\} = \left[L(i)\right] \{B(i-1)\} + \{M(i)\} \tag{3-70}$$

for i greater than 1, and for i equal 1,

$$\left[A(1)\right] = \left[L(1)\right] \tag{3-71}$$

$$\{B(1)\} = \{M(1)\} . \tag{3-72}$$

573 126

By recursion, $[A(i)]$ and $\{B(i)\}$ across the cylinder wall can be obtained, with the result that

$$\{\sigma\}_N = [A(N-1)] \{\sigma\}_1 + \{B(N-1)\} \tag{3-73}$$

where N is the index of the node at the outside surface of the cylinder. At the outside surface, $\sigma_r = -P_o$, where P_o is the external pressure acting upon the cladding. Thus, the following condition can be obtained:

$$-P_o = A_{11}(N-1)\,\sigma_r(1) + A_{12}(N-1)\sigma_\theta(1) + A_{13}(N-1)\,\sigma_z(1) + B_1(N-1) \tag{3-74}$$

At the inside surface of the cylinder, one of the following conditions holds:

$$\begin{cases} \sigma_r(1) = -P_i & \text{if } r_1 \neq 0 \\ \sigma_r(1) = \sigma_\theta(1) & \text{if } r_1 = 0. \end{cases} \tag{3-75}$$

Finally, the condition of axial equilibrium

$$\int\int \sigma_z dA = \sum \sigma_z(j)\, dA(j) = F_z$$

must be satisfied. Using the recursion matrices, this becomes

$$\begin{aligned} \sum \sigma(j) dA_j = &\left\{ [I]\, dA_1 + \left[A_1\right] dA_2 + \ldots + \left[A_{N-1}\right] dA_N \right\} \left\{ \sigma_1 \right\} \\ &+ \left\{ 0 + \left\{ B_1 \right\} dA_2 + \ldots + \left\{ B_{N-1} \right\} dA_N \right\} \\ &\triangleq [C] \left\{ \sigma_1 \right\} + \left\{ D \right\}. \end{aligned} \tag{3-76}$$

The axial force condition is the third component of this matrix equation, which can be written as

$$F_z = C_{31}\,\sigma_r(1) + C_{32}\,\sigma_\theta(1) + C_{33}\,\sigma_z(1) + D_3. \tag{3-77}$$

Equations (3-74), (3-75), (3-76) are solved simultaneously for the stresses at the inside node $\{\sigma\}_1$, after which all the other stresses and strains can be determined from the recursion relations given in Equation (3-68).

Thus, once the transfer matrices $[L(i)]$ and $\{M(i)\}$ in Equation (3-67) are known for each annulus in the cylinder, finding the stresses throughout the cylinder becomes a straightforward procedure.

The advantage of using the transfer matrix approach in solving for fuel rod deformations is that different transfer matrices can be used, depending on whether the fuel is cracked axially or radially or both, and whether or not the cladding and fuel are in contact. The basic solution technique is not changed. The various transfer matrices required are illustrated in the following.

(1) Homogeneous Cylinder. Here the transfer matrices for a cylinder which is not cracked, and in which the radial displacements and axial strains are everywhere continuous, are presented. The temperature and material properties, however, vary (radially) in an arbitrary manner.

The cylinder (either hollow or solid) is broken up into N-1 annular regions, with N node points, where r_1 is the radius to the first node as shown in Figure 22. (For a solid cylinder $r_1 = 0.$) Values of stresses, elastic strains, and plastic strains are found at each of the node points.

The derivatives are evaluated at the center of each annular region, that is, for the j^{th} annulus, at

$$r = 0.5(r_{j+1} + r_j).$$

Equations (3-61) and (3-66) are written for the midpoint of each annular region. Thus for the j^{th} annulus, for example,

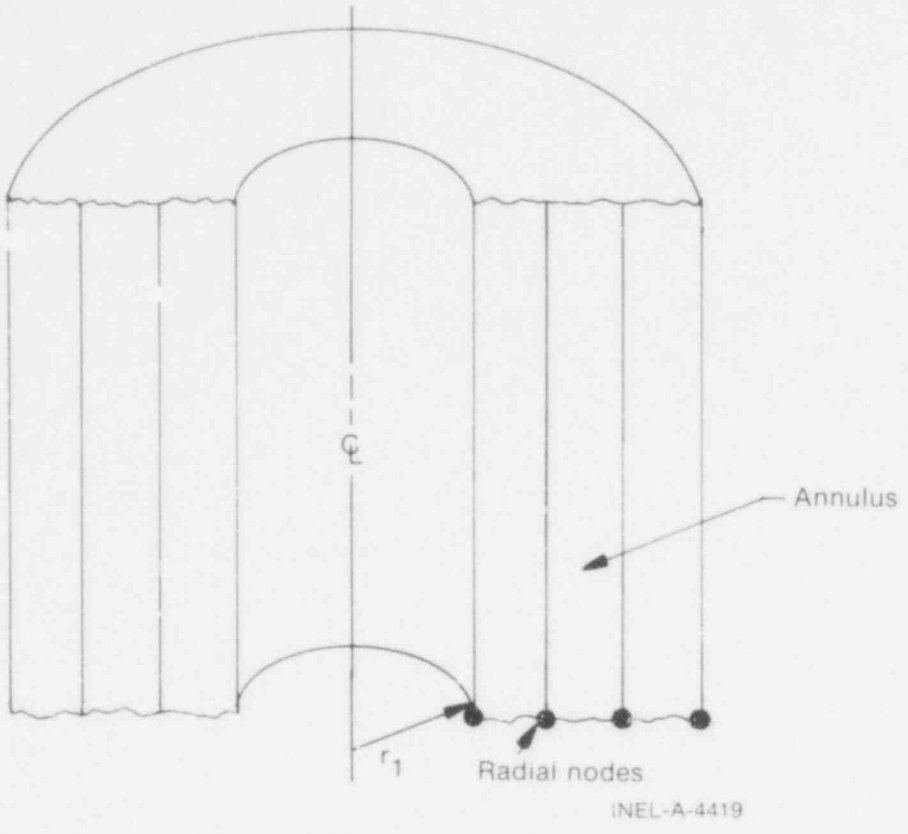

Fig. 22 Node and annuli geometry.

$$\frac{d}{dr}\left(\frac{\sigma_\theta}{E}\right) = \left[\frac{\sigma_\theta(j+1)}{E(j+1)} - \frac{\sigma_\theta(j)}{E(j)}\right] \Big/ (r_{j+1} - r_j)$$

and

$$\frac{\sigma_\theta}{E} = \left[\frac{\sigma_\theta(j+1)}{E(j+1)} + \frac{\sigma_\theta(j)}{E(j)}\right] /2$$

where function values at the midpoint are taken as the average of the function values at the end points. Denoting $\Delta r_j = r_{j+1} - r_j$, Equations (3-59), (3-61), and (3-66) become

$$\left[\frac{1}{r_{j+1} - r_j} + \frac{1}{2\, r_{j+1}}\right] \sigma_r(j+1) + \left[\frac{-1}{2\, r_{j+1}}\right] \sigma_\theta(j+1)$$

$$= \left[\frac{1}{r_{j+1} - r_j} - \frac{1}{2r_j}\right] \sigma_r(j) + \left[\frac{1}{2r_j}\right] \sigma_\theta(j) \qquad (3\text{-}78)$$

and

$$\left\{\frac{-\nu(j+1)}{E(j+1)\ \Delta r(j)}\right\}\ \sigma_z(j+1)\ +\ \left\{\frac{\nu(j)}{E(j)\ \Delta r(j)}\right\}\ \sigma_z(j)$$

$$\left\{\frac{-\nu(j+1)}{E(j+1)\ \Delta r_j}\ -\ \frac{1\ +\ \nu(j+1)}{2\ E(j+1)r_{j+1}}\right\}\ \sigma_r(j+1)$$

$$+\ \left\{\frac{1}{E(j+1)\ \Delta r(j)}\ +\ \frac{1\ +\ \nu(j+1)}{2E(j+1)\ r_{j+1}}\right\}\ \sigma(j+1)$$

$$+\ \left\{\frac{+\nu(j)}{E(j)\ \Delta r(j)}\ -\ \frac{1+\nu(j)}{2\ E(j)\ r_j}\right\}\ \sigma_r(j)$$

$$+\ \left\{\frac{-1}{E(j)\ r(j)}\ +\ \frac{1+\nu(j)}{2\ E(j)\ r_j}\right\}\ \sigma_\theta(j)$$

$$+\ \left\{\left[\alpha_\theta T(j+1)\ +\ \varepsilon_\theta^p(j+1)\ +\ d\varepsilon_\theta^p(j+1)\right]\left(\frac{1}{\Delta r(j)}\ +\ \frac{1}{2\ r_{j+1}}\right)\right\}$$

$$+\ \left\{\left[\alpha_\theta T(j)\ +\ ^p(j)\ +\ d\ ^p(j)\right]\ \ \frac{-1}{\Delta r(j)}\ +\ \frac{1}{2r_j}\right.$$

$$+\ \left\{\frac{-1}{2r_{j+1}}\ \left[\alpha_r T(j+1)\ +\ \varepsilon_r^p(j+1)\ +\ d\varepsilon_r^p(j+1)\right]\right\}$$

$$+\ \left\{\frac{-1}{2r_j}\ \left[\alpha_r T(j)\ +\ \varepsilon_r^p(j)\ +\ d\varepsilon_r^p(j)\right]\right\}\ =\ 0 \qquad (3\text{-}79)$$

and finally

$$\frac{1}{E(k+1)} \left\{\sigma_z(k+1) - \nu(k+1)\left[\sigma_r(k+1) + \sigma_\theta(k+1)\right]\right\}$$

$$+ \left[\alpha_z T + \varepsilon_z^p + d\varepsilon_z^p\right]_{k+1}$$

$$= \frac{1}{E(k)} \left\{\sigma_z(k) - \nu(k)\left[\sigma_r(k) + \sigma_\theta(k)\right]\right\}$$

$$+ \left[\alpha_z T + \varepsilon_z^p + d\varepsilon_z^p\right]_k . \qquad (3\text{-}80)$$

For the j^{th} annulus, Equations (3-78), (3-79), and (3-80) may be compactly written as

$$\left[E(J)\right] \begin{Bmatrix}\sigma_r \\ \sigma_\theta \\ \sigma_z\end{Bmatrix}_{j+i} = \left[F(j)\right] \begin{Bmatrix}\sigma_r \\ \sigma_\theta \\ \sigma_z\end{Bmatrix}_j + \left\{G(j)\right\}$$

where $[E]$, $[F]$, $\{G\}$ depend only on the material properties, plastic strains and thermal strains. The axial strains ε_z do not occur in the above. Multiplication of this equation by the inverse of $[E]$ results in:

$$\begin{Bmatrix}\sigma_r \\ \sigma_\theta \\ \sigma_z\end{Bmatrix}_{j+1} = \left[L(j)\right] \begin{Bmatrix}\sigma_r \\ \sigma_\theta \\ \sigma_z\end{Bmatrix}_j + \left\{M(j)\right\}.$$

Since neither $[E]$ nor $[F]$ depend on the plastic strains, the matrices $[E]^{-1}$ and $[L]$ need to be found only once for each load step. Hence only $[E]^{-1}\{G\}$ need be recomputed at each step of the iteration in the Method of Successive Substitutions.

(2) Transfer Matrix Across a Surface of Displacement Discontinuity. One annulus of zero thickness is used as a surface of discontinuity, across which the radial displacement and axial strain may be discontinuous. The displacements on each side of the surface are related by

$$u_r(k) = u_r(k+1) + \Delta u_r \tag{3-81}$$

$$\varepsilon_z(k) = \varepsilon_z(k+1) + \Delta\varepsilon_z \tag{3-82}$$

where k is the annulus corresponding to the surface of discontinuity. In addition, the radial stress must be continuous, so that

$$\sigma_r(k) = \sigma_r(k+1). \tag{3-83}$$

Then by use of the compatibility equations and $\varepsilon_\theta = u_r/r$, Equations (3-81), (3-82), and (3-83) can be written in matrix form as

$$[P]_{k+1} \{\sigma\}_{k+1} = [P]_k \{\sigma\}_k + [Q]. \tag{3-84}$$

The inverse of [P] is easily evaluated explicitly, so that, finally, the appropriate transfer relations across the pellet cladding interface are

$$\{\sigma\}_{k+1} = [P]^{-1}_{k+1} [P]_k \{\sigma\}_k + [P]^{-1}_{k+1} \{Q\}$$

which is in the form of Equation (3-68). Similar transfer relations are used for different combinations of axial and radial crack patterns.

3.3 Cladding Ballooning Model

After the small cladding deformation has been calculated by FRACAS-1, a check is made to determine whether or not the cladding ballooning subcode should be called[a]. This step was previously illustrated in the flow chart shown in Figure 12. The check consists of comparing the cladding effective plastic strain, which is part of the calculated deformation, against the cladding instability strain given by the MATPRO subcode. If the cladding effective plastic strain is greater than the cladding instability strain, the ballooning subcode is called and FRACAS-1 is bypassed at that axial node.

a. Ballooning calculations are not performed in FRAP-T5 when the FRACAS-2 option has been specified.

The ballooning subcode (BALLOON) computes the extent and shape of the localized large cladding deformation that occurs between the time that the cladding effective strain exceeds the instability strain and the time of cladding rupture. The cladding is assumed to consist of a network of membrane elements subjected to a pressure difference between the inside surface and the outside surface as shown in Figure 23. The equations for the model in the subcode are derived from the thin shell membrane equilibrium equation and geometric constraints. In addition, the model accounts for the extra cooling the cladding receives as it bulges outward.

The ballooning model is based on the following assumptions:

(1) Stability of the deformed shape can be described by the thin shell membrane theory

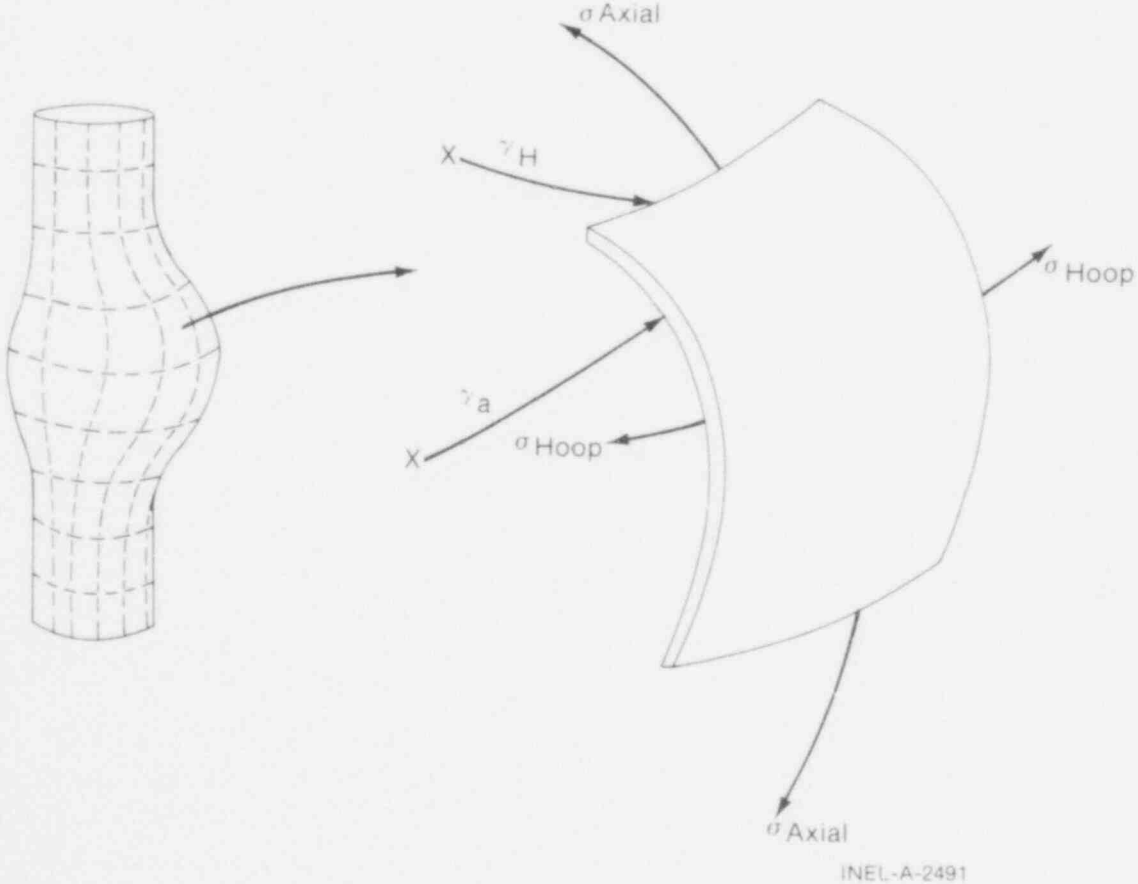

Fig. 23 Membrane swelling model.

573 133

(2) Stresses and temperatures are uniform thrcugh the cladding thickness

(3) Axial and circumferential stresses at a point can be defined as a function of temperature, strain, and strain rate by a single relationship

(4) The centroid of each nodal element remains on an extension of the radial vector to the undeformed element centroid

(5) Cladding hoop stress and axial stress are equal

(6) No change in cladding volume due to deformation

(7) No heat conduction in axial or azimuthal directions

(8) Heat flux through cladding changes slowly with time

(9) At the ballooning region, the surface heat transfer coefficient is a factor of two higher than that of the nonballooned cladding adjacent to the ballooning region

(10) The cladding thickness at the point of initiation of ballooning (cladding weak spot) is 99% of input-specified cladding thickness

(11) The length of the cladding balloon region is four inches.

3.3.1 Equilibrium Equation. The equilibrium equation for the membrane element in Figure 23 is

$$\frac{\sigma_a}{r_a} + \frac{\sigma_\theta}{r_c} = \frac{p}{t_c} \qquad (3\text{-}85)$$

573 134

where

p = difference between internal gas pressure and coolant pressure

σ_a = axial stress

σ_θ = hoop stress

r_a = axial radius of curvature

r_c = circumferential radius of curvature

t_c = cladding thickness.

Considering the assumption that no significant deformation is obtained until both axial and radial stresses have exceeded the yield stress, Equation (3-85) is expressed as

$$\sigma_y \left(\frac{1}{r_a} + \frac{1}{r_c}\right) \Big/ \frac{p}{t_c} = f \qquad (3\text{-}86)$$

where

σ_y = yield stress of cladding

f = node stability factor.

For a given internal pressure, P, cladding thickness, t_c, cladding yield stress, σ_y, and local curvatures, r_a and r_c, the value of f given by solution of Equation (3-86) determines whether an element is stable or will deform under the applied pressures. If the value of f is less than one, the element will displace outward. Otherwise, the element remains stable. When an unstable element is detected, the cladding is deformed in such a manner as to make the system more stable. This adjustment in the geometry of the cladding is described in the following paragraphs.

3.3.2 Geometric Models. To compute the radius of curvature in the axial direction, the configuration shown in Figure 24 is assumed. The angle between the chord connecting nodes i-1 and i+1 and the fuel rod centerline is given by the equation

$$\theta = \tan^{-1}\left|\frac{d_{i+1} - d_{i-1}}{2w'}\right| \qquad (3\text{-}87)$$

where

d_i = perpendicular distance between node i and fuel rod centerline

w' = specified mesh spacing in axial direction (set to 0.2 inches in balloon model subcode).

One-half the length of the chord connecting nodes i-1 and i+1 is

$$w = w'/\cos\theta. \qquad (3\text{-}88)$$

If the radius of curvature, r_a, is assumed to be constant between nodes i-1 and i+1, the radius of curvature at node i and the chord connecting nodes i-1 and i+1 are perpendicular to each other. Then, the perpendicular distance between node i and the chord connecting nodes i-1 and i+1 is given by the equation

$$\delta = \left[d_i - \frac{d_{i+1} - d_{i-1}}{2}\right]\cos\theta. \qquad (3\text{-}89)$$

Application of the Pythagorean theorem gives the following relation between the radius of curvature r_a, chord length 2w, and δ:

$$(r_a - \delta)^2 + w^2 = r_a^2.$$

Solving for r_a,

$$r_a = \left[\frac{w^2 + \delta^2}{2\delta}\right]. \qquad (3\text{-}90)$$

573 136

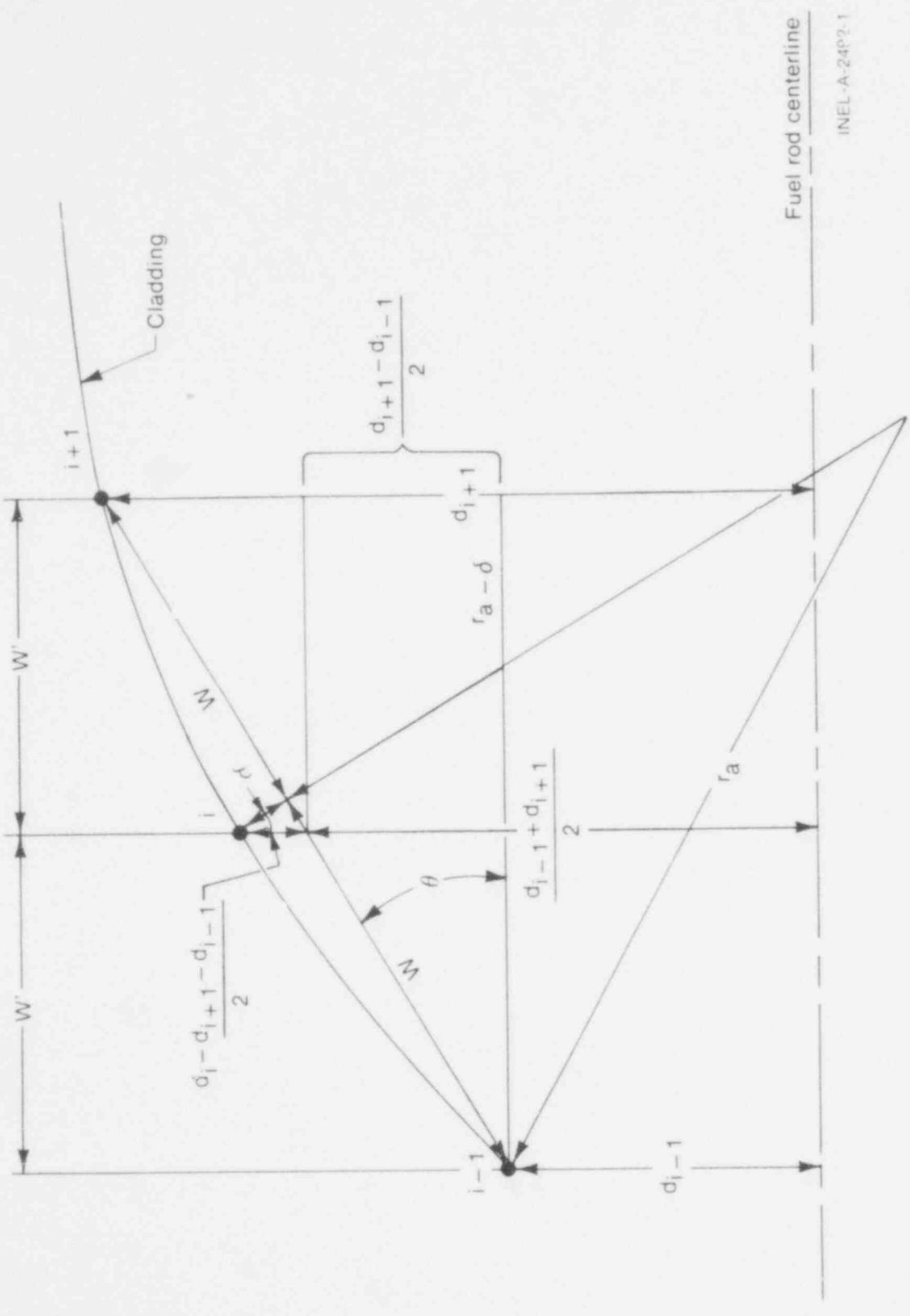

Fig. 24 Radius of curvature in axial direction.

To compute the radius of curvature in the circumferential direction, the configuration shown in Figure 25 is assumed. By assuming that the local radius of curvature can be computed by averaging the radial coordinates d_{i-1} and d_{i+1}, one-half the length of the chord connecting nodes i-1 and i+1 is

$$w = \sin \phi \ \frac{d_{i-1} + d_{i+1}}{2} \qquad (3\text{-}91)$$

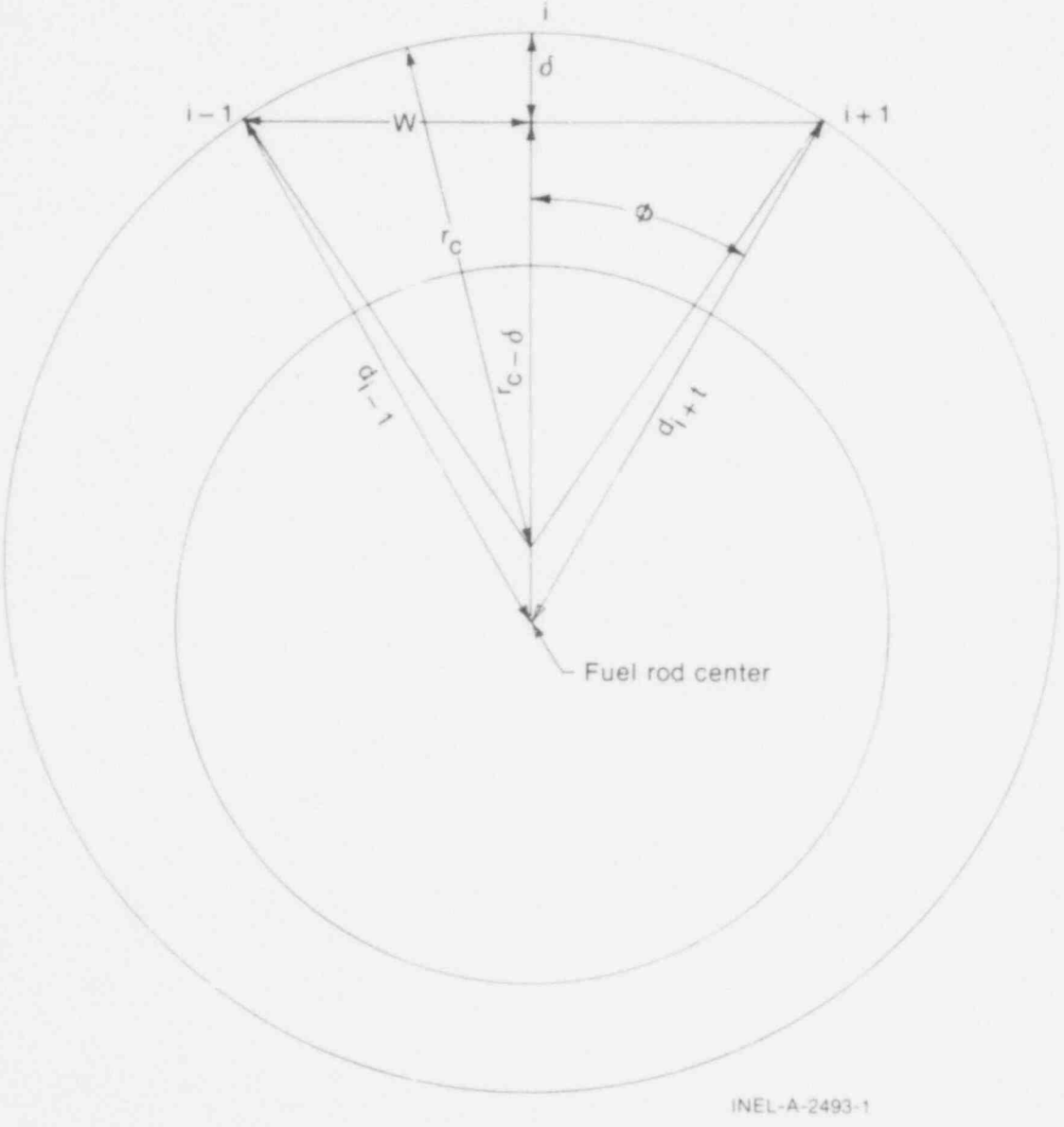

Fig. 25 Radius of curvature in circumferential direction.

where

w = one-half length of chord connecting nodes i-1 and i+1

$\emptyset$ = angular mesh spacing (set to $\pi/7$ balloon model subcode)

d_i = distance from fuel rod center to node i.

The perpendicular distance between node i and the chord connecting nodes i-1 and i+1 is

$$\delta = \left[d_i\right] - \left[\frac{d_{i-1} + d_{i+1}}{2}\right]\cos\emptyset. \qquad (3\text{-}92)$$

By application of the Pythagorean theorem, the radius of curvature at node i is related to δ and w by the equation

$$(r_c - \delta)^2 + w^2 = r_c^2.$$

Solution for r_c gives the equation

$$r_c = \left[\frac{\delta^2 + w^2}{2\delta}\right]. \qquad (3\text{-}93)$$

Calculation of the surface area and cladding thickness at each node is based on the assumption that the volume of the cladding does not change with deformation. The calculations assume the configuration shown in Figure 26. The surface area of node i in the deformed state is calculated by the equation

$$A_{D_i} = d_i \emptyset \omega \qquad (3\text{-}94)$$

where

A_{D_i} = cladding surface area at node i

573 139

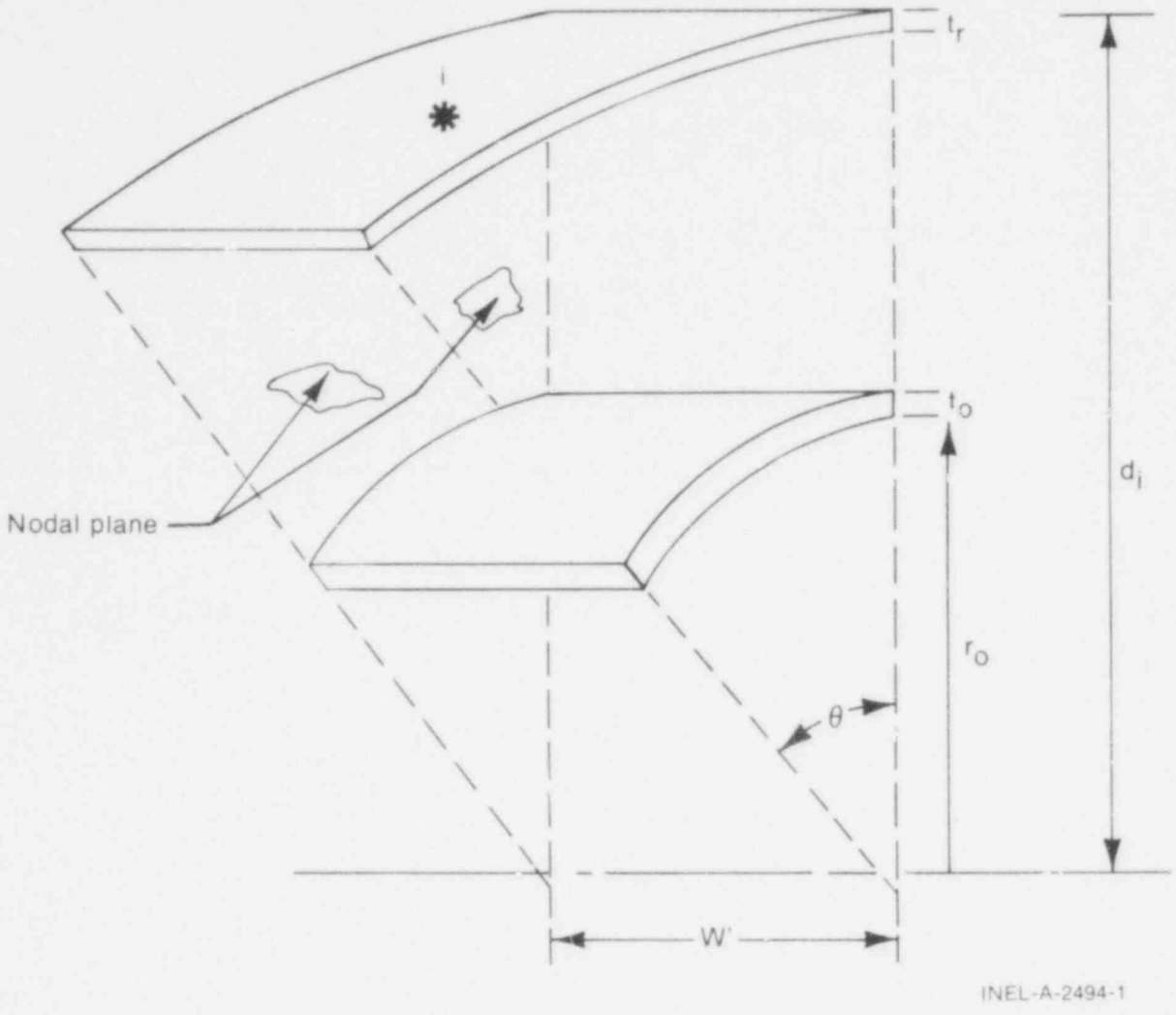

Fig. 26 Surface area and cladding thinning model.

d_i = radial coordinate of node i

$\emptyset$ = circumferential nodal spacing (radians)

ω = axial node spacing after swelling (see Figure 24).

Assuming constant element volume, the following relation is obtained for local cladding thickness

$$t_c = r_o \phi \omega' t_o / A_{D_i} \qquad (3\text{-}95)$$

573 140

where

t_c = cladding thickness at node i

r_o = original cladding radius

ω' = axial mesh spacing (see Figure 24)

t_o = original cladding thickness.

The volume of the region inside the cladding is required for input to the fuel rod pressure model. Incremental nodal volumes are calculated as the node is displaced and summed to produce a new, swelled volume for each time step. The relationship defining the incremental nodal volume is

$$\Delta V_i = d_i \phi \omega' d_i \tag{3-96}$$

where

Δd_i = incremental displacement of node i during the time step.

The total swelling volume for the time step is then

$$V = V_o + \sum_{i=1}^{n} \Delta V_i \tag{3-97}$$

where

n = number of nodes

V_o = volume from previous time step.

3.3.3 Numerical Analysis. The analytical sequence used in the cladding ballooning model consists of

(1) Solution for the stability of each nodal point on the cladding using Equation (3-86)

(2) Modification of the cladding geometry as a function of cladding instability.

The stability of each node is determined by solution of Equation (3-86) for the local stability factor f_i, with $f_i > 1$ indicating a stable node.

With the assumption that unstable nodes ($f_i < 1$) will deform, the solution is to specify a deformation for these unstable nodes. Specification of these deformations is based on the following assumptions:

(1) Nodal deformations are a function of the nodal instability at that node which is the most unstable (F_m = maximum f_i) and will deform the most

(2) The specified displacements must be small enough that adjacent stable nodes are not unrealistically affected.

The process of specifying deformations consists of the addition of a finite deformation to the nodal deformation calculated during the last time tep as

$$d_i = d_{i_o} + dh_i \qquad (3\text{-}98)$$

where

d_i = the new radial coordinate of node i

d_{i_o} = the old radial coordinate of node i

dh_i = specified incremental radial displacement of node i.

The effect of adding an incremented deformation to node i is shown in Figure 27 to decrease the radius of curvature at i. Examination of Equation (3-86) shows this decrease in curvature to increase the stability function f_i and, thus, the local stability at node i. An additional effect to be noted from Figure 27 is that an increase in deformation at node i causes an increase in curvature at node i+1 and i-1 (possibly to the point of producing negative curvature).

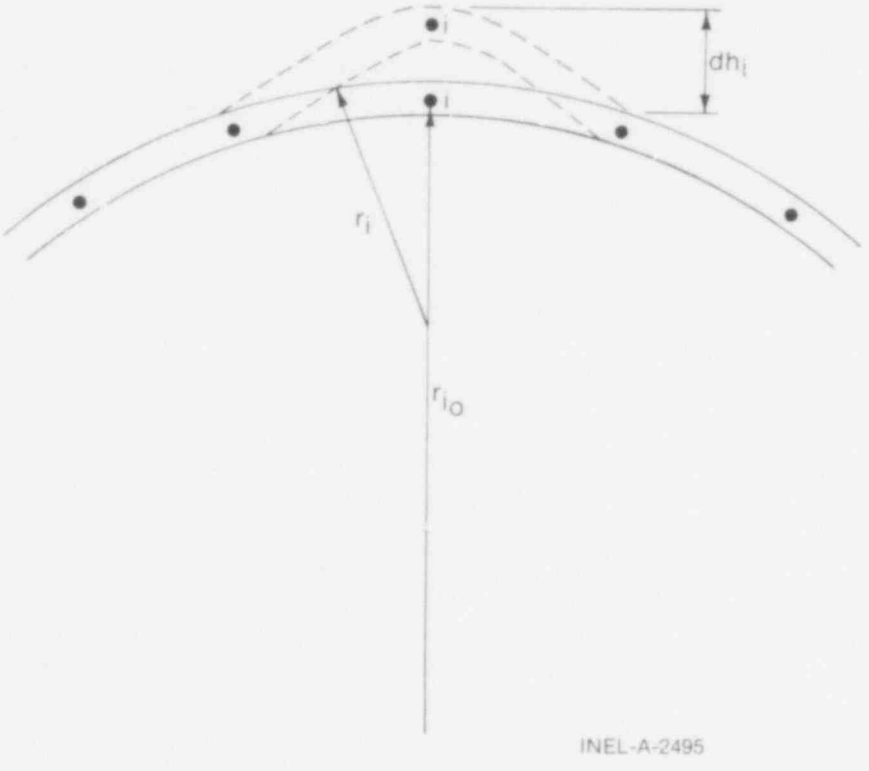

Fig. 27 Incremental deformation at node i.

Examination of Equation (3-86) shows an increase in curvature to decrease the stability function and, thus, local cladding stability. The effect, therefore, of locally deforming a weak spot is to strengthen the weak spot but propagate the weakness into the surrounding material, possibly causing additional new instability and further propagation. Careful examination of membrane instabilities on ballooning tubes indicates that initial deformation is quite localized and then proceeds to either rupture or an enlarged stable geometry.

Deformations are specified according to the relation

$$dh_i = dh_m \left(\frac{(1-f_i)^2}{1-F_m} \right) + 0.1 \qquad (3\text{-}99)$$

where

dh_i = incremental radial displacement of node i

dh_m = maximum displacement to be added to any node

f_i = instability factor at node i

F_m = maximum instability factor.

A value of dh_m equal to the cladding thickness has been found to produce a rapid convergence with no apparent numerical or structural instabilities. The 0.1 factor in Equation (3-98) serves to "push" the function past the stability point, since corrections very close to stability are very small. The overall numerical procedure for the balloon model is shown in Figure 28.

3.3.4 Conduction Model. As the cladding extends away from the hot fuel pellet surface, the cladding temperature will change due to the combined effects of:

(1) Decreased gap conductance with increasing gap thickness

(2) Increased surface cooling due to increased area

(3) Increased surface cooling due to local flow phenomena

(4) Increased fuel surface temperature due to decreased gap conductance

(5) Heat capacitance of cladding.

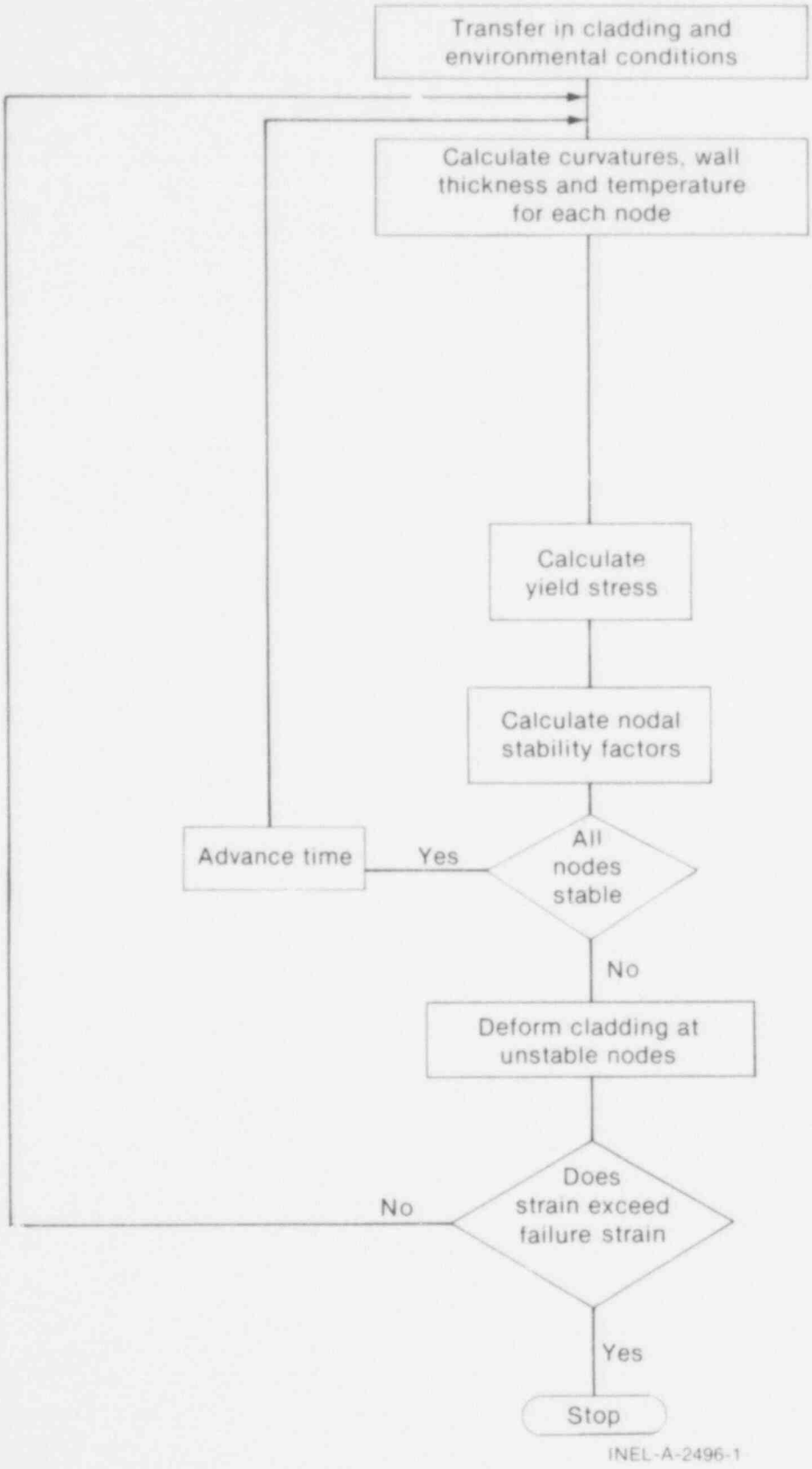

Fig. 28 Balloon model flow diagram.

The conduction model formulated to include these combined effects considers the cladding temperature as a function of the local power or surface heat flux value. The major assumption of the model is that the heat flux, $\ddot{q}$, from an area of the fuel, A_f, is transferred through a corresponding area of cladding, A_{cl}, throughout the transient. Considering this assumption, the temperature of the cladding is determined by

$$\rho C_p V_{cl} \frac{\partial T_{cl}}{\partial t} = \ddot{q} A_f + A_{cl} h_s (T_B - T_{cl}) \qquad (3\text{-}100)$$

where

C_p = cladding heat capacity

ρ = cladding density

V_{cl} = cladding nodal volume

T_{cl} = cladding average temperature

T_B = bulk coolant temperature

h_s = cladding surface heat transfer coefficient (see following section)

A_{cl} = cladding nodal area

A_f = fuel nodal area

$\ddot{q}$ = fuel surface heat flux

t = time.

Solution of Equation (3-100) for the time-dependent cladding temperature gives

573 146

$$T_{cl} = (T_o - B/A)\, e^{-At} + B/A \qquad (3\text{-}101)$$

where

T_o = initial cladding temperature

A = $A_{cl}/(\rho C_p V_{cl})$

B = $(\ddot{q}\, A_f + A_{cl}\, h\, T_B)/(\rho C_p V_{cl})$.

Additional cladding cooling will result as the cladding swells into the coolant channel. This additional cooling is modeled as an increase in the surface heat transfer coefficient by the relation

$$h_s = [1 + (C_1 - 1)\,(d_i - r_o)/r_o]\, h_o \qquad (3\text{-}102)$$

where

h_s = cladding heat transfer coefficient for ballooned cladding

h_o = cladding heat transfer coefficient calculated by the HEAT-1 subcode of FRAP-T, which assumes that no local variation in geometry exists

d_i = current radial coordinate of i^{th} node

r_o = initial radius of i^{th} node

C_1 = heat transfer enhancement factor (assumed to be 2.0).

3.4 Fuel Rod Failure Models

After the cladding stresses and strains have been computed by either the FRACAS-1 or FRACAS-2 subcodes, a check is made to determine whether or not the cladding has failed, as illustrated in the

flow chart shown in Figure 12. If the cladding has failed, the internal gas pressure is set equal to the coolant pressure, which eliminates the differential pressure loading on the cladding and also changes the gap conductance.

The determination of whether or not the cladding has failed (suffered loss of integrity) is made by the FRAIL[22,23] subcode. Models for predicting four types of fuel rod failure are contained in the FRAIL subcode. The failure types are: (a) overstress, (b) overstrain, (c) oxide layer wall thinning, and (d) eutectic melt. The models assume fuel rod failure to be a function of the following parameters:

(1) Temperature history

(2) Cold work

(3) Irradiation dosage

(4) Effective strain

(5) Effective stress

(6) Strain rate.

Because of scatter in the experimental data and uncertainties in the characterization of the experiment specimens, the FRAIL subcode uses a probabilistic approach. Instead of simply computing whether or not a fuel rod has failed, the subcode computes the probability of fuel rod failure.

3.4.1 Model for Overstress. The assumptions in the overstress failure model are:

(1) The mean hoop stress at failure can be correlated with temperature by least-square fitting to the failure stress data base

(2) The distribution of failure stress about the mean failure stress can be approximated with a Beta probability distribution

(3) The failure stress is not an explicit function of the hydrogen, cesium, iodine, or oxygen content of the cladding

(4) The failure stress is not a function of stress rate

(5) The failure stress is not a function of neutron irradiation.

The overstress model is based on an empirical correlation which relates average failure stress to cladding temperature. The data used to develop the correlation were taken from a number (305) of isothermal and transient temperature burst tests[24-31]. These tests include burst tests on tubing with varying degrees of irradiation and cold work. Since hoop stress at failure was not a measured quantity for these tests, that stress was computed using the maximum measured internal pressure and the equation of static equilibrium for a cylinder. The empirical correlation was generated by least-squares fitting of the failure stress data. All points were assigned a weight of one since the experimental errors were not reported. The best fit (minimum standard deviation) was found to be given by the equation

$$\log \sigma_f = 5.00 + 3.27 \times 10^{-4} T - 1.14 \times 10^{-6} T^2 + 2.56 \times 10^{-10} T^3$$

σ_f = failure stress (psi)

T = temperature (^{o}F). (3-102)

This correlation is plotted in Figure 29.

To compute the probability of failure as a function of stress and temperature, a distribution of failure stress about the mean line must

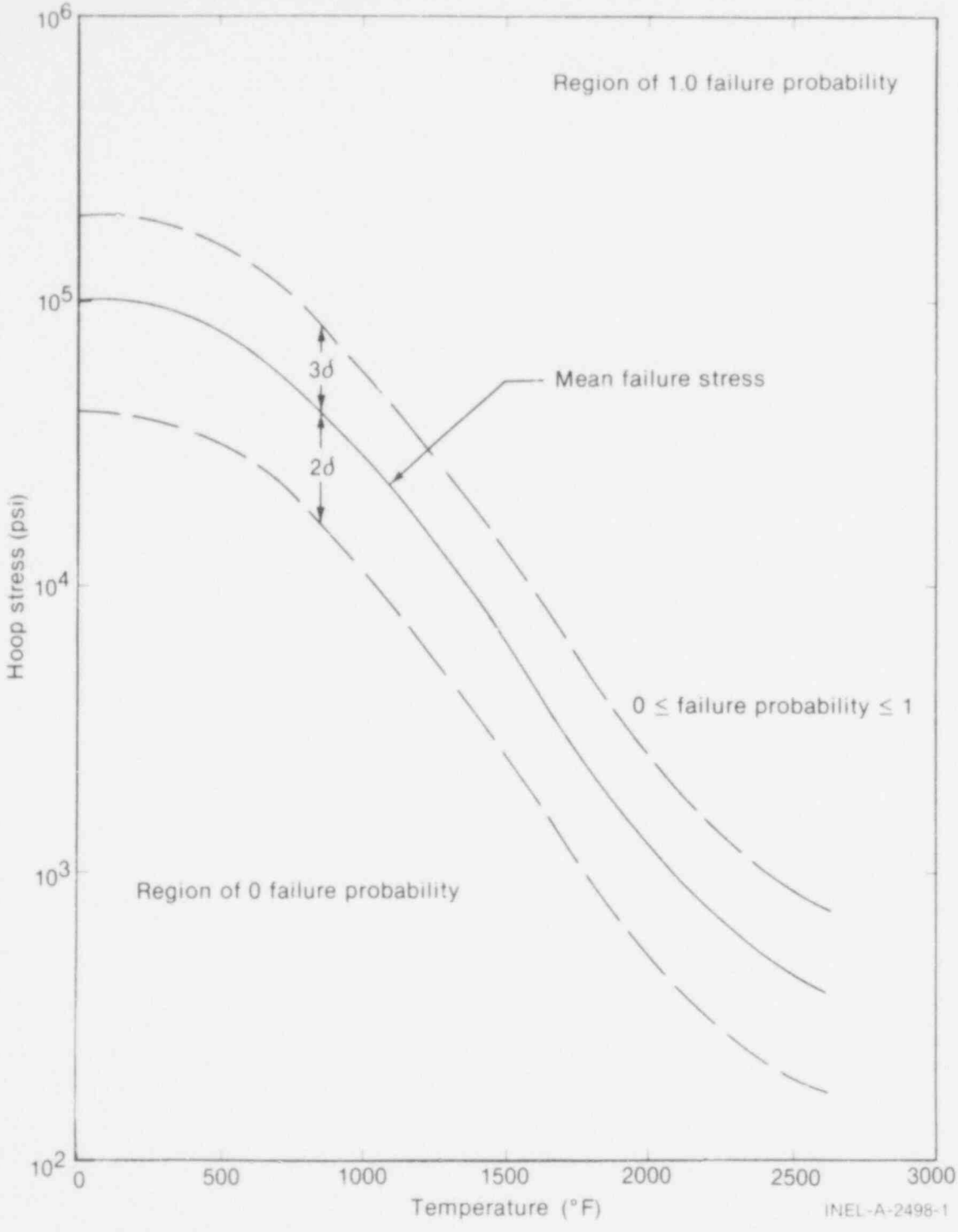

Fig. 29 Mean failure stress versus temperature.

be defined. The beta distribution was chosen because this distribution is limited to a finite interval. Estimates of the shape parameters of the beta distribution were found from the equations

$$n = \frac{(1 - \bar{x})}{s^2} \bar{x}(1-\bar{x}) - s^2 \qquad (3\text{-}103)$$

and

$$\gamma = \frac{\bar{x}\, n}{1-\bar{x}} \qquad (3\text{-}104)$$

where

$\bar{x}$ = normalized failure stress

s = normalized standard deviation

n,γ = shape parameters.

The normalized failure stress is found from the expression

$$\bar{x} = \frac{\sigma_F - B}{T - B} \qquad (3\text{-}105)$$

where

$\bar{x}$ = normalized failure stress ($0 \leq \bar{x} \leq 1$)

σ_F = mean failure stress

and B and T define the interval of allowable failure stresses. This interval was chosen to be three standard deviations above and two standard deviations below the mean failure stress. These limits are depicted in Figure 29.

The normalized standard deviation is found from the equation

$$s = s' \frac{\partial \bar{x}}{\partial \sigma_F} = \frac{s'}{T - B} \qquad (3\text{-}106)$$

573 151

where

s = normalized standard deviation, that is, the standard deviation of $\bar{x}$

s' = standard deviation of $\sigma_F = 0.305\ \sigma_F$.

Because of the large spread in the failure stress data, the overstress failure model does not currently distinguish between the failure of irradiated and unirradiated fuel rods.

3.4.2 Model for Overstrain Failure. The assumptions used in the overstrain failure model are

(1) The mean failure strain can be correlated with temperature by least-squares fitting to the failure strain data base

(2) The distribution of the failure strain about the mean failure strain can be approximated by a Beta probability distribution

(3) The failure strain is not a function of the hydrogen, oxygen, cesium, or iodine content of the cladding.

The overstrain failure model calculates the probability of failure as a function of strain and temperature. The strain at failure is assumed to be distributed according to the beta distribution. The upper and lower limits are set at +2 and -2 standard deviations, respectively, from the mean failure strain. The standard deviation is 16% of the mean failure strain.

The mean failure strain as a function of temperature is obtained from the MATPRO subroutine CMLIMT. The effects of cold work and irradiation level are taken into account.

3.4.3 Model for Oxide Layer Wall Thinning Failure. If the thickness of the oxide layer is greater than 17% of the original cladding wall thickness, failure of the cladding is assumed to occur. No probability of failure by this mode is computed. If the oxide layer thickness is less than 17% of the original wall thickness, the probability for failure is zero. If greater, the probability for failure is one.

3.4.4 Model for Eutectic Melt. This model requires the cladding temperature at the point of contact of the cladding with the spacer grids. Since the temperature distribution subcode only computes cladding temperature in the absence of spacer grids, this failure model contains an equation that estimates the temperature at spacer grids. Basically, the equation modifies the temperature calculated in the temperature distribution subcode in the vicinity of the spacer grids according to the ratio of the heat transfer coefficient at the spacer grids to that in the absence of spacer grids.

The assumptions in the model for eutectic melt are

(1) The fuel rod heat transfer coefficient at a spacer grid is 1.4 times the heat transfer coefficient in absence of the spacer grid[32]

(2) The total heat transferred at a spacer grid is 1.06 times that transferred in the absence of the spacer grid

(3) The cladding temperature at a spacer grid is governed by the equation

$$\frac{T_2 - T_1}{T_1 - T_c} = \frac{h_1 q_2}{h_2 q_1}$$

where

T = temperature

573 153

h = heat transfer coefficient

q = total heat transferred

and the subscripts are

c = coolant

1 = fuel rod cladding at a spacer grid

2 = fuel rod cladding in absence of spacer grid

(4) At the position of a spacer grid, there is no oxide layer on the surface of the cladding because of fretting action

(5) Nickel from the spacer grids is the only material that can react with the cladding to form a eutectic

(6) The melting temperature of the zircaloy-nickel eutectic is 1233 K.

(7) If the cladding temperature reaches 1233 K at a spacer grid, the zircaloy-nickel eutectic forms instantly, which results simultaneously in localized cladding melting.

By application of assumptions (1) and (2) to the equation which constitutes assumption (3), the equation for cladding temperature at a spacer grid is

$$T_1 = 0.666\ (T_2 + 0.5\ T_c) \qquad (3\text{-}107)$$

where

T_1 = cladding temperature at a spacer grid

T_2 = cladding temperature in absence of the spacer grid (as computed by the temperature subcode)

T_c = coolant temperature.

The cladding is assumed to fail if T_1 exceeds 1233 K. No probability of failure for this mode is computed. If the cladding temperature at the spacer grids is less than 1233 K, the probability of failure is zero. If the cladding temperature is greater than 1233 K, the probability of failure is unity.

4. FUEL ROD INTERNAL PRESSURE

After the temperature and deformation calculations have been completed, the pressure of the gas in the fuel rod is computed. To calculate the pressure, the temperature and volume of the gas are required. The temperature subcode output gives the temperature of the gas in the fuel rod plenum, gas gap, and fuel voids. The deformation subcode output gives the volume of the fuel rod plenum, gas gap, and fuel voids.

The internal gas pressure can be computed by either a static pressure model (which assumes that all volumes inside the fuel rod equilibrate instantaneously) or by a transient pressure model which takes into account the viscous flow of the fill gas in the fuel rod. The transient model is an input option. Unless the gas gap is small (< 25 microns) or closed, the static and transient models give identical results.

The static fuel rod internal pressure model is based on the following assumptions:

573 155

(1) The perfect gas law holds

(2) The gas pressure is the same throughout the fuel rod

(3) The gas in the fuel cracks is at the average fuel temperature.

The transient fuel rod pressure model is based on the following assumptions.

(1) The gas behaves as a perfect gas

(2) The gas flow past the fuel column is a quasi-steady state process

(3) The gas flow is compressible and laminar

(4) The gas flow past the fuel column can be analyzed as Poiseuille flow (that is, by force balance only)

(5) The gas expansion in the plenum and ballooning zone is isothermal

(6) The entire gas gap can be represented as one volume containing gas at a uniform pressure

(7) The flow distance is equal to the distance from plenum to centroid of the gas gap

(8) The minimum cross-sectional area of flow is equivalent to an annulus with inner radius equal to that of fuel pellet radius and a radial thickness of 2.5 microns.

4.1 Static Fuel Rod Internal Pressure

The static pressure is computed by the perfect gas law, modified to include volumes at different temperatures:

$$P_G = \frac{M_G R}{\frac{V_p}{T_p} + \sum_{n=1}^{N} \left[\frac{\pi(r_{cn}^2 - r_{fn}^2)}{T_{Gn}} + \frac{V_{cn}}{T_{aven}} + \frac{V_{Dn}}{T_{Dn}} + \frac{V_{pn}}{T_{aven}} + \frac{V_{rfn}}{T_{fsn}} + \frac{V_{rcn}}{T_{csn}} \right] \Delta Z_n} \quad (4\text{-}1)$$

where

P_G = internal fuel rod pressure

M_g = moles of gas in fuel rod

R = universal gas constant

V_P = plenum volume

T_P = temperature of gas in plenum

n = axial node number

N = number of axial nodes

r_{cn} = radius of inside surface of cladding at axial node n

r_{fn} = radius of outside surface of fuel at axial node n

T_{Gn} = temperature of gas in gas gap at axial node n

ΔZ_n = fuel rod length associated with axial node n

V_{cn} = fuel crack volume per unit length at axial node n

573 157

T_{cn} = temperature of gas in fuel cracks at axial node n

V_{Dn} = volume of fuel pellet dishes per unit length of fuel stack at axial node n

T_{Dn} = temperature of gas in fuel dishes at axial node n

V_{pn} = volume of gas in fuel open pores per unit length at axial node n

T_{aven} = volumetric average fuel temperature at axial node n

V_{rfn} = volume of gas in voids due to fuel surface roughness per unit length at axial node n

T_{fsn} = temperature of fuel surface

V_{rcn} = volume of gas in voids due to roughness on cladding inside surface per unit length

T_{csn} = temperature of cladding inside surface.

4.2 Transient Internal Gas Flow

Transient flow of gas between the plenum and gas gap of a fuel rod is calculated by the Poiseuille equation for viscous flow along an annulus. The equation is

$$\dot{m} = \frac{\pi (P_p^2 - P_s^2)}{Ru \sum_{i=I_s}^{I_p} \frac{\ell_i T_i Ha}{D_g D_h^3}} \qquad (4\text{-}2)$$

where

$\dot{m}$ = mass flow rate

573 158

μ = gas viscosity at temperature T_A

T_i = gas temperature at node i

T_A = volume averaged temperature of gas in gas gap

ℓ_i = axial length of node i

t_{gi} = gap thickness (radial) at node i

I_p = number of top axial node

I_s = number of axial node closest to centroid of gas gap (see Figure 30).

Ha = Hagen number (defined below)

P_p = fuel rod plenum pressure

P_s = pressure in gas gap

R = universal gas constant

D_g = mean diameter of gas gap

D_h = hydraulic diameter of gas gap = $2t_{gi}$ for a small gap.

The Hagen number is computed by the equation

$$Ha = 22 + 0.24558/(2t_{gi} - 0.0007874). \quad (4\text{-}3)$$

A plot of the relation between Hagen number and gap thickness given by Equation (4-3) is shown in Figure 31. For gaps smaller than 1 mil (25 microns), the function is cut off at a value of 1177.

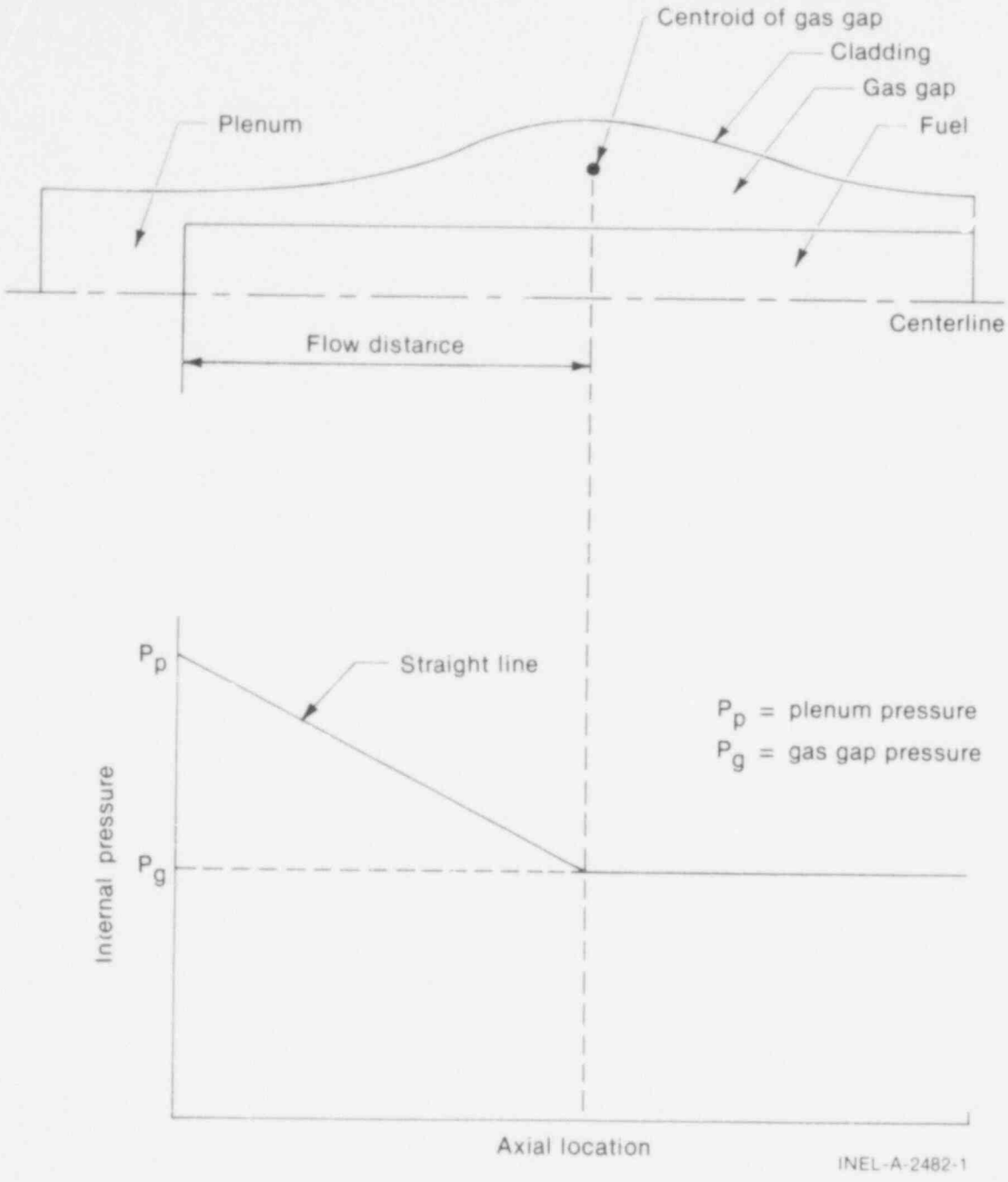

Fig. 30 Internal pressure distribution model.

To calculate the gas gap pressure, a modified form of Equation (4-1) is used. The plenum term is deleted and the moles of gas in the gas gap substituted in place of the moles of gas in the fuel rod.

The subroutine GSFLOW is programmed to solve Equation (4-2) and calculate the transient gas flow within a fuel rod. Operation of the computer model is as follows:

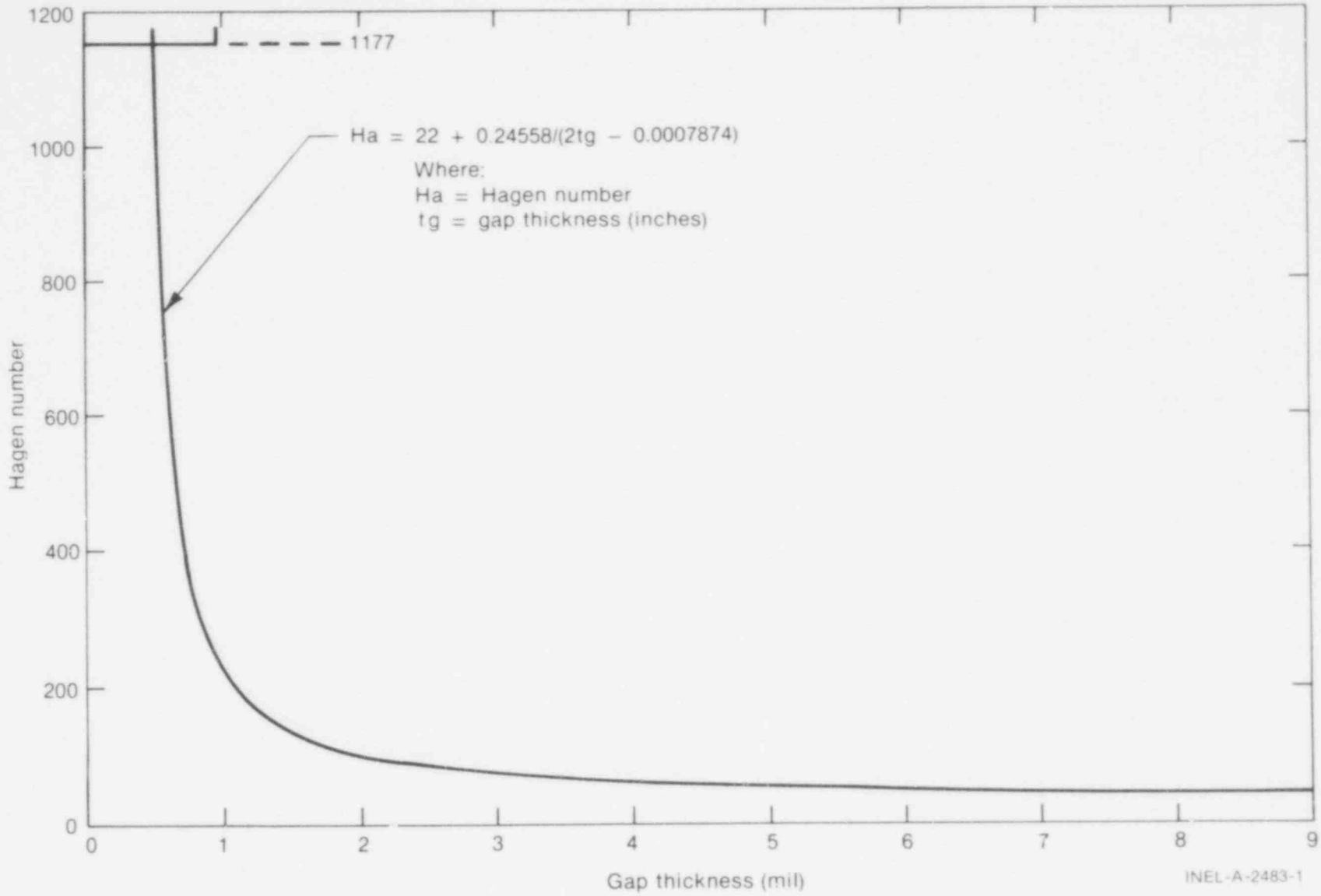

Fig. 31 Hagen number versus gap thickness.

(1) During each iteration step of FRAP-T, the subroutine GSFLOW is called to calculate the pressure distribution along the length of the fuel rod

(2) At each call, FRAP-T supplies the following information to GSFLOW:

   (a) Moles of gas in plenum at start of time step

   (b) Moles of gas in gas gap at start of time step

   (c) Fuel-cladding gap at each node

   (d) Gas temperature at each node

   (e) Axial length of each node

   (f) Volume of plenum

   (g) Volume of gas gap

   (h) Axial location of centroid of gas gap (Figure 30)

   (i) Time over which flow is to occur (FRAP-T time step)

(3) Using the above input data, the subroutine GSFLOW calculates the following:

   (a) Plenum pressure at the end of time step

   (b) Gas gap pressure at the end of time step

   (c) Moles of gas in plenum and gas gap at end of time step

(d) Axial pressure distribution as a function of plenum pressure and gas gap pressure (this distribution is shown in Figure 30).

5. FISSION GAS PRODUCTION AND RELEASE

Transient fission gas production and release is calculated by the GRASS[3] subcode, which calculates the generation of fission gas within UO_2 grains, the migration of fission gas from the interior of the grains to the grain boundaries, and the subsequent release of fission gas to the fuel rod gas gap and plenum. The fission gas production is a function of the fuel rod power. The gas is retained within the fuel grains, among the fuel grains, and in closed porosity. The fission gas migration and release is a function of the fuel temperature and microstructure. In particular, grain boundary separation increases fission gas release. The calculation of fuel swelling due to retained fission gas is also calculated, but is not passed to the deformation subcode.

The GRASS subcode was developed at the Argonne National Laboratory. The reader is referred to Reference 3 for a detailed description of the GRASS subcode.

IV. UNCERTAINTY ANALYSIS OPTION

The FRAP-T5 uncertainty analysis option has been developed so that a user may easily obtain estimates of the uncertainty in calculated code outputs. The option has been specifically designed so that a user may perform an uncertainty analysis on any FRAP problem in an understandable, systematic manner. To aid the user, default uncertainty values for approximately 50 input variables have been built into the code. The option further provides for a sequential development of output complexity by allowing the user to restart and continue an analysis from intermediate points. One goal of the option is to provide to all users a straightforward technique based on sound methodology for estimating code uncertainties.

1. METHODOLOGY

The uncertainty analysis option is based on the response surface method. Any of the output variables of a computer code may be termed a response. There is some functional relationship between a response and the input variables. In the space of the input variables, this relationship defines a surface, and hence the term "response surface." When the code is rather simple, this surface may be determined analytically over the entire range of the input values. More often, as in the case of the FRAP-T5 code, the surface may be known only through the code, and the range of inputs and problem types is very large. Thus, the complete true-response surface cannot be determined analytically. The response surface method of uncertainty analysis is based on a systematic sampling of the true surface which is then approximated by a polynomial equation in the independent (input) variables. In effect, the true surface is approximated by a smooth surface[33].

The polynomial equation approximating the true surface is derived as follows. Let $Y(x_i)$ denote the code response as a function of $x_i = x_1, x_2, \ldots, x_k$ inputs. The Taylor's series expansion about any point μ_i is then given by:

573 164

$$Y(x_i) = Y(\mu_i) + \sum_{i=1}^{k} \frac{\partial Y(u_i)}{\partial x_i} (x_i - \mu_i) + 1/2 \sum_{i=1}^{k} \frac{\partial^2 Y(u_i)}{\partial x_i^2} (x_i - \mu_i)^2$$

$$+ \sum_{\substack{i,j \\ i<j}}^{k} \frac{\partial^2 Y(\mu_i)}{\partial x_i \partial x_j} (x_i - \mu_i)(x_j - \mu_j) + \text{higher order terms.} \qquad (1\text{-}1)$$

Truncating the Taylor's series at second order terms, the desired polynomial equation is obtained by identifying the coefficients of the polynomial with the partial derivatives of the series expansion. The coefficients are estimated from sample values of the true response surface obtained by perturbing the nominal inputs. For a second-order polynomial to reasonably approximate the true response surface, the region of the surface being sampled must be small enough so that large irregularities are not present. Experience has shown that a range of plus and minus one standard deviation ($\pm 1\sigma$) in the input variable uncertainties will usually satisfy this requirement for the FRAP-T5 code.

The polynomial approximation may be used to examine the behavior of the true surface in the region of the sample space without the burden of excessive cost. In particular, the polynomial can be used to study the propagation of errors through the code and their effect on the uncertainty in the computed outputs. Thus, an estimate of response uncertainty and the relative contributions of input variables to this uncertainty may be obtained using the response surface method.

Once the user has selected a base-case problem and made a choice of output responses and input variables, the following procedures will be followed by the code to obtain the estimates of response uncertainties.

(1) An experimental design will be chosen. This is simply a pattern for perturbing the independent variables of the problem. The pattern is obtained in matrix format where

the columns correspond to inputs and the rows correspond to the individual analyses that must be computed. The problem is run as many times as the design dictates, each time varying the input variable perturbations according to the pattern.

(2) The response surface equations are then generated using the information derived from step one. Basically, a multiple regression routine is used with certain simplifications arising from orthogonal properties of the experimental design.

(3) The response surface equations are used to generate uncertainty distributions for the response parameters. Second-order error propagation analysis is used to estimate the means and variances of the responses.

(4) Finally, estimates of the fractional contributions to the response variances are made to indicate the relative importance of individual input variables.

2. APPLICATION

Calculations illustrating the use of the FRAP-T5 uncertainty analysis method have been performed. The base case was a nominal PWR fuel rod subjected to a 200% cold leg break LOCA at normal operation power. Only the blowdown phase of the LOCA was analyzed. Thirty-seven input variables representing almost all material properties and fabrication parameters, and a few operating conditions, were chosen as independent variables. Seven responses selected from both thermal and mechanical parameters were used as dependent variables. Since the fuel rod response during a transient can be significantly affected by variations in thermal-hydraulic boundary conditions, the results of the calculations are conditional. A more realistic analysis would include nondeterministic boundary conditions. However, when these

conditions are available (either from analysis or experiment), they can easily be incorporated in the uncertainty analysis structure as currently programmed.

Figure 32 shows the nominal calculated rod cladding surface temperature with a calculated uncertainty of one standard deviation due to fuel rod related uncertainties. Figure 33 shows the fractional contributions to the total variance of cladding surface temperature of the seven most influential fuel rod variables in the analysis. As the calculation of the problem progresses, both the absolute and relative contributions of different variables to the total uncertainty are shown to vary significantly.

These results demonstrate how an uncertainty analysis can be used to identify the significant sources of uncertainty in a computed response. Such knowledge provides insight with which to formulate direction for planning experimental programs and code development efforts.

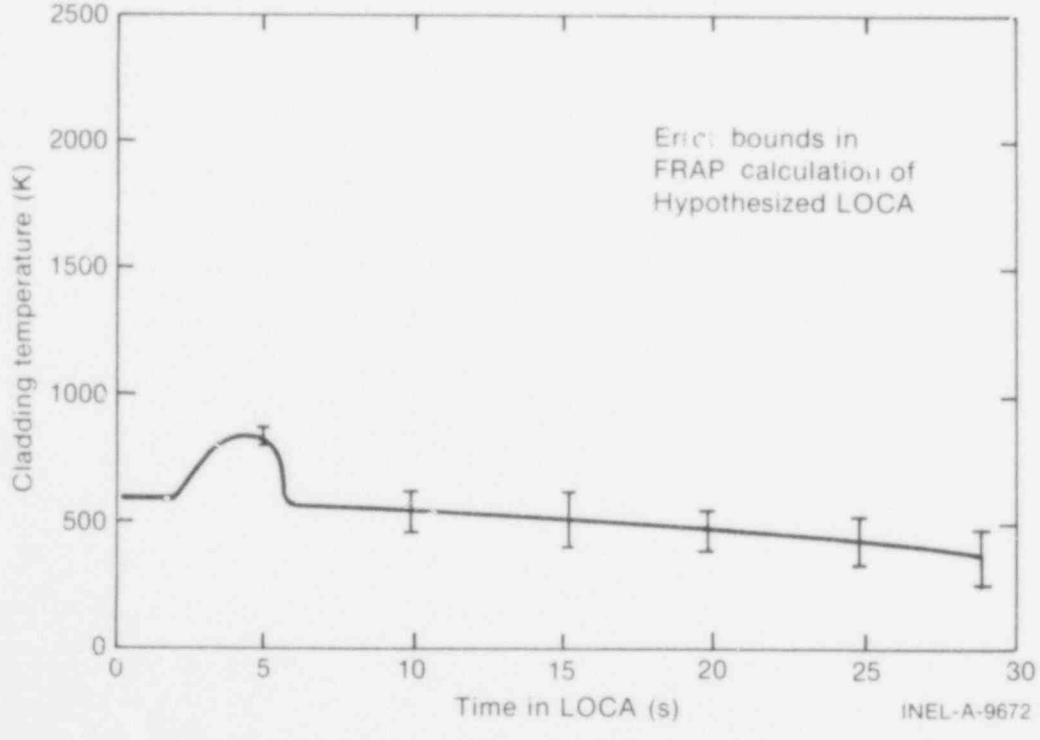

Fig. 32 Uncertainty in calculated cladding surface temperature due to fuel rod related uncertainties during the blowdown phase of a LOCA.

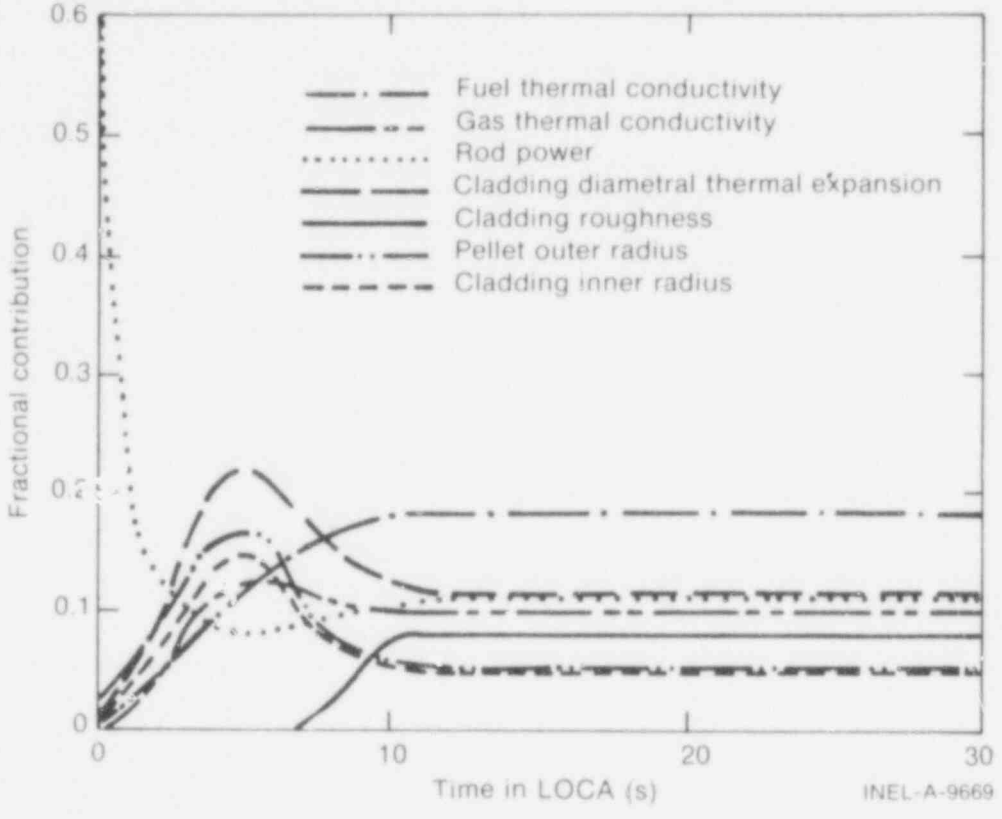

Fig. 33 Fractional contribution of the seven most influential variables to uncertainty of cladding surface temperature.

573 168

V. REFERENCES

1. Aerojet Nuclear Company, RELAP4/MOD5 - A Computer Program For Transient Thermal-Hydraulic Analysis of Nuclear Reactors and Related Systems, Vols I-III, ANCR-NUREG-1335 (September 1976).

2. G. A. Reymann et al, MATPRO - Version 11: A Handbook of Materials Properties for Use in the Analysis of Light Water Reactor Fuel Rod Behavior, NUREG/CR-0497 TREE-1280 (February 1979).

3. J. Rest, GRASS-SST: A Comprehensive Mechanistic Model for the Prediction of Fission Gas Behavior in UO_2 Based Fuels During Steady State and Transient Conditions, NUREG/CR-0202, ANL-78-53 (June 1978).

4. G. J. Scatena, G. L. Upham, Power Generation in a BWR Following Normal Shutdown or Loss-Of-Coolant Accident Conditions, NEDO-10625, March 1973.

5. A. M. Ross and R. L. Stoute, Heat Transfer Coefficient Between UO_2 and Zircaloy-2, AECL-1552 (June 1962).

6. C. R. Hann, C. E. Beyer, L. J. Parchen, GAPCON-THERMAL-1: A Computer Program for Calculating the Gap Conductance in Oxide Fuel Pins, BNWL-1778 (September 1973).

7. F. F. Cadek et al, PWR FLECHT Final Report Supplement, WCAP-7931 (October 1972).

8. F. W. Dittus and L. M. K. Boelter, Heat Transfer in Automobile Radiators of the Tubular Type, University of California Publications, 2 (1930) pp 443-461.

9. J. R. S. Thom et al, "Boiling in Subcooled Water During Flow Up Heated Tubes or Annuli," Proceedings Instrumentation of Mechanical Engineers, (London), 180 (Part 3C (1966)) pp 226-246.

10. V. E. Schrock and L. M. Gr[illegible], Forced Convection Boiling Studies, Final Report on For[illegible]onvection Vaporization Project, TID-14632 (1959).

11. J. B. McDonough, W. Mil[illegible]ing, Partial Film Boiling with Water at 2000 ps[illegible]nd Tube, MSA Research Corporation, Technical Report 62 (1[illegible]).

12. L. S. Tong and J. D. Young, "A Phenomenological Transition and Film Boiling Heat Transfer Correlation," Fifth International Heat Transfer Conference, Japan, July 1974, Journal of Heat Transfer (1974) pp 20-124.

13. K. G. Condie et al, "Regression Analysis of Post-CHF Flow Boiling Data," Fifth International Heat Transfer Conference, Japan, September 1974, pp 115-119.

14. D. C. Groeneveld, An Investigation of Heat Transfer in the Liquid Deficient Regime, AECL-3281 (Rev.) (December 1968; Revised August 1969).

15. R. L. Dougall and W. M. Rohsenow, Film Boiling on the Inside of Vertical Tubes with Upward Flow of the Fluid at Low Qualities, MIT-TR-9079-26 (1963).

16. R. J. Wagner, HEAT-1: A One-Dimensional Time Dependent or Steady State Heat Conduction Code, IDO-16887 (1963).

17. J. Crank and P. Nicolson, "A Practical Method for Numerical Evaluation of Solutions of Partial Differential Equations of the Heat Conduction Type," Proceedings, Cambridge Philosophical Society, 43 (1974) pp 50-64.

18. F. Kreith, Principles of Heat Transfer, 8th edition, Scranton: International Text Book Company, 1964.

19. W. H. McAdams, Heat Transmission, 3rd edition, New York: McGraw-Hill Book Company, Inc., 1954.

20. A. Mendelson, Plasticity: Theory and Applications, New York: The MacMillian Company, 1968.

21. C. Wang, Applied Elasticity, New York: McGraw-Hill Book Company, Inc., 1953.

22. K. A. Dietz (ed.), Quarterly Technical progress Report on Water Reactor Safety Programs Sponsored by the Nuclear Regulatory Commission's Division of Reactor Safety Research, July-September 1976, TREE-NUREG-1017 (January 1977).

23. J. B. Ferguson (ed.), Quarterly Technical Progress Report on Water Reactor Safety Programs Sponsored by the Nuclear Regulatory Commission's Division of Reactor Safety Research, October-December 1976, TREE-NUREG-1070 (April 1977).

24. C. C. Busby and K. B. March, High Temperature Deformation and Burst Characteristics of Recrystallized Zircaloy-4 Tubing, WAPD-T-900 (January 1970).

25. D. O. Hobson and P. L. Rittenhouse, Deformation and Rupture Behavior of Light Water Reactor Fuel Cladding, ORNL-4727 (October 1971).

26. M. R. Osborne and G. W. Parker, The Effect of Irradiation on the Failure of Zircaloy-Clad Fuel Rods, ORNL-3626 (January 1972).

27. D. O. Hobson, M. F. Osborne, G. W. Parker, "Comparison of Rupture Data from Irradiated Fuel Rods and Unirradiated Cladding," Nuclear Technology, 11 (August 1971).

28. D. G. Hardy, "The Effect of Neutron Irradiation on the Mechanical Properties of Zirconium Alloy Fuel Cladding in Uniaxial and Biaxial Tests," Symposium on Irradiation Effects on Structural Alloys for Nuclear Reactor Application, Niagra Falls, Canada, June 29 - July 1, 1970, ASTM-STP 484 (1971) pp 215-216.

29. W. J. Langford, "Metallurgical Properties of Cold-Worked Zircaloy-2 Pressure Tubes Irradiated Under CANDU-PHW Power Reactor Conditions," Symposium on Irradiation Effects on Structural Alloys for Nuclear Reactor Application, Niagra Falls, Canada, June 29 - July 1, 1970, ASTM-STP 484 (1971) pp 259-286.

30. W. R. Smalley, Saxton Core II Fuel Performance Evaluation Material, WCAP-3385-56 (September 1971) pp 4-84, 4-65; W. R. Smalley, Evaluation of Saxton Core III Fuel Materials Performance, WCAP-3385-57 (July 1974) pp 3-69, 3 -132, 3-134.

31. D. G. Hardy, "Burst Testing of Zircaloy Cladding for Irradiated Pickering-Type Fuel Bundles," Symposium on the Effects of Radiation on Substructure and Mechanical Properties of Metals and Alloys, Los Angeles, June 25-30, 1972, ASTM-STP 529 (1973) pp 415-435.

32. W. A. Sutherland, "Experimental Heat Transfer in Rod Bundles, "Heat Transfer in Rod Bundles, ASME (1968).

33. N. D. Cox, "Comparison of Two Uncertainty Analysis Methods," Nuclear Science and Engineering, 64 (September 1977) pp. 258-265.

573 171

APPENDIX A

COMPUTER CONTROL CARDS AND INPUT DATA REQUIREMENTS

APPENDIX A

COMPUTER CONTROL CARDS AND INPUT DATA REQUIREMENTS

The job control cards for compiling and executing the FRAP-T5 code on the CDC 7600 computer at the Idaho National Engineering Laboratory (INEL) are shown in Section 1 of this appendix. The input data requirements are shown in Section 2.

1. CONTROL CARDS FOR CDC 7600 COMPUTER

The control cards below will compile the tape transmitted source cards of FRAP-T and execute an example input data deck stored on the transmittal tape.

Job Card

Account Card

STAGE,TRAN,PE,PRE,VSN = T91234.	(Stage FRAP-T tape.)
CØPYBF,TRAN,FRAPSCR.	(Copy source cards of FRAP-T5, which are on file 1, to data set FRAPSRC.)
CØPYBF,TRAN,STH2ØT.	(Copy water properties table to data set STH2ØT. This data set consists of one record that is several thousand words long.)
CØPYBF,TRAN,FRPL.	(Copy source cards of plot code to data set FRPL.)
CØPYBF,TRAN,FCØØL.	(Copy source cards of FCOOL subcode, which is defined in Appendix E.)

```
CØPYBF,TRAN,STRIP4.
```
(Copy source cards of STRIP4 subcode, which is defined in Appendix E.)

```
REWIND,FRAPSCR,STH2ØT.

RFL,160000.
FTN,I = FRAPSRC, ØPT = 1, R = 3,L = 0.
```
(Compile FRAP-T source cards.)

```
SEGLØAD,B = FRAPABS,I = INPUT
```
(Create load module, named FRAPABS, of entire FRAP-T program. Directives for segmentation are given by input data cards.)

```
LØAD,LGØ
NØGØ.
CØPYBF,STH2ØT,TAPE15.
```
(FRAP-T reads water properties table with FORTRAN Logical Unit 15.)

```
RETURN,STH2ØT.

REWIND,FRAPABS,TAPE15.
REWIND, TAPE17.
RFL,160000.
```
(Information for FRAP-T plotting program is written to file TAPE 17.)

```
FRAPABS.
```
(Execute FRAP-T. Input data supplied by input cards.)

```
EXIT,U.

UNLØAD,TAPE2.
```
(If restart tape created, save it in case of abnormal termination.)

A summary of the tape files used by FRAP-T5 is given in Table A-I. Examples are shown below of control cards which set up these files.

If transient spatially varying coolant conditions are to be specified, a file for TAPE4 needs to be input. An example of this is shown below.

```
STAGE,TAPE4,PE,E,VSN = T9aaaa.
```

(T9aaaa is the number of the tape containing transient coolant conditions.)

If a FRAP-T restart tape is to be read, a STAGE card is required which assigns the restart tape to FORTRAN Logical Unit 1. An example of this is shown below.

```
STAGE,TAPE1,PE,E,VSN = T9bbbb.
```

(T9bbbb is tape number of previously created restart tape staged out for FORTRAN Logical Unit 2.)

If a restart tape is to be output, a file for FORTRAN Logical Unit 2 needs to be set up. An example of this is shown below.

```
STAGE,TAPE2,PE,E,PØST.
```

If FRAPCON computed fuel rod conditions are to be used as initial conditions to a FRAP-T transient analysis, a STAGE card for file TAPE31 must be supplied similar to that shown for TAPE1.

If an uncertainty analysis restart is to be performed, an additional restart tape is required. The restart tape is read by FORTRAN Logical Unit 44 and output on FORTRAN Logical Unit 45. The STAGE control card parameters are similar to those shown for TAPE1 and TAPE2, respectively.

TABLE A-I

TAPE FILES USED BY FRAP-T

File Name	File Status	Type of Data
TAPE1	Input	Restart information for single rod calculations. Tape must have been created by TAPE2 file of run to be restarted.
TAPE2	Output	Restart information.
TAPE3	Input	Restart information for multirod calculations. Tape must have been created by TAPE2 file of a previous run.
TAPE 4	Input	Coolant conditions according to format shown in Appendix E.
TAPE10	Output	Output tape of plot code. This tape is input to the FR-80 at INEL for microfiche copies of plots.
TAPE15	Input	Water properties table.
TAPE17	Output	Input tape to plot code.
TAPE31	Input	FRAPCON-1 created tape of burnup dependent variables.
TAPE44	Input	Data for restart or refinement of uncertainty analysis.
TAPE45	Output	Data for restart or refinement of uncertainty analysis.

To avoid exceeding the small core memory space (which is 160,000 octal words) of the CDC 7600 computer at INEL, the FRAP-T5 code is overlayed. The overlay is generated by the SEGLOAD program, which is part of the CDC 7600 computer software. This program is given directives which specify the manner in which subroutines are to be put into groups. The groups may occupy common positions in small core memory. But only one group is in small core memory at any given time, while the other groups are stored in large core memory or on disk.

The directives that the SEGLOAD program is given are shown in Table A-II. In addition to the directives which specify the manner in which the subroutines are grouped together, GLOBAL directives are also necessary. These directives make all of the common blocks in FRAP-T5 accessible to all of the subroutine groups.

The overlay generated by the SEGLOAD directives is similar to the root system of a tree. This is shown in Figure A-1. Eleven groups of subroutines are shown. Each group is defined to be a branch. The branches are numbered at the top of each group. The first word in each branch has a common point of storage in small core memory. Two of the branches, 3 and 5, have additional branches. These additional branches are shown in Figures A-2 and A-3, respectively. The highest level of small core memory storage, which has a word location of 153,000, occurs in branch 3.

TABLE A-II

SEGLOAD DIRECTIVES FOR FRAP-T5

```
T1  TREE  HEAT-(T3,REFLOOD,GAPHTR,HTISST,COOL)
T2  TREE  DEFORM-(FCM1,FRAIL,FCM12,BALOON)
T3  TREE  HTRC-(QDOT,EMQDOT)
T4  TREE  ANSWER-(READIN,DESIGN)
  TREE FRAPT5-(CARDIN,INITIA,T1,PLNT,T2,GSFLOW,MARYJN,PRNTOT,FRIDAY,LACE
,DE,T4)
      GLOBAL   DESNBL
   GLOBAL STH2OC
      GLOBAL FTBLCM
      GLOBAL BLK1
      GLOBAL EXCB,LACEMDL,FLECHT,HTCB,FRPSTO,MATPRC,PHYPRO
      GLOBAL RESTR1,REST11,PASSVB,RESTB2,RESI12,RESTR3,REST13
      GLOBAL PRNTB,DIALB
      GLOBAL DFRMB,ERCB,FCM1WA,FCM1W2
      GLOBAL FRAPC
    GLOBAL  DUMP,GRS2A4,GRS2A3,BDGR2,BDGR5,BDGR4
   GLOBAL BJMS,GRS023,GRS0A3,GRS0A2,GRS0A4,BDG020,BDGR
      GLOBAL IO,BUF,,Q8,IO,,FCL,C,
      INCLUDE INCOM=;
FRAPT5 INCLUDE  FRAPI,FRAP,BLCDAT,ERROR1,ERROR1
FRAPT5 INCLUDE       PLOTW,TIMSET,ZEROUT,MOVE
FRAPT5 INCLUDE PLENU,PRNTMP,TIMSTP,USWELL,CELMOD,SPROPI,SWLCUV
FRAPT5  INCLUDE  CCP,CTHCON,ZOEMIS
FRAPT5  INCLUDE PACHED
FRAPT5 INCLUDE GRSDAT
FRAPT5  INCLUDE  DRIVER
GSFLOW  INCLUDE  GAPPRS,CUISCO
INITIA  INCLUDE  GAPPRS,POWINP
CARDIN INCLUDE  EXCINP
CARDIN  INCLUDE                FLDINP,LACE,KTABLE;
CARDIN INCLUDE POWINP,THMPRP,HTIINP,BOOBOO,DIALST,ECHOT,NBNDY
CARDIN INCLUDE INP,INP2,INP5,INP6,INP8,CUI,LINK,MODER,INPUPK
CARDIN INCLUDE       PLTINP,GPRINP,COOLIN,CARDPR,GPCINP,MODPID
CARDIN  INCLUDE  RLPST2,FTHCON
```

TABLE A-II (continued)

```
HEAT   INCLUDE        POWER,METWTB,EMSSF2,HADATA
HEAT   INCLUDE   BDCOND,EMSSF1,ROOT1,FEMISS,CMHARD
HEAT   INCLUDE  HTITDP,SURFGC
HEAT   INCLUDE  PRNTC,SLP2,SLIPR,SURTEN,THCON,CHITOX
HEAT   INCLUDE  VISC,VOID,QCON:
HEAT   INCLUDE ARYMDI,ASTOR
HEAT   INCLUDE  SIMQ,GAPHTC,ASET,IDXGN1,IDXGN2,FTHCON
HEAT   INCLUDE  GTHCON,EMGTON,GVISCO
HTRC   INCLUDE  PCHF,PROFAC,EHHTRC
REFLOOD INCLUDE  WCORR
PLNT   INCLUDE  GTHCON,EMGTON,GVISCO
PLNT   INCLUDE  THETAV,SIMQ,IDXGN1,IDXGN2
DEFORM  INCLUDE CHLIMT,CTHEXP,REPACK
DEFORM INCLUDE  STRAIN,STRESS,FBLOCK
DEFORM  INCLUDE  FELHOD,CSTRAN,FPOIR
FCM1   INCLUDE                          CLADF,CLOSE,COUPLE
FCM1   INCLUDE  GAPT,STACK
FRAIL  INCLUDE          BDTR,BFRAC,CDTR,CRERUP,DFRAC,DLGAM,EUMELT
FRAIL  INCLUDE  FSIGT,FSTEMP,FSTRS,HCFF,LCFF,MELT,NDTR

FCM12  INCLUDE  CLOS2,GAPT2,PELLET,AXRACH,TRANSF,EQUAL1,EQUAL2
FCM12  INCLUDE  STRAN1,CREP1,CRIP1,STRES1,EPRESS,STRAN2,STRES2
FCM12  INCLUDE   CREEP
BALOON  INCLUDE  RADII,WRITE
PRNTOT INCLUDE         FEMISS,ENERGY,PRNTAZ
PRNTOT  INCLUDE  CANEAL,COBILD
PRNTOT  INCLUDE  ASET,IDXGN1,IDXGN2,GAPHTC,FTHCON:
PRNTOT  INCLUDE  EMSSF2,CMHARD,GTHCON,EMGTON,GVISCO
PRNTOT  INCLUDE  WRITER,RESTRW,RLPST3
MARYJN  INCLUDE  GRASS,GRASS2,GRASS3,GRASS4,GRASS5
      END  DRIVER
```

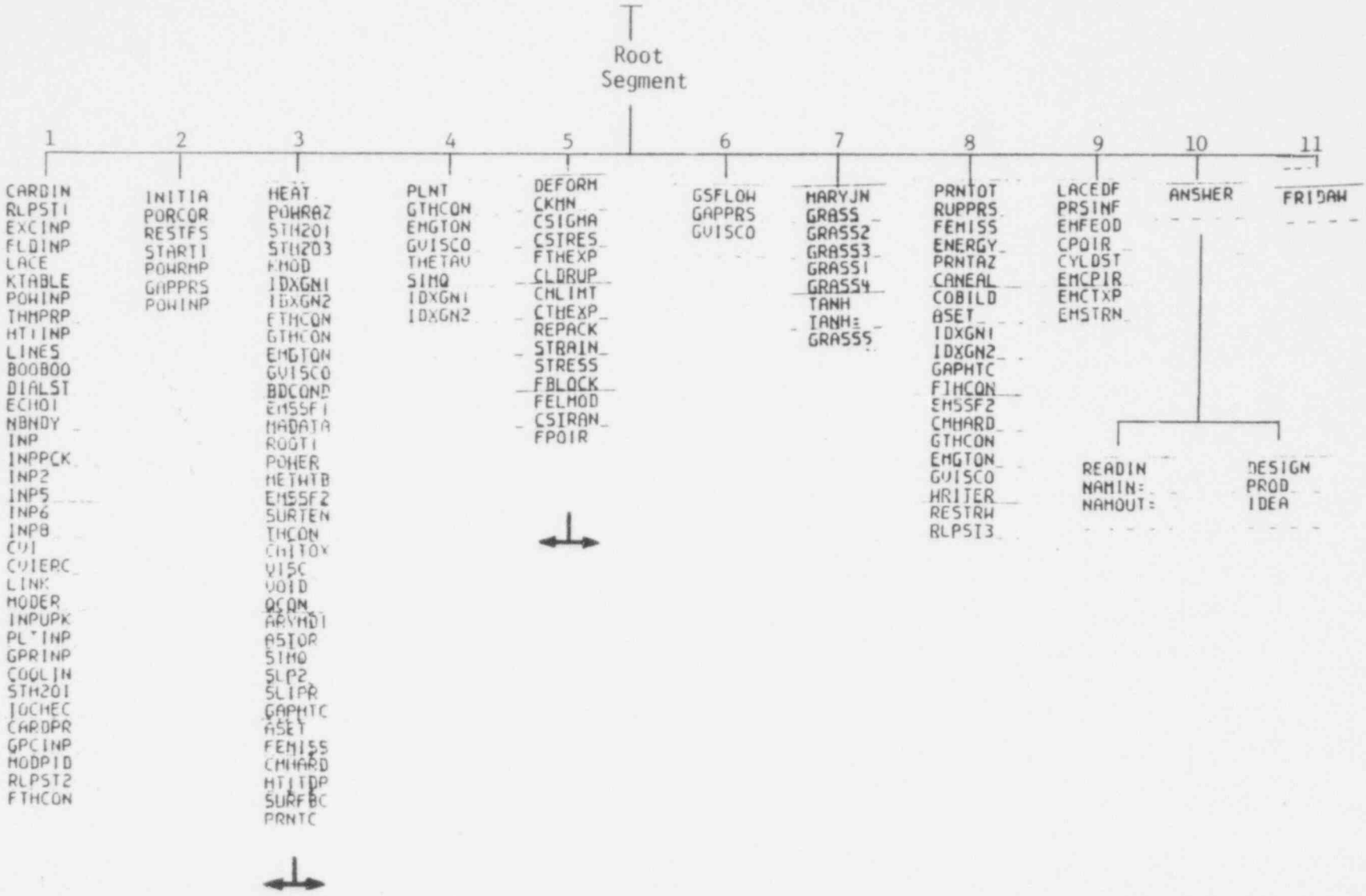

Fig. A-1 Overlay structure of FRAP-T5.

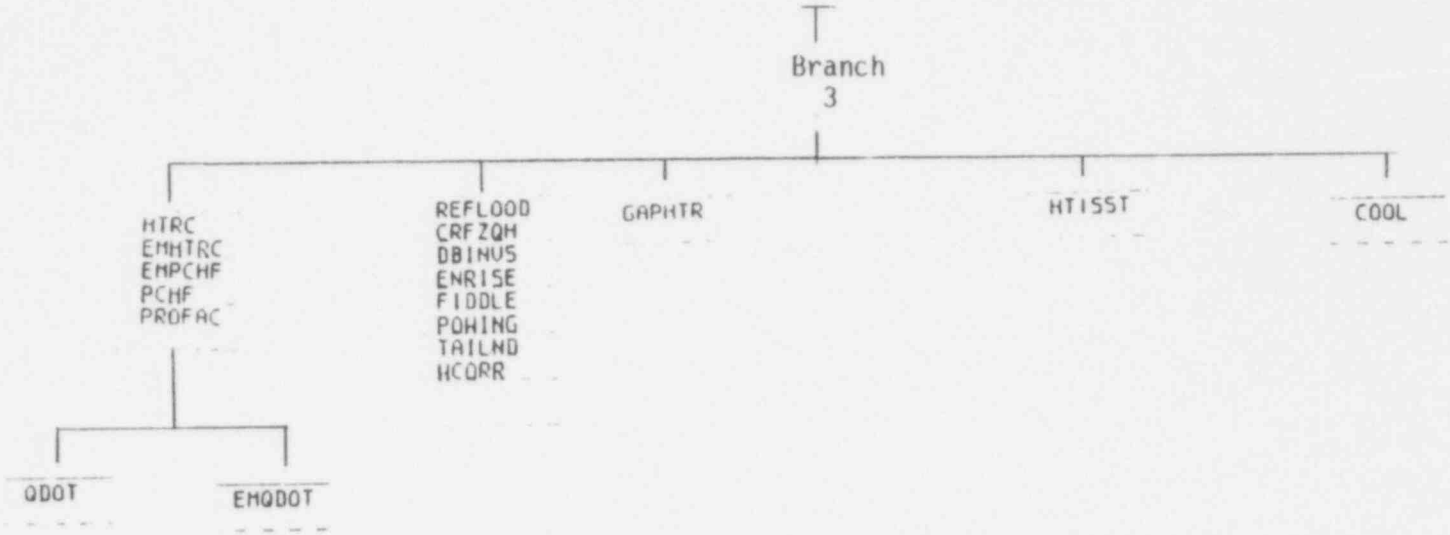

Fig. A-2 Overlay structure of Branch 3.

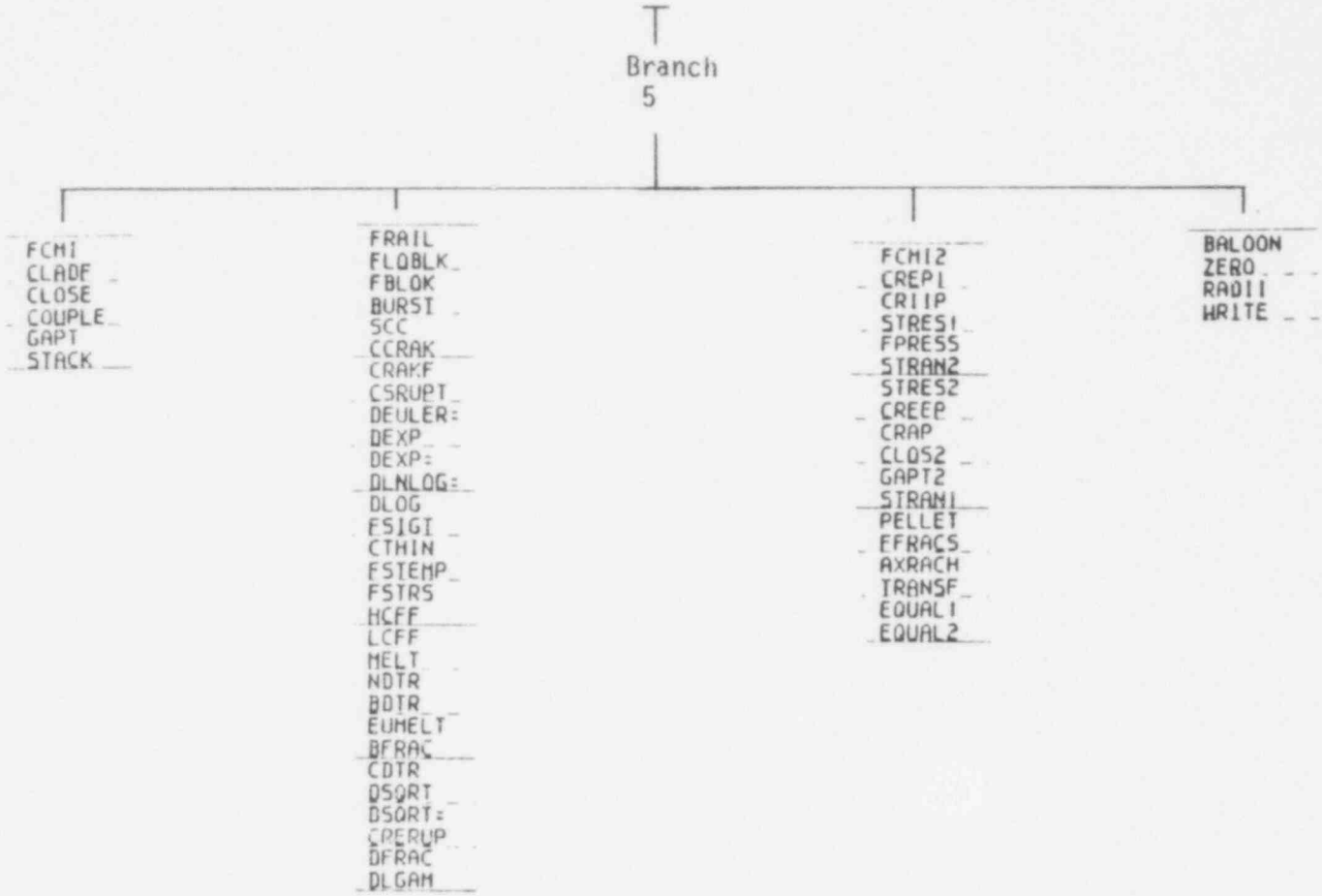

Fig. A-3 Overlay structure of Branch 5.

2. INPUT DATA CARDS

For the purpose of better describing the contents of FRAP-T5 input data cards, the data deck has been divided into several data blocks. Each data block is read in by a different input subroutine of the code. The information contained in each data block is summarized in Table A-III. The data blocks are described below in the order they follow in the input data deck. The type of data contained in each data block is identified, and the column location, format, name, and definition of each piece of input data is given.

The input data can be in either the British or SI system of units. The two systems of units cannot be mixed. If SI units are specified,

TABLE A-III

INFORMATION CONTAINED IN EACH DATA BLOCK

Data Block	Information
U	Uncertainty analysis data.
1	Axial nodalization, numerical solution control, options for phenomena models, fuel and cladding design parameters, restart control, multipliers on models, reflood model input.
2	Specification of range and detail of generated thermal property tables.
3	Radial mesh layout, accuracy of temperature solution, radial power distribution.
4	Power history, axial and azimuthal power distribution.
5	Boundary conditions, critical heat flux and film boiling correlation options, coolant condition input.
6	Fuel and cladding surface roughness.
7	Internal gas content and quantity, plenum size, plenum spring geometry.
8	Plotting parameters.

all data must be input in SI units. Within either system, the required unit for each input quantity is given below.

Input format is indicated by the character F, I, and A. F denotes that floating point numbers are to be input. For this case, exponents must be right hand adjusted and a decimal point must be present. An I denotes that integer numbers are to be input. The integers must be right hand adjusted. No decimal point can be present. An A denotes that alphanumeric characters are to be input. This input is used to specify labels for plot axes and titles.

When the restart option is used, the problem solution starts from the end time of a previous computer run. Only a portion of the previous input cards is required. This is a change from previous versions of FRAP-T, which required submittal of the entire input deck.

A FRAP-T4 input deck requires a few changes to be compatible with FRAP-T5. First, two extra cards are required. These are the cards numbered 0.1 and 1.4.2. Next, Card 1.7 has been changed. This card is input if two-dimensional heat conduction calculations are to be performed. The first variable on this card in the FRAP-T4 input has been eliminated and the other variables shifted to the left by ten columns. Next, if an unequal spacing of axial nodes has been specified, node elevations instead of node length are input to FRAP-T5. This change occurs on Card 1.12. Last, some minor changes have been made to Card 1.14, which controls restarting.

The first card in the input deck specifies options for restart and uncertainty analysis. This card was not required in FRAP-T4 input.

Card 0.1 Input Control Card.

Columns	Format	Name	Quantity
1-5	I	NCARDS	If NCARDS = 0, a previous calculation is to be continued. This continuation requires a STAGE control card, which assigns the restart tape number for file TAPE1. Card 0.1 and Data Block 8 are the only input cards read. If NCARDS = 1, a new calculation is to be performed. A complete input deck is required. If NCARDS = 2, a second transient calculation is performed considering the history effects of a previous transient. The time read on the restart tape is backshifted to zero. This time backshift permits analysis of a second transient with initiation at a time of zero. The power history and coolant condition history can then assume that a time of zero corresponds with time of transient initiation. The steady state condition of the fuel rod is calculated to determine the fuel rod initial conditions. If NCARDS = 2, Card Group 1.10, Data Blocks 4, 5, and 8 must be input. These cards contain time step, power, coolant condition, and plot scaling data, respectively.

Columns	Format	Name	Quantity
6-10	I	IUNCRT	If IUNCRT = 0, no uncertainty analysis is to be performed. If IUNCRT = 1, an uncertainty analysis is to be performed. Data Block U must be input.
11-20	F	TEND	End time of calculations (sec). If NCARDS = 1, leave these columns blank. Since the reference frame for time is always the same, end time for a restart run is equal to the end time of the previous run plus the additional amount of problem time for which a transient response is wanted. If NCARDS = 2, the end time of the previous run should not be added.

Data Block U Uncertainty Analysis Data.

If IUNCRT = 0 on Card 0.1, omit Data Block U. If IUNCRT = 1, input this data block between Cards 0.1 and 1.1.

All input for Data Block U is NAMELIST format. The first card in the data block only contains "$IN" in columns 1 through 3. The last card only contains "$END" in columns 1 through 4. All input variables have been assigned default values. If no default values are to be modified, no further input cards are required. If an input variable is to be modified, a card must be input which contains the variable name and the new variable value. This is further clarified in the sample input section following the list of uncertainty analysis input variables.

The list of uncertainty analysis input variables follows. Only those variables whose default values are to be overridden need to be input.

Variable	Value
IFLAG	Flag for check runs. 0 - design and confounding arrays (default) 1 - add nominal FRAP run 2 - add complete uncertainty analysis
LTYPE	Type of analysis desired. 1 - linear (default) 2 - linear plus foldover 3 - linear plus quadratic 4 - linear plus foldover plus quadratic
LPB	Plackett-Burman design flag. 0 - fractional factorial design (default) 1 - Plackett-Burman design
IPRINT	Flag for additional experimental design data including design generators and one and two factor aliases. 0 - no (default) 1 - yes
ISTART	Flag for restarting from previous analysis. 0 - no (default) 1 - yes

Variable	Value
LFAC(N)	List of factors from Table A-IV to be included in the analysis. Order is important. Example, LFAC(1) = 2, 4, 8, 5, 6, will include these five factors in the analysis in this order in the experimental design and confounding arrays (default is 0).
LRES(N)	List of responses from Table A-V. Order is not important. Individual responses may be listed more than once. (For example, a given response may be desired at more than one axial node). Not to exceed 10 total responses (default is 0).
NODE(N)	Axial node at which LRES(N) is to be computed. List must match LRES(N) one for one. For example, NØDE(3) must be axial node at which LRES(3) is to be computed (default is 1).
C(I, J, K)	Uncertainty factors. Factors are described by polynomials of up to third order in temperature (I) in four temperature ranges (J) for approximately 50 factors (K).
	Values are one standard deviation. Multiplication factors should be input as a decimal fraction. Example: An uncertainty factor of

Variable	Value
	1.25 indicating a 25% one-sigma uncertainty should be input as 0.25. The code will add the 1.00 when default values are as given in Table A-IV.
TL(J, K)	Upper temperature limits describing ranges applicable to uncertainty factor polynomials. If no temperature range or uppermost limit, enter 0. Default values are given in Table A-IV.
AMU(L, K)	First four dimensionless central moments of the uncertainty factor distributions. Assumed to apply over all temperature ranges. Normal distribution is default.
FACTOR(K)	Flag for additive or multiplicative uncertainty factors. 0 - additive 1 - multiplicative Default values are given in Table A-IV.

To amplify the input instructions for Data Block U, input data is shown below for an example problem.

Assume that an uncertainty analysis is to be performed using factors 1, 5, 13, 3, and 37 from Table A-IV, in that order, as independent variables. Responses 1, 2, 3, 4, and 5 are chosen from Table A-V and are desired at node 8 except that response 2 is desired at nodes 1 and 15 as well. A linear fractional factorial design is chosen with no

TABLE A-IV

DEFAULT UNCERTAINTY FACTORS

LFAC	Source	Additive (A) or Multiplicative (M)[a]	Factor	Temperature Range (K)
1	Fuel specific heat	M	1.02	T < 500
			1.012 + 1.6E - 5xT	500 < T < 3000
			1.06	3000 < T
2	Fuel thermal conductivity	A	0.4 $\frac{W}{m-K}$	--
3	Fuel emissivity	M	1.10	--
4	Fuel thermal expansion	A	0.25E-5 xT $\frac{m}{m}$	T < 500
			0.00125	500 < T
5	Fuel elastic modulus	A	.037E11 (Pascals)	--
6	Poisson's ratio	A	0.094	
7	Fuel creep	--	(TBD)[b]	--
8	Fuel fracture strength	A	0.19 (Pascals)	--
9	Fuel swelling	--	(TBD)	--
10	Fuel restructuring	--	(TBD)	--
11	Fuel densification	--	(TBD)	--
12	Fission gas release	--	(TBD)	--
13	Cladding specific heat	A	10 (J/kg-K)	T < 300
			10	300 < T < 1090
			25	1090 < T < 1300
			100	1300 < T
15	Zirc oxide emissivity	A	0.10	--

TABLE A-IV (continued)

LFAC	Source	Additive (A) or Multiplicative (M)[a]	Factor	Temperature Range (K)
16	Zirc oxide thermal conductivity	M	1.20	--
17	Cladding axial thermal expansion	M	1.20 1.50	T < 1073 1073 < T
18	Cladding diametral thermal expansion	M	1.10 1.50	T < 1073 1073 < T
19	Cladding elastic modulus	M	1.10 1.20	T < 1083 1083 < T
20	Cladding strength coefficient	A	29.E6 (Pascals)	--
21	Cladding circumferential rupture strain	A	0.08 -0.91 + 1.25E - 3 T 4.94 - 4.125E - 3xT 0.11	T ≤ 800 800 < T < 1090 1090 < T < 1170 1170 < T
22	Cladding Meyer hardness	--	(TBD)	--
23	Cladding creep rate	--	(TBD)	--
24	Cladding shear modulus	A	9.E9 (Pascals)	--
25	Cladding oxidation	M	1.175 1.065	T < 1523 1523 < T
26	Gas thermal conductivity	A	-0.0068 + 1.61E - 5xT	--
27	Gas viscosity	M	1.05	--
28	Gap heat transfer	M	1.25	--

TABLE A-IV (continued)

LFAC	Source	Additive (A) or Multiplicative (M)[a]	Factor	Temperature Range (K)
29	Alpha-Beta transition temperature	A	10 (K)	--
30	Pellet stack height	M	1.001	--
31	Cladding outer diameter	M	1.001	--
32	Fuel density	M	1.0067	--
33	Pellet shoulder radius	M	1.034	--
34	Pellet dish depth	M	1.034	--
35	Pellet height	M	1.001	--
36	Pellet dish volume	M	1.034	--
37	Pellet outer radius	M	1.001	--
38	Cladding inner radius	M	1.001	--
39	Cladding outer radius	M	1.001	--
40	Cladding roughness	M	1.100	--
41	Fuel roughness	M	1.100	--
42	Amount of gas in rod	M	1.034	--
43	Plenum volume	M	1.001	--
44	Cold pressure	M	1.034	--
45	Mole fractions of gas components	--	(TBD)	--
46	Unused	--	--	--

TABLE A-IV (continued)

LFAC	Source	Additive (A) or Multiplicative (M)[a]	Factor	Temperature Range (K)
47	Initial temperature estimate	--	(TBD)	--
48	Power history	M	1.050	--
49	ANS decay heat curve	M	1.067	--
50	Unused	--	--	--
51	CHF factor	M	1.080	--
52-60	Unused	--	--	--

a. Additive (A) or Multiplicative (M) refers to the manner in which the factor was applied. That is, percentage uncertainties were multiplicative whereas absolute uncertainties were additive.

b. (TBD) - to be determined or presently inactive.

TABLE A-V

RESPONSES

LRES	Response
1	Fuel centerline temperature (K)
2	Cladding surface temperature (K)
3	Cladding hoop stress (Pascals)
4	Cladding axial stress (Pascals)
5	Permanent cladding hoop strain
6	Permanent cladding axial strain
7	Gap pressure (Pascals)
8	Cladding axial displacement (mm)
9	Heat transfer coefficient at rod surface $\frac{W}{m^2 - K}$
10	Heat transfer coefficient across gas gap $\frac{W}{m^2 - K}$
11	Structural radial gas gap (mm)
12	Cladding hoop strain
13	Cladding radial strain
14	Cladding effective stress (Pascals)
15	Fraction of failed fuel rods

additional printout or restarts. Uncertainty factor 1 is to be changed, for the purpose of illustration, to the values given in Table A-IV. This is a check run executing the nominal FRAP-T deck once. The necessary input is as follows:

```
$IN
LFAC(1)      =  1, 5, 13, 3, 37,
LRES(1)      =  1, 2, 2, 2, 3, 4, 5,
NODE(1)      =  8, 8, 1, 15, 8, 8, 8,
```

```
IFLAG          =  1,
C(1, 1, 1)     =  0.2, 0., 0., 0.,
C(1, 2, 1)     =  0.12, 1.6E-5, 0., 0.,
C(1, 3, 1)     =  06, 0., 0., 0.,
C(1, 4, 1)     =  0., 0., 0., 0.,
TL(1, 1)       =  500., 3000., 0., 0.,
AMU(1, 1)      =  0., 1., 0., 3.,
FACTOR(1)      =  0., 1., 0., 3.,
$END
```

Data Block 1. General Data.

Cards 1.1 and 1.2 contain several input variables that control the selection of models. These input variables are model option switches. The model recommended for general use is specified by setting the model option switch to zero. Special conditions or the requirements of a more detailed analysis may, however, preempt the use of the thus-recommended model.

Card 1.1

Columns	Format	Name	Quantity
1-5	I	NROD	Number of fuel rods. Always input the integer 1.
5-10	I	NCHN	Number of coolant subchannels surrounding fuel rods. Because of array dimension limitations, NCHN must equal 1.
11-15	I	NAXN	Number of axial nodes (NAXN $\leq$ 20). If NGSFLØ = 1 (columns 31-35), NAXN $\geq$ 3. If no minus sign in front of NAXN, code generates evenly spaced mesh. An example of generated mesh is shown in

			Figure A-4. At each axial node, calculations of fuel rod state from fuel center to cladding surface are performed on a plane perpendicular to fuel rod longitudinal axis and passing through the center of the axial node. If minus sign input, axial node elevations are specified by Card Group 1.12.
16-20	I	NPLNT	If NPLNT = 0, plenum gas temperature model is used. If NPLNT = 1, plenum gas temperature set to coolant temperature at top axial node plus $10^{o}F$.
21-25	I	NDT	Number of time step - time pairs used to prescribe time step during problem solution. See Card Group 1.10 input instruction for further clarification. NDT $\leq$ 20. If constant time step, NDT = 0.
26-30	I	NUNIT	If this field is zero or left blank, data are input in British units. If the integer 1 is put in column 30, data are input in SI units. Code output for NUNIT = 0 or 1 is in the same system of units that is selected for input. If the integer 2 is put in column 30, data are input in British unit, but calculations and plots are output in SI units.
31-35	I	NGSFLO	If NGSFLO = 0, gas flow between plenum and gas gap is not modeled. Instead, pressure equilibrium is assumed to

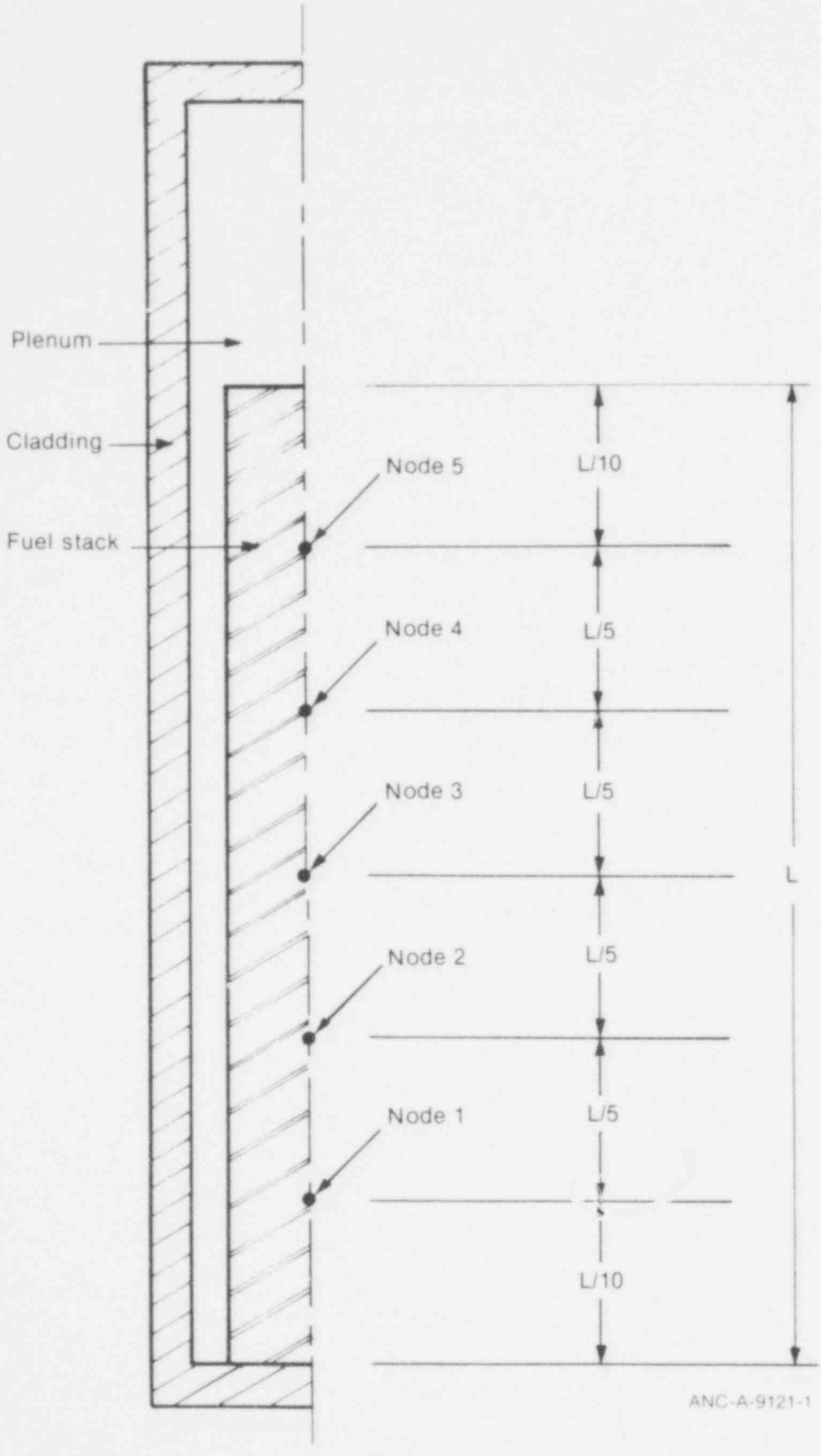

Fig. A-4 Example of evenly spaced axial node mesh for case NAXN = 5.

			instantly occur, so that plenum and gas gap are always at the same pressure. If NGSFLO = 1, gas flow between plenum and gas is modeled. This requires NAXN $\geq$ 3.
36-40	I	MØDMW	If MØDMW = 0, metal-water reaction calculated according to Cathcart model. Also, oxygen diffusion inside the oxide layer is calculated. If MØDMW = 1, metal-water reaction is not modeled. If MØDMW = 2, cladding oxidation calculated according to Baker-Just model.
41-45	I	MØDFD	Two deformation models are available. The first model, called FRACAS-I, assumes no stress deformation of the fuel. The second model, called FRACAS-II, accounts for stress deformation of the fuel. If fuel deformation due to stress is considered insignificant or if a reduction in computer running time has high priority the FRACAS-I model should be chosen. If fuel deformation due to stress is significant, the FRACAS-II model should be chosen. If MØDFD = 0, the FRACAS-I deformation model is used, with the fuel assumed to have radial cracks extending from fuel surface to fuel center (free thermal expansion) and a relocation of 0.25% times fuel pellet radius for structural calculations. No relocation in thermal or pressure calculations. If

			MØDFD = 1, the GAPCON-THERMAL-1 code[A-1] fuel deformation model is used. No fuel relocation assumed. If MØDFD = 2, same as MØDFD = 0, but no fuel relocation is assumed. If MØDFD = 3, same as MØDFD = 0, but variable fuel relocation assumed in thermal and pressure calculations. Fuel conductivity modified to account for cracks associated with fuel relocation. No relocation assumed in structural calculations. If MØDFD = 7, the FRACAS-II deformation model is used.
46-50	I	MØDGPC	IF MØDGPC = 0, the Ross and Stoute[A-1] gap conductance model is used.
51-55	I	NFASTF	If NFASTF = 0, fast neutron flux assumed to have same axial profile as power profile specified by Card Group 4.4. Otherwise, NFASTF = number of pairs of normalized fast neutron flux versus elevation used to prescribe axial distribution of fast neutron flux on Card Group 1.13. NFASTF $\leq$ 25.
56-60	I	MPDCAY	If MPDCAY = 0, decay heat not added to fuel rod power specified by card group 4.2. If MPDCAY = 1, decay heat is added to fuel rod power and is computed according to ANS formula for decay heat.

66-70	I	NDIM	Indicator of number of dimensions in heat conduction calculations. If NDIM = 0, only radial heat conduction is considered. If NDIM = 1, radial-azimuthal heat conduction at one or more axial nodes is considered.

Card 1.2

Columns	Format	Name	Quantity
1-5	I	NVØID	Switch to model partial length central void in fuel. 0 = no, 1 or 2 = yes. If NVØID = 1, no instrumentation in void. If NVØID = 2, instrumentation is present.
6-10	I	NFMOD	Switch to set fuel rod failure model. 0 = FRAIL subcode general model, 1 = FRAIL subcode tube burst model with flow blockage calculations.
11-15	I	NDIAL	Switch to apply multipliers or addition terms (dials) to selected fuel rod models. 0 = no, 1 = yes. If NDIAL = 1, Card Group 1.19 must be input.
16-20	I	NSWHTC	Switch to modify cladding surface heat transfer coefficient to account for ballooning of neighboring fuel rod. NSWHTC = 0 = no modification. NSWHTC = 1 = modification. If NSWHTC = 1, Cards 1.15 and 1.16 must be input.
21-25	I	NREFLD	Switch to compute cladding surface heat transfer coefficient during

			reflooding of core following reactor vessel blowdown. 0 = no, 1 = yes. If NREFLD = 1, Card Group 1.20 must be input.
26-30	I	NSWLAC	Switch for Licensing Audit Code (LAC) calculations. If NSWLAC = 1, Card Group 1.21 must be input. 0 = no 1 = yes
31-35	I	NPØ	Number of printout interval-time pairs used to specify problem time intervals at which fuel rod state is to be printed. If constant printout interval, leave these columns blank. NPØ $\leq$ 20. If NPØ > 0, Card 1.17 must be input.
36-40	I	NFCMI	Switch to force calculations by the FRACAS subcode after cladding failure predicted, so that post-failure stresses due to pellet cladding mechanical interaction are computed. 0 = no, 1 = yes. If NFCMI = 1, however, the balloon model calculations are bypassed. If NFCMI = 0, the only deformation assumed to occur after cladding failure is that due to thermal expansion.
41-45	I	NPRSW	Internal power ramp switch. At the problem start, FRAP-T internally generates a power ramp that increases fuel rod power from zero to full power in small increments of power. If

			fuel-cladding contact at full power not expected, the internal power ramp can be bypassed and computer time saved. 0 = generate power ramp 1 = bypass power ramp
51-55	I	NSWGRS	Switch to perform fission gas production and release with the GRASS[A-2] Subcode. 0 = no, 1 = yes. If NSWGRS = 1, the computer run time will increase about a factor of four due to the complex nature of the GRASS subcode. Calculations cannot be restarted. Maximum number of axial nodes = 10. Maximum number of radial nodes in fuel = 15.
56-60	I	NRADSH	Switch to model radiation heat transfer between fuel rod and surrounding flow shroud. If radiation heat transfer not to be modeled, NRADSH = 0. Otherwise, NRADSH = number of temperature-time pairs in Card Group 1.18, which supplies temperature history of flow shroud, NRADSH $\leq$ 25. Flow shroud assumed to be zircaloy with an oxide layer 1.4 microns thick on inside surface. If NRADSH > 0, NSWC = 4 on Card 5.1 is required.
61-65	I	NBOTPL	Switch to model lower gas plenum in fuel rod. 0 = no, 1 = yes. If NBOTPL = 1, the lower plenum geometry must be specified on Card 7.2.

66-70	I	NPRPRN	Switch to print out fuel rod conditions at each power level of initial power ramp. 0 = no 1 = yes

Card 1.3

Columns	Format	Name	Quantity
1-10	F	TO	Initial problem time (seconds).
11-20	F	TMAX	Final problem time (seconds).
21-30	F	DT	Time step (seconds). If NDT > 0 on Card 1.1, this field is not used. If used, DT > 0. If NDIM > 0 on Card 1.1 (multidimensional heat conduction calculations performed), DT should not exceed value of about 0.02, because the explicit numerical solution of multidimensional heat conduction is not stable for a time step much larger than 0.02 sec.
31-40	F	DTPO	Problem time intervals at which calculated fuel rod state will be printed (seconds). If printout desired at end of each time step, set DTPO to zero. If NPO > 1 on Card 1.2, omit DTPO input.
41-50	F	RL	Cold length fuel pellet stack (ft or m).
51-60	F	DROD	Cold outer diameter of fuel rod (ft or m).

61-70	F	TEMPO	Cold state temperature of fuel rod (^{o}F or K). The fuel rod dimensions given in the input must correspond with this temperature.
71-80	F	COLDW	Reduction of cross-sectional area of cladding by cold working process. COLDW = $(A_o-A)/A_o$ Where A_o = cross-sectional area prior to cold working, A = cross-sectional area after cold working.

Card 1.4.1 Pellet Data

Columns	Format	Name	Quantity
1-10	F	RHØF	Cold state density of fuel (lbf/ft^3 or kg/m^3).
11-20	F	RSHD	Cold state radius to pellet shoulder (ft or m). Shoulder defined to be point of primary contact at pellet interfaces. See Figure A-5.
21-30	F	DISHD	Cold state depth of pellet dish (ft or m).
31-40	F	PELH	Cold state height of fuel pellet (ft or m).
41-50	F	DISHVO	Cold state volume of pellet dish (ft^3 or m^3); sum of top and bottom dish volumes.
51-60	F	FRPO2	Fraction by weight of fuel that is PuO_2.

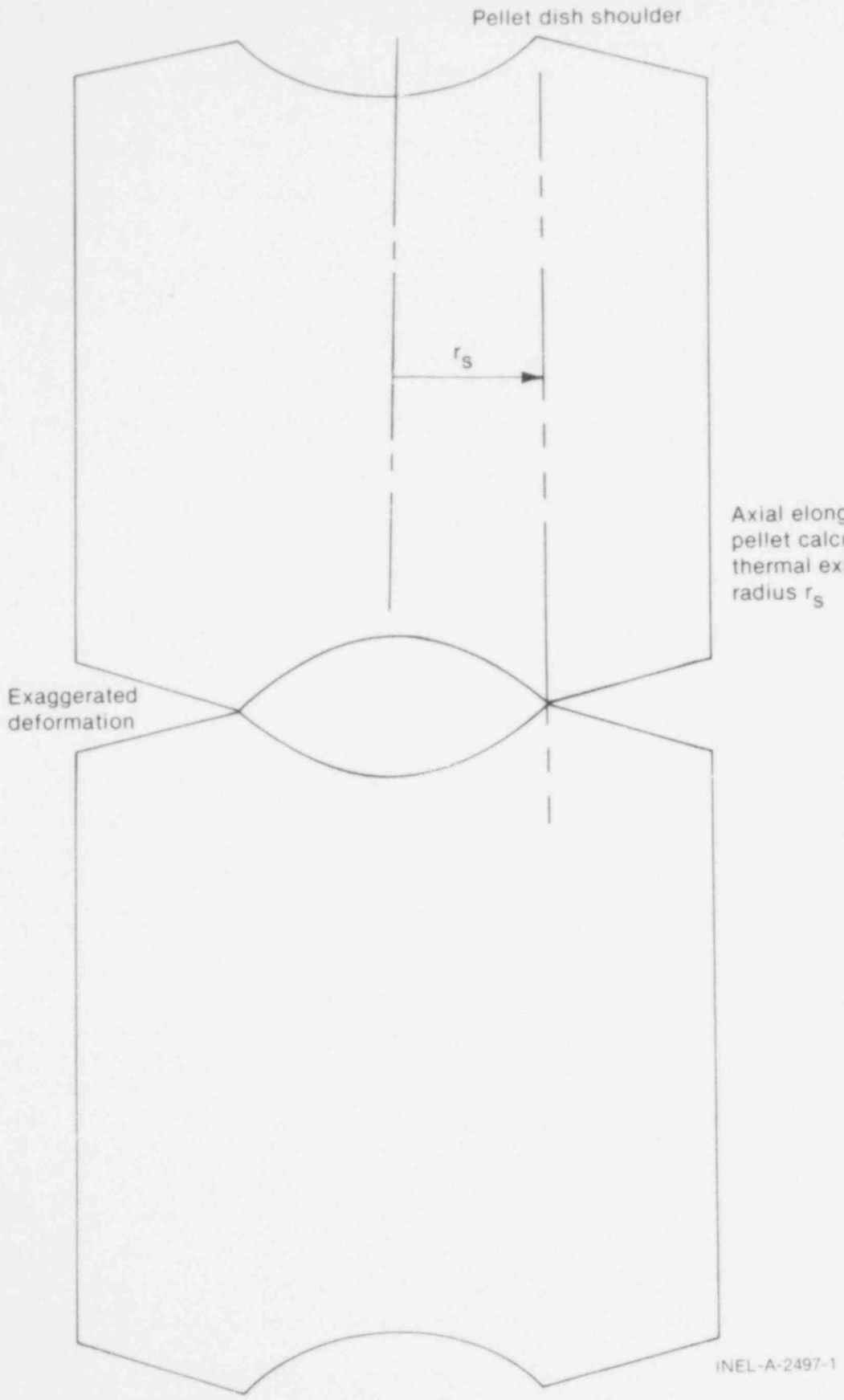

Fig. A-5 Definition of pellet shoulder radius.

61-70	F	BU	Burnup of fuel (MWs/kg). Burnup (MWd/MT) x 86.4 = Burnup (MWs/kg)
71-80	F	PITCH	Center to center spacing of fuel rods (ft or m). If PITCH = 0.0, no restraint to cladding ballooning is modeled. If PITCH > 0.0, restraint to cladding ballooning given by adjacent fuel rods is modeled. Also, the cladding instability strain is set equal to the rupture strain, so that full strain range of cladding ballooning is modeled by the FRACAS-I subcode. The BALLOON subcode is not used.

Card 1.4.2 Pellet Data.

Columns	Format	Name	Quantity
1-10	F	FOTMTL	Ratio of fuel oxygen atoms to uranium and plutonium atoms. Normally, FOTMTL = 2.0.
11-20	F	TSNTRK	Fuel sintering temperature (K). Normally, TSNTRK = 1600°C (1883 K).

Card 1.5 (Omit this card if NVOID = 0 Card 1.2.)

Columns	Format	Name	Quantity
1-10	F	ZVOID1	Distance from bottom of fuel stack to bottom of central void (ft or m).
11-20	F	ZVOID2	Distance from bottom of fuel stack to top of central void (ft or m). If central void extends along entire length of fuel stack, set ZVOID1 = 0 and ZVOID2 equal to fuel stack length.

Card 1.6 Numerical Solution Control and Cladding Flux History.

Columns	Format	Name	Quantity
1-10	F	PRSACC	Minimum fractional change in internal fuel rod pressure between two successive iterations before convergence is declared. If these columns left blank, program sets PRSACC to the recommended value of 0.001. This minimum change must occur at every axial node before convergence is declared. The test is $(p^{r+1} - p^r)/p^r < PRSACC$, where p^r symbolizes pressure at iteration number r. If PRSACC > 1.0, explicit solution method used. No iterations performed. Both deformation-pressure and temperature-deformation-pressure loops are only cycled once. Accuracy controlled only by time step. For steady state solution at first time step, accuracy internally set to 0.001. If implicit solution runs into convergence difficulties, explicit solution should be considered.
11-20	F	TMPACC	Minimum fractional change in temperature at any radial node between two successive iterations before convergence is declared. If these columns left blank, program sets TMPACC to the recommended value of 0.001.
21-30	F	FQCRIT	Factor which critical heat flux is multiplied by. If these columns left blank, program sets value of 1.0. If

			FQCRIT assigned a large value, prediction of film boiling can be precluded.
31-40	F	DTSS	Time step threshold (sec) for steady state heat conduction model. If time step as set by DT on Card 1.3 or DTMAXA array of Card Group 1.10 is greater than DTSS, steady state heat conduction model used. If not, transient heat conduction model used. If DTSS left blank, transient heat conduction model always used after first time step.
41-50	F	CFLUX	Axially averaged and time averaged fast neutron flux cladding exposed to during lifetime (neutrons/m^2-sec). Fast neutron is defined to be a neutron with an energy greater than 1 MeV.
51-60	F	TFLUX	Time span of cladding exposure to fast neutron flux (sec). The quantity CFLUX*TFLUX must equal axially averaged fast neutron fluence received by cladding.
61-70	F	PFAIL	If probability for fuel rod failure exceeds PFAIL, then fuel rod assumed to be failed. If these columns left blank, PFAIL set to value of 0.5.
71-80	F	DTMPCL	Maximum circumferential variation in cladding temperature during ballooning. If DTMPCL = 0.0, the temperature is assumed to be uniform.

Card 1.7 (Omit Cards 1.7 through 1.9 if NDIM = 0 on Card 1.1.)

Columns	Format	Name	Quantity
1-10	F	DØFSET	Offset of fuel stack centerline from cladding longitudinal axis (ft or m). Leave blank if fuel stack longitudinal axis corresponds with cladding longitudinal axis. If fuel pellet always in contact with one side of pellet, input the number 1.0.
11-20	F	DØFANG	Azimuthal angle along which fuel pellet shifted toward cladding inside surface (degrees). Azimuthal coordinate system must be consistent with that used to input azimuthal power variation on Card 4.5. Leave blank if DØFSET = 0.

Card 1.8 (Omit if NDIM = 0.)

Columns	Format	Name	Quantity
1-5	I	NAZ	Number of azimuthal sectors in heat conduction calculations (azimuthal sector defined in Figure A-6). Because dynamic storage is used, the upper bound of NAZ is only set by computer core storage limits.
6-10	I	NAZN	Number of axial nodes at which azimuthal heat conduction is to be considered.
11-5	I	NSYMM	Symmetry indicator. If NSYMM = 0, twofold symmetry (temperature distribution computed in quarter of fuel

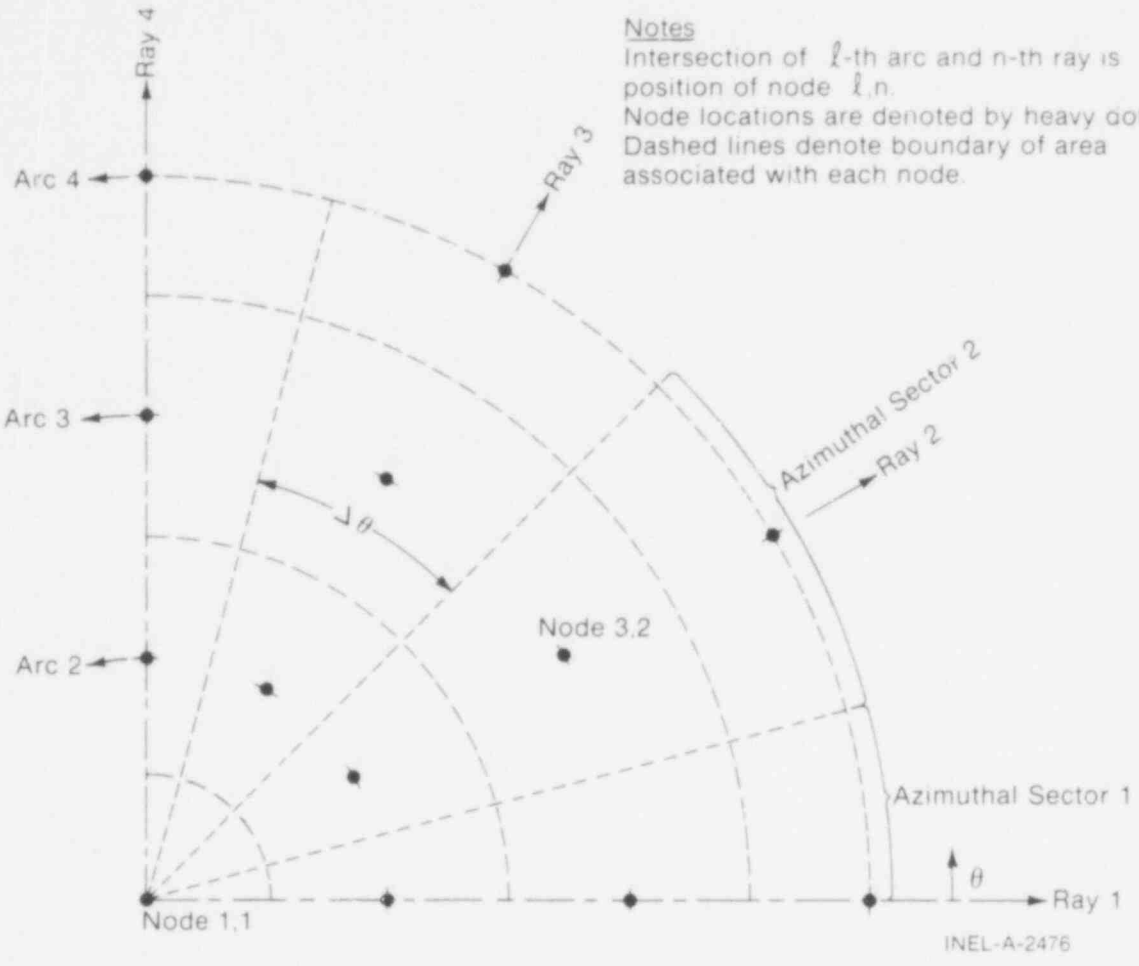

Fig. A-6 Mesh configuration for R-θ heat conduction.

rod). If NSYMM = 1, onefold symmetry (temperature distribution computed in half of fuel rod). If NSYMM = 2, no symmetry.

The computer core requirements increase as the spatial detail specified for the multidimensional temperature distribution increases. Storage requirements increase according to the equation $S = 5\ N_\theta\ N_Z\ N_R + 20\ N_\theta\ N_Z$, where S = words of storage required, N_θ = number of azimuthal sectors, N_Z = number of axial nodes at which azimuthal heat conduction is to be considered, and N_R = number of radial nodes. Symmetry conditions are taken advantage of to reduce storage requirements. If twofold symmetry exists, a given azimuthal spatial detail is accomplished with a quarter of the azimuthal sectors required when no symmetry exists.

Card(s) 1.9 (Omit if NDIM = 0.)

Columns	Format	Name	Quantity
1-5	I	N1	First axial node at which azimuthal heat conduction is to be considered
6-10	I	N2	Second axial node at which azimuthal heat conduction is to be considered.

Repeat as necessary.

Card Group 1.10 Time Step History Cards.

If NDT $\leq$ 0 on Card 1.1, no cards are input. On these cards, every other 10-column field contains the maximum time step desired at the time specified in the 10-column field immediately to the right of it. The data are entered four pairs per card in order of increasing time until NDT pairs are described. A straight line interpolation between points specified by input is performed by the code. If quantities such as mass flux or pressure are oscillating rapidly, the time step history cards should be used to enforce a program step that is small compared to the period of the oscillations. Examples of the time step history specified for several different types of accidents are shown in Table A-VI. As a general rule, the time step should not exceed 0.1 sec for an implicit solution and 0.05 sec for an explicit solution. Cases in which the fuel rod temperature is changing slowly are an exception. If multidimensional heat conduction is being computed (NDIM > 0 on Card 1.1), then the time step should never exceed about 0.02 sec. The time step needs to be limited to this value in order to assure stability of the heat conduction calculations.

573 210

TABLE A-VI

EXAMPLES OF TIME STEP HISTORIES

Loss-of-Coolant Accident		Power-Cooling-Mismatch Accident		Reactivity Initiated Accident		Anticipated Transient Without Scram Accident		Slow Power Ramp		Power Ramp at 0.5 kW/m-sec, 2-D rθ Heat Conduction	
Time (sec)	Time step (sec)	Time (sec)	Time step (sec)	Time (sec)	Time step (sec)	Time (sec)	Time step (sec)	Time (sec)	Time step (sec)	Time (sec)	Time step (sec)
0.0	0.02	0.0	0.1	0.0	0.001	0.0	0.05	0	3600	0	0.02
0.05	0.02	100.0	0.1	2.0	0.001	10	0.05	36,000	3600	10	0.02
				2.1	0.005						
				10	0.005						
0.0501	0.05					10.1	0.1				
1.9	0.05					20	0.1				
2.0	0.1										
30.0	0.1										

Card 1.10.1 Number of Data Pairs.
(Omit if NCARDS = 0 or 1 on Card 0.1.)

Columns	Format	Name	Quantity
1-5	I	NDT	Number of time step-time pairs used to prescribe time step during problem solution. NDT $\leq$ 20.
11-20	F	DTPO	Problem time span between printout.

Card 1.10.2 Time Step-Time Data Pairs.

Columns	Format	Name	Quantity
1-10	F	DTMAXA(1)	Time step at time DTMAXA(2) (sec).
11-20	F	DTMAXA(2)	Time (sec).
21-30	F	DTMAXA(3)	Time step at time DTMAXA(4) (sec).
31-40	F	DTMAXA(4)	Time (sec) DTMAXA(4) > DTMAXA(2).

Repeat as necessary. After first card is filled with four pairs of data, continue putting data in same manner on second card. Continue in this manner until all pairs of data have been put on cards. An example of the time step history specified by Card Group 1.10 is shown in Figure A-7. A maximum of 20 time step pairs are allowed.

Card Group 1.11 Rod-to-Coolant Channel Connection Data.

The coolant channel geometry is assumed to be the same along the entire length of the fuel rods. No coolant subchannel can have an identification number greater than NCHN of Card 1.1. For only one coolant subchannel, input for Card Group 1.11 consists of one card with a 1 in column 5, 1 in column 15, and 1.0 in columns 16 through 20; rest of card is blank. A pictorial explanation of data input for Card Group 1.11 is shown in Figure A-8.

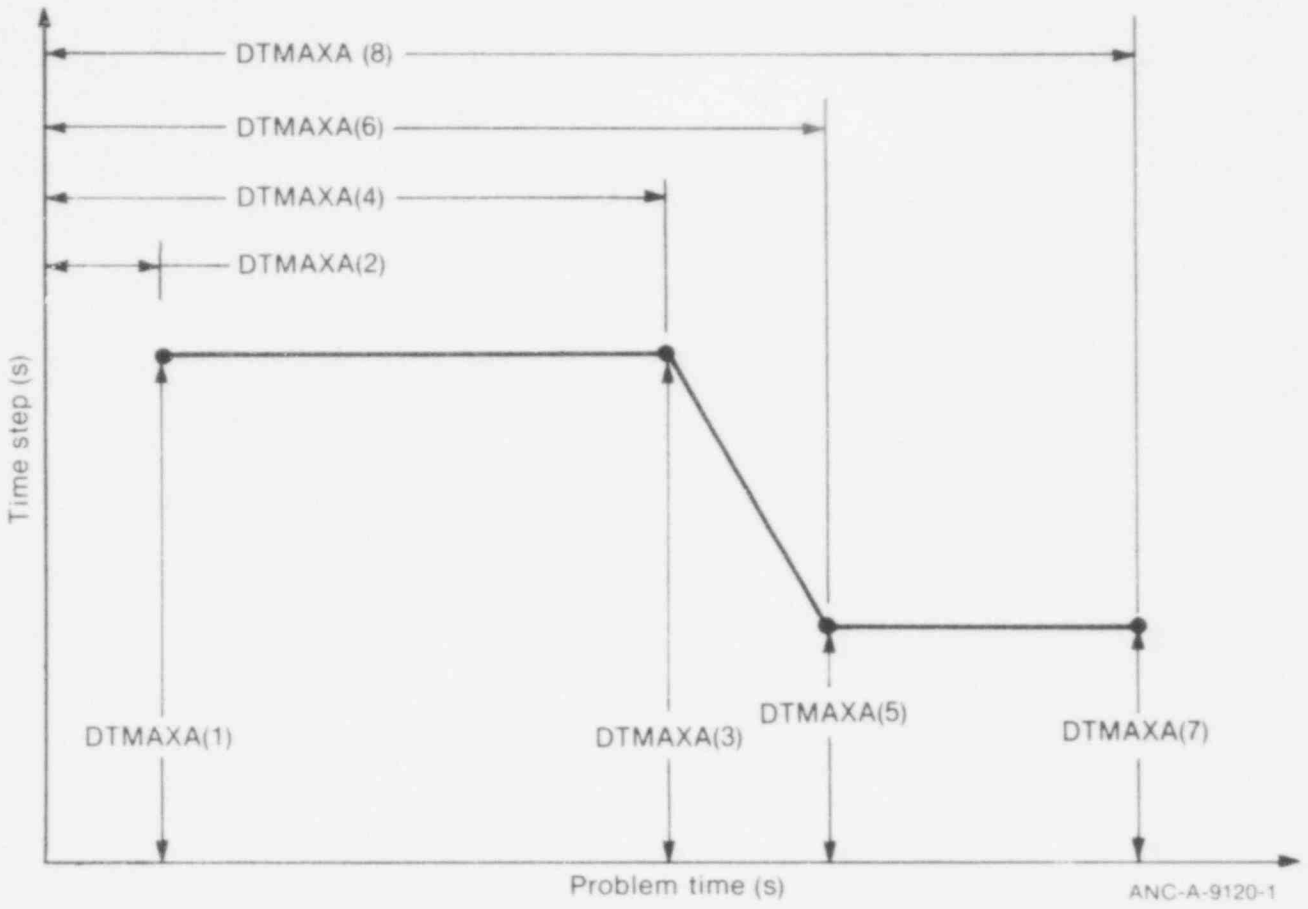

Fig. A-7 Example of time step history specified by Card Group 1.10.

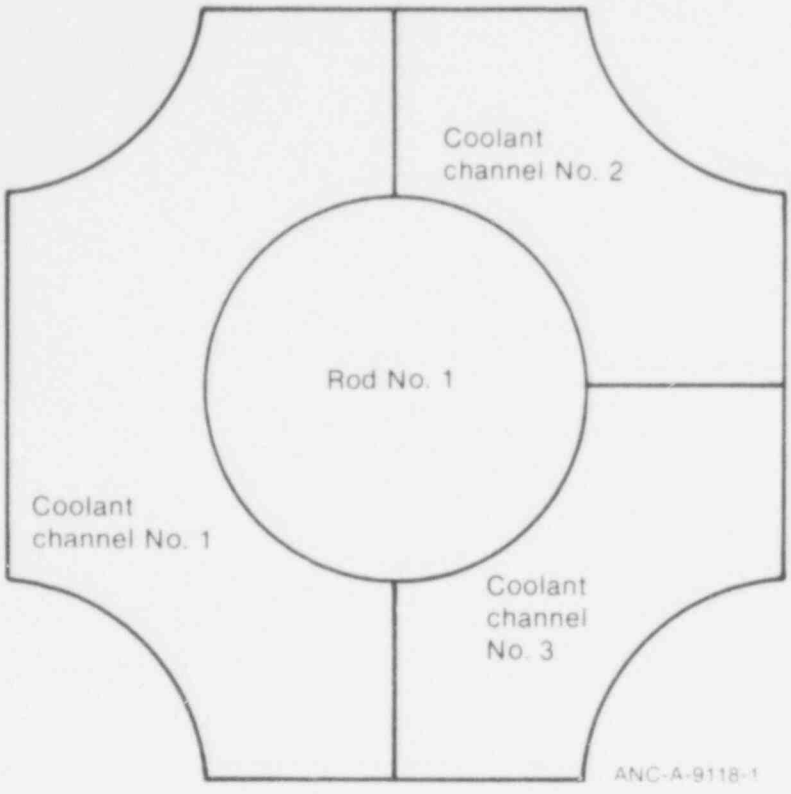

RØDNØ = 1
CHNNØ1 = 1
FRP1 = 0.5
CHNNØ2 = 2
FRP2 = 0.25
CHNNØ3 = 3
FRP3 = 0.25

Fig. A-8 Example of data input for Card Group 1.11 (coolant channel data).

Columns	Format	Name	Quantity
1-5	I	RØDNØ	Number of a rod in cluster being analyzed.
11-5	I	CHNNØ1	Number of a subchannel cooling RØDNØ.
16-20	F	FRP1	Fraction of surface area of RØDNØ bordering CHNNØ1.
21-25	I	CHNNØ2	Number of a subchannel cooling RØDNØ.
26-30	F	FRP2	Fraction of surface area of RØDNØ bordering CHNNØ2.
31-35	I	CHNNØ3	Number of a subchannel cooling RØDNØ.

36-40	F	FRP3	Fraction of surface area of RØDNØ bordering CHNNØ3.
41-45	I	CHNNØ4	Number of subchannel cooling RØDNØ.
46-50	F	FRP4	Fraction of surface area of RØDNØ bordering CHNNØ4.

Card Group 1.12 Axial Node Elevation Data.

If no minus sign is put in front of NAXN of Card 1.1, omit this card group.

Columns	Format	Name	Quantity
1-10	F	Z(1)	Elevation of axial node 1 (ft or m).
11-20	F	Z(2)	Elevation of axial node 2 (ft or m).
21-30	F	Z(3)	Elevation of axial node 3 (ft or m).

Continue as necessary with eight elevations per card until NAXN elevations have been put on cards. An example of the axial node mesh layout generated by Card Group 1.12 is shown in Figure A-9 for the case of NAXN = 5.

Card Group 1.13 Normalized Fast Neutron Flux Axial Distribution.
(Omit this card group if NFASTF = 0 on Card 1.1.)

Fast neutrons considered to be those with energy greater than 1 MeV. The time averaged fast neutron axial distribution during normal reactor operation should be input rather than that during a reactor transient.

Columns	Format	Name	Quantity
1-10	F	FLUXZ(1)	Ratio of fast neutron flux at elevation FLUXZ(2) to axially averaged fast neutron flux. FLUXZ(1) * CFLUX *

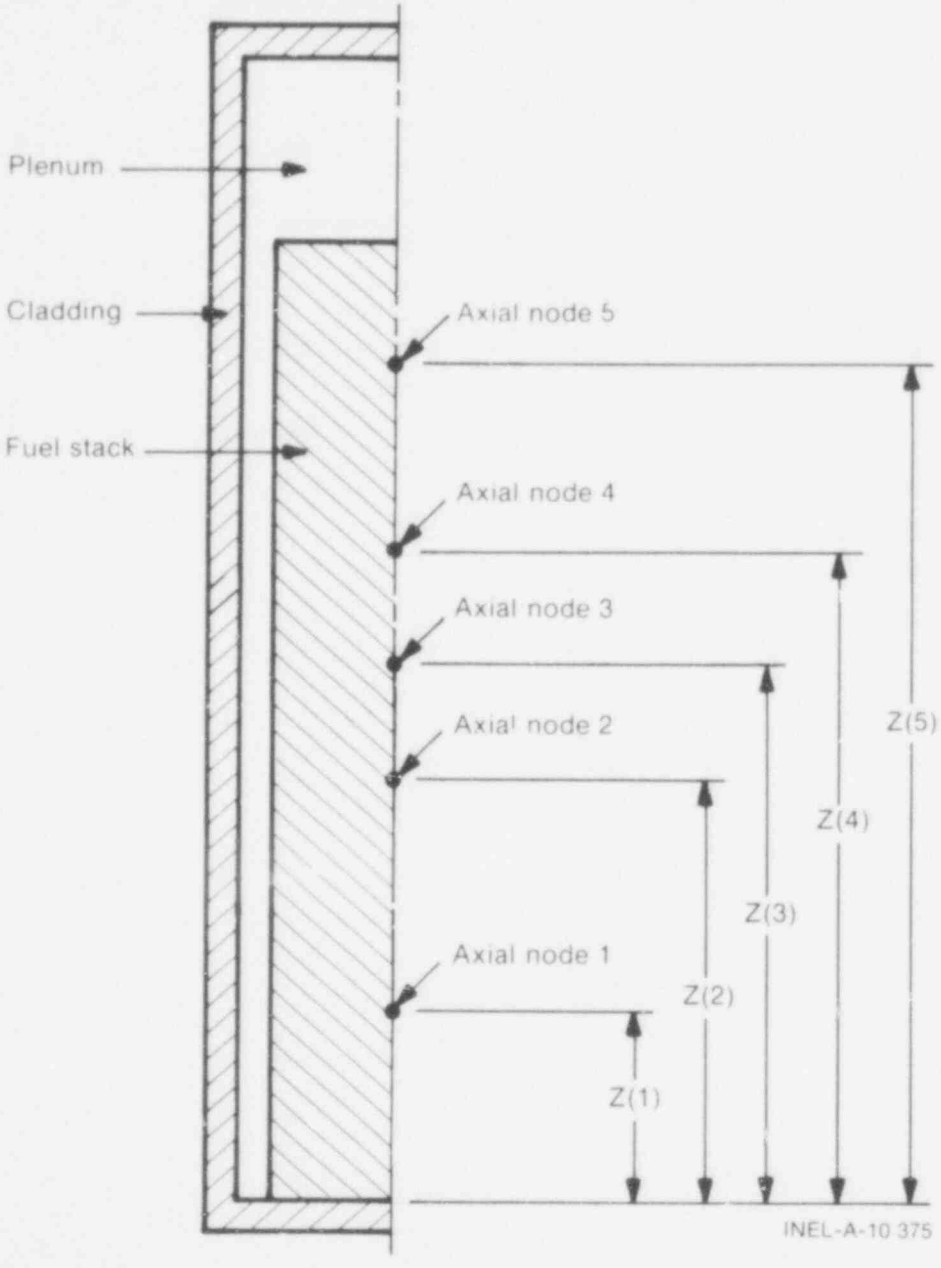

Fig. A-9 Example of axial node mesh specified by Card Group 1.12 for case NAXN = 5.

			TFLUX = fast neutron fluence (neutrons/m^2) at elevation FLUXZ(2). (CFLUX and TFLUX input on Card 1.6.)
11-20	F	FLUXZ(2)	Elevation above bottom of fuel stack (ft or m).
21-30	F	FLUXZ(3)	Ratio of fast neutron flux at elevation FLUXZ(4) to axially averaged fast neutron flux.
31-40	F	FLUXZ(4)	Elevation above bottom of fuel stack (ft or m).

Repeat until NFASTF pairs of data have been placed on cards, four pairs per card. Maximum of six and one-fourth cards of data. Also FLUXZ(4) > FLUXZ(2), etc.

Card 1.14 Restart Switches.

Columns	Format	Name	Quantity
6-10	I	NSWINW	If NSWINW = 0, no restart tape to be written. If restart tape to be written, set NSWINW equal to 2.
11-15	I	NRADFS	Switch to use FRAPCON computed fuel rod steady state conditions as initial conditions for transient calculations. 0 = no, 1 = yes. If NRADFS = 1, a STAGE or ATTACH card must be supplied which specifies the location of the FRAPCON created data set.
21-30	F	TREST	Time of fuel rod conditions on FRAPCON restart tape that will be used to

			specify initial fuel rod condition (sec). If NRADFS = 0, leave these columns blank.

Card 1.15 Specification of Surface Heat Transfer Coefficient Multiplier. (Omit if NSWHTC = 0 on Card 1.2.)

The mutiplier accounts for the effect of ballooning of neighboring fuel rod on heat transfer at the cladding surface.

Columns	Format	Name	Quantity
1-5	I	KAXHTC	Axial node at which surface heat transfer coefficient is to be modified to account for ballooning of neighboring fuel rod.
6-10	I	NPAIRS	Number of multiplier-time pairs used to specify history of multiplier on surface heat transfer coefficients. NPAIRS $\leq$ 10.
11-20	F	TSHTC	Time at which modification of surface heat transfer coefficient to start (sec).

Card 1.16 Heat Transfer Coefficient Multiplier History. (Omit if NSWHTC = 0 on Card 1.2).

Continuous history of multiplier generated by connecting straight lines to multiplier-time points specified on this card.

Columns	Format	Name	Quantity
1-10	F	FHTC(1)	Multiplier on cladding surface heat transfer coefficient at axial node KAXHTC at time TSHTC + FHTC(2).

11-20	F	FHTC(2)	Time relative to time TSHTC at which FHTC(1) applies. If FHTC(2) = 0, then FHTC(1) applied at absolute time TSHTC (sec).
21-30	F	FHTC(3)	Multiplier on cladding surface heat transfer coefficient at absolute time TSHTC + FHTC(4).
31-40	F	FHTC(4)	Time since time TSHTC at which FHTC(3) applies (sec).

Repeat until NPAIRS of multiplier-time data have been placed on cards, four pairs per card. Maximum of two and one-half cards.

Card(s) 1.17 Printout Interval Specification. (Omit if NPO = 0 on Card 1.2).

Columns	Format	Name	Quantity
1-10	F	DTPØA(1)	Problem time between printout of fuel rod state at problem time DTPØA(2)(sec). Set DTPØA(1) = 0 if printout desired at every time step.
11-20	F	DTPØA(2)	Problem time (sec).

Repeat until NPO pairs of data have been placed on cards, four pairs per card. Maximum of five cards. DTPØA(4) > DTPØA(2), etc.

Card Group 1.18 Flow Shroud Temperature. (Omit if NRADSH = 0 on Card 1.2).

Card 1.18.1

Columns	Format	Name	Quantity
1-10	F	DSHRD	Inner diameter of flow shroud (ft or m).

Card(s) 1.18.2 Flow Shroud Temperature History.

Columns	Format	Name	Quantity
1-10	F	TSHRDA(1)	Temperature of inside surface of flow shroud at time TSHRDA(2) (F or K).
11-20	F	TSHRDA(2)	Time (sec).

Repeat until NRADSH pairs of data have been placed on cards, four pairs per card. Maximum of six and one-fourth cards.

Card Group 1.19 Multipliers and Addition terms. (If NDIAL = 0 on Card 1.2, omit this card group).

Card 1.19.1

Specification of models to which multiplication factor is applied.

Columns	Format	Name	Quantity
1-5	I	NDHGAP	Switch to adjust gap conductance calculations. 0 = no, 1 = yes.
6-10	I	NDFCON	Switch to adjust fuel thermal conductivity. 0 = no, 1 = yes.
11-15	I	NDHFB1	Switch to adjust transition flow film boiling heat transfer coefficient. 0 = no, 1 = yes.
16-20	I	NDHFB2	Switch to adjust stable flow film boiling heat transfer coefficient. 0 = no, 1 = yes.
21-25	I	NDHFB3	Switch to adjust pool film boiling heat transfer coefficient. 0 = no, 1 = yes.

573 220

26-30	I	NDHFB4	Switch to adjust free convection heat transfer coefficient. 0 = no, 1 = yes.

Card(s) 1.19.2 Gap Conductance Multiplication Factors. (Omit if NDHGAP = 0.)

Columns	Format	Name	Quantity
1-5	F	FHGAP(1)	Multiplication factor on gap conductance at axial node 1.
6-10	F	FHGAP(2)	Multiplication factor on gap conductance at axial node 2.

Repeat until FHGAP has been specified at each axial node. If more than 16 axial nodes, continue on second card in same manner.

Card 1.19.3 (Omit if variables NDFCON through NDHFB4 on Card 1.19.1 are set equal to zero.)

Columns	Format	Name	Quantity
1-5	F	FFCON	Addition term to fuel thermal conductivity (Watts/M-K); leave blank if NDFCON = 0.
6-10	F	FHFB1	Multiplication factor to be applied to transition flow film boling heat transfer coefficient (leave blank if NDHFB1 = 0).
11-15	F	FHFB2	Multiplication factor to be applied to stable flow film boiling heat transfer coefficient (leave blank if NDHFB2 = 0).

573 221

16-20	F	FHFB3	Multiplication factor to be applied to pool film boiling heat transfer coefficient (leave blank if NDHFB3 = 0).
21-25	F	FHFB4	Multiplication factor to be applied to free convection heat transfer coefficient (leave blank if NDHFB4 = 0).

Card Group 1.20 Reflood Heat Transfer Data. (Omit this card group if NREFLD = 0 on Card 1.2.)

Card 1.20.1

Columns	Format	Name	Quantity
10-11	A	NSWRLD	Input the character string ON in columns 10-11.
15-24	F	EMPYTM	Problem time, in seconds, at which the core is dry and begins adiabatic heatup.
27-36	F	REFDTM	Problem time, in seconds, at which flooding of fuel rods begins.
39-48	F	HRAD	Radiation heat transfer coefficient. If HRAD < 0.0, HRAD is computed. (BtU/hr-ft^2-F)
51-55	I	NBR1	Number of inlet temperature (^{o}F) versus time (sec) pairs, NBR1 ≤ 20
55-60	I	NBR2	Number of flooding rate (in./sec) versus time (sec) pairs, NBR2 ≤ 20

66-70	I	NBR4	Number of reactor vessel pressure (psi) versus time (sec) pairs, NBR4 ≤ 20

Card 1.20.2

Columns	Format	Name	Quantity
1-6	A	LODMRK	Specifies the line of demarcation. If RUPTUR is input, line of demarcation is plane of cladding rupture. If LIQLEV is input, line of demarcation is the collapsed liquid level. If the cladding rupture plane is the line of demarcation, and cladding rupture does occur, steam cooling is modeled depending upon the flooding rate. If the flooding rate is greater than 1 in./sec, the FLECHT correlation is assumed to apply along the entire length of the fuel rod. But if the flooding rate is less than 1 in./sec, the FLECHT correlation is assumed to apply up to the elevation of cladding rupture. Above this elevation, the cladding heat transfer coefficient is calculated by the steam cooling model. If the collapsed liquid level is the line of demarcation, and the flooding rate is greater than 1 in./sec, the FLECHT correlation is assumed to apply along the entire length of the fuel rod. But if the FLECHT correlation is less than 1 in./sec, the FLECHT correlation is applied up to the elevation of the collapsed liquid level, and above this elevation the cladding heat transfer coefficient is calculated by the steam cooling model.

Columns	Format	Name	Quantity
9-18	F	HYDIAM	The flow channel hydraulic diameter (ft).
21-30	F	FLXSEC	The flow channel cross-sectional area per fuel rod (ft^2).

On all the following history cards, all time references are from the beginning of reflood; not beginning of problem.

Card 1.20.3

For the reflood water inlet temperature-time history cards, the inlet temperature-time data pairs are entered, three pairs to a card. A total of NBR1, from Card 1.19.1, pairs must be entered. The data pairs start at a reflood time of 0 sec into reflood.

Columns	Format	Name	Quantity
1-10	F	TEMP(1)	Inlet temperature in degrees F at TIME(1) into reflood.
11-20	F	TIME(1)	Time from beginning of reflood (must be 0.0).
21-30	F	TEMP(2)	Inlet temp. . in degrees F at TIME(2) into ref .od.
31-40	F	TIME(2)	Time in seconds into reflood.
41-50	F	TEMP(3)	Inlet temperature in degrees F at time TIME(3) into reflood.
51-60	F	E(3)	Time in seconds into reflood.

Continue on additional card until NBR1 pairs have been entered. Maximum of six and one-half cards are allowed.

573 224

Card 1.20.4 Reflood rate-time history cards.

The reflood rate-time data pairs are entered, three pairs to a card. There must be NBR2 pairs, from Card 1.20.1, entered. The data pairs start with a reflood time of 0 sec into reflood.

Columns	Format	Name	Quantity
1-10	F	FLDRAT(1)	Reflood rate in inches per second at time TIME(1).
11-20	F	TIME(1)	Time from beginning of reflood (second) (must be 0.0).
21-30	F	FLDRAT(2)	Reflood rate in inches per second at TIME(2).
31-40	F	TIME(2)	Time in seconds into reflood.
41-50	F	FLDRAT(3)	Reflood rate in inches per second at time TIME(3).
51-60	F	TIME(3)	Time in seconds into reflood.

Continue an additional card until NBR2 pairs have been entered. A maximum of six and one-half cards are allowed.

Card 1.20.5 Reactor Vessel Pressure - Time Pairs. (Input same as previous card group.)

Columns	Format	Name	Quantity
1-10	F	PRESTM(1)	Reactor vessel pressure at time PRESTM (2) (psia).
11-20	F	PRESTM(2)	Time from beginning of reflood (sec).

Continue with three pairs to a card until NBR4 pairs have been entered. A maximum of six and one-half cards are allowed.

Continue on additional card until NBR4 pairs have been entered.

Card Group 1.21 The Licensing Assistance Modeling Card Group.
(Include this card group only if NSWLAC = 1 on Card 1.2.)

This card group allows the user to specify which, if any, of the Licensing Audit Code (LAC) models are to be substituted for the otherwise best estimate (BE) model.

The input format is free form requiring only blanks as separators. The input numbers do not need to be placed in certain card columns.

Since there are several options available, the user may choose to use all, all except a few, just a select few, or none of the available modeling options.

Card 1.21.1

Data Field	Format	Variable	Input
1	A	PRNTOP	ALL = all LAC models to be used. NONE = no LAC models to be used. SOME = use only the specified LAC models. EXCEPT = use of all LAC models except for the specified BE models.

For options ALL and NONE, nothing additional need be specified.

For options SOME and EXCEPT, the next data fields must specify how many and which LAC models are to be used. The number of LAC or BE models is first entered, then the number codes for the models are entered. Each number code must be separated by at least one blank column.

573 226

Examples:

SOME 3 12 5 11

This card specifies that only the three LAC models, 12, 5, and 11, will be used.

EXCEPT 2 9 4

This card specifies that all LAC models except 9 and 4 will be used.

The number code for each LAC model option is listed as follows:

Model	Number Code
CLADDING AXIAL THERMAL EXPANSION	3
CLADDING DIAMETRAL THERMAL EXPANSION	3
CLADDING SPECIFIC HEAT	4
CLADDING ELASTIC MODULUS	5
CLADDING POISSON RATIO	6
CLADDING THERMAL CONDUCTIVITY	7
FUEL SPECIFIC HEAT	8
FUEL ELASTIC MODULUS	9
FUEL EMISSIVITY	10
FUEL POISSON RATIO	11
FUEL THERMAL CONDUCTIVITY	12
FUEL THERMAL EXPANSION	13
CLADDING PLASTIC HOOP STRAIN	14
CLADDING SURFACE HEAT TRANSFER COEFFICIENT	15
GAS THERMAL CONDUCTIVITY	16
METAL-WATER REACTION	17
FUEL DEFORMATION	18
GAP CONDUCTANCE	19
OPERATING POWER * 1.02	20
ANS DECAY POWER * 1.2	21

The model specifications on Card 1.21.1 override those specified on other input cards. For example, if Card 1.1 specifies the Cathcart model for metal-water reaction, but Card 1.21.1 specifies the LAC model, the LAC model will be used.

Card 1.21.2

Omit this card if NSWLAC = 0 on Card 1.2. Also, omit this card if the LAC cladding plastic hoop strain model is not used. This card follows Card 1.21.1.

Columns	Format	Name	Quantity
1.5	I	NPTRVP	Number of pairs of rupture temperature versus cladding differential pressure (inside pressure minus coolant pressure) (ΔP) in Card Group 1.21.3. NPTRVP $\leq$ 25.
6-10	I	NPSRVP	Number of pairs of rupture strain versus ΔP in Card Group 1.21.4. NPSRVP $\leq$ 25.
11-15	I	NPFBLK	Number of pairs of flow blockage versus ΔP in Card Group 1.21.5. NPFBLK $\leq$ 25.

Card 1.21.3 Rupture Temperature Versus ΔP Table.

Columns	Format	Name	Quantity
1-10	F	TAB1(1)	Minimum temperature at which cladding will rupture when cladding differential pressure equals TAB1(2); ^{o}F.
11-20	F	TAB1(2)	Cladding differential pressure (psi).

Repeat as necessary, with four pairs per card, and a maximum of six and one-fourth cards. TAB1(4) > TAB1(2), etc.

Card 1.21.4 Rupture Strain Versus ΔP Table.

Columns	Format	Name	Quantity
1-10	F	TAB2(1)	Cladding rupture strain if cladding rupture occurs at cladding differential pressure of TAB2(2).
11-20	F	TAB2(2)	Cladding differential pressure (psi).

Repeat as necessary, with four pairs per card, and a maximum of six and one-fourth cards. TAB2(4) > TAB(2), etc.

Card 1.21.5 Flow Blockage Versus ΔP Table.

Columns	Format	Name	Quantity
1-10	F	TAB3(1)	Flow blockage if cladding rupture occurs at cladding differential pressure of TAB3(2); percent.
11-20	F	TAB3(2)	Cladding differential pressure (psi).

Repeat as necessary, with four pairs per card, and a maximum of six and one-fourth cards. TAB3(4) > TAB3(2), etc.

Data Block 2. Thermal Property Data.

To reduce computer time, FRAP-T generates tables containing fuel and cladding thermal properties versus temperature from MATPRO correlations of these properties. Thermal properties at temperatures intermediate to those in the tables are found by linear interpolation.

573 229

Card 2.1

Specification of temperature intervals at which thermal properties are put into tables. No restriction placed on the upper bound value for the quantities read in on this card. Larger values demand more computer memory, however.

Columns	Format	Name	Quantity
1-5	I	NKF	Number of thermal conductivity versus temperature pairs to be generated by code for fuel. If NKF < 2 it is reset to 2. Normally NKF = 100.
6-10	I	NSF	Number of specific heat versus temperature pairs to be generated for fuel. Computer memory requirements are reduced if NSF = NKF.
11-15	I	NKC	Number of thermal conductivity versus temperature pairs to be generated for cladding. If NKC < 2 it is reset to 2. Normally, NKC = 50.
16-20	I	NSC	Number of specific heat versus temperature pairs to be generated for cladding. Computer memory requirements are reduced by setting NSC = NKC.
21-25	I	IDEBUG	If IDEBUG is greater than zero, thermal property tables generated for fuel and cladding are printed.

573 230

Card 2.2

Specification of temperature bounds of thermal property tables.

Columns	Format	Name	Quantity
1-10	F	TOF	Minimum temperature in fuel thermal property tables (^{O}F or K) (must be less than minimum fuel temperature expected during calculations).
11-20	F	TMAXF	Maximum temperature in fuel thermal property tables (^{O}F or K) (must be greater than maximum fuel temperature expected during calculations).
21-30	F	TOC	Minimum temperature in thermal property tables of cladding (^{O}F or K).
31-40	F	TMAXC	Maximum temperature in thermal property tables of cladding (^{O}F or K).

Data Block 3. Temperature Computation Subcode Input Data

All of the input data cards must have an eight-digit card number as the first entry on the card. The input data is free form and does not need to be placed in certain card columns. Each piece of input data must be separated on both sides by at least one blank column or a comma. A piece of input data that is integer format must not have a decimal point or an exponent. Title cards must have an "=" as the first nonblank character. Comment cards are allowed in this block of the input data and are identified by an "*" or a "$" as the first nonblank character. Data on a card may be continued on a following card by entering a plus sign as the first nonblank character on the continuation card. The last card in Data Block 3 must have a "." character in column 1.

Card 3.1 Title Card.

This card must have the "=" symbol as the first nonblank character, usually placed in column 1. The remainder of the card is used to specify the problem title, which will be printed out in the input listing.

Card 3.2 General Data.

This card must have the number 01010001 in columns 1 through 8.

Data Field	Format	Variable	Quantity
1	I	COLS	Number of radial mesh points (radial nodes) at each axial node (COLS $\leq$ 20).
2	I	IGEOM	Geometry type. Always input the integer 2 (cylindrical).
3	F	XO	Left boundary coordinate. Always input 0.0.
4	F	FCTR	Source multiplication factor. Always set equal to 1.
5	I	MAXIT	Maximum number of iterations in steady state solution (normally about 200).
6	F	EPS	Convergence criterion for temperature calculation subcode (^{o}F or K) (normally about 1.^{o}F). If temperature change between two successive interations exceeds this value, no convergence is declared and another iteration ordered with updated material properties.

573 232

7	I	NOITER	Maximum number of iterations on material properties for time dependent solution. (Normally about 200).

Card 3.3 Format for Radial Mesh Specifications.

This card must have the number 01010200 in columns 1 through 8. The card specifies the format for the input of the radial mesh data. The data for Card 3.3 is fixed as shown below.

Data Field	Format	Quantity
1	I	ID of problem in which geometry data are defined. Always input 0.
2	I	Format of mesh spacing data. Always input the integer 1.

Card 3.4 Specification of Radial Mesh.

This cards(s) must have the number 010102nn in columns 1 through 8, where $1 \leq nn \leq 99$. Radial intervals with a constant mesh spacing are specified. Normally, the fuel is given a constant mesh spacing, the cladding a different constant mesh spacing, and the gas gap is specified to have one mesh spacing. An example of a radial mesh is shown in Figure A-10. Pairs of data are input for each radial interval. The first number in the pair specifies the number of mesh spacings in the interval, the second number the outer radius of the interval. The interval data is entered in order of ascending outer radius. If the fuel has a central void, the interval data for it is entered first. The interval data for the cladding is entered last. If the fuel has no central void, and the fuel is given a constant mesh spacing and the cladding a different constant mesh spacing, the card will have three pairs of data, as shown below.

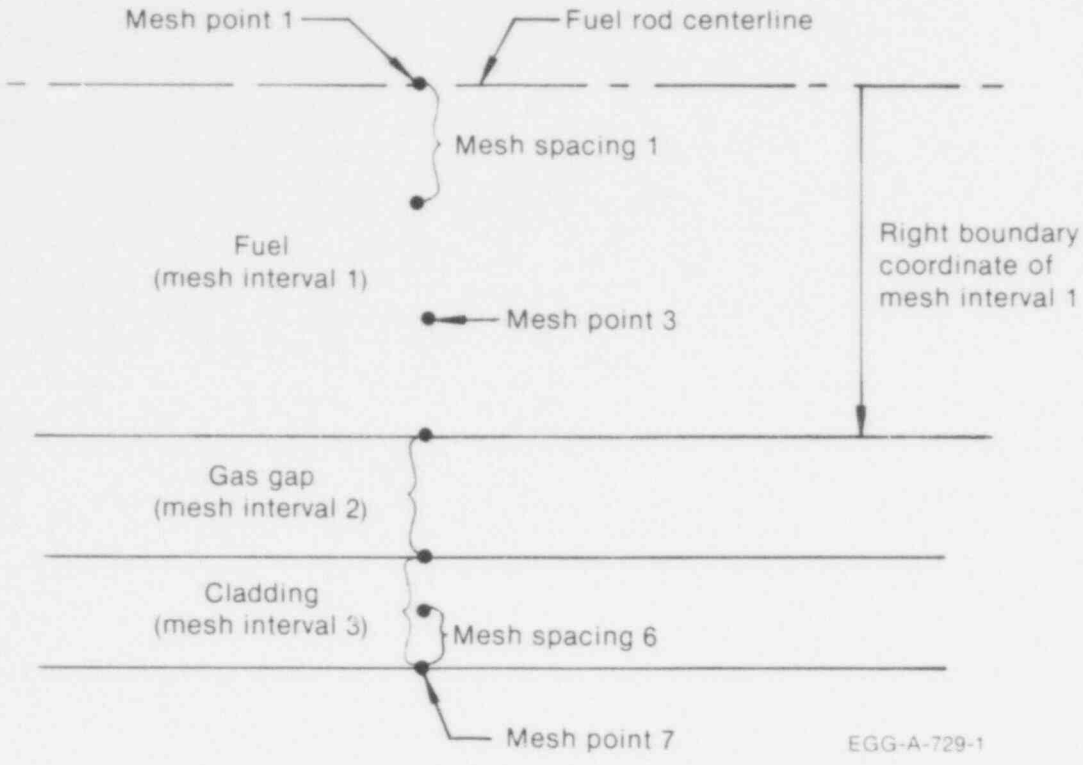

Fig. A-10 Example of radial mesh layout.

Data Field	Format	Quantity
1	I	If no central void, leave this field blank. If central void, input the integer "1".
2	F	If no central void, leave this field blank. If central void, input the radius of central void (ft or m).
3	I	Number of mesh spaces overlaying the fuel.
4	F	Radius of outside surface of fuel pellets (ft or m).
5	I	Number of mesh spacings overlaying the gas gap (always input the integer 1).

573 234

6	F	Radius of inside surface of cladding (ft or m).
7	I	Number of mesh spacings overlaying cladding.
8	F	Radius of outside surface of cladding (ft or m).

The integers in data fields 1, 3, 5, and 7 must sum to CØLS-1, where CØLS is specified in data field 1 of Card 3.2.

Card 3.5 Composition Overlay.

This card must have the number 01010301 in columns 1 through 8. Compositions are defined as homogeneous material regions bounded on either side by mesh points. Composition data are input pairs of numbers in integer format; the first being the composition number, and the second the number of the last mesh spacing (not mesh point) containing material with the specific composition number. Mesh spacings which overlay the fuel region must be given a composition number of 1. Similarly, cladding mesh spacings must be given a composition number of 2 and the gas gap mesh spacing a composition number of 3.

Data Field	Format	Quanitity
1	I	Composition of fuel region. Always input the integer 1.
2	I	The number of the mesh spacing which overlays fuel and borders fuel outer surface.
3	I	Composition of gas gap. Always input the integer 3.

4	I	The number of the mesh spacing overlaying the gas gap (the number in data field 2, plus 1).
5	I	Composition of cladding region. Always input the integer 2.
6	I	The number of the mesh spacing which overlays cladding and borders cladding outer surface. This number must equal CØLS-1, where COLS is specified in field 1 of Card 3.2.

Card 3.6 Normalized Radial Power Distribution.

This card(s) must have the number 010104nn in columns 1 through 8, where $1 \leq nn \leq 99$. The radial power profile factor is defined to be the ratio of power in a mesh spacing to the radially averaged power in the fuel. Power factors for each mesh spacing are specified by pairs of numbers. The first number specifies the radial power profile factor and the second number the mesh spacings where the radial power profile factor applies. The power factors must satisfy the equation

$$\sum_{n=1}^{N} \frac{P_n(r^2_{n+1} - r^2_n)}{r_f^2} = 1$$

where

r_f = radius to outside of fuel pellet

P_n = power profile factor for n^{th} mesh spacing

r_n = inner radial coordinate (cold state) of n^{th} mesh spacing

N = number of mesh spacings in fuel

r_{n+1} = outer radial coordinate of n^{th} mesh spacing.

The radial power profile factor should represent the average power in the mesh spacings. All axial nodes are assumed to have the same normalized radial power distribution. This card still needed even if azimuthal variation in power specified on Card 4.5. The card specifies power distribution at axial nodes at which no azimuthal heat conduction is specified. If azimuthal heat conduction specified at all axial nodes, put dummy data on this card.

Data Field	Format	Name	Quantity
1	F	P(1)	Radial power profile factor for region defined by N1.
2	I	N1	The largest mesh spacing number for which P(1) applies.
3	F	P(2)	Radial power profile factor for region defined by N2.
4	I	N2	The largest mesh spacing number for which P(2) applies.

Repeat as necessary. The last mesh spacing number input must be CØL-1. If each mesh spacing is given a different radial power profile factor, then N1, N2, etc., will have values going from 1 to CØL-1 in increments of one.

Card Group 3.7 Initial Temperature Estimate.

This card(s) must have the number 010106nn in columns 1 through 8, where $1 \leq nn \leq 99$. The initial temperature distribution is input in the same format as the radial power distribution except that the temperatures are defined at mesh points rather than for mesh spacings.

This input is only used to supply initial guess to steady state temperature calculations. Normally, the steady state temperature calculations will converge if the entire fuel rod is assumed to be at initial coolant temperature.

Data Field	Format	Name	Quantity
1	F	T(1)	Initial temperature of region defined by N1 (^{O}F or K).
2	I	N1	The number of the mesh point on the right boundary of region for which T(1) applies.
3	F	T(2)	Initial temperature of region defined by N2 (^{O}F or K).
4	I	N2	The number of the mesh point on the right boundary of region for which T(2) applies.

Repeat as necessary. The last mesh point number input must be CØLS.

End card. Place period symbol, ".", in column 1.

Data Block 4. Power History and Axial Power Profile Input Data.

Card 4.1

Columns	Format	Name	Quantity
1-5	I	N	Number of a fuel rod in rod bundle being analyzed. (Always input the integer 1.)
6-10	I	NH	Number of power-time pairs used to describe power history of rod (NH $\leq$ 50).

11-15	I	NA	Number of power factor-elevation pairs used to describe axial power profile of rod N (NA $\leq$ 25).
16-20	I	NAAZP	Number of azimuthal angles for which a radial power profile distribution is input to specify azimuthal power variation (1 $\leq$ NAAZP) $\leq$ 10). Leave blank if NDIM = 0 on Card 1.1. If NAAZP = 1, power distribution in fuel is assumed concave parabolic[A-3] in shape. The shape is that given by a parabola offset from center of fuel rod and rotated through 180^{o}. The shape is shown in Figure A-11. The point of peak fuel power occurs on the fuel surface. The shape is specified by the equation; $P(r,\theta)=A[r^2 + B^2 - 2Br\cos\theta] + C$, where $P(r,\theta)$ = ratio of power at radial coordinate r and azimuthal coordinate θ to area averaged power, and A, B and C are coefficients determined from user input values on Card 4.5.
21-25	I	NRAZP	Number of pairs of relative power versus radius in each radial power profile (2 $\leq$ NRAZP $\leq$ 15). Leave blank if NDIM = 0 on card 1.1 or NAAZP = 1 on Card 4.1.

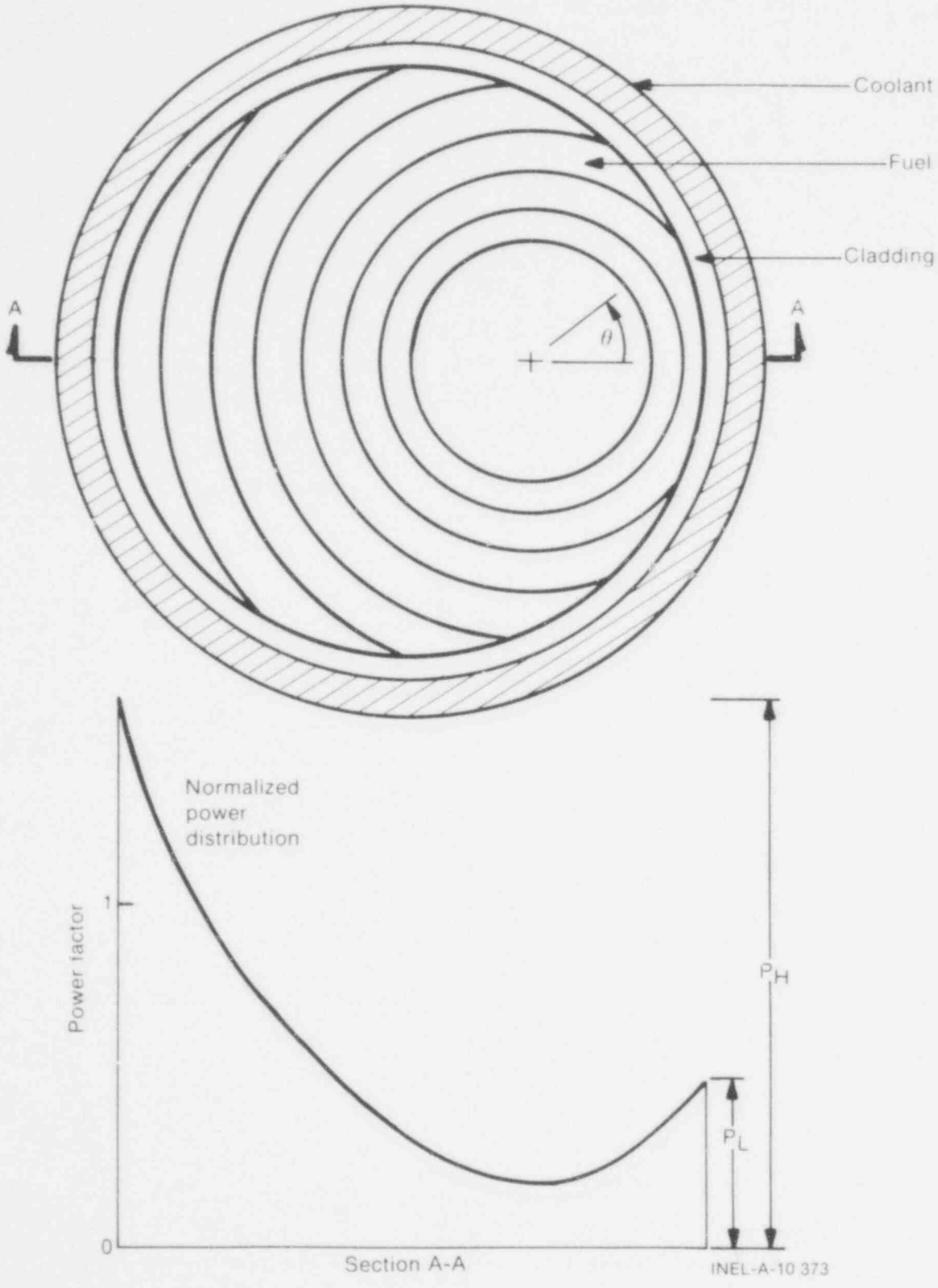

Fig. A-11 Concave parabolic power distribution.

573 240

Card Group 4.2 Power History Cards.

Columns	Format	Name	Quantity
1-10	F	PH(1)	Average linear power in fuel rod N at time PH(2) (kW/ft or kW/m). If MPDCAY = 1 on Card 1.1, the power should not include heat generation due to radioactive decay of fission products.
11-20	F	PH(2)	Time (sec).

Repeat until NH pairs of data have been placed on cards, four pairs per card. Maximum of 12-1/2 cards of data. Input is in same format as that of Card Group 1.10.

Card Group 4.3 ANS Decay Heat Formula Parameters. (Omit this card group if MPDCAY = 0 on Card 1.1.)

Columns	Format	Name	Quantity
1-10	F	PØWØP	Average linear fuel rod power just prior to accident initiation (normal operation power - kW/ft or kW/m).
11-20	F	TIMØP	Time span at which fuel rod was at operating power (sec).
21-30	F	FPDCAY	Factor applied to power given by ANS decay heat formula. If power specified by ANS formula not to be modified, set FPDCAY = 1.

573 241

Card Group 4.4 Axial Power Distribution.

Columns	Format	Name	Quantity
1-10	F	PA(1)	Axial power profile factor at elevation PA(2).
11-20	F	PA(2)	Elevation (ft or m). This elevation does not need to correspond to elevation of an axial node.

Repeat until NA pairs of data have been input. PA(4) > PA(2), etc. Maximum of six and one-fourth cards of data. A pictorial explanation of axial power profile specified by Card Group 4.4 for case of NA = 4 is shown in Figure A-12.

Card Groups 4.2 and 4.4 specify fuel rod power according to the equation

$$P(Z,t) = A_f(Z)\, P_h(t)$$

where

$P(Z,t)$ = fuel rod power at elevation Z and time t (kW/ft or kW/m)

$A_f(Z)$ = axial power profile factor at elevation Z (this value found by interpolating in table specified by Card Group 4.4)

$P_h(t)$ = average fuel rod power at time t (this value found by interpolating in table specified by Card Group 4.2).

573 242

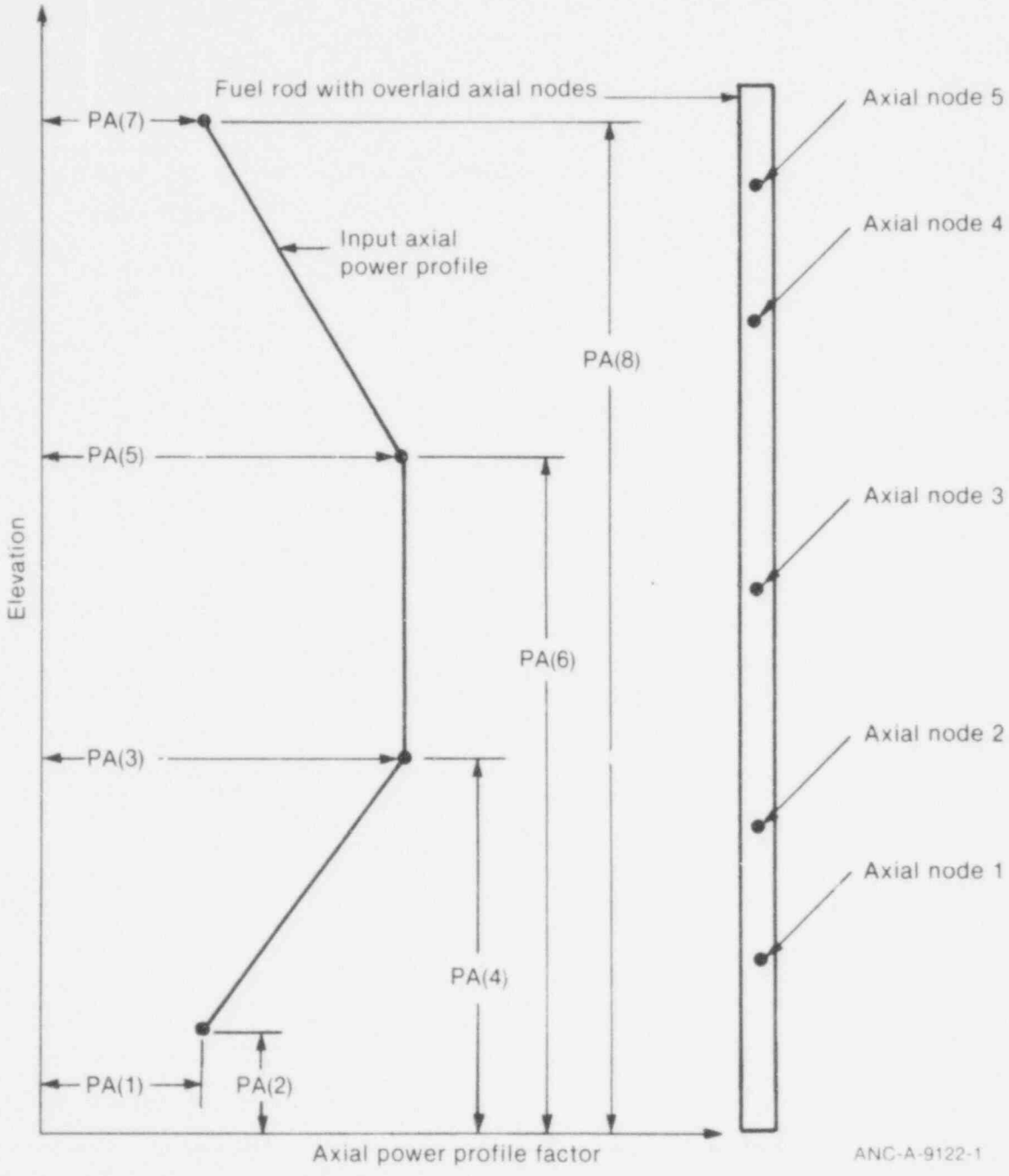

Fig. A-12 Example of axial power profile specified by data on Card Group 4.4.

573 243

Card 4.5 Concave Parabolic Power Distribution. (Omit if NDIM = 0 on Card 1.1 or NAAZP > 1 on Card 4.1.)

Columns	Format	Name	Quantity
1-10	F	PH	Maximum power peaking factor in fuel. The factor is maximum value of the ratio of heat generation rate at a point to the cross-section area averaged heat generation rate. The point must occur on the fuel surface.
11-20	F	PL	Power peaking factor at point on the fuel surface diametrically opposite of point at which PH occurred.
21-30	F	DØFFST	Azimuthal angle of diametric line connecting points PH and PL (degrees). Azimuthal coordinate system defined in Figure A-6. Unless DØFANG > 0 on Card 1.7, set DØFFST=0.

Cards 4.6 and 4.7 are input as a set. There must be NAAZP (specified on Card 4.1) sets of these cards. These cards are omitted if NDIM = 0 on Card 1.1 or NAAZP = 1 on Card 4.1. These cards specify the radial power profile at various azimuthal angles.

Card 4.6 (Omit if NDIM = 0 on Card 1.1 or NAAZP = 1 on Card 4.1.)

Columns	Format	Name	Quantity
1-10	F	AZ(L)	Azimuthal angle (degrees) of L^{th} radial power profile. The first azimuthal angle must have a value of zero degrees. The last azimuthal angle must have a value of 90 degrees if NSYMM = 0, and 180 degrees if NSYMM = 1.

573 244

Card 4.7 (Omit if NDIM = 0 on Card 1.1) or NAAZP = 1 on Card 4.1.)

Columns	Format	Name	Quantity
1-10	F	PAZ(1,L)	Radial power profile factor at radius PAZ(2,L).
11-20	F	PAZ(2,L)	Radius (ft or m).
21-30	F	PAZ(3,L)	Radial power profile factor at radius PAZ(4,L).
31-40	F	PAZ(4,L)	Radius (ft or m).

Repeat until NRAZP (specified on Card 4.1) power factor versus radius pairs have been input. The radius of the last power factor for each radial profile must equal the outer radius of the fuel.

The set of radial power profile curves must be normal. The set is normal if the following relation is satisfied:

$$\sum_{j=1}^{NAAZP}\left[\frac{\theta_{j+1} - \theta_{j-1}}{2\phi}\right]$$

$$\sum_{n=1}^{NRAZP} \frac{\frac{PAZ(2n+1,j) + PAZ(2n-1,j)}{2}\left[PAZ(2n+2,j)^2 - PAZ(2n,j)^2\right]}{r_f^2} = 1$$

where

θ_j = azimuthal angle of j^{th} radial power profile (degrees)

NAAZP = total number of radial power profiles

r_f = radius to outside surface of fuel

ϕ = 90 if NSYMM = 0

ϕ = 180 if NSYMM = 1

ϕ = 360 if NSYMM = 2.

Data Block 5. Coolant Condition History Input Data.

Five input options are available. In the first option, the enthalpy, quality, and void fraction of the coolant are computed by the code. These quantities are coupled to the calculated fuel rod surface heat flux. In the second option, core average transient coolant conditions are input on cards. In the third option, transient spatially varying coolant conditions are input by reading a data set stored on tape or disk. In the fourtn option, transient spatially varying heat transfer coefficients are input on cards. In the fifth option, transient spatially varying heat transfer coefficients are input by reading a data set stored on tape or disk.

Card 5.1

Columns	Format	Name	Quantity
1-5	I	NSWC	Coolant input switch. If NSWC = 0, enthalpy histories of lower and upper vessel plenums, core average pressure history, and core average mass flux history are specified by card input. The code computes the coolant enthalpy, temperature, quality, and void fraction. These are coupled to the fuel rod surface heat flux and vary with elevation.

573 246

If NSWC = 1, enthalpy histories of lower and upper plenums, core average pressure history, mass flux history, and enthalpy history are specified by card input. The core average coolant conditions are applied to all fuel rod axial nodes. The code computes the coolant quality and void fraction.

If NSWC = 2, transient coolant conditions are read from data set stored on disk or tape. The format of the data set is specified in Appendix E. With this option, different coolant conditions can be specified for each axial node. The coolant void fraction is computed by the code.

If NSWC = 3, fuel rod cooling is prescribed by heat transfer coefficient and bulk temperature histories input on cards.

If NSWC = 4, transient heat transfer coefficients, coolant temperatures, and pressure are read from a data set stored on disk or tape. The format of the data set is specified in Appendix E. With this option, the time and spatial variation of the heat transfer coefficients and coolant temperatures can be prescribed in unlimited detail.

6-10	I	NPBH	Number of pressure-time pairs used to describe to coolant pressure history. NPBH ≤ 50. Leave blank if NSWC = 2 or 4.
11-15	I	NHLP	Number of enthalpy-time pairs used to describe enthalpy history of lower plenum. NHLP ≤ 50. Leave blank if NSWC = 2, 3, or 4.
16-20	I	NHUP	Number of enthalpy-time pairs to describe enthalpy history of upper plenum. NHUP ≤ 50. Leave blank if NSWC = 2, 3, or 4.
21-25	I	NGBH	Number of mass flux-time pairs used to describe mass flux history in core. NGBH ≤ 100. Leave blank if NSWC = 2, 3, or 4.
26-30	I	NHBH	Number of enthalpy-time pairs used to describe average enthalpy history of coolant in core. NHBH ≤ 25. Leave blank if NSWC = 0, 2, 3, or 4.
31-35	I	NZØNE	Number of different zones for which coolant conditions are specified along the vertical flow path surrounding fuel rod. If the coolant conditions are computed by the RELAP4 code and NSWC = 2, NZØNE = number of volumes in RELAP model that overlay fuel rod being analyzed. If NSWC = 4, NZØNE = number of heat slabs in RELAP model of fuel rod being analyzed.

36-40	I	LCHF	Option switch to control application of axial power profile factor and cold-wall factor to critical heat flux correlations. Axial power profile factor models influence of axially nonuniform heat flux on CHF. Cold-wall factor models influence of cold walls surrounding fuel rod on CHF. If LCHF = 0, critical heat flux correlation multiplied by both axial power profile factor and cold-wall factor. If LCHF = 1, CHF correlation is multiplied only by axial power profile factor. If LCHF = 2, CHF correlation is multiplied only by cold-wall factor. If LCHF = 3, neither axial power profile factor nor cold-wall factor are applied to CHF correlation. If JCHF (next input variable on this card) = 1, 2, or 5; LCHF set internally to 3, independent of input value.
44	I	JCHF	Option switch to control critical heat flux correlation. The correlations are described in Appendix D of this report. If the mass flux is less than 200,000 lb/hr-ft^2, the modified Zuber correlation is used in place of the input specified correlation. If JCHF = 0, the B&W-2[A-4] correlation is used for high coolant pressure. Modified Barnett correlation[A-5] is used when coolant pressure is less than 725 psia. The local form of the Barnett correlation[A-6] is used for pressure between 1000 and 1300 psia.

			B&W-2 correlation is used when coolant pressure is greater than 1500 psia. For intermediate pressures, a combination of the two adjacent correlations is used. If JCHF = 1, General Electric correlation[A-7] is used. If JCHF = 2, Savannah River correlation[A-8] is used. If JCHF = 3, either modified Barnett or W-3 correlation[A-9] is used, depending on coolant pressure. Modified Barnett is used when coolant pressure is less than 735 psia. Combination of modified Barnett and W-3 is used for pressures between 725 and 1000 psia. W-3 correlation is used for pressures greater than 1000 psia. If JCHF = 4, the CE-1 correlation is used. If JCHF = 5, the Loss-of-Fluid Test correlation[A-10] is used. This correlation assumes the geometry of the LOFT reactor.
45	I	JFB	Option switch to control film boiling correlation. The correlations are described in Appendix D of this report. If JFB = 0, form 5.9 (cluster geometry) of Groeneveld correlation[A-11] is used when the coolant pressure is greater than 500 psia. When coolant pressure is less than 500 psia, the Dougall-Rohsenow correlation[A-12] is used. If JFB = 1, form 5.7 (open annulus geometry) of Groeneveld correlation is used when the coolant pressure is greater than 500 psia.

			Otherwise, the Dougall-Rohsenow correlation is used. If JFB = 2, Dougall-Rohsenow correlation is always used. If JFB = 3, Condie-Bengston correlation[A-13] is always used. If JFB = 4, Tong-Young correlation[A-14] is always used.
51-55	I	NFBSW	Number of axial nodes at which time span of film boiling is prescribed by card input. If film boiling region to be calculated by FRAP-T, set NFBSW = 0. This is normal option.
61-65	I	NQBOW	Switch to consider effect of fuel rod bowing on critical heat flux and fuel rod power. 0 = No, 1 = Yes. If NQBOW = 1, Cards 5.2.2 and 5.2.3 must be input, which prescribe deflection of fuel rod due to bowing.

Card(s) 5.2.1 (If NFBSW = 0, omit these cards.)

Columns	Format	Name	Quantity
1-5	I	N	Number of an axial node at which time span of film boiling is prescribed.
11-20	F	TS	Start time of film boiling at axial node N (sec).
21-30	F	TE	End time of prescribed film boiling at axial node N (sec). (Because of the high cladding temperature attained during the period of prescribed film boiling, film boiling will usually continue after the prescribed period).

Repeat Card(s) 5.2.1 until the time span of film boiling has been prescribed at NFBSW different axial nodes.

Card 5.2.2 Effect of Bowing on Critical Heat Flux. (If NQBOW = 0 on Card 5.1, omit this card.)

Columns	Format	Name	Quantity
1-10	F	FBCHF	Multiplier in equation for CHF reduction due to bowing. Equation is described in Section 2 of Appendix D.
11-20	F	BØWTHR	Maximum amount of bowing that can occur without any effect on CHF. The amount of bowing is input as a fraction of amount of bowing required for contact with adjacent fuel rod.

Card 5.2.3 Deflection of Fuel Rod Due to Bowing. (If NQBOW = 0, omit this card.)

Columns	Format	Name	Quantity
1-10	F	BØWFR(1)	Ratio of deflection due to bowing at axial node 1 to maximum possible deflection. The maximim possible deflection is equal to fuel rod spacing minus fuel rod diameter.
11-20	F	BØWFR(2)	Bowing deflection at axial node 2 as a fraction of maximum possible.
21-30	F	BØWFR(3)	Bowing deflection at axial node 2 as a fraction of maximum possible.

Repeat until bowing deflection specified for all axial nodes. If more than eight axial nodes, continue on second card, with bowing fraction for axial node 9 specified in columns 1-10.

Card Groups 5.3 through 5.14 complete the data input that is required for the coolant condition data block. Depending on the value of NSWC (input on Card 5.1), not all of these card groups are input. The card groups required for each value of NSWC are shown in Table A-VII.

TABLE A-VII

CARD GROUPS REQUIRED FOR COOLANT CONDITION DATA BLOCK

NSWC	Required Card Groups
0	5.1, 5.3 - 5.6, 5.8 - 5.10
1	5.1, 5.3 - 5.10
2	5.1, 5.8 - 5.10, tape of transient coolant condition, according to format shown in Appendix E
3	5.1, 5.3, 5.11 - 5.14
4	5.1, tape of transient heat transfer coefficients, coolant temperature and pressure, according to format shown in Appendix E

Card Group 5.3

Specification of pressure history of coolant. Input in same format as Card Group 1.10, four pairs per card.

Columns	Format	Name	Quantity
1-10	F	PBH(1)	Average core coolant pressure at time PBH(2); (psia or N/m^2).
11-20	F	PBH(2)	Time (sec).

Repeat until NPBH pairs have been input. Maximum of 12-1/2 cards of data. The pressure at any given time is found by linearly interpolating the pressure between the input time points.

573 253

If NSWC = 3, or 4, do not input Card Groups 5.4 through 5.10. If NSWC = 2, do not input Card Groups 5.4 through 5.7.

Card Group 5.4

Specification of enthalpy history of lower plenum (coolant at bottom of fuel rods). Input in same format as Card Group 1.10.

Columns	Format	Name	Quantity
1-10	F	HLP(1)	Enthalpy of coolant in lower plenum at time HLP(2); Btu/lbm or joules/kg.
11-20	F	HLP(2)	Time (sec).

Repeat until NHLP pairs have been input. Maximum of 12-1/2 cards of data.

Card Group 5.5

Specification of enthalpy history of upper plenum (coolant at top of fuel rods). If coolant always flows upward, enthalpy of upper plenum can be set equal to any value greater than enthalpy of lower plenum. In this case, the upper plenum enthalpy values are only used to specify that coolant is always flowing upward. If the coolant is flowing downward through the core, however, the upper plenum enthalpy must be accurately specified. The lower plenum enthalpy can then be set to any value greater than upper plenum enthalpy. Input in manner as Card Group 1.10.

Columns	Format	Name	Quantity
1-10	F	HUP(1)	Enthalpy of upper plenum at time HUP(2); Btu/lbm or joules/kg.
11-20	F	HUP(2)	Time (sec).

Repeat until NHUP pairs have been input. Maximum of 12-1/2 cards of data.

Card Group 5.6

Specification of mass flux history of coolant. Input in same manner as Card Group 1.10.

Columns	Format	Name	Quantity
1-10	F	GBH(1)	Mass flux of coolant surrounding fuel rods at time GBH(2); lbm/hr-ft^2 or kg/s m^2.
11-20	F	GBH(2)	Time (sec).

Repeat until NGBH pairs have been input. Maximum of 25 cards of data.

Card Group 5.7

Specification of core average enthalpy history. Input this card group only if NSWC = 1. Input in same format as Card Group 1.10.

Columns	Format	Name	Quantity
1-10	F	HBH(1)	Enthalpy of coolant surrounding fuel rods at time HBH(2); Btu/lbm or joules/kg.
11-20	F	HBH(2)	Time (sec).

Repeat until NHBH pairs have been input. Maximum of six and one-fourth cards of data.

Card Groups 5.8 through 5.10 specify coolant channel geometry needed by the heat transfer and critical heat flux correlations. A set of three parameters describes the geometry. The parameters are heated equivalent diameter, hydraulic diameter, and flow cross-sectional area. They should be computed as follows.

573 255

The heated equivalent diameter and hydraulic diameter are computed according to the equations

$$d_{he} = 4\ A_f/P_h$$

$$d_{hy} = 4\ A_f/P_w$$

where

d_{he} = heated equivalent diameter

d_{hy} = hydraulic diameter.

The parameters A_f, P_h, and P_w are computed according to the equations shown below.

Case 1: Fuel Rod In Middle Of Cluster

$$A_f = S^2 - \pi d_r^{\,2}/4$$

$$P_h = \pi d_r$$

$$P_w = \pi d_r$$

where

A_f = flow cross-sectional area

s = fuel rod spacing (pitch)

d_r = fuel rod outer diameter

P_h = heated perimeter

P_w = wetted perimeter.

573 256

Case 2: Single Fuel Rod Surrounded By Unheated Flow Shroud

$$A_f = \pi d_s^2/4 - \pi d_r^2/4$$

$$P_h = \pi d_r$$

$$P_w = \pi d_s + \pi d_r$$

where

d_s = inside diameter of flow shroud.

Card Group 5.8

Specification of heated equivalent diameter of flow channel. For more information on flow channels, see Card Group 1.11.

Columns	Format	Name	Quantity
1-10	F	DHE(1)	Heated equivalent diameter of flow channel 1 (ft or m) [4 x (flow area)/(heated perimeter)].

Card Group 5.9

Specification of hydraulic diameter of flow channel.

Columns	Format	Name	Quantity
1-10	F	DHY(1)	Hydraulic diameter of flow channel 1 (ft or m) [4 x (flow area)/(wetted perimeter)].

Card Group 5.10 If NSWC not equal to zero on Card 5.1 and NREFLD = 0 on Card 1.2, leave this card blank.

573 257

Specification of cross-sectional area of flow channel.

Columns	Format	Name	Quantity
1-10	F	ACHN(1)	Cross-sectional area of flow channel 1 (ft^2 or m^2).

If NSWC = 3, input Cards 5.11 through 5.14. Otherwise, omit these cards.

Card Group 5.11

Columns	Format	Name	Quantity
1-5	I	NHTCZ	Number of different vertical zones for which heat transfer coefficient and bulk temperature histories will be prescribed. NHTCZ ≤ 10.

Cards 5.12 through 5.14 must be input as a set for each vertical zone. A total of NHTCZ sets must be supplied.

Card 5.12

Columns	Format	Name	Quantity
1-5	I	L	Number of a vertical zone (1 ≤ L ≤ NHTCZ).
6-10	I	NHPRS(L)	Number of heat transfer coefficient-time pairs specified for zone L [NHPRS(L) ≤ 49].
11-15	I	NTPRS(L)	Number of bulk temperature-time pairs specified for zone L [NTPRS (L) ≤ 49].
21-30	F	ZP(L)	Elevation of top boundary of zone L. Elevation of bottom boundary of zone L is assumed to be same as top boundary

of zone L - 1. Bottom boundary of zone 1 assumed to have elevation of zero. Top boundary of top vertical zone must have elevation greater than or equal to active fuel stack length (ft or m).

Card(s) 5.13

Heat transfer coefficient history for vertical zone L. Input is same format as Card Group 1.10, four pairs per card.

Columns	Format	Name	Quantity
1-10	F	HTCA(1)	Heat transfer coefficient at time HTCA(2); (Btu/hr-ft^2-^{o}F or W/m^2·K).
11-20	F	HTCA(2)	Time (sec).
21-30	F	HTCA(3)	Heat transfer coefficient at time HTCA (4); (Btu/hr-ft^2-^{o}F or W/m^2·K).
31-40	F	HTCA(4)	Time (sec).

Repeat until NHPRS(L) pairs have been input. Maximum of 12-1/4 cards.

Card(s) 5.14

Bulk temperature history for vertical zone L. Input in same format as Card Group 1.10, four pairs per card.

Columns	Format	Name	Quantity
1-10	F	TBLKA(1)	Coolant temperature at time TBLKA(2); ^{o}F or K.
11-20	F	TBLKA(2)	Time (sec).

573 259

Repeat until NTPRS(L) pairs have been input. Maximum of 12-1/4 cards.

Repeat Card Groups 5.12 through 5.14 until heat transfer coefficient and coolant temperature-time pairs have been supplied for a total of NHTCZ zones.

If NSWC = 2 or 4, a data set describing the transient coolant conditions is read from disk or tape. The data set is accessed by FORTRAN logical unit 4. The required form of the coolant condition data set is given in Appendix E.

One program in the FRAP package has the purpose of transforming RELAP4 plot data sets to FRAP coolant condition data stes. The information required to use this program is given in Appendix E.

Card 6.1 Specification of Surface Roughness.

Columns	Format	Name	Quantity
1-10	F	RC	Arithmetic mean roughness of inside surface of cladding (microns).
11-20	F	RF	Arithmetic mean roughness of outside surface of fuel pellets.

Data Block 7. Internal Gas and Plenum Data.

Card 7.1

Columns	Format	Name	Quantity
1-5	I	N	Number of fuel rods in rod bundle being analyzed. Always input the integer "1".
6-10	I	NC(N)	Number of coils in upper plenum spring [NC(N) $\geq$ 1].

11-20	F	GSMS(N)	Amount of gas in fuel rod (gram-moles) (leave blank if TGASO(N) > 0 in columns 71 through 80 of this card).
21-30	F	VPLEN(N)	Cold state upper plenum volume of fuel rod (ft^3 or m^3); include volume of plenum spring.
31-40	F	PO(N)	Cold state pressure in fuel rod (psia or N/m^2). If TGASO(N) = 0, only use of this quantity is that of supplying guess of internal fuel rod pressure on first iteration of first time step. Accurate value, therefore, is not required. But, if TGASO(N) > 0, PO(N) is term in calculation of moles of gas in fuel rod. Accurate value, then, is required.
41-50	F	SL(N)	Uncompressed height of upper plenum spring of fuel rod (ft or m).
51-60	F	CD(N)	Uncompressed outer diameter of upper plenum spring coils of fuel rod (ft or m).
61-70	F	DS(N)	Wire diameter of upper plenum spring of fuel rod (ft or m).
71-80	F	TGASO(N)	Temperature of fuel rod gas when at cold state pressure PO(N); ^{o}F or K. This temperature is term in calculation to compute moles of gas in fuel rod. If moles of gas input in columns 11-20, leave these columns blank.

Card 7.2 Geometry of Lower Plenum. (Omit if NBOTPL = 0 on Card 1.2.)

Columns	Format	Name	Quantity
1-5	I	NCOLBP	Number of coils in bottom plenum spring (NCOLBP ≥ 1).
11-20	F	VOLBP	Volume of bottom plenum (ft^3 or m^3).
21-30	F	SPLBP	Uncompressed height of spring (ft or m).
31-40	F	COLDBP	Uncompressed outer diameter of spring (ft or m).
41-50	F	SPDBP	Wire diameter of spring (ft or m).

Card 7.3 Gas Composition Data.

Mole fractions of gas components specified. Total of fractions should sum to 1. If they do not, the code normalizes them so that sum is 1.

Columns	Format	Name	Quantity
1-10	F	GF(1)	Fraction of helium in fuel rod N.
11-20	F	GF(2)	Fraction of argon in fuel rod N.
21-30	F	GF(3)	Fraction of krypton in fuel rod N.
31-40	F	GF(4)	Fraction of xenon in fuel rod N.
41-50	F	GF(5)	Fraction of hydrogen in fuel rod N.

573 262

51-60	F	GF(6)	Fraction of air in fuel rod N.
61-70	F	GF(7)	Fraction of water vapor in fuel rod N.

If, for example, a fuel rod contained 0.008 moles of helium and 0.002 moles of argon, then GF(1) = 0.8, GF(2) = 0.2, and GF(3), GF(4) . . . are equal to zero.

Data Block 8. Plot Subcode Input Data. (If plots are not wanted, omit the cards in this data block.)

Card 8.1

Columns	Format	Name	Quantity
1-5	I	NPLTS	Number of axial nodes at which plots of fuel rod response are wanted.
6-10	I	NOGRID	If NOGRID = 0, grid is placed on plots. If NOGRID = 1, grid is not placed on plots.

Card 8.2

Columns	Format	Name	Quantity
1-5	I	N1	Number of an axial node for which temperature, deformation, and pressure histories are to be plotted.
6-10	I	N2	Number of an axial node for which temperature, deformation, and pressure histories are to be plotted.

Repeat for all nodes to be plotted.

If plots are wanted, all input cards from Cards 8.3 through 8.23 must be supplied.

573 263

Card 8.3 Time Axis.

Columns	Format	Name	Quantity
1-10	F	TSTART	Minimum time on time axis (sec).
11-20	F	TEND	Maximum time on time axis (sec).
21-30	F	AXLT	Length of time axis (in.). A tick mark or vertical line is placed on the plots at every (TEND-TSTART)/AXLT increment of time on the time axis. For example, if TSTART = 0, TEND = 100 sec, AXLT = 10 in., a tick mark is placed every 10 sec on time axis.
31-70	A	LABLT	Label to be given time axis.

Card 8.4 Cladding Surface Temperature Axis.

Columns	Format	Name	Quantity
1-10	F	TSMIN	Minimum cladding surface temperature on axis (^{o}F or K).
11-20	F	TSMAX	Maximum cladding surface temperature on axis (^{o}F or K).
21-30	F	AXLTS	Length of surface temperature axis (in.). A tick mark or horizontal line is placed on the plots at every (TSMAX-TSMIN)/AXLTS increment of temperature on the temperature axis.
31-70	A	LABLTS	Label to be given surface temperature axis.

Card 8.5 Fuel Centerline Temperature Axis.

Columns	Format	Name	Quantity
1-10	F	TCLMIN	Minimum fuel centerline temperature on axis (^{o}F or K).
11-20	F	TCLMAX	Maximum fuel centerline temperature on axis (^{o}F or K).
21-30	F	AXLTMP	Length of centerline temperature axis (in.).
31-70	A	LABLTM	Label to be given centerline temperature axis.

Card 8.6 Gas Gap Pressure Axis.

Columns	Format	Name	Quantity
1-10	F	PMIN	Minimum gas gap pressure on axis (psia or N/m^2).
11-20	F	PMAX	Maximum gas gap pressure on axis (psia or N/m^2).
21-30	F	AXLP	Length of gas gap pressure axis (in.)
31-70	A	LABLP	Label to be given gas gap pressure axis.

Card 8.7 Cladding Hoop Strain Axis.

Columns	Format	Name	Quantity
1-10	F	EPSMIN	Minimum cladding hoop strain on axis (dimensionless).
11-20	F	EPSMAX	Maximum cladding hoop strain on axis (dimensionless).

21-30	F	AXLEPS	Length of cladding hoop strain axis (in.).
31-70	A	LABLE	Label to be given cladding hoop strain axis.

Card 8.8 Fuel Axial Displacement Axis.

Columns	Format	Name	Quantity
1-10	F	UZFMIN	Minimum fuel stack length change on axis (in. or m).
11-20	F	UZFMAX	Maximum fuel stack length change on axis (in. or m).
21-30	F	AXLUZF	Length of fuel stack length change axis (in.).
31-70	A	LABLUF	Label to be given fuel stack length change axis.

Card 8.9 Cladding Axial Displacement Axis.

Columns	Format	Name	Quantity
1-10	F	UZCMIN	Minimum cladding length change on axis (in. or m).
11-20	F	UZCMAX	Maximum cladding length change on axis (in. or m).
21-30	F	AXLUZC	Length of cladding length change axis (in.).
31-70	A	LABLUC	Label to be given cladding length change axis.

Card 8.10 Fuel Rod Power Axis.

Columns	Format	Name	Quantity
1-10	F	PMIN	Minimum linear fuel rod power on axis (kW/ft or kW/m).
11-20	F	PMAX	Maximum linear fuel rod power on axis (kW/ft or kW/m).
21-30	F	PLEN	Length of linear fuel rod power axis (in.).
31-70	A	PLABL	Label to be given linear fuel rod power axis.

Card 8.11 Fuel Surface Temperature Axis.

Columns	Format	Name	Quantity
1-10	F	TFSMIN	Minimum fuel surface temperature on axis (^{o}F or K).
11-20	F	TFMAX	Maximum fuel surface temperature on axis (^{o}F or K).
21-30	F	TFSLEN	Length of fuel surface temperature axis (in.).
31-70	A	TFSLAB	Label to be given fuel surface temperature axis.

Card 8.12 Gas Gap Heat Transfer Coefficient Axis.

Columns	Format	Name	Quantity
1-10	F	HGMIN	Minimum gap heat transfer coefficient on axis (Btu/hr-^{o}F-ft^{2} or W/M^{2}.K).

573 267

11-20	F	HGMAX	Maximum gap heat transfer coefficient on axis (Btu/hr-^{o}F-ft^{2} or W/M^{2}.K).
21-30	F	HGLEN	Length of gap heat transfer coefficient axis (in.).
31-70	A	HGLABL	Label to be given gap heat transfer coefficient axis.

Card 8.13 Surface Heat Transfer Coefficient Axis. (Logarithmic scale.)

Columns	Format	Name	Quantity
1-10	F	HSMIN	Minimum surface heat transfer coefficient on axis (Btu/hr-^{o}F-ft^{2} or W/M^{2}.K).
11-20	F	HSMAX	Maximum surface heat transfer coefficient on axis (Btu/hr-^{o}F-ft^{2} or W/M^{2}.K).
21-30	F	HSLEN	Length of surface heat transfer coefficient axis (in.).
31-70	A	HSLAB	Label to be given surface heat transfer coefficient axis.

Card 8.14 Average Cladding Temperature Axis.

Columns	Format	Name	Quantity
1-10	F	TAMIN	Minimum average cladding temperature on axis (^{o}F or K).
11-20	F	TAMAX	Maximum average cladding temperature on axis (^{o}F or K).

21-30	F	TALEN	Length of average cladding temperature axis (in.).
31-70	A	LABLTA	Label to be given average cladding temperature axis.

Card 8.15 Heat Per Unit Length Transferred Out of Fuel Rod Axis. This plot designed to overlay plot specified by Card 8.10.

Columns	Format	Name	Quantity
1-10	F	QMIN	Minimum heat out value on axis (kW/ft or kW/m).
11-20	F	QMAX	Maximum heat value on axis (kW/ft or kW/m).
21-30	F	QLEN	Length of heat out axis (in.).
31-70	A	QLABL	Label to be given heat out axis.

Card 8.16 Plenum Pressure Axis.

Columns	Format	Name	Quantity
1-10	F	PPMIN	Minimum plenum pressure on axis (psia or N/m^2).
11-20	F	PPMAX	Maximum plenum pressure on axis (psia or N/m^2).
21-30	F	PPLEN	Length of plenum pressure axis (in.).
31-70	A	PPLABL	Label to be given plenum pressure axis.

573 269

Card 8.17 Fuel Rod Upper Plenum Temperature Axis.

Columns	Format	Name	Quantity
1-10	F	TPMIN	Minimum plenum temperature on axis (^{o}F of K).
11-20	F	TPMAX	Maximum plenum temperature on axis (^{o}F or K).
21-30	F	TPLEN	Length of plenum temperature axis (in.).
31-70	A	TPLABL	Label to be given plenum temperature axis.

Card 8.18 Gas Flow Rate Axis. Plot of rate at which gas flows from plenum.

Columns	Format	Name	Quantity
1-10	F	GFMIN	Minimum gas flow rate on axis (gram-moles/ sec).
11-20	F	GFMAX	Maximum gas flow rate on axis (gram-moles/sec).
21-30	F	GFLEN	Length of gas flow rate axis (in.).
31-70	A	GFLABL	Label to given gas flow rate axis.

Card 8.19 Mass Flux Axis.

Plot of mass flux of coolant surrounding fuel rod. (If NSWC = 3 or 4 on Card 5.1, put dummy values on this card such that GMAX > GMIN and GLEN > 0.)

Columns	Format	Name	Quantity
1-10	F	GMIN	Minimum mass flux on axis (lbm/ft^2-hr or $kg/s \cdot m^2$).
11-20	F	GMAX	Maximum mass flux on axis (lbm/ft^2-hr or $kg/s \cdot m^2$).
21-30	F	GLEN	Length of mass flux axis (in.).
31-70	A	GLABL	Label to be given mass flux axis.

Card 8.20 Coolant Quality Axis.

Plot of average quality in coolant channel at level of axial node being plotted. (If NSWC = 3 or 4 on Card 5.1 put dummy values on this card such that XMAX > XMIN and XLEN > 0.)

Columns	Format	Name	Quantity
1-10	F	XMIN	Minimum quality on axis (dimensionless).
11-20	F	XMAX	Maximum quality on axis (dimensionless).
21-30	F	XLEN	Length of quality axis (in.).
31-70	A	XLABL	Label to be given quality axis.

Card 8.21 Coolant Pressure Axis. Plot of average pressure in coolant channel at level of axial node being plotted.

Columns	Format	Name	Quantity
1-10	F	PCMIN	Minimum pressure on axis (psia or N/m^2).
11-20	F	PCMAX	Maximum pressure on axis (psia or N/m^2).

573 271

21-30	F	PCLEN	Length of pressure axis (in.).
31-70	A	PCLABL	Label to be given coolant pressure axis.

Card 8.22 Fuel Rod Radial Gas Gap Thickness Axis.

Columns	Format	Name	Quantity
1-10	F	THKMIN	Minimum gap thickness on axis (mils or m).
11-20	F	THKMAX	Maximum gap thickness on axis (mils or m).
21-30	F	THLEN	Length of gap thickness axis (in.).
31-70	A	THKLAB	Label to be given gap thickness axis.

Card 8.23 Coolant Temperature Axis.

Columns	Format	Name	Quantity
1-10	F	TBMIN	Minimum coolant temperature on axis (^{o}F or K).
11-20	F	TBMAX	Maximum coolant temperature on axis (^{o}F or K).
21-30	F	TBLEN	Length of coolant temperature axis (in.).
31-70	A	TBLAB	Label to be given coolant temperature axis.

3. REFERENCES

A-1. C. R. Hann, C. E. Beyer, L. J. Parchen, GAPCON-THERMAL-1: A Computer Program for Calculating the Gap Conductance in Oxide Fuel Pins, BNWL-1778 (September 1973).

A-2. J. Rest, GRASS-SST: A Comprehensive Mechanistic Model for the Prediction of Fission Gas Behavior in UO_2 Based Fuels During Steady State and Transient Conditions, NUREG/CR-0202, ANL-78-53 (June 1978).

A-3. Yasus Harayama, "Calculated Effect of Radially Asymmetric Heat Generation on Temperature and Heat Flux Distribution in a Fuel Rod," Nuclear Engineering and Design (31), 1974.

A-4. J. S. Gellerstedt et al, "Correlation of Critical Heat Flux in a Bundle Cooled by Pressurized Water," Two-Phase Flow and Heat Transfer in Rod Bundles, Symposium Presented at the Winter Annual Meeting of the American Society of Mechanical Engineers, Los Angeles, California, November 1969, pp 63-71.

A-5. E. D. Hughes, A Correlation of Rod Bundle Critical Heat Flux for Water in the Pressure Range 150 to 725 psia, IN-1412 (July 1970).

A-6. P. G. Barnett, A Correlation of Burnout Data for Uniformly Heated Annuli and Its Use for Predicting Burnout in Uniformly Heated Rod Bundles, AEEW-R463 (1966).

A-7. B. C. Slifer and J. E. Hench, Loss of Coolant Accident and Emergency Cooling Models for General Electric Boiling Water Reactors, NEDO-10329 (April 1971).

A-8. D. H. Knoebel et al, Forced Convection Subcooled Critical Heat Flux, D2O and H2O Coolant with Aluminum and Stainless Steel Heaters, DP-1306 (February 1973).

A-9. L. S. Tong, Boiling Crisis and Critical Heat Flux, TID-25887 (August 1972).

A-10. S. A. Eide and R. G. Gottula, Evaluation and Results of LOFT Steady State Departure from Nucleate Boiling Tests, TREE-NUREG-1043 (April 1977).

A-11. D. C. Groeneveld, An Investigation of Heat Transfer in a Liquid Deficient Regime, AECL-3281 (Revised December 1968; Revised August 1969).

A-12. R. S. Dougall and W. M. Rohsenow, Film Boiling on the Inside of Vertical Tubes with Upward Flow of The Fluid at Low Qualities, MIT-TR-9079-26 (1963).

573 273

A-13. K. G. Condie et al, "Regression Analysis of Post-CHF Flow Boiling Data," Fifth International Heat Transfer Conference, Japan, September 1974, pp 115-119.

A-14. L. S. Tong and J. D. Young, "A Phenomenological Transition and Film Boiling Heat Transfer Correlation," Fifth International Heat Transfer Conference, Japan, July 1974, Journal of Heat Transfer (1974) pp 20-124.

APPENDIX B

SAMPLE PROBLEM

APPENDIX B

SAMPLE PROBLEM

A FRAP-T prediction of the behavior of the hot fuel rod of the hot coolant channel in a PWR after a double-ended cold leg break is shown. The input data, calculation printout, and plots of calculation results are presented. A summary description of the fuel rod analyzed is shown in Table B-I. The peak rod power at initiation of the accident was 51.9 kW/m. The internal gas in the fuel rod consisted of 0.030 gram-moles of helium. The fuel rod was assumed to be at beginning-of-life, so a FRAPCON-1 calculation of the fuel rod initial conditions was not required. The boundary conditions were determined by the RELAP code, and then input to FRAP-T5 on cards.

TABLE B-I

FUEL ROD DATA (COLD STATE)

Measurement	British Units	SI Units
Fuel stack length	12 ft	3.658 m
Cladding outside diameter	0.422 in.	0.01072 m
Cladding thickness	24 mils	0.6096×10^{-3} m
Amount of internal gas		0.030 gram-moles
Plenum volume	0.657 $in.^3$	1.076×10^{-5} m^3
Fuel density	638 lbf/ft^3	1.022×10^4 kg/m^3
Cladding density	409 lbf/ft^3	5.5602×10^3 kg/m^3
Arithmetic mean roughness of fuel		0.114×10^{-5} m
Arithmetic mean roughness of cladding		0.216×10^{-5} m
Radius to outside edge of pellet dishes	0.121 in.	0.307×10^{-2} m

573 277

The input cards for the problem are listed on computer printout sheets 1 and 2[a] included at the end of this appendix. A descriptive printout of the input data is shown on sheets 3 through 13. The data are printed out in about the same order as they are stored on the input cards. The input data of a general nature are shown on sheets 3 through 6. The temperature calculation subcode input data are shown on sheets 7 through 9. The radial mesh that was used by both the temperature and deformation subcodes is shown in this printout. The radial heat source distribution is also shown. The average fuel rod power history and axial power profile are shown on sheet 10. The input data used to specify the transient fuel rod to coolant heat transfer coefficients and coolant temperature are shown on sheets 11 and 12. The heat transfer coefficients are prescribed for three axial zones. Fuel rod to coolant heat transfer is uniform within each zone. The input data for the gap conductance and gap pressure subcodes are shown on sheet 13.

Computer printout showing fuel rod behavior for the first 20 seconds following the cold leg break are shown on sheets 14 through 27. The fuel rod state just prior to accident initiation is shown on sheets 14 through 18. Localized ballooning and rupture of the cladding occurred 11 seconds after accident initiation. Rupture occurred near the point of peak fuel rod power (axial node 5). When cladding rupture occurred, the fuel rod internal pressure dropped to the value of the coolant pressure (shown in Figure B-1). The peak cladding surface temperature was 1284 K and occurred 10.5 seconds after the pipe break at axial node 5. The surface temperature history at axial node 5 is shown in Figure B-2. The fuel centerline temperature continuously dropped during the LOCA. This is shown in Figure B-3. The uniform cladding hoop strain history at axial node 5 is shown in Figure B-4. The maximum uniform cladding hoop strain is 17%. Localized ballooning and rupture occurred at axial node 5. This deformation is not shown in Figure B-4. The gap conductance history at axial node 5 is shown in Figure B-5. The plenum gas temperature is shown in Figure B-6. Length change of the cladding is shown in Figure B-7.

---

a. All sheet numbers mentioned in this appendix refer to the numbers located in the upper right corner of the computer printout sheets.

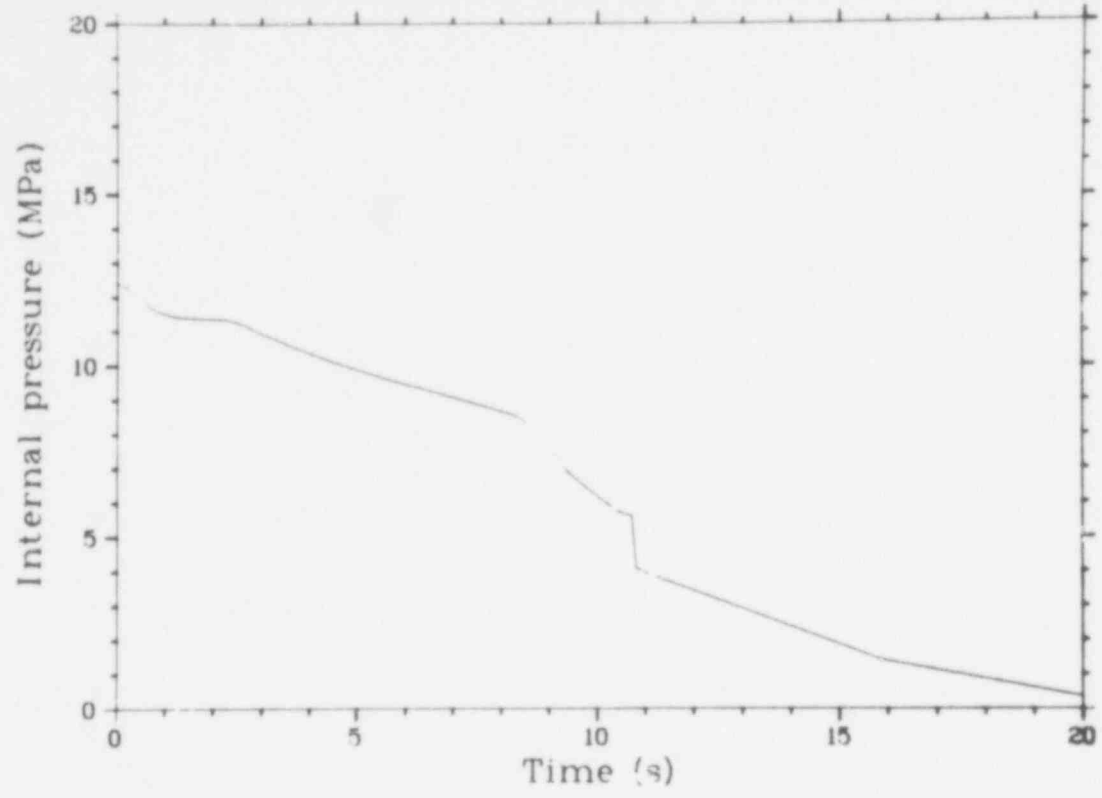

Fig. B-1 Fuel rod internal pressure history.

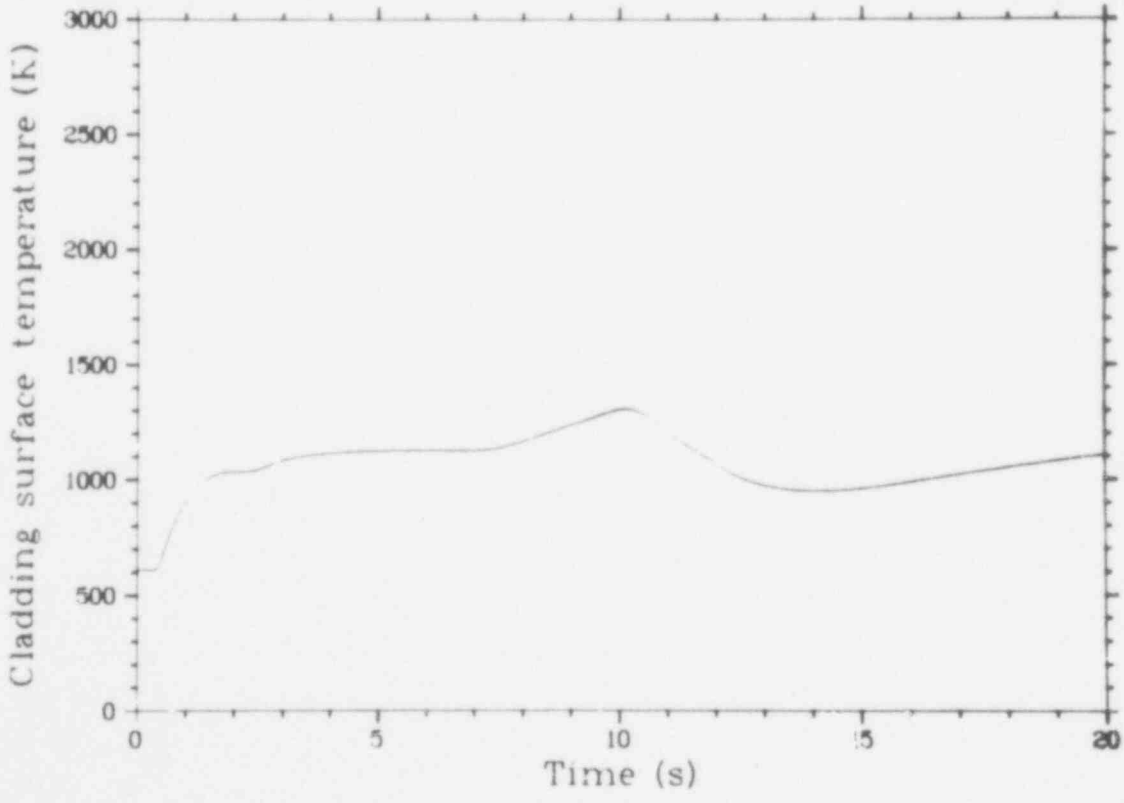

Fig. B-2 Cladding surface temperature history.

573 279

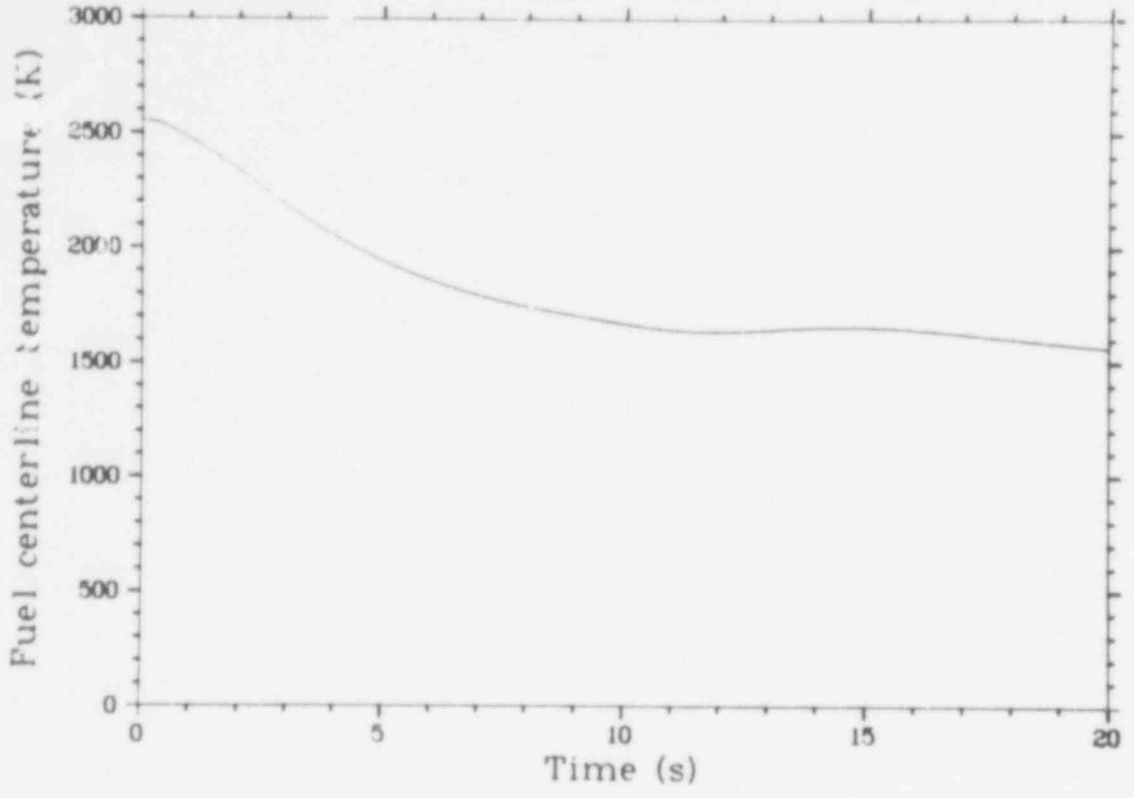

Fig. B-3 Fuel centerline temperature history.

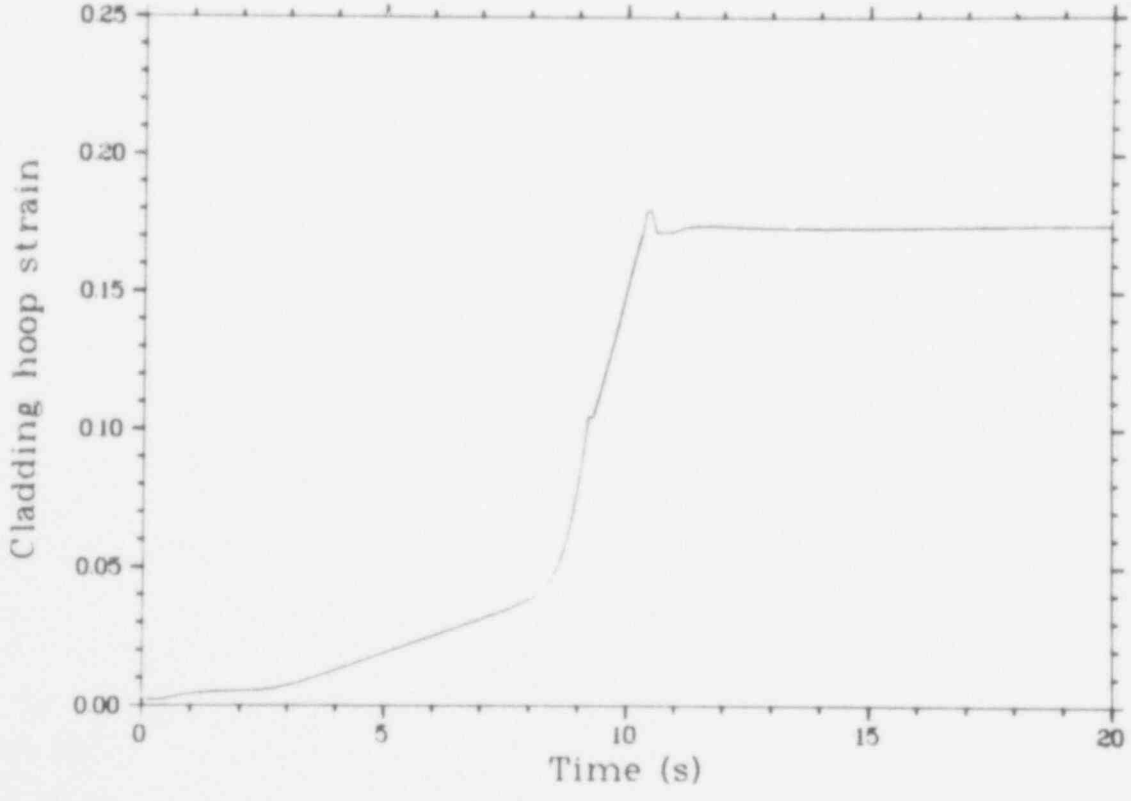

Fig. B-4 Cladding hoop strain history.

573 280

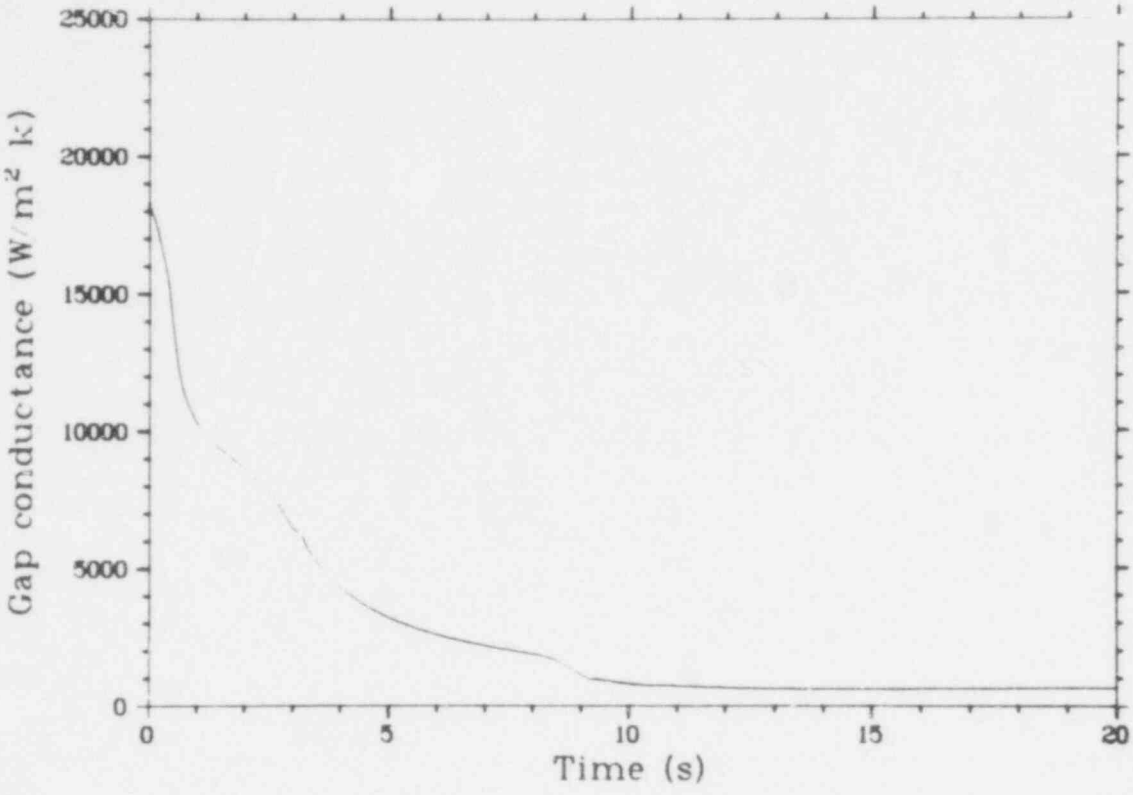

Fig. B-5 Gap conductance history.

The strain quantities printed at each axial node are those computed by the FRACAS subcode. Since the FRACAS subcode is not used after the balloon subcode is turned on, the printed strains after cladding ballooning has begun stay fixed to the values calculated just prior to initiation of localized cladding ballooning. Thus, the cladding plastic hoop strain after cladding failure at the rupture node is shown to be 17% (the instability strain), even though the hoop strain in the region of localized cladding ballooning reached a value of 37%.

The calculations were performed on the CDC 7600 computer at INEL and took five minutes of computer time.

573 281

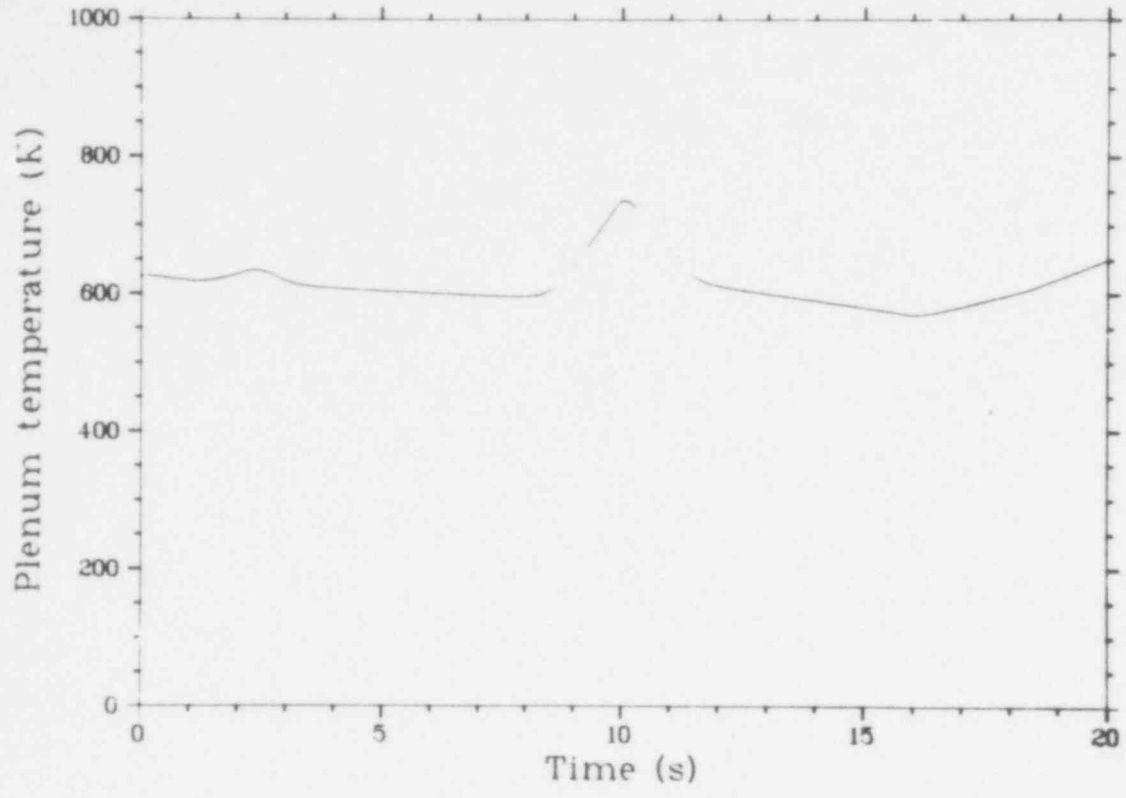

Fig. B-6 Plenum gas temperature history.

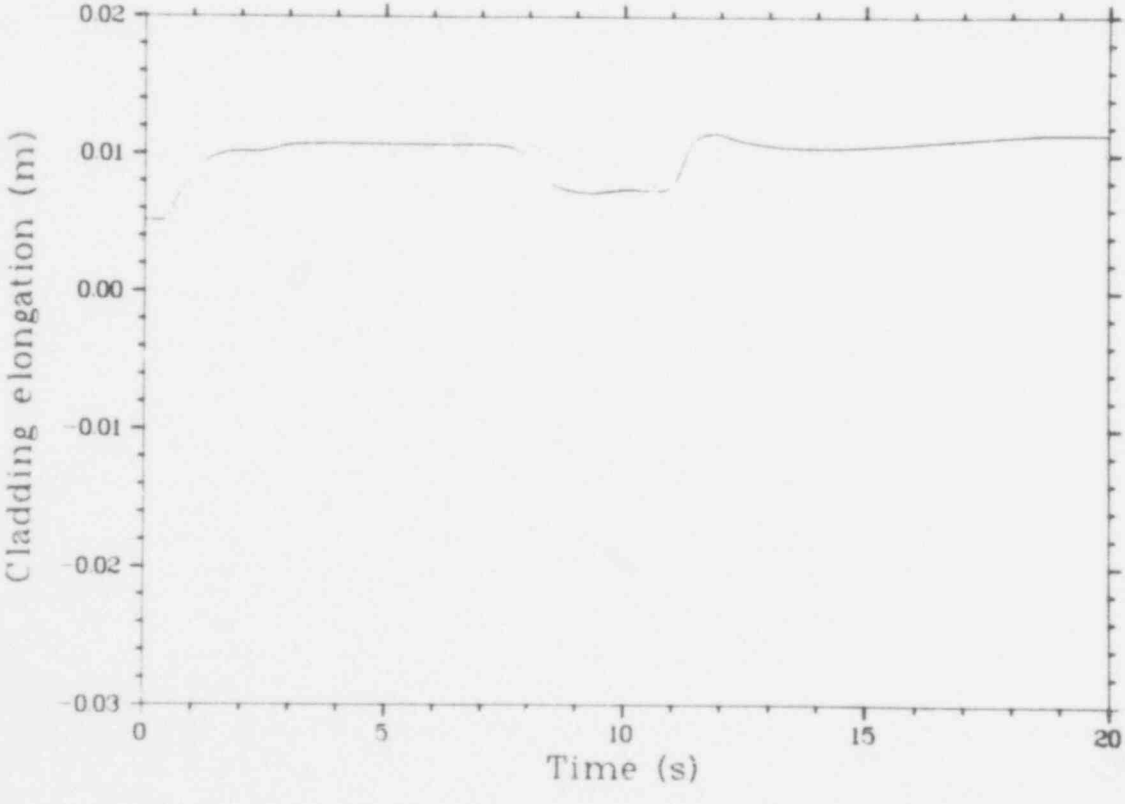

Fig. B-7 Cladding length change history.

573 282

```
        1         2         3         4         5         6         7         8
12345678901234567890123456789012345678901234567890123456789012345678901234567890
    1    1  -16        00    2    0    0          0
    C
    0.        20.        .1         .5        12.       .03516      70.        .1
  638.       .01008     .000625     .6251      .2E-06                           0.
    2
  .001       .001                                                    1.
    1          1 1.
    .5        1.5        2.5        3.5        4.25       4.75       5.25       5.75
   6.25       6.75       7.25       7.75       8.5        9.5        10.5       11.5

  100  100    50   50
   70.       8500.      70.        3500.
* BLOWDOWN ANALYSIS OF SINGLE ROD
* GENERAL DATA FOR HEAT-1
01010001    14          2          0.         1.        100         1.        100
* GEOMETRY LOCATION AND MESH INCREMENT
01010200    C           1
* MESH INCREMENT DATA - UNITS ARE FT
01010201    10        .01525       1          .015575    2         .01758
* COMPOSITION OVERLAY
01010301    1           10         3          11         2          13
* SOURCE DISTRIBUTION CARDS
01010401  .982 1 .983 2  .984 3  .985 4  .988 5  .991 6  .996 7
01010402  1.002  8 1.009  9 1.017  10  0.  13
* INITIAL TEMPERATURE DISTRIBUTION
01010601    650.        14
*
    1    8   11
   11.08       0.        3.695      0.6        2.01       2.3        1.413      3.7
   0.815      10.0       1.902      13.0       0.543      16.3       0.402      45.
    .56       0.545      1.17      1.6333      1.46       2.7        1.61      3.8125
   1.58       4.9        1.48      5.99166     1.34       7.075      1.15      8.15833
   6.94       9.25       0.70       10.3       0.36      11.39166
    3   12
  2273.        0.        1561.      0.51       1405.      1.01       1198.      2.15
  1166.       2.75       940.       6.95       908.       7.55       856.       8.15
   686.       9.87       368.       11.07      206.       15.87       50.       20.07
    3
    1   12    12          3.
 51600.        0.        166.       0.51        36.       1.01       281.       2.15
   120.       2.75       100.       6.95        52.       7.55        50.       8.15
     5.       9.87       160.       11.07      60.       15.87       50.       20.07
   638.3        0.       601.5      0.51       587.5      1.01       743.8      2.15
   563.5       2.75      537.2      6.94       533.1      7.55       533.2      8.15
  1333.8       9.87       531.      11.07      384.2      15.87      893.2      20.07
    2   12    12          9.
 62300.        0.        158.       0.51        36.       1.01       281.       2.15
   116.       2.75       100.       6.95        52.       7.55        50.       8.15
     5.       9.87       160.      11.07       60.       15.87       50.       20.07
   638.3        0.       601.5      0.51       587.5      1.01       743.8      2.15

        1         2         3         4         5         6         7         8
12345678901234567890123456789012345678901234567890123456789012345678901234567890
```

Sheet 2

```
         1         2         3         4         5         6         7         8
12345678901234567890123456789012345678901234567890123456789012345678901234567890

   563.5      2.75      537.2       6.95      533.1      7.55      553.2      8.15
  1333.8      9.87      531.       11.07      384.2     15.87      893.2     20.07
     3   12  12          12.
   39300.     0.        250.        0.51       40.       1.01      281.       2.15
   128.       2.75      110.        6.95       52.       7.55        5.       8.15
     5.       9.87      160.       11.07       60.      15.87       50.      20.07
   638.3      0.        601.5       0.51      587.5      1.01      743.8      2.15
   563.5      2.75      537.2       6.95      533.1      7.55      553.2      8.15
  1333.8      9.87      531.       11.07      384.2     15.87      893.2     20.07
   2.16      1.14
     1   22  3.00E-02   .38E-03   2243.      .4583     .0291     .006333

     4    1
     4    5     6    7
    0.        20.         5.               TIME (S)
      0.      3000.        6.      SURFACE TEMPERATURE OF CLAD (K)
      0.      3000.        6.      CENTERLINE TEMPERATURE OF FUEL (K)
  1.0E+05    2.0E+07      8.     GAS GAP PRESSURE (N/M**2)
      0.       .25         5.       CLADDING HOOP STRAIN (M/M)
    0.        .05        10.     FUEL AXIAL DISPLACEMENT (M)
   -.03       .02         5.0    CLADDING AXIAL DISPLACEMENT (M)
      0.      80.         8.     FUEL ROD POWER (KW/M)
    0.      2000.         8.0    FUEL SURFACE TEMP. (K)
     0.0     5.0E+04      5.     GAP HEAT TRANSFER COEFFICIENT (W/M**2-K)
  1.0E+01    1.0E+07      6.0    SURF. HEAT TRANSF. COEFF. (W/M**2-K)
    0.      2000.         8      AVERAGE CLADDING TEMP. (K)
   -20.       +20.        8.0    SURFACE HEAT FLUX PER UNIT LENGTH (KW/M)
  1.0E+05   1.26E+07      5.0    PLENUM PRESSURE (N/M**2)
    0.       1000.        5.     PLENUM TEMPERATURE (K)
 -2.5E-10   2.5E-10      10.     GAS FLOW RATE (GRAM-MOLES/SEC)
  -1.E+03    2.E+03       6.     MASS FLUX (KG/M**2-SEC)
    0.        1.          5.   COOLANT QUALITY
    0.0      2.0E+07      10.0   COOLANT PRESSURE (N/M**2)
    0.0      2.0E-03      10.    GAP THICKNESS (M)
    0.       1000.        5.     BULK TEMPERATURE (K)

         1         2         3         4         5         6         7         8
12345678901234567890123456789012345678901234567890123456789012345678901234567890
85 INPUT CARDS
```

```
                *** ROD CODE GENERAL INPUT ***
INPUT IN BRITISH SYSTEM OF UNITS - OUTPUT IN S.I. UNITS
NUMBER OF FUEL RODS          =   1
NUMBER OF FLOW CHANNELS      =   1
NUMBER OF AXIAL NODES        =  16

FUEL DEFORMATION MODEL TYPE =    0
FREE THERMAL EXPANSION FUEL DEFORMATION MODEL SPECIFIED

CATHCART CLADDING OXIDATION MODEL SPECIFIED

MODIFIED ROSS AND STOUTE MODEL FOR GAP CONDUCTANCE TO BE USED

GAS FLOW MODEL NOT TO BE USED - INSTANT PRESSURE EQUILIBRIUM ASSUMED

INITIAL TIME              =0.            SEC
FINAL TIME                = .260000E+02 SEC
MAXIMUM TIME STEP         = .100000E+00 SEC
IF TIME STEP EXCEEDS  .100000E+06 SEC , STEADY-STATE HEAT CONDUCTION MODEL TO BE USED.
TIME SPAN BETWEEN EDITS = .500000E+00 SEC
ACTIVE FUEL STACK LENGTH = 12.0000 FT          3.658 M
ROD DIAMETER     =  .03516 FT          .01072 M
CLADDING COLD WORK = .10000
PROBABILITY THRESHOLD FOR FUEL ROD FAILURE =1.10000


         *** FUEL PELLET DATA ***

FUEL DENSITY      = .63800E+03 LBM/FT3      .10220E+05 KG/M3
FRACTION OF THEORETICAL DENSITY =  .932457

SHOULDER RADIUS =  .01008 FT          .00307 M
  (AXIAL EXPANSION OF FUEL STACK IS ON A LINE THRU THIS SHOULDER)
DISH DEPTH       = .62500E-03 FT      .19050E-03 M
PELLET HEIGHT    = .25100E-01 FT      .76505E-02 M
DISH VOLUME/PELLET = .20000E-06 FT3      .56634E-08 M**3
FRACTION BY WEIGHT OF FUEL THAT PLUTONIUM OXIDE =0.000000
BURNUP OF FUEL =0.           MWS/KG


RATIO OF ATOMS OXYGEN TO ATOMS URANIUM IN FUEL (AS FABRICATED) = .200000E+01
AVERAGE FAST NEUTRON FLUX (N/M**2-SEC) =0.
TIME SPAN OF FAST NEUTRON FLUX (SEC) =0.
COLD STATE TEMPERATURE OF ROD =  70.0 F        294.3 K
CONVERGENCE FRACTION FOR INTERNAL PRES.  = 1.00E-03
CONVERGENCE FRACTION FOR TEMPERATURES    = 1.00E-03
```

// ROD TO COOLANT CHANNEL CONNECTIONS //

ROD NO.	CHANNEL	FRACTION	CHANNEL	FRACTION	CHANNEL	FRACTION	CHANNEL	FRACTION
1	1	1.000E+00	0	0.	0	0.	0	0.

AXIAL NODE	MID-PLANE ELEVATIONS (FT)	(M)	NODE LENGTHS (FT)	(M)
1	.5000	.1524	1.0000	.3048
2	1.5000	.4572	1.0000	.3048
3	2.5000	.7620	1.0000	.3048
4	3.5000	1.0668	.8750	.2667
5	4.2500	1.2954	.6250	.1905
6	4.7500	1.4478	.5000	.1524
7	5.2500	1.6002	.5000	.1524
8	5.7500	1.7526	.5000	.1524
9	6.2500	1.9050	.5000	.1524
10	6.7500	2.0574	.5000	.1524
11	7.2500	2.2098	.5000	.1524
12	7.7500	2.3622	.6250	.1905
13	8.5000	2.5908	.8750	.2667
14	9.5000	2.8956	1.0000	.3048
15	10.5000	3.2004	1.0000	.3048
16	11.5000	3.5052	1.0000	.3048

NORMALIZED AXIAL VARIATION IN FAST FLUX ASSUMED SAME AS THAT OF FUEL ROD POWER

*** NO DIALS TURNED ON ***

****

********** REFLOOD FLAG IS SET TO OFF
****

```
                    / THERMAL PROPERTY DATA /

FUEL PROPERTY TABLES IN THE TEMPERATURE RANGE   70.0 TO 8500.0 F          294.3 TO 4977.6 K
WILL USE 100 POINTS FOR THERMAL CONDUCTIVITY, 100 FOR HEAT CAPACITY.

CLAD PROPERTY TABLES IN THE TEMPERATURE RANGE   70.0 TO 3500.0 F          294.3 TO 2199.8 K
WILL USE  50 POINTS FOR THERMAL CONDUCTIVITY,  50 FOR HEAT CAPACITY.

FUEL DENSITY =          6.3800E+02 LBM/FT**3     1.0220E+04 KG/M**3
FRACTION OF THEORETICAL DENSITY = 93.25 (

CLAD DENSITY =          4.0954E+02 LBM/FT**3     6.5602E+03 KG/M**3

GAS GAP HEAT CAPACITY =  1.200E-02 BTU/FT**3.F    8.048E+02 J/M**3.K

FUEL MELTING TEMPERATURE =  5144.0 F                3113.2 K

FUEL HEAT OF FUSION =   7.5156E+04 BTU/FT**3     2.8002E+09 J/M**3

CLAD MELTING TEMPERATURE =  3317.0 F                2098.2 K

CLAD HEAT OF FUSION =   3.9616E+04 BTU/FT**3     1.4760E+09 J/M**3
ERROR IN POLATE

INITIAL INDEX =     1          FINAL INDEX =     0          ARRAY LENGTH =    13          ARGUMENT =   .294261E+03

TABLE OF X VALUES =
   .300000E+03    .400000E+03    .640000E+03    .109000E+04    .109300E+04    .111300E+04    .113300E+04    .115300E+04
   .117360E+04    .121300E+04    .121300E+04    .123300E+04    .124800E+04
```

LISTING OF INPUT DATA FOR CASE 1

```
    1    * BLOWDOWN ANALYSIS OF SINGLE ROD
    2    * GENERAL DATA FOR HEAT-1
    3    01010001      14          2          0.          1.        100          1.        100
    4    * GEOMETRY LOCATION AND MESH INCREMENT
    5    01010200       0          1
    6    * MESH INCREMENT DATA - UNITS ARE FT
    7    01010201      10       .01525        1        .015575     2         .01758
    8    * COMPOSITION OVERLAY
    9    01010301       1         10          3         11          2         13
   10    * SOURCE DISTRIBUTION CARDS
   11    01010401   .982 1 .983 2  .984 3  .985 4  .988 5  .991 6  .996 7
   12    01010402  1.002  8  1.009  9  1.017  10  0.  13
   13    * INITIAL TEMPERATURE DISTRIBUTION
   14    01010601    650.       14
   15    *
```

GENERAL DATA

HEAT1 PROBLEM NUMBER	= 1
NUMBER OF MESH POINTS	= 14
GEOMETRY TYPE	= CYLINDRICAL
LEFT BOUNDARY COORD.	= 0.
SOURCE SCALING FACTOR	= 1.00000E+00
TOTAL INTEG. SOURCE	= 7.30565E-04

DATA FOR STEADY STATE CALCULATIONS

MAX NO. OF ITERATIONS	= 100
CONVERGENCE CRITERION	= 1.00000E+00

DATA FOR TIME DEPENDENT CALCULATIONS

MAX NO. OF ITERATIONS	= 100

MESH INTERVALS - (J(I), DELTA X(I))
MESH INCREMENT, DELTA X(I), CONSTANT BETWEEN MESH POINTS J(I-1) AND J(I)

11. 1.52500E-03 12. 3.25000E-04 14. 1.00250E-03

CUMULATIVE MESH COORDINATES - (J, X(J))

1.	0.	2.	1.52500E-03	3.	3.05000E-03	4.	4.57500E-03	5.	6.10000E-03	6.	7.62500E-03
7.	9.15000E-03	8.	1.06750E-02	9.	1.22000E-02	10.	1.37250E-02	11.	1.52500E-02	12.	1.55750E-02
13.	1.65775E-02	14.	1.75800E-02								

COMPOSITION OVERLAY - (J(I), COMP ID(I))
COMPOSITION CONSTANT BETWEEN MESH POINTS J(I-1) AND J(I)

11. 1 12. 3 14. 2

SOURCE DISTRIBUTION - (J(I), Q(I))
SOURCE Q(I) CONSTANT BETWEEN MESH POINTS J(I-1) AND J(I)

2.	9.82000E-01	3.	9.83000E-01	4.	9.84000E-01	5.	9.85000E-01	6.	9.88000E-01	7.	9.91000E-01
8.	9.96000E-01	9.	1.00200E+00	10.	1.00900E+00	11.	1.01700E+00	14.	0.		

INITIAL TEMPERATURE DISTRIBUTION - (J(I), T(I))
TEMPERATURE T(I) CONSTANT BETWEEN MESH POINTS J(I-1) AND J(I)

14. 6.50000E+02

POWER HISTORY AND AXIAL PROFILE INPUT DATA FOR 1 FUEL RODS

ROD NO.	DATA PAIRS	LINEAR POWER (KW/FT)	TIME (SEC)	LINEAR POWER (KW/FT)	TIME (SEC)	LINEAR POWER (KW/FT)	TIME (SEC)	LINEAR POWER (KW/FT)	TIME (SEC)
1	8	1.1060E+01	0.	3.6950E+00	6.0000E-01	2.0100E+00	2.3000E+00	1.4130E+00	8.7000E+00
		8.1500E-01	1.0000E+01	1.9020E+00	1.3000E+01	5.4300E-01	1.6300E+01	4.0200E-01	4.5000E+01

DATA PAIRS	AXIAL POWER RATIO	AXIAL DISTANCE (FT)	AXIAL POWER RATIO	AXIAL DISTANCE (FT)	AXIAL POWER RATIO	AXIAL DISTANCE (FT)	AXIAL POWER RATIO	AXIAL DISTANCE (FT)
11	5.6000E-01	5.4500E-01	1.1700E+00	1.6333E+00	1.4600E+00	2.7000E+00	1.6100E+00	3.8125E+00
	1.5800E+00	4.9000E+00	1.4800E+00	5.9917E+00	1.3400E+00	7.0750E+00	1.1500E+00	8.1563E+00
	9.4000E-01	9.2500E+00	7.0000E-01	1.0300E+01	3.6000E-01	1.1392E+01		

*** INTEGRAL OF AXIAL POWER PROFILE FACTORS OVER FUEL ROD LENGTH SUMS TO .1120E+01FOR FUEL ROD = 1 ***
SUM SHOULD BE 1.0. CHECK CARD GROUP 4.3 INPUT.

*** CORE PRESSURE HISTORY *** 12 PAIRS

TIME (SEC)	PRESSURE (PSIA)	PRESSURE (N/M**2)
0.	2.2730E+03	1.5672E+07
5.1000E-01	1.5610E+03	1.0763E+07
1.0100E+00	1.4050E+03	9.6871E+06
1.5000E+00	1.1980E+03	8.2599E+06
2.7500E+00	1.1660E+03	8.0393E+06
6.9500E+00	9.4000E+02	6.4811E+06
7.5500E+00	9.0800E+02	6.2604E+06
8.1500E+00	8.5600E+02	5.9019E+06
9.8700E+00	6.8600E+02	4.7298E+06
1.1070E+01	5.6800E+02	3.9162E+06
1.5870E+01	2.0600E+02	1.4203E+06
2.0070E+01	5.0000E+01	3.4474E+05

*** TRANSIENT HEAT TRANSFER COEFFICIENT AND BULK TEMPERATURE SPECIFIED BY CARD INPUT ***

*** ZONE 1 TOP BOUNDARY ELEVATION = 3.0000 FT OR .9144 M ***

TIME(SEC)	H.T.C.(BTU/HR-F-FT2)	H.T.C.(WATT/M2-K)
0.	.3560E+03	.2020E+04
.5100E+00	.1650E+03	.9362E+03
.1010E+01	.3600E+02	.2044E+03
.2550E+01	.2610E+03	.1481E+04
.2750E+04	.1200E+03	.6814E+03
.6955E+01	.1060E+03	.5978E+03
.7015E+01	.5200E+02	.2953E+03
.6815E+01	.5000E+01	.2839E+02
.5967E+01	.3960E+01	.2239E+02
.1107E+02	.1620E+03	.9085E+03
.1157E+02	.6030E+02	.3407E+03
.2007E+02	.5000E+02	.2839E+03

TIME(SEC)	TEMPERATURE(F)	TEMPERATURE(K)
0.	.6383E+03	.6105E+03
.5100E+00	.6015E+03	.5857E+03
.1010E+01	.5865E+03	.5818E+03
.2550E+01	.7438E+03	.6688E+03
.2750E+04	.5960E+03	.5684E+03
.6955E+01	.5938E+03	.5538E+03
.7015E+01	.5533E+03	.5515E+03
.6815E+01	.5522E+03	.5627E+03
.5967E+01	.2336E+04	.9964E+03
.1107E+02	.5931E+03	.5504E+03
.1157E+02	.3842E+03	.4668E+03
.2007E+02	.8932E+03	.7516E+03

*** ZONE 2 TOP BOUNDARY ELEVATION = 9.0000 FT OR 2.7432 M ***

TIME(SEC)	H.T.C.(BTU/HR-F-FT2)	H.T.C.(WATT/M2-K)
0.	.6020E+03	.3538E+04
.5100E+00	.1650E+03	.9372E+03
.1010E+01	.3600E+02	.2044E+03
.2550E+01	.2610E+03	.1596E+04
.2750E+04	.1160E+03	.6587E+03
.6955E+01	.1060E+03	.5978E+03
.7015E+01	.5200E+02	.2953E+03
.6815E+01	.5000E+01	.2839E+02
.5967E+01	.3960E+01	.2239E+02
.1107E+02	.1620E+03	.9085E+03
.1157E+02	.6030E+02	.3407E+03
.2007E+02	.5000E+02	.2839E+03

TIME(SEC)	TEMPERATURE(F)	TEMPERATURE(K)
0.	.6383E+03	.6100E+03
.5100E+00	.6015E+03	.5855E+03
.1010E+01	.5865E+03	.5818E+03
.2550E+01	.7438E+03	.6688E+03
.2750E+04	.5960E+03	.5684E+03
.6955E+01	.5938E+03	.5538E+03
.7015E+01	.5533E+03	.5515E+03
.6815E+01	.5522E+03	.5627E+03
.5967E+01	.2336E+04	.9964E+03
.1107E+02	.5931E+03	.5504E+03
.1157E+02	.3842E+03	.4668E+03
.2007E+02	.8932E+03	.7516E+03

*** ZONE 3 TOP BOUNDARY ELEVATION = 12.0000 FT OR 3.6576 M ***

TIME(SEC)	H.T.C.(BTU/HR-F-FT2)	H.T.C.(WATT/M2-K)
0.	.3930E+03	.2232E+04
.5100E+00	.2500E+03	.1420E+04
.1010E+01	.4600E+02	.2271E+03
.2550E+01	.2810E+03	.1596E+04
.2750E+04	.1290E+03	.7268E+03
.6955E+01	.1100E+03	.6246E+03
.7050E+01	.5200E+02	.2953E+03

.18500E+01	.5000E+01	.2839E+02
.98700E+01	.5000E+01	.2839E+02
.11070E+02	.1600E+03	.9085E+03
.15870E+02	.6000E+02	.3407E+03
.20070E+02	.5000E+02	.2839E+03

TIME(SEC)	TEMPERATURE(F)	TEMPERATURE(K)
0.	.6383E+03	.6100E+03
.51000E+00	.5875E+03	.5895E+03
.10100E+01	.7438E+03	.6486E+03
.21500E+01	.[illegible]	.[illegible]
.[illegible]	.[illegible]	.[illegible]
.[illegible]	.[illegible]	.[illegible]
.[illegible]	.[illegible]	.[illegible]
.[illegible]	.[illegible]	.[illegible]
.98700E+01	.1334E+04	.9964E+03
.11070E+02	.5310E+03	.5504E+03
.15670E+02	.3842E+03	.4688E+03
.20070E+02	.6932E+03	.7516E+03

```
 *** GAP CONDUCTANCE SUBCODE INPUT ***
ARITHMETIC MEAN ROUGHNESS OF CLADDING (MICRONS) =  .2160E+01
ARITHMETIC MEAN ROUGHNESS OF FUEL     (MICRONS) =  .1140E+01

*** GAS GAP DATA ***
  XXX DATA FOR ROD  1 XXX
GAS QUANTITY  = 3.000E-02 MOLES
PLENUM VOLUME = 3.800E-04 FT**3  ( 1.076E-05 M**3 )
GAP PRESSURE  = 2.243E+03 PSIA   ( 1.546E+07 N/M**2 )
SPRING LENGTH= 4.583E-01 FT      ( 1.397E-01 M      )
COIL OD SPRING = 2.910E-02 FT    ( 8.870E-03 M      )
NUMBER OF COILS =   22
WIRE OD OF SPRING = 6.333E-03 FT   ( 1.930E-03 M    )
MOLE FRACTIONS OF GAS COMPONENTS
 HELIUM       ARGON        KRYPTON      XENON        HYDROGEN     NITROGEN       H2O
 .1000E+01  0.           0.           0.           0.           0.           0.
PLOTS REQUESTED FOR  4 NODES
   4    5    6    7

     MINIMUM         MAXIMUM         AXIS LENGTH     -------LABEL----------
     0.              .2000E+02       .5000E+01         TIME (S)
     0.              .3000E+04       .6000E+01       SURFACE TEMPERATURE OF CLAD (K)
     0.              .3000E+04       .6000E+01       CENTERLINE TEMPERATURE OF FUEL (K)
     .1000E+06       .2000E+08       .8000E+01     GAS GAP PRESSURE (N/M**2)
     0.              .2500E+00       .5000E+01       CLADDING HOOP STRAIN (M/M)
     0.              .5000E-01       .1000E+02     FUEL AXIAL DISPLACEMENT (M)
    -.3000E-01       .2000E-01       .5000E+01     CLADDING AXIAL DISPLACEMENT (M)
     0.              .8000E+02       .8000E+01     FUEL ROD POWER (KW/M)
     0.              .2000E+04       .8000E+01     FUEL SURFACE TEMP. (K)
     0.              .5000E+05       .5000E+01     GAP HEAT TRANSFER COEFFICIENT (W/M**2-K
     .1000E+02       .1000E+08       .6000E+01     SURF. HEAT TRANSF. COEFF. (W/M**2-K)
     0.              .2000E+04       .8000E+06     AVERAGE CLADDING TEMP. (K)
    -.2000E+02       .2000E+02       .8000E+01     SURFACE HEAT FLUX PER UNIT LENGTH (KW/M
     .1000E+06       .1200E+08       .5000E+01     PLENUM PRESSURE (N/M**2)
     0.              .1000E+04       .5000E+01     PLENUM TEMPERATURE (K)
    -.2500E-09       .2500E-09       .1000E+02     GAS FLOW RATE (GRAM-MOLES/SEC)
    -.1000E+04       .2000E+04       .6000E+01     MASS FLUX (KG/M**2-SEC)
     0.              .1000E+01       .5000E+01   COOLANT QUALITY
     0.              .2000E+08       .1000E+02     COOLANT PRESSURE (N/M**2)
     0.              .2000E-02       .1000E+02     GAP THICKNESS (M)
     0.              .1000E+04       .5000E+01     BULK TEMPERATURE (K)

*** LENGTH REQUIRED FOR A1 ARRAY =    1081 ***
```

COOLANT CONDITIONS AT TIME = 0. SEC

ELEVATION(M)	COOLANT TEMPERATURE(K)	PRESSURE(N/M**2)
.1524E+00	.6100E+03	.1567E+08
.4572E+00	.6100E+03	.1567E+08
.7620E+00	.6100E+03	.1567E+08
.1067E+01	.6100E+03	.1567E+08
.1295E+01	.6100E+03	.1567E+08
.1448E+01	.6100E+03	.1567E+08
.1600E+01	.6100E+03	.1567E+08
.1753E+01	.6100E+03	.1567E+08
.1905E+01	.6100E+03	.1567E+08
.2057E+01	.6100E+03	.1567E+08
.2210E+01	.6100E+03	.1567E+08
.2362E+01	.6100E+03	.1567E+08
.2591E+01	.6100E+03	.1567E+08
.2896E+01	.6100E+03	.1567E+08
.3200E+01	.6100E+03	.1567E+08
.3505E+01	.6100E+03	.1567E+08

FUEL ROD # 1 CONDITIONS AT TIME =0. SEC (0. HOURS)

TIME STEP= .100000E+07 SEC NUMBER OF TEMPERATURE-DEFORMATION-PRESSURE LOOP ITERATIONS = 8
NUMBER OF DEFORMATION-PRESSURE LOOP ITERATIONS = 1 ACCUMULATED CPU TIME = 65.21 SEC

AVERAGE FUEL ROD POWER (KW/M)	3.635E+01
VOLUME AVERAGED FUEL TEMPERATURE (K)	1365.1
ENERGY GENERATED BY METAL-WATER REACTION(KW)	0.
FUEL STACK AXIAL EXTENSION (MM)	4.285E+01
CLADDING AXIAL EXTENSION (MM)	5.169E+00
PLENUM GAS TEMPERATURE (K)	626.2
PLENUM GAS PRESSURE (N/M**2)	1242E+08
GAS FLOW RATE FROM PLENUM (GM-MOLES/SEC)	0.
FRACTION OF MOLTEN FUEL IN FUEL ROD	0.0000
FRACTION OF FUEL RODS FAILED	0.

TOTAL FREE GAS VOLUME(MM) **3	.157754E+05
PLENUM VOLUME FRACTION	.423944
CRACK VOLUME FRACTION	.100370
GAP VOLUME FRACTION	.275926
OPEN POROSITY VOLUME FRACTION	.037914
DISH VOLUME FRACTION	.138987
CENTRAL VOID VOLUME FRACTION	0.000000
FUEL SURFACE ROUGHNESS VOLUME FRACTION	.007851
CLADDING SURFACE ROUGHNESS VOLUME FRACTION	.015006

FRAP-T MOD005 V04/19/79 FUEL ROD ANALYSIS PROGRAM * * EG&G - IDAHO *** MATPRO MODULE MOD 011

TIME(SEC)=0.

AXIAL NODE NUMBER	1	2	3	4	5	6
ELEVATION (M)	.152	.457	.762	1.067	1.295	1.448
LOCAL FUEL ROD POWER (KW/M)	1.944E+01	3.982E+01	5.110E+01	5.699E+01	5.809E+01	5.759E+01
AVERAGE FUEL ENTHALPY (JOU/KG)	213168.2	333127.7	385691.2	408567.4	412532.0	410726.6
COOLANT BULK TEMPERATURE(K)	610.0	610.0	610.0	610.0	610.0	610.0
COOLANT QUALITY	0.	0.	0.	0.	0.	0.
COOLANT MASS FLUX,KG/SEC-M2	0.	0.	0.	0.	0.	0.
SURFACE HEAT FLUX (WATT/M**2)	5.763E+05	1.180E+06	1.515E+06	1.689E+06	1.722E+06	1.707E+06
CRITICAL HEAT FLUX (WATT/M**2)	0.	0.	0.	0.	0.	0.
CRITICAL HEAT FLUX / SURFACE HEAT FLUX	0.	0.	0.	0.	0.	0.
SURFACE HEAT TRANSFER COEF. (WATT/M**2.K)	2.930E+05	2.930E+05	2.930E+05	3.538E+05	3.538E+05	3.538E+05
HEAT TRANSFER MODE	1	1	1	1	1	1
GAP HEAT TRANSFER COEF. (WATT/M**2.K)	3.862E+03	7.061E+03	1.176E+04	1.692E+04	1.832E+04	1.765E+04
THERMAL RADIAL GAS GAP (MM)	.0716	.0401	.0238	.0163	.0150	.0156
STRUCTURAL RADIAL GAS GAP (MM)	.0599	.0285	.0121	.0047	.0034	.0040
GAP PRESSURE (N/M**2)	1.242E+07	1.242E+07	1.242E+07	1.242E+07	1.242E+07	1.242E+07
COOLANT PRESSURE(N/M**2)	1.567E+07	1.567E+07	1.567E+07	1.567E+07	1.567E+07	1.567E+07
DISPLACEMENT OF FUEL OUTER SURFACE (MM)	4.752E-02	7.938E-02	9.597E-02	1.035E-01	1.048E-01	1.042E-01
DISPLACEMENT OF CLAD OUTER SURFACE (MM)	1.004E-02	1.052E-02	1.077E-02	1.087E-02	1.090E-02	1.089E-02
CLADDING HOOP STRAIN (MIDPLANE)	1.826E-03	2.914E-03	3.962E-03	4.980E-03	4.985E-03	4.983E-03
CLADDING RADIAL STRAIN	2.669E-03	2.767E-03	2.820E-03	2.841E-03	2.846E-03	2.844E-03
CLADDING PERMANENT HOOP STRAIN	0.	0.	0.	0.	0.	0.
CLADDING PERMANENT AXIAL STRAIN	0.	0.	0.	0.	0.	0.
CLADDING PERMANENT RADIAL STRAIN	0.	0.	0.	0.	0.	0.
INTERFACE PRESSURE, THERMAL GAP(N/M**2)	0.	0.	0.	0.	0.	0.
INTERFACE PRESSURE, STRUCT. GAP(N/M**2)	0.	0.	0.	0.	0.	0.
CLADDING HOOP STRESS (N/M**2)	-4.094E+07	-4.094E+07	-4.094E+07	-4.094E+07	-4.094E+07	-4.094E+07
CLADDING AXIAL STRESS (N/M**2)	-2.754E+07	-2.754E+07	-2.754E+07	-2.754E+07	-2.754E+07	-2.754E+07
EFFECTIVE CLADDING STRESS (N/M**2)	3.615E+07	3.615E+07	3.615E+07	3.615E+07	3.615E+07	3.615E+07
CLADDING YIELD STRESS(N/M**2)	3.715E+08	3.601E+08	3.539E+08	3.515E+08	3.509E+08	3.512E+08
CLAD STRESS AT INSTABILITY STRAIN(N/M**	3.967E+08	3.842E+08	3.773E+08	3.746E+08	3.739E+08	3.742E+08
CLADDING EFFECTIVE PLASTIC STRAIN	0.	0.	0.	0.	0.	0.
CLADDING INSTABILITY STRAIN	1.343E-01	1.365E-01	1.378E-01	1.383E-01	1.384E-01	1.384E-01
OXIDE DEPTH, CLAD OUTER SURFACE(MM)	0.000E-03	0.000E-03	0.000E-03	0.000E-03	0.000E-03	0.000E-03
OXYGEN STABILIZED ALPHA THICKNESS(MM)	0.	0.	0.	0.	0.	0.
OXIDE DEPTH, CLAD INNER SURFACE(MM)	0.000E-03	0.000E-03	0.000E-03	0.000E-03	0.000E-03	0.000E-03
METAL-WATER REACTION ENERGY (KW/M)	0.	0.	0.	0.	0.	0.

TEMPERATURES BY RADIAL MESH POINTS

NO.	MESH RADIUS (MM)	TEMPERATURES (K)					
1	0.	1278.9	2049.6	2386.5	2529.3	2553.3	2542.4
2	4.648E-01	1273.4	2035.3	2370.3	2512.5	2536.4	2525.5
3	9.296E-01	1256.8	1992.0	2321.0	2460.4	2484.8	2474.0	
4	1.394E+00	1229.4	1918.7	2236.8	2372.4	2395.4	2384.9	
5	1.859E+00	1191.9	1816.4	2112.9	2241.6	2263.3	2253.4	
6	2.324E+00	1144.9	1688.6	1946.6	2063.0	2082.6	2073.7	
7	2.789E+00	1089.5	1539.5	1774.8	1883.1	1901.4	1893.1	
8	3.254E+00	1026.3	1374.6	1583.0	1679.0	1695.0	1687.7	
9	3.719E+00	957.0	1200.5	1375.9	1459.1	1473.0	1466.7	
10	4.183E+00	882.7	1023.8	1041.7	1104.9	1115.5	1110.7	
11	4.648E+00	804.9	850.6	820.5	870.3	878.7	874.9	
12	4.647E+00	634.3	659.4	673.8	679.2	680.5	679.9	
13	5.093E+00	622.8	636.2	643.2	646.4	647.1	646.8	
14	5.356E+00	611.9	614.0	615.2	614.8	614.8	614.8	

FRAP-T MOD0J5 VJ4/19/79 FUEL ROD ANALYSIS PROGRAM * * EG&G - IDAHO *** MATPRO MODULE MOD 011

TIME(SEC)=0.

AXIAL NODE NUMBER	7	8	9	10	11	12
ELEVATION (M)	1.600	1.753	1.905	2.057	2.210	2.362
LOCAL FUEL ROD POWER (KW/M)	5.627E+01	5.461E+01	5.259E+01	5.024E+01	4.760E+01	4.441E+01
AVERAGE FUEL ENTHALPY (JOU/KG)	405885.7	399548.3	391542.1	381795.8	370285.4	355608.4
COOLANT BULK TEMPERATURE(K)	610.0	610.0	610.0	610.0	610.0	610.0
COOLANT QUALITY	0.	0.	0.	0.	0.	0.
COOLANT MASS FLUX,KG/SEC-M2	0.	0.	0.	0.	0.	0.
SURFACE HEAT FLUX (WATT/M**2)	1.668E+06	1.619E+06	1.559E+06	1.489E+06	1.411E+06	1.316E+06
CRITICAL HEAT FLUX (WATT/M**2)	0.	0.	0.	0.	0.	0.
CRITICAL HEAT FLUX / SURFACE HEAT FLUX	0.	0.	0.	0.	0.	0.
SURFACE HEAT TRANSFER COEF. (WATT/M**2.K)	3.538E+05	3.538E+05	3.538E+05	3.538E+05	3.538E+05	3.538E+05
HEAT TRANSFER MODE	1	1	1	1	1	1
GAP HEAT TRANSFER COEF. (WATT/M**2.K)	1.608E+04	1.442E+04	1.276E+04	1.121E+04	9.827E+03	8.500E+03
THERMAL RADIAL GAS GAP (MM)	.0172	.0192	.0218	.0250	.0286	.0332
STRUCTURAL RADIAL GAS GAP (MM)	.0055	.0076	.0102	.0133	.0170	.0216
GAP PRESSURE (N/M**2)	1.242E+07	1.242E+07	1.242E+07	1.242E+07	1.242E+07	1.242E+07
COOLANT PRESSURE(N/M**2)	1.567E+07	1.567E+07	1.567E+07	1.567E+07	1.567E+07	1.567E+07
DISPLACEMENT OF FUEL OUTER SURFACE (MM)	1.026E-01	1.005E-01	9.791E-02	9.473E-02	9.104E-02	8.638E-02
DISPLACEMENT OF CLAD OUTER SURFACE (MM)	1.086E-02	1.082E-02	1.078E-02	1.072E-02	1.067E-02	1.059E-02
CLADDING HOOP STRAIN (MIDPLANE)	1.977E-03	1.971E-03	1.962E-03	1.953E-03	1.942E-03	1.928E-03
CLADDING RADIAL STRAIN	2.838E-03	2.830E-03	2.821E-03	2.810E-03	2.798E-03	2.783E-03
CLADDING PERMANENT HOOP STRAIN	0.	0.	0.	0.	0.	0.
CLADDING PERMANENT AXIAL STRAIN	0.	0.	0.	0.	0.	0.
CLADDING PERMANENT RADIAL STRAIN	0.	0.	0.	0.	0.	0.
INTERFACE PRESSURE, THERMAL GAP(N/M**2)	0.	0.	0.	0.	0.	0.
INTERFACE PRESSURE, STRUCT. GAP(N/M**2)	0.	0.	0.	0.	0.	0.
CLADDING HOOP STRESS (N/M**2)	-4.094E+07	-4.094E+07	-4.094E+07	-4.094E+07	-4.094E+07	-4.094E+07
CLADDING AXIAL STRESS (N/M**2)	-2.754E+07	-2.754E+07	-2.754E+07	-2.754E+07	-2.754E+07	-2.754E+07
EFFECTIVE CLADDING STRESS (N/M**2)	3.615E+07	3.615E+07	3.615E+07	3.615E+07	3.615E+07	3.615E+07
CLADDING YIELD STRESS(N/M**2)	3.519E+08	3.528E+08	3.538E+08	3.551E+08	3.565E+08	3.582E+08
CLAD STRESS AT INSTABILITY STRAIN(N/M**	3.750E+08	3.760E+08	3.772E+08	3.786E+08	3.802E+08	3.821E+08
CLADDING EFFECTIVE PLASTIC STRAIN	0.	0.	0.	0.	0.	0.
CLADDING INSTABILITY STRAIN	1.382E-01	1.380E-01	1.378E-01	1.376E-01	1.373E-01	1.369E-01
OXIDE DEPTH, CLAD OUTER SURFACE(MM)	3.000E-03	3.000E-03	3.000E-03	3.000E-03	3.000E-03	3.000E-03
OXYGEN STABILIZED ALPHA THICKNESS(MM)	0.	0.	0.	0.	0.	0.
OXIDE DEPTH, CLAD INNER SURFACE(MM)	3.000E-03	3.000E-03	3.000E-03	3.000E-03	3.000E-03	3.000E-03
METAL-WATER REACTION ENERGY (KW/M)	0.	0.	0.	0.	0.	0.

TEMPERATURES BY RADIAL MESH POINTS

NO.	MESH RADIUS (MM)	TEMPERATURES (K)					
1	0.	2512.8	2473.8	2423.9	2363.1	2291.1	2197.2
2	4.648E-01	2496.1	2457.2	2407.6	2347.0	2275.4	2182.0
3	9.296E-01	2444.9	2406.6	2357.6	2298.0	2227.6	2135.8
4	1.394E+00	2356.6	2319.4	2271.8	2214.0	2145.9	2057.2
5	1.859E+00	2226.6	2191.4	2146.3	2091.7	2027.6	1944.1
6	2.324E+00	2049.5	2017.7	1976.8	1927.3	1869.3	1797.1
7	2.789E+00	1820.3	1793.0	1763.8	1725.9	1681.1	1624.8
8	3.254E+00	1563.4	1547.5	1527.7	1502.9	1473.0	1434.6
9	3.719E+00	1297.3	1290.8	1282.3	1270.7	1255.6	1235.0
10	4.183E+00	1037.9	1039.5	1040.8	1040.9	1039.1	1034.8
11	4.648E+00	797.1	804.9	813.9	823.3	832.3	841.5
12	4.747E+00	678.4	676.4	674.0	671.2	668.0	664.2
13	5.053E+00	645.9	644.9	643.6	642.1	640.4	638.4
14	5.358E+00	614.7	614.6	614.4	614.2	614.0	613.7

FRAP-T MOD005 V04/19/79 FUEL ROD ANALYSIS PROGRAM * * EG&G - IDAHO *** MATPRO MODULE MOD 011

TIME(SEC)=0.

AXIAL NODE NUMBER	13	14	15	16
ELEVATION (M)	2.591	2.896	3.200	3.505
LOCAL FUEL ROD POWER (KW/M)	3.942E+01	3.209E+01	2.318E+01	1.186E+01
AVERAGE FUEL ENTHALPY (JOU/KG)	330850.0	291340.9	237302.4	163590.1
COOLANT BULK TEMPERATURE(K)	610.0	610.0	610.0	610.0
COOLANT QUALITY	0.	0.	0.	0.
COOLANT MASS FLUX,KG/SEC-M2	0.	0.	0.	0.
SURFACE HEAT FLUX (WATT/M**2)	1.168E+06	9.514E+05	6.872E+05	3.516E+05
CRITICAL HEAT FLUX (WATT/M**2)	0.	0.	0.	0.
CRITICAL HEAT FLUX / SURFACE HEAT FLUX	0.	0.	0.	0.
SURFACE HEAT TRANSFER COEFF. (WATT/M**2.K)	3.538E+05	2.232E+05	2.232E+05	2.232E+05
HEAT TRANSFER MODE	1	1	1	1
GAP HEAT TRANSFER COEFF. (WATT/M**2.K)	6.946E+03	5.418E+03	4.230E+03	3.278E+03
THERMAL RADIAL GAS GAP (MM)	.0408	.0523	.0661	.0818
STRUCTURAL RADIAL GAS GAP (MM)	.0292	.0407	.0545	.0701
GAP PRESSURE (N/M**2)	1.242E+07	1.242E+07	1.242E+07	1.242E+07
COOLANT PRESSURE(N/M**2)	1.567E+07	1.567E+07	1.567E+07	1.567E+07
DISPLACEMENT OF FUEL OUTER SURFACE (MM)	7.870E-02	6.707E-02	5.309E-02	3.719E-02
DISPLACEMENT OF CLAD OUTER SURFACE (MM)	1.048E-02	1.037E-02	1.016E-02	9.879E-03
CLADDING HOOP STRAIN (MIDPLANE)	1.908E-03	1.887E-03	1.847E-03	1.796E-03
CLADDING RADIAL STRAIN	2.760E-03	2.737E-03	2.692E-03	2.635E-03
CLADDING PERMANENT HOOP STRAIN	0.	0.	0.	0.
CLADDING PERMANENT AXIAL STRAIN	0.	0.	0.	0.
CLADDING PERMANENT RADIAL STRAIN	0.	0.	0.	0.
INTERFACE PRESSURE, THERMAL GAP(N/M**2)	0.	0.	0.	0.
INTERFACE PRESSURE, STRUCT. GAP(N/M**2)	0.	0.	0.	0.
CLADDING HOOP STRESS (N/M**2)	-4.094E+07	-4.094E+07	-4.094E+07	-4.094E+07
CLADDING AXIAL STRESS (N/M**2)	-2.754E+07	-2.754E+07	-2.754E+07	-2.754E+07
EFFECTIVE CLADDING STRESS (N/M**2)	3.615E+07	3.615E+07	3.615E+07	3.615E+07
CLADDING YIELD STRESS(N/M**2)	3.609E+08	3.636E+08	3.688E+08	3.754E+08
CLADDING STRESS AT INSTABILITY STRAIN(N/M**	3.850E+08	3.880E+08	3.937E+08	4.011E+08
CLADDING EFFECTIVE PLASTIC STRAIN	0.	0.	0.	0.
CLADDING INSTABILITY STRAIN	1.364E-01	1.359E-01	1.348E-01	1.335E-01
OXIDE DEPTH, CLAD OUTER SURFACE(MM)	3.000E-03	3.000E-03	3.000E-03	3.000E-03
OXYGEN STABILIZED ALPHA THICKNESS(MM)	0.	0.	0.	0.
OXIDE DEPTH, CLAD INNER SURFACE(MM)	3.000E-03	3.000E-03	3.000E-03	3.000E-03
METAL-WATER REACTION ENERGY (KW/M)	0.	0.	0.	0.

TEMPERATURES BY RADIAL MESH POINTS

NO.	MESH RADIUS (MM)	TEMPERATURES (K)			
1	0.	2035.1	1766.9	1422.5	1001.7
2	4.648E-01	2020.9	1755.5	1415.3	998.9
3	9.296E-01	1977.9	1721.4	1393.8	990.5
4	1.394E+00	1905.2	1665.3	1358.6	976.6
5	1.859E+00	1804.2	1588.7	1310.4	957.4
6	2.324E+00	1678.1	1493.4	1250.2	933.2
7	2.789E+00	1531.0	1382.2	1179.5	904.1
8	3.254E+00	1368.4	1258.6	1099.8	870.7
9	3.719E+00	1196.5	1126.8	1013.0	833.2
10	4.183E+00	1021.9	989.4	920.8	792.0
11	4.648E+00	850.6	851.7	825.3	747.8
12	4.747E+00	658.2	650.9	639.7	625.2
13	5.053E+00	635.2	632.1	626.0	618.2
14	5.358E+00	613.3	614.2	613.1	611.6

FUEL ROD # 1 CONDITIONS AT TIME = .1050002+02 SEC (.291667E-02 HOURS)

TIME STEP= .100000E+00 SEC NUMBER OF TEMPERATURE-DEFORMATION-PRESSURE LOOP ITERATIONS = 2
NUMBER OF DEFORMATION-PRESSURE LOOP ITERATIONS = 1 ACCUMULATED CPU TIME = 306.33 SEC

AVERAGE FUEL ROD POWER (KW/M)	3.268E+00
VOLUME AVERAGED FUEL TEMPERATURE (K)	1252.3
ENERGY GENERATED BY METAL-WATER REACTION(KW)	4.2617E-01
FUEL STACK AXIAL EXTENSION (MM)	3.496E+01
CLADDING AXIAL EXTENSION (MM)	7.341E+00
PLENUM GAS TEMPERATURE (K)	709.4
PLENUM GAS PRESSURE (N/M**2)	.5708E+07
GAS FLOW RATE FROM PLENUM (GM-MOLES/SEC)	0.
FRACTION OF MOLTEN FUEL IN FUEL ROD	0.0000
FRACTION OF FUEL RODS FAILED	.5151E+00
MODE OF FUEL ROD FAILURE	6

TOTAL FREE GAS VOLUME(MM) **3	.497628E+05
PLENUM VOLUME FRACTION	.148115
CRACK VOLUME FRACTION	.003466
GAP VOLUME FRACTION	.775591
OPEN POROSITY VOLUME FRACTION	.012019
MESH VOLUME FRACTION	.055303
CENTRAL VOID VOLUME FRACTION	0.000000
FUEL SURFACE ROUGHNESS VOLUME FRACTION	.002477
CLADDING SURFACE ROUGHNESS VOLUME FRACTION	.005028

FRAP-T MOD005 V04/19/79 FUEL ROD ANALYSIS PROGRAM * * EG&G - IDAHO *** MATPRO MODULE MOD 011

TIME(SEC)= .105000E+02

AXIAL NODE NUMBER	1	2	3	4	5	6
ELEVATION (M)	.152	.457	.762	1.067	1.295	1.448
LOCAL FUEL ROD POWER (KW/M)	1.748E+00	3.580E+00	4.594E+00	5.124E+00	5.222E+00	5.177E+00
AVERAGE FUEL ENTHALPY (JOU/KG)	183109.9	284001.0	335850.4	366543.3	371832.7	369474.5
COOLANT BULK TEMPERATURE(K)	762.2	762.2	762.2	762.2	762.2	762.2
COOLANT QUALITY	0.	0.	0.	0.	0.	0.
COOLANT MASS FLUX,KG/SEC-M2	0.	0.	0.	0.	0.	0.
SURFACE HEAT FLUX (WATT/M**2)	7.109E+04	1.960E+05	2.391E+05	2.531E+05	2.559E+05	2.539E+05
CRITICAL HEAT FLUX (WATT/M**2)	0.	0.	0.	0.	0.	0.
CRITICAL HEAT FLUX / SURFACE HEAT FLUX	0.	0.	0.	0.	0.	0.
SURFACE HEAT TRANSFER COEF. (WATT/M**2.K)	4.905E+02	4.905E+02	4.905E+02	4.905E+02	4.905E+02	4.905E+02
HEAT TRANSFER MODE	1	1	1	1	1	1
GAP HEAT TRANSFER COEF. (WATT/M**2.K)	3.565E+03	3.925E+03	1.457E+03	8.045E+02	7.396E+02	7.451E+02
THERMAL RADIAL GAS GAP (MM)	.0924	.1021	.3434	.8484	.9983	.9762
STRUCTURAL RADIAL GAS GAP (MM)	.0808	.0905	.3318	.8368	.9867	.9646
GAP PRESSURE (N/M**2)	5.708E+06	5.708E+06	5.708E+06	5.708E+06	5.708E+06	5.708E+06
COOLANT PRESSURE(N/M**2)	4.303E+06	4.303E+06	4.303E+06	4.303E+06	4.303E+06	4.303E+06
DISPLACEMENT OF FUEL OUTER SURFACE (MM)	3.846E-02	5.668E-02	6.708E-02	7.338E-02	7.448E-02	7.398E-02
DISPLACEMENT OF CLAD OUTER SURFACE (MM)	2.269E-02	4.841E-02	6.690E-01	7.220E-01	8.559E-01	8.358E-01
CLADDING HCOP STRAIN (MIDPLANE)	4.234E-03	9.554E-03	5.628E-02	1.517E-01	1.799E-01	1.757E-01
CLADDING RADIAL STRAIN	4.052E-03	4.534E-04	-5.042E-02	-1.458E-01	-1.739E-01	-1.697E-01
CLADDING PERMANENT HOOP STRAIN	0.	4.436E-03	5.315E-02	1.548E-01	1.857E-01	1.806E-01
CLADDING PERMANENT AXIAL STRAIN	0.	1.072E-05	1.166E-04	2.797E-04	3.169E-04	3.110E-04
CLADDING PERMANENT RADIAL STRAIN	0.	-4.447E-03	-5.327E-02	-1.551E-01	-1.860E-01	-1.809E-01
INTERFACE PRESSURE, THERMAL GAP(N/M**2)	0.	0.	0.	0.	0.	0.
INTERFACE PRESSURE, STRUCT. GAP(N/M**2)	0.	0.	0.	0.	0.	0.
CLADDING HOOP STRESS (N/M**2)	6.619E+06	6.723E+06	7.923E+06	1.066E+07	1.159E+07	1.145E+07
CLADDING AXIAL STRESS (N/M**2)	8.281E+05	8.798E+05	1.478E+06	2.645E+06	3.310E+06	3.239E+06
EFFECTIVE CLADDING STRESS (N/M**2)	6.547E+06	6.329E+06	7.297E+06	9.565E+06	1.035E+07	1.023E+07
CLADDING YIELD STRESS(N/M**2)	4.788E+07	9.570E+06	2.151E+06	1.358E+07	1.439E+07	1.426E+07
CLAD STRESS AT INSTABILITY STRAIN(N/M**	4.931E+07	1.052E+07	2.214E+06	1.364E+07	1.439E+07	1.427E+07
CLADDING EFFECTIVE PLASTIC STRAIN	0.	1.129E-03	9.144E-02	1.789E-01	2.146E-01	2.088E-01
CLADDING INSTABILITY STRAIN	1.864E-01	5.710E-03	6.844E-02	1.414E-01	2.173E-01	2.130E-01
OXIDE DEPTH, CLAD OUTER SURFACE(MM)	3.000E-03	3.129E-03	3.500E-03	3.656E-03	3.695E-03	3.675E-03
OXYGEN STABILIZED ALPHA THICKNESS(MM)	0.	4.973E-07	1.149E-06	1.406E-06	1.468E-06	1.434E-06
OXIDE DEPTH, CLAD INNER SURFACE(MM)	3.000E-03	3.000E-03	3.000E-03	3.000E-03	3.000E-03	3.000E-03
METAL-WATER REACTION ENERGY (KW/M)	0.	6.487E-02	1.854E-01	2.516E-01	2.662E-01	2.595E-01

TEMPERATURES BY RADIAL MESH POINTS

NO.	MESH RADIUS (MM)	TEMPERATURES (K)					
1	0.	955.9	1332.0	1528.0	1635.5	1653.8	1645.3
2	4.648E-01	955.3	1329.7	1524.6	1631.6	1649.8	1641.3
3	9.296E-01	953.4	1323.5	1514.6	1620.1	1638.1	1629.7
4	1.394E+00	950.3	1313.5	1498.3	1601.8	1619.4	1611.2
5	1.859E+00	946.4	1298.6	1477.4	1577.6	1595.3	1587.3
6	2.324E+00	941.8	1282.4	1453.2	1550.7	1567.3	1559.6
7	2.789E+00	937.0	1264.8	1427.3	1521.5	1537.5	1530.2
8	3.254E+00	932.1	1246.7	1401.4	1492.5	1508.0	1501.0
9	3.719E+00	927.5	1229.0	1377.1	1465.4	1480.3	1473.9
10	4.183E+00	923.3	1211.8	1355.2	1441.5	1456.4	1450.1
11	4.648E+00	919.6	1194.6	1335.0	1420.4	1435.6	1429.8
12	4.747E+00	908.8	1165.7	1298.9	1382.4	1398.2	1392.4
13	5.053E+00	908.1	1164.1	1252.1	1280.8	1286.5	1282.3
14	5.358E+00	907.2	1161.9	1249.7	1278.3	1284.1	1279.9

FRAP-T MOD005 V34/19/79 FUEL ROD ANALYSIS PROGRAM * * E66G - IDAHO *** MATPRO MODULE MOD 011

TIME(SEC)= .10500E+02

AXIAL NODE NUMBER	7	8	9	10	11	12
ELEVATION (M)	1.600	1.753	1.905	2.057	2.210	2.362
LOCAL FUEL ROD POWER (KW/M)	5.059E+00	4.909E+00	4.728E+00	4.517E+00	4.279E+00	3.993E+00
AVERAGE FUEL ENTHALPY (JOU/KG)	362800.7	354014.7	343503.3	332195.0	319962.8	304987.0
COOLANT BULK TEMPERATURE(K)	762.2	762.2	762.2	762.2	762.2	762.2
COOLANT QUALITY	0.	0.	0.	0.	0.	0.
COOLANT MASS FLUX,KG/SEC-M2	0.	0.	0.	0.	0.	0.
SURFACE HEAT FLUX (WATT/M**2)	2.519E+05	2.483E+05	2.435E+05	2.367E+05	2.266E+05	2.146E+05
CRITICAL HEAT FLUX (WATT/M**2)	0.	0.	0.	0.	0.	0.
CRITICAL HEAT FLUX / SURFACE HEAT FLUX	0.	0.	0.	0.	0.	0.
SURFACE HEAT TRANSFER COEF. (WATT/M**2.K)	4.905E+02	4.905E+02	4.905E+02	4.905E+02	4.905E+02	4.905E+02
HEAT TRANSFER MODE	1	1	1	1	1	1
GAP HEAT TRANSFER COEF. (WATT/M**2.K)	8.570E+02	9.887E+02	1.214E+03	1.586E+03	2.085E+03	3.045E+03
THERMAL RADIAL GAS GAP (MM)	.7586	.5985	.4408	.3072	.2171	.1386
STRUCTURAL RADIAL GAS GAP (MM)	.7470	.5869	.4292	.2955	.2055	.1270
GAP PRESSURE (N/M**2)	5.708E+06	5.708E+06	5.708E+06	5.708E+06	5.708E+06	5.708E+06
COOLANT PRESSURE(N/M**2)	4.303E+06	4.303E+06	4.303E+06	4.303E+06	4.303E+06	4.303E+06
DISPLACEMENT OF FUEL OUTER SURFACE (MM)	7.260E-02	7.077E-02	6.861E-02	6.633E-02	6.389E-02	6.089E-02
DISPLACEMENT OF CLAD OUTER SURFACE (MM)	6.417E-01	4.982E-01	3.566E-01	2.362E-01	1.544E-01	8.294E-02
CLADDING HOOP STRAIN (MIDPLANE)	1.348E-01	1.046E-01	7.475E-02	4.938E-02	3.214E-02	1.700E-02
CLADDING RADIAL STRAIN	-1.289E-01	-9.873E-02	-6.889E-02	-4.349E-02	-2.604E-02	-9.641E-03
CLADDING PERMANENT HOOP STRAIN	1.368E-01	1.014E-01	7.159E-02	4.625E-02	2.893E-02	1.319E-02
CLADDING PERMANENT AXIAL STRAIN	3.555E-04	2.624E-04	1.514E-04	1.028E-04	6.658E-05	3.131E-05
CLADDING PERMANENT RADIAL STRAIN	-1.370E-01	-1.016E-01	-7.174E-02	-4.639E-02	-2.899E-02	-1.322E-02
INTERFACE PRESSURE, THERMAL GAP(N/M**2)	0.	0.	0.	0.	0.	0.
INTERFACE PRESSURE, STRUCT. GAP(N/M**2)	0.	0.	0.	0.	0.	0.
CLADDING HOOP STRESS (N/M**2)	1.014E+07	9.239E+06	8.410E+06	7.746E+06	7.312E+06	6.930E+06
CLADDING AXIAL STRESS (N/M**2)	2.581E+06	2.134E+06	1.721E+06	1.389E+06	1.173E+06	9.829E+05
EFFECTIVE CLADDING STRESS (N/M**2)	9.123E+06	8.378E+06	7.695E+06	7.153E+06	6.801E+06	6.495E+06
CLADDING YIELD STRESS(N/M**2)	1.312E+07	1.139E+07	2.230E+06	1.950E+06	7.372E+06	8.138E+06
CLAD STRESS AT INSTABILITY STRAIN(N/M**	1.312E+07	2.169E+06	2.279E+06	2.015E+06	7.704E+06	8.674E+06
CLADDING EFFECTIVE PLASTIC STRAIN	1.581E-01	1.172E-01	8.276E-02	5.346E-02	3.344E-02	1.525E-02
CLADDING INSTABILITY STRAIN	2.088E-01	1.613E-01	1.914E-01	1.823E-01	1.735E-01	1.629E-01
OXIDE DEPTH, CLAD OUTER SURFACE(MM)	5.644E-03	3.612E-03	1.561E-03	3.472E-03	3.361E-03	3.220E-03
OXYGEN STABILIZED ALPHA THICKNESS(MM)	1.385E-06	1.329E-06	1.246E-06	1.101E-06	9.145E-07	6.981E-07
OXIDE DEPTH, CLAD INNER SURFACE(MM)	3.000E-03	3.000E-03	3.000E-03	3.000E-03	3.000E-03	3.000E-03
METAL-WATER REACTION ENERGY (KW/M)	2.453E-01	2.274E-01	2.047E-01	1.790E-01	1.477E-01	1.034E-01

TEMPERATURES BY RADIAL MESH POINTS

NO.	MESH RADIUS (MM)	TEMPERATURES (K)					
1	0.	1622.4	1591.1	1553.8	1514.6	1471.0	1414.9
2	4.648E-01	1618.5	1587.4	1550.8	1511.3	1467.9	1412.1
3	9.296E-01	1607.1	1576.3	1539.8	1500.4	1458.8	1404.1
4	1.394E+00	1589.0	1559.1	1523.3	1485.7	1444.3	1391.2
5	1.859E+00	1565.8	1536.6	1501.8	1465.3	1425.3	1374.2
6	2.325E+00	1538.8	1510.6	1477.0	1441.6	1403.2	1353.7
7	2.789E+00	1510.9	1483.9	1450.8	1416.6	1379.4	1331.7
8	3.254E+00	1481.4	1455.4	1424.2	1390.7	1354.7	1310.4
9	3.719E+00	1454.8	1429.6	1399.6	1366.7	1331.1	1288.7
10	4.183E+00	1431.2	1407.0	1377.6	1344.8	1309.2	1267.2
11	4.648E+00	1410.3	1386.7	1357.7	1324.9	1288.4	1246.4
12	4.747E+00	1279.9	1272.6	1262.7	1248.9	1228.4	1204.0
13	5.053E+00	1278.2	1270.9	1261.0	1247.2	1226.6	1202.2
14	5.358E+00	1275.8	1268.5	1258.6	1244.8	1224.2	1199.9

FRAP-T MOD005 V04/19/79 FUEL ROD ANALYSIS PROGRAM * * EG&G - IDAHO *** MATPRO MODULE MOD 011

TIME(SEC)= .1650000E+02

AXIAL NODE NUMBER	13	14	15	16
ELEVATION (M)	2.591	2.896	3.200	3.505
LOCAL FUEL ROD POWER (KW/M)	3.544E+00	2.885E+00	2.084E+00	1.066E+00
AVERAGE FUEL ENTHALPY (JOU/KG)	282544.9	245903.9	200808.1	142087.1
COOLANT BULK TEMPERATURE(K)	762.2	762.2	762.2	762.2
COOLANT QUALITY	0.	0.	0.	0.
COOLANT MASS FLUX,KG/SEC-M2	0.	0.	0.	0.
SURFACE HEAT FLUX (WATT/M**2)	1.946E+05	1.525E+05	9.415E+04	1.543E+04
CRITICAL HEAT FLUX (WATT/M**2)	0.	0.	0.	0.
CRITICAL HEAT FLUX / SURFACE HEAT FLUX	0.	0.	0.	0.
SURFACE HEAT TRANSFER COEF. (WATT/M**2,K)	4.905E+02	4.903E+02	4.905E+02	4.905E+02
HEAT TRANSFER MODE	1	1	1	1
GAP HEAT TRANSFER COEF. (WATT/M**2,K)	3.935E+03	4.247E+03	3.764E+03	3.124E+03
THERMAL RADIAL GAS GAP (MM)	.1016	.0880	.0989	.0952
STRUCTURAL RADIAL GAS GAP (MM)	.0900	.0764	.0793	.0636
GAP PRESSURE (N/M**2)	5.708E+06	5.708E+06	5.708E+06	5.708E+06
COOLANT PRESSURE (N/M**2)	4.303E+06	4.303E+06	4.303E+06	4.303E+06
DISPLACEMENT OF FUEL OUTER SURFACE (MM)	5.639E-02	4.941E-02	4.145E-02	3.190E-02
DISPLACEMENT OF CLAD OUTER SURFACE (MM)	4.778E-02	2.976E-02	2.436E-02	1.847E-02
CLADDING HOOP STRAIN (MIDPLANE)	9.414E-03	5.595E-03	4.556E-03	3.456E-03
CLADDING RADIAL STRAIN	7.003E-04	4.649E-03	4.367E-03	3.296E-03
CLADDING PERMANENT HOOP STRAIN	4.243E-03	2.202E-04	0.	0.
CLADDING PERMANENT AXIAL STRAIN	1.026E-03	5.369E-07	0.	0.
CLADDING PERMANENT RADIAL STRAIN	-4.254E-03	-2.207E-04	0.	0.
INTERFACE PRESSURE, THERMAL GAP(N/M**2)	0.	0.	0.	0.
INTERFACE PRESSURE, STRUCT. GAP(N/M**2)	0.	0.	0.	0.
CLADDING HOOP STRESS (N/M**2)	6.719E+06	6.625E+06	6.619E+06	6.619E+06
CLADDING AXIAL STRESS (N/M**2)	8.776E+05	8.307E+05	8.282E+05	8.280E+05
EFFECTIVE CLADDING STRESS (N/M**2)	6.326E+06	6.251E+06	6.247E+06	6.246E+06
CLADDING YIELD STRESS(N/M**2)	9.698E+06	1.007E+07	2.709E+07	1.844E+08
CLAD STRESS AT INSTABILITY STRAIN(N/M**	1.069E+07	1.103E+07	2.890E+07	1.916E+08
CLADDING EFFECTIVE PLASTIC STRAIN	4.906E-03	2.546E-04	0.	0.
CLADDING INSTABILITY STRAIN	1.818E-01	2.208E-01	1.959E-01	1.645E-01
OXIDE DEPTH, CLAD OUTER SURFACE(MM)	3.125E-03	3.017E-03	3.000E-03	3.000E-03
OXYGEN STABILIZED ALPHA THICKNESS(MM)	4.857E-07	1.515E-07	0.	0.
OXIDE DEPTH, CLAD INNER SURFACE(MM)	3.000E-03	3.000E-03	3.000E-03	3.000E-03
METAL-WATER REACTION ENERGY (KW/M)	6.256E-02	1.928E-02	0.	0.

TEMPERATURES BY RADIAL MESH POINTS

NO.	MESH RADIUS (MM)	TEMPERATURES (K)			
1	0.	1325.8	1185.4	1020.6	810.9
2	4.648E-01	1323.6	1183.8	1019.7	810.6
3	9.296E-01	1319.0	1179.1	1017.1	809.2
4	1.394E+00	1306.7	1172.3	1013.0	808.2
5	1.859E+00	1293.1	1162.9	1007.6	806.3
6	2.324E+00	1277.3	1155.2	1001.4	804.1
7	2.789E+00	1260.0	1140.8	994.8	801.8
8	3.254E+00	1242.4	1129.4	988.2	799.6
9	3.719E+00	1225.0	1118.5	982.0	797.7
10	4.183E+00	1208.1	1107.9	976.0	796.4
11	4.648E+00	1191.2	1096.7	969.9	795.6
12	4.747E+00	1162.8	1076.3	956.3	794.0
13	5.053E+00	1161.2	1075.0	955.4	793.9
14	5.358E+00	1159.1	1073.1	954.2	793.7

```
NLOOP =     12
FI =    -.19597233E+01
PRESSURE =     .21680615E+03
TIME (SEC) =     .10000000E+00
TOTL C ELONG =     .36874511E+00
VOLUME =     .15195674E+00
CLAD FAILURE
```

```
  FUEL ROD # 1  CONDITIONS AT TIME = .110000E+02 SEC       ( .305556E-02 HOURS)

TIME STEP= .100000E+00 SEC    NUMBER OF TEMPERATURE-DEFORMATION-PRESSURE LOOP ITERATIONS =   2
  NUMBER OF DEFORMATION-PRESSURE LOOP ITERATIONS =   1    ACCUMULATED CPU TIME =    312.10 SEC

AVERAGE FUEL ROD POWER (KW/M)                    3.863E+00
VOLUME AVERAGED FUEL TEMPERATURE (K)             1252.9
ENERGY GENERATED BY METAL-WATER REACTION(KW)     2.6414E-01
FUEL STACK AXIAL EXTENSION (MM)                  3.514E+01
CLADDING AXIAL EXTENSION (MM)                    7.821E+00
PLENUM GAS TEMPERATURE (K)                        664.9
PLENUM GAS PRESSURE (N/M**2)                     8.3964E+07
GAS FLOW RATE FROM PLENUM (GM-MOLES/SEC)         0.
FRACTION OF MOLTEN FUEL IN FUEL ROD              0.0000
FRACTION OF FUEL RODS FAILED                      .1000E+01
MODE OF FUEL ROD FAILURE                         6

TOTAL FREE GAS VOLUME(MM)  **3                    .500392E+05
PLENUM VOLUME FRACTION                            .147242
CRACK VOLUME FRACTION                             .003305
GAP VOLUME FRACTION                               .776980
OPEN POROSITY VOLUME FRACTION                     .011953
DISH VOLUME FRACTION                              .053071
CENTRAL VOID VOLUME FRACTION                     0.000000
FUEL SURFACE ROUGHNESS VOLUME FRACTION            .002457
CLADDING SURFACE ROUGHNESS VOLUME FRACTION        .004992


**** FAILURE PREDICTED  1.295  M) FROM BOTTOM OF ROD ****

FLOW BLOCKAGE (%) = 58.94
```

FRAP-T MOD005 w04/19/79 FUEL ROD ANALYSIS PROGRAM * * EG&G - IDAHO *** MATPRO MODULE MOD 011

TIME(SEC)= .116000E+02

AXIAL NODE NUMBER	1	2	3	4	5	6
ELEVATION (M)	.152	.457	.762	1.067	1.295	1.448
LOCAL FUEL ROD POWER (KW/M)	2.066E+00	4.231E+00	5.429E+00	6.056E+00	6.172E+00	6.119E+00
AVERAGE FUEL ENTHALPY (JOU/KG)	182961.6	283604.7	336264.3	367720.5	372995.8	370633.0
COOLANT BULK TEMPERATURE(K)	576.4	576.4	576.4	576.4	576.4	576.4
COOLANT QUALITY	0.	0.	0.	0.	0.	0.
COOLANT MASS FLUX,KG/SEC-M2	0.	0.	0.	0.	0.	0.
SURFACE HEAT FLUX (WATT/M**2)	2.523E+05	4.680E+05	5.263E+05	5.351E+05	5.383E+05	5.365E+05
CRITICAL HEAT FLUX (WATT/M**2)	0.	0.	0.	0.	0.	0.
CRITICAL HEAT FLUX / SURFACE HEAT FLUX	0.	0.	0.	0.	0.	0.
SURFACE HEAT TRANSFER COEF. (WATT/M**2.K)	8.572E+02	8.572E+02	8.572E+02	8.572E+02	8.572E+02	8.572E+02
HEAT TRANSFER MODE	1	1	1	1	1	1
GAP HEAT TRANSFER COEF. (WATT/M**2.K)	3.577E+03	3.819E+03	1.393E+02	7.446E+02	7.331E+02	7.364E+02
THERMAL RADIAL GAS GAP (MM)	.0907	.1037	.3534	.9084	.9501	.9363
STRUCTURAL RADIAL GAS GAP (MM)	.0907	.1037	.3534	.9084	.9501	.9363
GAP PRESSURE (N/M**2)	3.964E+06	3.964E+06	3.964E+06	3.964E+06	3.964E+06	3.964E+06
COOLANT PRESSURE(N/M**2)	3.964E+06	3.964E+06	3.964E+06	3.964E+06	3.964E+06	3.964E+06
DISPLACEMENT OF FUEL OUTER SURFACE (MM)	2.683E-02	4.493E-02	5.535E-02	6.172E-02	6.282E-02	6.232E-02
DISPLACEMENT OF CLAD OUTER SURFACE (MM)	2.087E-02	3.005E-02	2.806E-02	7.885E-01	8.276E-01	8.145E-01
CLADDING HOOP STRAIN (MIDPLANE)	3.895E-03	5.852E-03	4.084E-03	3.694E-03	3.743E-03	3.690E-03
CLADDING RADIAL STRAIN	3.895E-03	5.327E-03	4.075E-03	3.512E-03	3.371E-03	3.451E-03
CLADDING PERMANENT HOOP STRAIN	0.	4.528E-03	5.434E-02	1.607E-01	1.690E-01	1.662E-01
CLADDING PERMANENT AXIAL STRAIN	0.	1.094E-05	1.189E-04	2.874E-04	2.405E-04	2.382E-04
CLADDING PERMANENT RADIAL STRAIN	0.	-4.539E-03	-5.446E-02	-1.610E-01	-1.692E-01	-1.664E-01
INTERFACE PRESSURE, THERMAL GAP(N/M**2)	0.	0.	0.	0.	0.	0.
INTERFACE PRESSURE, STRUCT. GAP(N/M**2)	0.	0.	0.	0.	0.	0.
CLADDING HOOP STRESS (N/M**2)	-3.964E+06	-3.964E+06	-3.964E+06	-3.964E+06	-3.964E+06	-3.964E+06
CLADDING AXIAL STRESS (N/M**2)	-3.964E+06	-3.964E+06	-3.964E+06	-3.964E+06	-3.964E+06	-3.964E+06
EFFECTIVE CLADDING STRESS (N/M**2)	0.	0.	0.	0.	0.	0.
CLADDING YIELD STRESS(N/M**2)	0.	0.	0.	0.	0.	0.
CLAD STRESS AT INSTABILITY STRAIN(N/M**	0.	0.	0.	0.	0.	0.
CLADDING EFFECTIVE PLASTIC STRAIN	0.	0.	0.	0.	0.	0.
CLADDING INSTABILITY STRAIN	0.	0.	0.	0.	0.	0.
OXIDE DEPTH, CLAD OUTER SURFACE(MM)	3.000E-03	3.156E-03	3.554E-03	3.734E-03	3.776E-03	3.754E-03
OXYGEN STABILIZED ALPHA THICKNESS(MM)	0.	5.486E-07	1.234E-06	1.502E-06	1.567E-06	1.566E-06
OXIDE DEPTH, CLAD INNER SURFACE(MM)	3.000E-03	3.000E-03	3.000E-03	3.000E-03	3.051E-03	3.029E-03
METAL-WATER REACTION ENERGY (KW/M)	0.	4.573E-02	1.027E-01	1.177E-01	2.420E-01	2.351E-01

TEMPERATURES BY RADIAL MESH POINTS

NO.	MESH RADIUS (MM)	TEMPERATURES (K)				
1	0.	954.5	1325.0	1517.7	1643.0	1634.4
2	4.648E-01	954.0	1323.1	1514.7	1639.3	1631.0
3	9.296E-01	952.4	1317.3	1505.9	1629.2	1620.8
4	1.394E+00	950.0	1308.2	1493.9	1613.8	1604.8
5	1.859E+00	946.9	1296.0	1478.0	1593.2	1584.0
6	2.324E+00	943.2	1280.8	1458.2	1567.7	1558.4
7	2.789E+00	938.9	1262.8	1434.8	1537.6	1528.3
8	3.254E+00	934.1	1242.3	1408.2	1503.2	1494.0
9	3.719E+00	928.7	1219.4	1378.6	1465.0	1456.0
10	4.183E+00	922.8	1194.5	1346.4	1423.5	1414.9
11	4.648E+00	916.5	1168.0	1312.0	1379.2	1370.9
12	4.747E+00	909.8	1140.3	1276.0	1332.6	1324.6
13	5.053E+00	874.1	1027.6	1122.4	1190.7	1200.8	1204.4
14	5.358E+00	870.7	1022.4	1116.7	1184.3	1194.5	1198.1

FRAP-T MOD005 04/19/79 FUEL ROD ANALYSIS PROGRAM * * EG&G - IDAHO *** MATPRO MODULE MOD 011

TIME(SEC)= .110000E+02

AXIAL NODE NUMBER	7	8	9	10	11	12
ELEVATION (M)	1.600	1.753	1.905	2.057	2.210	2.362
LOCAL FUEL ROD POWER (KW/M)	5.979E+00	5.802E+00	5.588E+00	5.338E+00	5.057E+00	4.719E+00
AVERAGE FUEL ENTHALPY (JOU/KG)	363889.2	354881.7	344126.1	332306.5	319984.9	307762.9
COOLANT BULK TEMPERATURE(K)	576.4	576.4	576.4	576.4	576.4	576.4
COOLANT QUALITY	0.	0.	0.	0.	0.	0.
COOLANT MASS FLUX,KG/SEC-M2	0.	0.	0.	0.	0.	0.
SURFACE HEAT FLUX (WATT/M**2)	5.344E+05	5.323E+05	5.291E+05	5.245E+05	5.156E+05	5.011E+05
CRITICAL HEAT FLUX (WATT/M**2)	0.	0.	0.	0.	0.	0.
CRITICAL HEAT FLUX / SURFACE HEAT FLUX	0.	0.	0.	0.	0.	0.
SURFACE HEAT TRANSFER COEF. (WATT/M**2.K)	8.[illegible]2E+02	8.572E+02	8.572E+02	8.572E+02	8.572E+02	8.572E+02
HEAT TRANSFER MODE	1.	1.	1.	1.	1.	1.
GAP HEAT TRANSFER COEF. (WATT/M**2.K)	7.955E+02	9.416E+02	1.160E+03	1.515E+03	1.997E+03	2.893E+03
THERMAL RADIAL GAS GAP (MM)	.8080	.6143	.4525	.3168	.2240	.1446
STRUCTURAL RADIAL GAS GAP (MM)	.8080	.6143	.4525	.3168	.2240	.1446
GAP PRESSURE (N/M**2)	3.964E+06	3.964E+06	3.964E+06	3.964E+06	3.964E+06	3.964E+06
COOLANT PRESSURE(N/M**2)	3.964E+06	3.964E+06	3.964E+06	3.964E+06	3.964E+06	3.964E+06
DISPLACEMENT OF FUEL OUTER SURFACE (MM)	6.093E-02	5.908E-02	5.690E-02	5.459E-02	5.213E-02	4.911E-02
DISPLACEMENT OF CLAD OUTER SURFACE (MM)	6.962E-02	6.187E-02	5.708E-02	5.473E-02	5.220E-02	4.966E-02
CLADDING HOOP STRAIN (MIDPLANE)	1.451E-03	1.082E-03	7.730E-04	5.142E-04	3.611E-04	2.824E-04
CLADDING RADIAL STRAIN	1.543E-03	1.656E-03	3.876E-03	4.199E-03	4.556E-03	4.941E-03
CLADDING PERMANENT HOOP STRAIN	1.415E-01	1.045E-01	7.342E-02	4.722E-02	2.905E-02	1.330E-02
CLADDING PERMANENT AXIAL STRAIN	2.622E-04	1.074E-04	3.548E-04	1.048E-04	6.685E-05	1.150E-05
CLADDING PERMANENT RADIAL STRAIN	-1.418E-01	-1.047E-01	-7.358E-02	-4.733E-02	-2.912E-02	-1.333E-02
INTERFACE PRESSURE, THERMAL GAP(N/M**2)	0.	0.	0.	0.	0.	0.
INTERFACE PRESSURE, STRUCT. GAP(N/M**2)	0.	0.	0.	0.	0.	0.
CLADDING HOOP STRESS (N/M**2)	-3.964E+06	-3.964E+06	-3.964E+06	-3.964E+06	-3.964E+06	-3.964E+06
CLADDING AXIAL STRESS (N/M**2)	-3.964E+06	-3.964E+06	-3.964E+06	-3.964E+06	-3.964E+06	-3.964E+06
EFFECTIVE CLADDING STRESS (N/M**2)	0.	0.	0.	0.	0.	0.
CLADDING YIELD STRESS(N/M**2)	0.	0.	0.	0.	0.	0.
CLAD STRESS AT INSTABILITY STRAIN(N/M**	0.	0.	0.	0.	0.	0.
CLADDING EFFECTIVE PLASTIC STRAIN	0.	0.	0.	0.	0.	0.
CLADDING INSTABILITY STRAIN	0.	0.	0.	0.	0.	0.
OXIDE DEPTH, CLAD OUTER SURFACE(MM)	3.720E-03	3.684E-03	3.629E-03	3.534E-03	3.414E-03	3.263E-03
OXYGEN STABILIZED ALPHA THICKNESS(MM)	1.480E-06	1.420E-06	1.332E-06	1.185E-06	9.918E-07	7.696E-07
OXIDE DEPTH, CLAD INNER SURFACE(MM)	0.000E-03	0.000E-03	0.000E-03	0.000E-03	0.000E-03	0.000E-03
METAL-WATER REACTION ENERGY (KW/M)	1.163E-01	1.122E-01	1.068E-01	1.000E-01	8.851E-02	7.388E-02

TEMPERATURES BY RADIAL MESH POINTS

NO.	MESH RADIUS (MM)	TEMPERATURES (K)					
1	0.	1611.6	1580.5	1543.5	1504.5	1461.4	1406.3
2	4.648E-01	1608.2	1577.3	1540.4	1501.6	1458.7	1403.9
3	9.296E-01	1598.3	1567.8	1531.3	1493.0	1450.8	1396.8
4	1.394E+00	1582.7	1552.7	1517.0	1479.4	1438.4	1385.5
5	1.859E+00	1562.5	1533.3	1498.5	1461.7	1421.6	1370.7
6	2.324E+00	1539.1	1510.8	1477.1	1441.2	1402.2	1353.2
7	2.789E+00	1514.1	1486.8	1454.1	1419.0	1381.0	1335.9
8	3.254E+00	1488.8	1462.4	1430.6	1396.1	1358.8	1317.5
9	3.719E+00	1463.9	1438.1	1407.6	1372.8	1335.9	1298.5
10	4.183E+00	1439.1	1413.4	1382.6	1348.2	1311.9	1278.6
11	4.648E+00	1412.1	1388.0	1356.7	1322.0	1286.6	1257.6
12	4.747E+00	1208.2	1205.8	1202.2	1196.8	1193.6	1169.4
13	5.053E+00	1205.1	1202.7	1199.0	1193.6	1188.2	1166.3
14	5.358E+00	1199.8	1197.4	1193.7	1188.2	1177.9	1161.0

FRAP-T MOD005 V04/19/79 FUEL ROD ANALYSIS PROGRAM * * EG&G - IDAHO *** MATPRO MODULE MOD 011

TIME(SEC)= .1100000E+02

AXIAL NODE NUMBER	13	14	15	16
ELEVATION (M)	2.591	2.896	3.200	3.505
LOCAL FUEL ROD POWER (KW/M)	4.188E+00	3.410E+00	2.463E+00	1.260E+00
AVERAGE FUEL ENTHALPY (JOU/KG)	282144.8	245175.0	200497.9	142321.3
COOLANT BULK TEMPERATURE(K)	576.4	576.4	576.4	576.4
COOLANT QUALITY	0.	0.	0.	0.
COOLANT MASS FLUX,KG/SEC-M2	0.	0.	0.	0.
SURFACE HEAT FLUX (WATT/M**2)	4.653E+05	3.817E+05	2.889E+05	1.652E+05
CRITICAL HEAT FLUX (WATT/M**2)	0.	0.	0.	0.
CRITICAL HEAT FLUX / SURFACE HEAT FLUX	0.	0.	0.	0.
SURFACE HEAT TRANSFER COEF. (WATT/M**2,K)	8.572E+02	8.572E+02	8.572E+02	8.572E+02
HEAT TRANSFER MODE	1.	1.	1.	1.
GAP HEAT TRANSFER COEF. (WATT/M**2,K)	5.885E+03	4.161E+03	3.776E+03	3.139E+03
THERMAL RADIAL GAS GAP (MM)	.1030	.0859	.0891	.0940
STRUCTURAL RADIAL GAS GAP (MM)	.1030	.0859	.0891	.0940
GAP PRESSURE (N/M**2)	3.964E+06	3.964E+06	3.964E+06	3.964E+06
COOLANT PRESSURE(N/M**2)	3.964E+06	3.964E+06	3.964E+06	3.964E+06
DISPLACEMENT OF FUEL OUTER SURFACE (MM)	4.463E-02	3.766E-02	2.979E-02	2.031E-02
DISPLACEMENT OF CLAD OUTER SURFACE (MM)	4.910E-02	3.740E-02	2.742E-02	1.718E-02
CLADDING HOOP STRAIN (MIDPLANE)	9.667E-03	7.138E-03	5.085E-03	3.205E-03
CLADDING RADIAL STRAIN	5.334E-03	4.918E-03	4.085E-03	3.205E-03
CLADDING PERMANENT HOOP STRAIN	4.334E-03	2.702E-03	0.	0.
CLADDING PERMANENT AXIAL STRAIN	2.048E-03	1.369E-03	0.	0.
CLADDING PERMANENT RADIAL STRAIN	-4.344E-03	-2.207E-04	0.	0.
INTERFACE PRESSURE, THERMAL GAP(N/M**2)	0.	0.	0.	0.
INTERFACE PRESSURE, STRUCT. GAP(N/M**2)	0.	0.	0.	0.
CLADDING HOOP STRESS (N/M**2)	-3.964E+06	-3.964E+06	-3.964E+06	-3.964E+06
CLADDING AXIAL STRESS (N/M**2)	-3.964E+06	-3.964E+06	-3.964E+06	-3.964E+06
EFFECTIVE CLADDING STRESS (N/M**2)	0.	0.	0.	0.
CLADDING YIELD STRESS(N/M**2)	0.	0.	0.	0.
CLADDING STRESS AT INSTABILITY STRAIN(N/M**	0.	0.	0.	0.
CLADDING EFFECTIVE PLASTIC STRAIN	0.	0.	0.	0.
CLADDING INSTABILITY STRAIN	0.	0.	0.	0.
OXIDE DEPTH, CLAD OUTER SURFACE(MM)	3.151E-03	3.017E-03	3.000E-03	3.000E-03
OXIDE STABILIZED ALPHA THICKNESS(MM)	3.354E-07	3.242E-07	0.	0.
OXIDE DEPTH, CLAD INNER SURFACE(MM)	3.000E-03	3.000E-03	3.000E-03	3.000E-03
METAL-WATER REACTION ENERGY (KW/M)	4.391E-02	0.	0.	0.

TEMPERATURES BY RADIAL MESH POINTS

NO.	MESH RADIUS (MM)	TEMPERATURES (K)			
1	0.	1319.0	1180.9	1018.2	810.4
2	4.648E-01	1317.0	1179.0	1017.5	810.4
3	9.296E-01	1311.3	1175.9	1015.4	808.4
4	1.394E+00	1302.5	1169.9	1012.2	808.4
5	1.859E+00	1290.8	1162.2	1007.8	807.0
6	2.324E+00	1277.6	1155.2	1002.2	805.4
7	2.789E+00	1267.6	1149.2	999.9	803.7
8	3.254E+00	1260.2	1145.1	999.5	801.9
9	3.719E+00	1227.2	1119.1	982.9	799.9
10	4.183E+00	1206.6	1102.0	973.0	797.0
11	4.648E+00	1188.2	1087.5	958.0	792.0
12	4.747E+00	1182.8	1029.8	919.8	772.8
13	5.053E+00	1124.4	1026.3	917.2	771.4
14	5.358E+00	1119.2	1021.6	913.4	769.1

APPENDIX C

CALCULATIONS OF CLADDING SURFACE TEMPERATURE

APPENDIX C

CALCULATION OF CLADDING SURFACE TEMPERATURE

The numerical solution of the heat conduction equation (Equation 1-13) reduces to solving a set of tridiagonal equations. This set of equations is shown as follows:

$$\begin{vmatrix} b_1 & C_1 & 0 & 0 & & \\ a_2 & b_2 & C_2 & 0 & & 0's \\ 0 & a_3 & b_3 & C_3 & & \\ . & . & . & . & & . \\ . & . & . & . & & . \\ & 0's & a_{n-1} & b_{n-1} & & C_{n-1} \\ & & & a_n & & b_n \end{vmatrix} \begin{vmatrix} T_1^{m+1} \\ T_2^{m+1} \\ T_3^{m+1} \\ . \\ . \\ T_{n-1}^{m+1} \\ T_n^{m+1} \end{vmatrix} = \begin{vmatrix} d_1 \\ d_2 \\ d_3 \\ . \\ . \\ d_{n-1} \\ d_n \end{vmatrix} \quad \text{(C-1)}$$

where a_n, b_n, c_n, d_n are terms in finite difference form of the heat conduction equation at the n^{th} mesh point.

T_n^{m+1} = temperature at n^{th} mesh point at time step m+1

n = number of mesh point at outer surface.

The mesh point temperatures are solved by the Gaussian elimination method.

573 311

$$T_n^{m+1} = (d_n - a_n F_{n-1})/(b_n - a_n E_{n-1})$$

$$T_j^{m+1} = -E_j T_{j+1}^{m+1} + F_j \text{ for } j = n-1, n-2, \ldots 2, 1$$

$$\left.\begin{aligned} E_1 &= C_1/b_1 \text{ and } F_1 = d_1/b_1 \\ E_j &= C_j/(b_j - a_j E_{j-1}) \\ F_j &= (d_j - a_j F_{j-1})/(b_j - a_j E_{j-1}) \end{aligned}\right\} \text{for } j = 2, 3 \ldots n-1. \qquad \text{(C-2)}$$

The coefficients a_n, b_n, and d_n in the first equation of equation set (C-2) are derived from the energy balance equation for the half mesh interval bordering the outside surface. The continuous form of the energy balance equation for this half mesh interval is

$$\rho C_p \Delta V \frac{\partial T}{\partial t} = -A_{n-1/2}\, k \frac{\partial T}{\partial r}\Bigg|_{r = r_n - \Delta r/2} - \emptyset A_n + q\Delta V \qquad \text{(C-3)}$$

where all the terms in Equation (C-3) are defined below.

The finite difference form of Equation (C-3) is

$$\underbrace{\frac{-0.5\, A_{n-1/2}\, k}{\Delta r}}_{a_n} T_{n-1}^{m+1} + \underbrace{\left(\frac{\rho C_p \Delta V}{\Delta t} + \frac{0.5 A_{n-1/2}\, k}{\Delta r}\right)}_{b_n} T_n^{m+1}$$

$$= \underbrace{\frac{\rho C_p\, \Delta V}{\Delta r} T_n^m \quad \frac{-0.5\, A_{n-1/2}\, k}{\Delta r} (T_n^m - T_{n-1}^m) - 0.5 A_n (\emptyset^m + \emptyset^{m+1}) + q^{m+1/2} \Delta V}_{d_n}. \qquad \text{(C-4)}$$

The complete expressions for the coefficients a_n, b_n, and d_n are then

$$a_n = \frac{-0.5A_{n-1/2}\ K}{\Delta r}$$

$$b_n = \left(\frac{\rho C_p\ \Delta V}{\Delta t} + \frac{0.5A_{n-1/2}\ K}{\Delta r} \right)$$

$$d_n = \frac{\rho C_p\ \Delta V}{\Delta t}\ T_n^m\ \frac{-0.5A_{n-1/2}\ K}{\Delta r}\ (T_n^m - T_{n-1}^m)$$

$$-0.5A_n\ (\emptyset^{m+1} + \emptyset^m) + q^{m+1/2}\ \Delta V$$

$$A_{n-1/2} = 2\P\ (r_n - \Delta r/2)$$

$$A_n = 2\P\ r_n$$

$$V = \P\ (r_n \Delta r - \Delta r^2/4) \qquad \text{(C-5)}$$

where

K = thermal conductivity of material in half mesh interval bordering the surface

C_p = specific heat of material in half mesh interval bordering the surface

ρ = density of material in half mesh interval bordering the surface

r_n = radius to outside surface

Δr = width of mesh interval bordering outside surface

Δt = time step

$\emptyset^m$ = surface heat flux at m^{th} time step

T_n^m = surface temperature at m^{th} time step

$q^{m-1/2}$ = heat generation rate in half mesh interval bordering outside surface (heat generation caused by metal-water reaction).

Since the coefficients a_n, b_n, d_n, E_{n-1}, and F_{n-1} in equation set (C-2) do not contain temperature, the first equation of equation set (C-2) can be rewritten.

$$A_1 T_n^{m+1} + B_1 = \emptyset^{m+1} \tag{C-6}$$

where

$$A_1 = -(b_n - a_n E_{n-1})0.5A_n$$

$$B_1 = -\left[\frac{0.5\,\emptyset^m A_n + a_n F_{n-1} \frac{-\rho C_p}{\Delta t} \Delta V T^m_n - a_n (T_n^m - T^m_{n-1}) - q^{m-1/2} \Delta V}{0.5A_n}\right] \tag{C-7}$$

As shown in equation set (C-2), the coefficients E_{n-1} and F_{n-1} are evaluated by forward reduction of equation set (C-1). So Equation (C-6) contains only T_n^{m+1} and $\emptyset^{m+1}$ as unknown quantities.

Empirically derived heat transfer correlations are available from which surface heat flux due to convection can be computed in terms of surface temperature, geometry parameters, and flow conditions. Also, the equation for radiation heat transfer from a surface to surrounding water is known. Thus, the total surface heat flux can be expressed by the equation

$$\phi^{m+1} = f_i\,(C,G,\,T_n^{m+1}\,) + \sigma\,F_A\,F_E\left[(T_n^{m+1}\,)^4 - T_w^4\right] \qquad \text{(C-8)}$$

where

ϕ^{m+1} = surface heat flux at time step m+1

f_i = function specifying rate at which heat is transferred from surface by convection heat transfer during heat transfer mode i. These functions are defined in Table D-I of Appendix D.

i = number identification of convective heat transfer mode (nucleate boiling, film boiling, etc.)

C = set of parameters describing coolant conditions

G = set of parameters describing geometry

T_n = Stefan-Boltzmann constant

F_A = configuration factor for radiation heat transfer

F_E = emissivity factor for radiation heat transfer

T_W = bulk temperature of water surrounding fuel rod surface.

Equations (C-6) and (C-8) are two independent equations with unknowns T_n^{m+1} and Q^{m+1}. Simultaneous solution of the two equations yields the new surface temperature T_n^{m+1}.

APPENDIX D

HEAT TRANSFER CORRELATIONS AND COOLANT MODELS

APPENDIX D

HEAT TRANSFER CORRELATIONS AND COOLANT MODELS

This appendix describes the heat transfer correlations in FRAP-T. The heat transfer correlations supply one of the equations required for calculation of the fuel rod surface temperature, as shown in Section III-1.3. Also described are the optional coolant enthalpy model and the calculation of coolant void fraction.

1. HEAT TRANSFER AND CRITICAL HEAT FLUX CORRELATIONS

Most of the heat transfer and critical heat flux correlations in FRAP-T were taken from the RELAP4 code. In some cases, more than one correlation is available for a given heat transfer mode. In these cases, the particular correlation to be used is specified by the input data. The available correlations for each heat transfer mode are described in Table D-I. The symbols used in Table D-I are defined in Table D-II.

The following critical heat flux correlations are available:

(1) B&W-2[D-1]

(2) Local Barnett[D-2]

(3) Modified Barnett[D-3]

(4) General Electric[D-4]

(5) Savannah River[D-5]

(6) W-3[D-6]

(7) LOFT[D-7]

573 317

TABLE D-I

HEAT TRANSFER CORRELATIONS[a]

Mode 1 Subcooled Liquid Forced Convection: Dittus and Boelter[D-9]

$$h = 0.023 \frac{K}{D_e} Pr^{0.4} Re^{0.8}$$

Mode 2 Nucleate Boiling: Thom[D-10]

$$q = \left[\frac{\Delta T_{sat} \exp (P/1,260)}{0.072}\right]^2$$

Mode 3 Forced Convection Vaporization: Schrock and Grossman[D-11]

$$h = (2.5)\ (0.023) \frac{K_f}{D_e} Pr_f^{0.4} \quad [Re_f\ (1-X)]^{0.8}$$

$$\left[\left(\frac{X}{1-X}\right)^{0.9} \left(\frac{\mu_g}{\mu_f}\right)^{0.1} \left(\frac{\rho_f}{\rho_g}\right)^{0.5}\right]^{0.75}$$

Mode 4 Transition Boiling: McDonough, Milich, and King[D-12]

$$q = q_{CHF} - C(P)\ (T_w - T_{w,CHF})$$

Pressure, psi	C(P)
2,000	979.2
1,200	1,180.8
800	1,501.2

where

$$T_{w,CHF} = T_{sat} + 0.072 \exp(-P/1260)(q_{CHF})^{0.5}$$

Mode 5 Stable Film Boiling: Groeneveld[D-13]

$$h = a \frac{k_g}{D_e} Pr_w^c \left\{Re_g \left[X + \frac{\rho_g}{\rho_f}\ (1-X)\right]\right\}^b$$

$$\left[1.0 - 0.1\ (1-X)^{0.4} \left(\frac{\rho_f}{\rho_g} - 1\right)^{0.4}\right]^d$$

TABLE D-I (continued)

Mode 5 Stable Film Boiling (continued)

	Groeneveld Equation (5.9) (cluster geometry)	Groeneveld Equation (5.7) (annular geometry)
a.	0.00327	0.052
b.	0.901	0.688
c.	1.32	1.26
d.	-1.50	-1.06

Condie - Bengston[D-14]

$$h = 42011.23 \exp\left(-0.5 \sqrt{\Delta T_{sat}}\right) + 659.91 \frac{K_g^{0.2007} Pr_w^{3.6155} Re_g^{[0.0483 + 0.7441 \ln(X+1)]}}{D_e^{0.2771} (X+1)^{10.8450}} - 16.04 \exp(Pr_w P/1000)$$

Dougall and Rohsenow[D-15]

$$h = 0.023 \frac{K_g}{D_e} Pr_g^{0.4} \left\{ Re_g \left[X + \frac{\rho_g}{\rho_f} (1-X) \right] \right\}^{0.8}$$

Tong - Young[D-16]

$$q = \frac{C_3 (T_w - T_v)}{1 - \exp\left[C_1 \left(\frac{\Delta T_{sat}}{100} \right)^{(1 + C_2 \Delta T_{sat})} \right]}$$

$$h = q/(T_w - T_{sat})$$

$$C_1 = -0.001 \, X_E^{2/3} \Big/ (dX_E/dz)$$

573 319

TABLE D-I (continued)

Mode 5 Stable Film Boiling (continued)

$$C_2 = 0.0016$$

$$C_3 = 0.023 \left[\frac{K_v}{D_e} \left(R_e \right)_v^{0.8} \left\{ \frac{nX_E \rho_v/\rho_g + S(1-nX_E) \rho_v/\rho_f}{nX_E + S(1 - nX_E)} \right\}^{0.8} \left(Pr \right)_v^{0.4} \right]_{T_v}$$

dX_E/dz = rate of change of equilibrium quality with elevation

The Marchaterre - Hoglund correlation[D-16] is used to compute the slip ratio.

Mode 6 Low Flow Film Boiling: Modified Bromley[b]

$$h = 0.62 \left[\frac{k_g^3 \, i_{fg} \, \rho_g \, g(\rho_f - \rho_g)}{\mu_g \, L \, \Delta T_{sat}} \right]^{0.25}$$

$$L = 2\pi \sqrt{\frac{g_c \sigma}{g \, (\rho_f - \rho_g)}}$$

Mode 7 Free Convection plus Radiation[b]

$$h = h_c + h_r$$

$$h_c = 0.4 \, (Gr \, Pr_f)^{0.2}$$

$$Gr = \frac{L_g^3 \, \beta_g \, \rho_g^2 \, \Delta T_{sat}}{\mu_g^2}$$

$$L = \frac{D_e}{2}$$

$$h_r = 0.23 \, \frac{1.714(10^{-9}) \, (T_w^4 - T_{sat}^4)}{\Delta T_{sat}}$$

573 320

TABLE D-I (continued)

Mode 8 Superheated Vapor Forced Convection: Dittus and Boelter[D-9]

$$h = 0.023 \frac{k}{D_e} Pr^{0.4} Re^{0.8}$$

Mode 9 Low Pressure Flow Film Boiling: Dougall and Rohsenow[D-15]

$$h = 0.023 \frac{K_g}{D_e} Pr_g^{0.4} \left\{ Re_g \left[X + \frac{\rho_g}{\rho_f} (1-X) \right] \right\}^{0.8}$$

a. Notation definitions follow in the next table.

b. RELAP4/MOD6 UPDATE4 Version III, Idaho National Engineering Laboratory Configuration Control Number H00441IB.

TABLE D-II

SYMBOL DEFINITIONS FOR TABLES D-I AND D-III

h = heat transfer coefficient, Btu/ft^2-hr-°F

k = thermal conductivity, Btu/ft-hr-°F

D_e = equivalent diameter based on wetted perimeter, inches

$D_{HY} = \sqrt{D_r (D_r + D_{HE})} - D_r$, inches

D_{HE} = heated equivalent diameter, inches

D_r = fuel rod diameter, inches

Pr = Prandtl number, $\frac{c_p \mu}{k}$

573 321

TABLE D-II (continued)

Re = Reynolds number, $\frac{GD_e}{\mu}$

μ = viscosity, $lb_m/ft\text{-}hr$

C_p = specific heat, $Btu/lb_m\text{-}°F$

H = enthalpy (Btu/lb)

H_{fg} = heat of vaporization

T_{sat} = saturation temperature, $°F$

T_w = wall temperature, $°F$

$\Delta T_{sat} = T_W - T_{sat}$, $°F$

q = heat flux, $Btu/ft^2\text{-}hr$

p = pressure, psia

X = quality

α = void fraction

$n = X_A/X_E$

ρ = density, lb_m/ft^3

L = channel length, in.

g = local acceleration due to gravity, ft/sec^2

g_c = gravitational constant, $ft\text{-}lb_m/lb_f\text{-}sec^2$

TABLE D-II (continued)

σ = surface tension, lb_f/ft

Q = volumetric flow rate, ft^3/sec

A_{flow} = flow area, ft^2

β = coefficient of thermal expansion, $\frac{1}{\circ F}$

S = ratio of velocity of vapor phase to velocity of liquid phase (slip ratio)

and subscripts

CHF = critical heat flux conditions

f = saturated liquid conditions

g = saturated vapor conditions

v = superheated vapor conditions

E = equilibrium

w = wall

A = actual

573 323

(8) Modified Zuber[D-8]

(9) Combustion Engineering (CE)-1.

The correlations are described in Table D-III.

The B&W-2, W-3, and CE-1 correlations are restricted to high pressure conditions. The B&W-2 correlation is restricted to coolant pressures greater than 1500 psia. If the coolant pressure is less than 1300 psia, the B&W-2 correlation is replaced with the Barnett correlation. A combination of the two correlations is used for intermediate pressures. Similarly, the W-3 correlation is restricted to coolant pressures greater than 1000 psia. If the coolant pressure is less than 725 psia, the W-3 correlation is replaced with the Barnett correlation. A combination of the two correlations is used for intermediate pressures.

If the LOFT correlation is selected and the coolant conditions fall outside of its valid range, the B&W-2 or its appropriate low pressure substitute is used.

2. INFLUENCE OF ROD BOWING UPON CRITICAL HEAT FLUX

The calculation of critical heat flux reduction due to fuel rod bowing is a user option. If this option is used, both critical heat flux and fuel rod power are reduced according to the amount of fuel rod bowing. The reductions are computed by empirical equations. The equations for critical heat flux reduction are

$$\Delta f_{CHF}(Z) = F_{BCHF} \quad (W(Z) - W_{Thr}) / (1 - W_{Thr})$$

$$\Delta f_{CHF}(Z) = 0 \quad \text{if} \quad W(Z) \leq W_{Thr}$$

$$q^{(Z)}_{CHFR} = (1 - \Delta f^{(Z)}_{CHF}) \, q^{(Z)}_{CHF}$$

TABLE D-III

CRITICAL HEAT FLUX CORRELATIONS

(1) Babcock & Wilcox Company, B&W-2[D-1] .

$$q_{CHF} = \frac{1.15509 - 0.40703(12De)}{12.71 \times (3.0545G')^{A}}$$

$$\left[(0.3702 \times 10^{8}) \ (0.59137G')^{B} - 0.15208XH_{fg}G\right] \Big/ F_{APk}$$

where

$$A = 0.71186 + (2.0729 \times 10^{-4}) \ (P-2,000)$$

$$B = 0.834 + (6.8479 \times 10^{-4}) \ (P-2,000)$$

and where

$$G' = \frac{G}{10^{6}}$$

H_{fg} = heat of vaporization

F_{APk} = axial power profile factor for the B&W-2 correlation at elevation station k.

The axial power profile factor is calculated by the equation[D-1]

$$F_{APk} = \Big\{1.02 \ S_1 + \sum_{i=2}^{k} \Big[\Big\{q_i - (dq/dZ)_i\Big\} \exp\Big(C_1(Z_i - Z_k)\Big)$$

$$- \Big\{q_{i-1} - (dq/dZ)_i\Big\} \exp\Big(C_1(Z_{i-1} - Z_k)\Big)\Big]\Big\} \Big/ C_2 q_k$$

573 325

where

q_i = surface heat flux at axial node i (Btu/ft^2-hr)

Z_i = elevation of axial node i (ft)

$(dq/dZ)_i = (q_i - q_{i-1})/C_1(Z_i - Z_{i-1})$

$C_1 = 2.988(1-X)^{7.82} / (G/10^6)^{0.457}$

$C_2 = -C_1 Z_K$

$S_1 = q_1 [\exp (C_1(Z_1 - Z_K)) - \exp (C_2)]$.

The correlation was developed from rod bundles in water data over the parametric ranges given by:

Equivalent diameter	0.2 to 0.5 in.
Length	72 in.
Pressure	2,000 to 2,400 psia
Mass flux	0.75 x 10^6 to 4.0 x 10^6 lb/ft^2-hr
Burnout quality	-0.03 to 0.20.

(2) Local Barnett. The local Barnett Correlation[D-2] is:

$$q_{CHF} = 10^6 \left[\frac{A + B(H_{fg} X)}{C} \right]$$

where

$A = 69.40\ D_{HE}^{0.751} G'^{0.226}\ \ 1.0 - 0.672 \exp (-6.090\ D_{HY} G')$

$B = -0.250\ D_{HE}^{1.000}\ G'^{1.000}$

$$C = 165.9\ D_{HY}^{1.246}\ G'^{0.329}.$$

The parametric range of the data is as follows:

Equivalent diameters	0.258 in. $< D_{HE} <$ 3.792 in.
	0.127 in. $< D_{HY} <$ 0.875 in.
Length	24 to 108 in.
Pressure	1,000 psi
Mass flux	0.14×10^6 to 6.20×10^6 lb_m/ft^2-hr
Inlet subcooling	0 to 412 Btu/lb.

(3) Modified Barnett[D-3]

$$q_{CHF} = 10^6 \left[\frac{A + B(H_f - H_{in})}{C + L}\right]$$

where

$$A = 73.71\ D_{HE}^{0.052}\ G'^{0.663} \left(1.0 - 0.315\ e^{(-11.34 D_{HY} G')}\right)$$

$$B = 0.104\ D_{HE}^{1.445} G'^{0.691}$$

$$C = 45.44\ D_{HY}^{0.0817} G'^{0.5866}.$$

Data were from rod bundles containing water and were over parametric ranges given by:

Rod diameter	0.395 to 0.543 in.
Length	32.9 to 174.8 in.
Pressure	150 to 725 psia
Mass Flux	0.03×10^6 to 1.7×10^6 lb_m/ft^2-hr
Inlet subcooling	6 to 373 Btu/lb.

(4) General Electric Company[D-4] . The General Electric Company Correlations are:

$$q_{CHF} = 10^6 \ (0.8 - X)$$

for $G \geq 0.5 \times 10^6$ lb_m/ft^2-hr

and

$$q_{CHF} = 10^6 \ (0.84 - X)$$

for $G < 0.5 \times 10^6$ lb_m/ft^2-hr.

(5) Savannah River[D-5] .

$$Q_{CHF} = 188{,}000 \ (1.0 + 0.0515V) \ (1.0 + 0.069 \ T_{SUB})$$

where

V = fluid velocity, ft/sec

T_{SUB} = fluid saturation temperature minus fluid temperature.

(6) Westinghouse Company, W-3[D-6] .

$$q_{CHF} = 1. \times 10^6 \left[2.022 - 4.302 \times 10^{-4}P + (0.1722 - 9.84 \times 10^{-5}P) \exp((18.177 - 4.129 \times 10^{-3}P)X)\right] \left[1.157 - 0.869X\right] \left[(0.1484 + X(-1.596 + 0.1729 \ ABS(X))) G' + 1.037\right] \left[0.8258 + 7.94 \times 10^{-4} (H_f - H_{IN})\right] \left[0.2664 + 0.8357 \exp(-3.151 \ D_{HE})\right] F_{CW}/F_{APK}$$

573 328

TABLE D-III (continued)

where

H_f = enthalpy of saturated liquid (BTU/lb)

H_{IN} = enthalpy of coolant at bottom of fuel rods (inlet enthalpy) (BTU/lb)

F_{CW} = cold wall factor

F_{APK} = axial power profile factor at elevation station K

G' = $G/10^6$.

The W-3 correlation is valid in the following parametric ranges:

Equivalent diameter	0.2 to 0.7 in
Length	10 - 144 in
Pressure	1000 - 2400 psia
Mass Flux	1×10^6 lbm/ft^2-hr
Exit quality	$\leq$ 0.15.

The cold wall factor is calculated by the equation[D-6]

$$F_{CW} = 1. - (1.-D_E/D_{HE}) \; [13.76-1.372 \exp(1.78X) -4.732 (G/10^6)^{-0.0535} -0.0619(P/1000)^{0.14} -8.509 D_{HE}^{0.107}].$$

573 329

The axial power profile factor is calculated by the equation

$$F_{APK} = \left\{ S_1 + \sum_{i=2}^{K} \left[\left\{ q_i - (dq/dZ)_i \right\} \exp(C_1(Z_i - Z_K)) - \left\{ q_{i-1} - (dq/dZ)_i \right\} \exp(C_1(Z_{i-1} - Z_K)) \right] \right\} / C_2 q_K$$

where

F_{APK} = axial power profile factor at axial node K

q_i = surface heat flux at axial node i

Z_i = elevation of axial node i (ft)

$(dq/dZ)_i = (q_i - q_{i-1})/C_1(Z_i - Z_{i-1})$

$C_1 = 1.8(1-X)^{4.31}/[(G/10^6)^{0.478}]$

$C_2 = -C_1 Z_K$

$S_1 = q_1 [\exp(C_1(Z_1 - Z_K)) - \exp(C_2)]$.

(7) LOFT Correlation[D-7].

For high pressure, the following correlation is used:

$$q_{CHF} = 0.11585G + 800P - 0.27442P^2 - 1.4383GX + 0.0002566\ GPX.$$

For the range $2000 \le P \le 2400$

$0.75 \times 10^6 \le G \le 2.5 \times 10^6$

$-0.35 \le X \le 0.2$.

If the pressure is less than 2000 psia, the following correlation is used:

$$q_{CHF} = 1.880919 \times 10^6 - 850.58P - 1.099GX + 0.13P^2 - 1.186207 \times 10^6 X^2$$

For the range $1000 \leq P \leq 2000$

$0.4 \times 10^6 \leq G \leq 2.0 \times 10^6$

$-0.05 \leq X \leq 0.50.$

(8) Modified Zuber Correlation[D-8] (used when G < 200,000)

$$q_{CHF} = (0.96-\alpha)\ (0.130)\ (H_{fg})\ (\rho_g)^{0.5}\ [\sigma g_c\ g\ (\rho_f-\rho_g)]^{0.25}\ (\rho_f/(\rho_f+\rho_g))^{0.5}$$

(9) CE-1 Correlation

$$\frac{q_{CHF}}{10^6} = \frac{b_1\left(\frac{d}{d_m}\right)^{b_2}\left[(b_3 + b_4P)\left(\frac{G}{10^6}\right)^{(b_5 + b_6P)} - \left(\frac{G}{10^6}\right)\ (X)\ (H_{fg})\right]}{(b_7P + b_8\ G/10^6)\ F_{APK}\ \left(\frac{G}{10^6}\right)}$$

where

q_{CHF} = critical heat flux, Btu/hr-ft^2

p = pressure, psia

$\frac{d}{d_m}$ = 1.0

G = local mass velocity at CHF location, lb/hr-ft^2

X = local coolant quality at CHF location, decimal fraction

573 351

TABLE D-III (continued)

H_{fg} = latent heat of vaporization, Btu/lb

b_1 = 2.8922×10^{-3}

b_2 = -0.50749

b_3 = 405.32

b_4 = -9.9290×10^{-2}

b_5 = -0.67757

b_6 = 6.8235×10^{-4}

b_7 = 3.1240×10^{-4}

b_8 = -8.3245×10^{-2}

F_{APK} = axial power profile factor at elevation station K, the factor is calculated the same as is shown for the W-3 correlation.

Parameter Ranges for the CE-1 Correlation

pressure (psia)	1785 to 2415
local coolant quality	-0.16 to 0.20
local mass velocity (lb/hr-ft^2)	0.87×10^6 to 3.21×10^6
inlet temperature (^oF)	382 to 644
subchannel wetted equivalent diameter (inches)	0.3588 to 0.5447
subchannel heated equivalent diameter (inches)	0.4713 to 0.7837
heated length (inches)	84, 150

where

$\Delta f(Z)$ = fractional decrease in critical heat flux due to fuel rod bowing at elevation Z.

q_{CHFR} = reduced critical heat flux.

q_{CHF} = critical heat flux in absence of fuel rod bowing.

$W(Z)$ = amount of fuel rod bowing (fraction of bowing required to contact adjacent fuel rod, 0 = no bowing, 1 = maximum possible).

W_{Thr} = maximum amount of bowing which can occur without an effect on CHF (fraction of maximum bowing possible). This quantity is specified by user input.

F_{BCHF} = multiplication factor specified by user input.

The reduction in fuel rod power due to bowing is computed by the equation

$$P_r = [1 + 0.01\ (0.94W(Z) - 2.84\ W(Z)^2)]P$$

$$P_r = P \qquad (W(Z) \leq 0.3)$$

where

P_r = power reduced to account for fuel rod bowing

P = power in absence of fuel rod bowing.

3. VOID FRACTION

The void fraction of the coolant is computed by the equation

$$\alpha = XV_g / [(1-X)V_{f\gamma} + XV_g] \qquad \text{(D-1)}$$

where

α = void fraction

X = coolant quality

V_f = specific volume of saturated liquid

V_g = specific volume of saturated gas

γ = slip velocity ratio.

The slip velocity ratio for void fraction calculations is always assumed to be 1.0 (homogeneous flow).

4. COOLANT ENTHALPY MODEL

In cases where the coolant flow is quasi-steady state, coolant conditions can be specified by a combination of card input and coolant enthalpy model. The coolant inlet enthalpy and transient spatially uniform coolant pressure and mass flux are prescribed by card input. The coolant enthalpy and temperatures are then computed by the enthalpy model. This input option is included in the code as a user convenience in scoping problems where coolant conditions from a thermal-hydraulic code are not readily available. The option is not meant to replace the calculations of thermal-hydraulic codes, especially in cases where transient flow conditions exist. Also, the option should not be used if coolant quality may exceed a value of about 0.3.

The coolant enthalpy model is based on the principle of energy balance. The enthalpy increase of the coolant is related to the heat received from the fuel rods. The model consists of equations which calculate the following quantities: (a) the rate at which heat is added to each flow channel, (b) enthalpy increase of the coolant in each flow channel, and (c) temperature of the coolant in each flow channel.

The rate at which heat is added to the flow channel is computed by the equation

$$q_i(z) = \pi \sum_{m=1}^{M} f_{im} \int_0^z d_m(z)\, \phi_i(z)\, dz \qquad \text{(D-2)}$$

where

$q_i(Z)$ = rate at which heat is added to flow channel i from flow inlet to distance z from flow inlet

f_{im} = fraction of perimeter of fuel rod m that borders flow channel i

M = number of fuel rods that border flow channel i

$d_m(z)$ = diameter of fuel rod m at distance z from flow inlet

$\phi_m(z)$ = surface heat flux of fuel rod m at distance z from flow inlet.

The coolant enthalpy is computed by the equation

$$h_i(z) = h_o + q_i(z)/GA_i(z) \qquad \text{(D-3)}$$

where

$h_i(z)$ = enthalpy of coolant in flow channel i at distance z from flow inlet

h_o = enthalpy of coolant at flow inlet

G = mass flux

$A_i(z)$ = cross-sectional area of flow channel i.

The coolant quality and temperature are computed by the following equations:

$$\text{Case 1.} \quad h_i(z) \leq H_F(P)$$
$$X_i(z) = 0$$
$$T_i(z) = \theta(h_i(z), P) \tag{D-4}$$

$$\text{Case 2.} \quad H_F(P) \leq h_i(z) \leq H_G(P)$$
$$X_i(z) = (h_i(z) - H_F(P))/(H_G(P) - H_F(P))$$
$$T_i(z) = T_s(P) \tag{D-5}$$

$$\text{Case 3.} \quad h_i(z) \geq H_G(P)$$
$$x_i(z) = 1$$
$$T_i(z) = \theta(h_i(z), P)) \tag{D-6}$$

where

x_i = quality of coolant in flow channel i at distance z from flow inlet

$T_i(z)$ = temperature of coolant in flow channel i at distance z from flow inlet

$H_F(P)$ = enthalpy of saturated liquid at coolant pressure P

$H_G(P)$ = enthalpy of saturated gas at coolant pressure P

$T_s(P)$ = saturation temperature at coolant pressure P

$\theta(h,P)$ = function specifying temperature of coolant as a function of enthalpy and pressure.

The functions H_F, H_G, $\theta(h,P)$, and T_s are supplied by the Water Properties Package in FRAP-T5.

5. REFERENCES

D-1. J. S. Gellerstedt et al, "Correlation of Critical Heat Flux in a Bundle Cooled by Pressurized Water," Two-Phase Flow and Heat Transfer in Rod Bundles, Symposium presented at the Winter Annual Meeting of the American Society of Mechanical Engineers, Los Angeles, California, (November 1969) pp 63-71.

D-2. P. G. Barnett, A Correlation of Burnout Data for Uniformly Heated Annuli and Its Use for Predicting Burnout in Uniformly Heated Rod Bundles, AEEW-R463 (1966).

D-3. E. D. Hughes, A Correlation of Rod Bundle Critical Heat Flux for Water in the Pressure Range 150 to 725 psia, IN-1412 (July 1970).

D-4. B. C. Slifer and J. E. Hench, Loss-of-Coolant Accident and Emergency Core Cooling Models for General Electric Boiling Water Reactors, NEDO-10329 (April 1971).

D-5. D. H. Knoebel et al, Forced Convection Subcooled Critical Heat Flux, D_2O, and H_2O Coolant with Aluminum and Stainless Steel Heaters, DP-1306 (February 1973).

D-6. L. S. Tong, Boiling Crisis and Critical Heat Flux, TID-25887 (August 1972).

D-7. S. A. Eide and R. G. Gottula, Evaluation and Results of LOFT Steady State Departure from Nucleate Boiling Tests, TREE-NUREG-1043 (April 1977).

D-8. R. A. Smith and P. Griffith, "A Simple Model for Estimating Time to CHF in a PWR LOCA," Transactions of American Society of Mechanical Engineers, Paper No. 76-HT-9 (1976).

D-9. F. W. Dittus and L. M. K. Boelter, Heat Transfer in Automobile Radiators of the Tubular Type, University of California Publications, 2 (1930) pp 443-461.

D-10. J. R. S. Thom et al, "Boiling in Subcooled Water During Flow Up Heated Tubes or Annuli," Proceedings Instrumentation of Mechanical Engineers, (London), 180 (Part 3C) (1966) pp 226-246.

D-11. V. H. Schrock and L. M. Grossman, Forced Convection Boiling Studies, Final Report on Forced Convection Vaporization Project, TID-14632 (1959).

D-12. J. B. McDonough, W. Milich, E. C. King, Partial Film Boiling with Water at 2000 psia in a Round Tube, MSA Research Corporation, Technical Report 62 (1958).

573 338

D-13. D. C. Groeneveld, An Investigation of Heat Transfer in the Liquid Deficient Regime, AECL-3281 (Rev.) (December 1968; Revised August 1969).

D-14. K. G. Condie et al, "Regression Analysis of Post-CHF Flow Boiling Data," Fifth International Heat Transfer Conference, Japan, September 1974, pp 115-119.

D-15. R. L. Dougall and W. M. Rohsenow, Film Boiling on the Inside of Vertical Tubes with Upward Flow of the Fluid at Low Qualities, MIT-TR-9079-26 (1963).

D-16. L. S. Tong and J. D. Young, "A Phenomenological Transition and Film Boiling Heat Transfer Correlation," Fifth International Heat Transfer Conference, Japan, July 1974, Journal of Heat Transfer (1974) pp 20-124.

573 339

APPENDIX E

FRAP-T PASSIVE LINK WITH THERMAL HYDRAULIC CODES

APPENDIX E

FRAP-T PASSIVE LINK WITH THERMAL HYDRAULIC CODES

An input option of FRAP-T allows the code to read transient coolant conditions directly from a data storage file. This appendix describes (a) the form of the data set required by FRAP-T and (b) the description of a routine which converts RELAP4 output to a form usable by FRAP-T as transient coolant condition input.

1. CONTENTS AND FORMAT OF COOLANT CONDITION DATA SET

1.1 NSWC = 2 Option

If NSWC = 2 (Input card 5.1), a data set specifying the transient coolant conditions must be stored on disk or tape. The data set will be accessed by FORTRAN logical unit 4. A STAGE or ATTACH card for file TAPE4 must be supplied which specifies the location of the data set.

The transient coolant condition data set must be created as follows:

```
      DØ100N=1,NTSTEP
      WRITE(LU)T(N)
      WRITE(LU)PLP(N),HLP(N),TBLP(N)
      DØ50M=1,NZØNE
 50   WRITE(LU)ZB(M),ZT(M),P(M,N),H(M,N),TB(M,N),G(M,N)
100   WRITE(LU)PUP(N),HUP(N),TBUP(N)
```

573 341

where

LU = fortran logical unit

T(N) = time of N-th time point (s)

PLP(N) = pressure of coolant in lower plenum at time T(N) (psia)

HLP(N) = enthalpy of coolant in lower plenum at time T(N) (BTU/lbm)

TBLP(N) = bulk temperature of coolant in lower plenum at time T(N) (^{o}F)

NZONE = number of different elevation spacings (vertical zones) at which thermal/hydraulic code has computed coolant conditions (for RELAP4 code, NZONE = number of stacked volumes surrounding fuel rods being analyzed)

ZB(M) = elevation of bottom of M-th elevation spacing (ft)

ZT(M) = elevation of top of M-th elevation spacing (ft) (ZB(M+1) must equal ZT(M))

P(M,N) = coolant pressure between zone bounded by ZB(M) and ZT(M)(psia)

H(M,N) = coolant enthalpy (BTU/lb)

TB(M,N) = coolant temperature (F)

G(M,N) = mass flux (lbm/ft^2 - hr)

PUP(N) = pressure in upper plenum (psia)

HUP(N) = enthalpy in upper plenum (BTU/lbm)

TBUP(N) = temperature in upper plenum (^{O}F).

1.2 NSWC = 4 Option

If NSWC = 4 on input card 5.1 of Appendix A, a coolant condition data set must be created as follows:

```
DO100N = 1,NTSTEP

WRITE(LU)T(N)

DO50M = 1,NZONE

 50 WRITE(LU)ZB(M),ZT(M),HTC(M,N)TB(M,N)P(M,N)

100 CONTINUE
```

where

HTC(M,N) = heat transfer coefficient in region of M-th elevation spacing at N-th time point (BTU/hr-ft^2-F).

If NSWC=4 on input card 5.1, the coolant temperature in the coolant condition data set must be such that

$$Q(M,N) = HTC(M,N)[TCLAD - TB(M,N)]$$

where

Q(M,N) = surface heat flux

573 343

TCLAD = cladding surface temperature

HTC(M,N) = heat transfer coefficient

TB(M,N) = coolant temperature for forced convection modes of heat transfer and saturation temperature for boiling modes of heat transfer.

The coolant condition data set will be accessed by FORTRAN logical unit 4. A control card for FORTRAN unit 4 must be supplied which copies the coolant condition data set to a data set with name "TAPE4".

2. CONVERSION OF RELAP PLOT TAPE TO FRAP COOLANT TAPE

Two subcodes are available which convert a RELAP4 plot tape to a FRAP-T coolant condition data set. The first subcode, named FCOOL, creates a data set containing the transient values of the coolant pressure, enthalpy, and mass flux. The second subcode, named STRIP4, creates a data set containing the transient values of cladding surface heat transfer coefficient, and coolant pressure and temperature.

The required input for FCOOL is described in Table E-I and consists of some editing parameters, the volume or heat slab index from the RELAP problem which is to be associated with each FRAP-T coolant zone, and some geometry data. The control cards for running the subcode on the INEL CDC 7600 computer are shown in Table E-II. The input RELAP4 plot tape is staged in on TAPE3. The output FRAP-T coolant condition tape is post staged on TAPE8.

The required input for STRIP4 is described in Table E-III. The control cards for running the subcode are shown in Table E-II. The input RELAP4 plot tape is prestaged on TAPE3. The output FRAP-T coolant condition data set is post staged on TAPE9.

TABLE E-I

INPUT FOR FCOOL SUBCODE

Card 0	Columns 1-6.	Insert -1, remainder may be used to identify the deck but is not used by program.	
Card 1	Control.		
Columns	Format	Name	
1-5	I	IPRINT	Print control code. If ≤ 0 - do not print channel data. If > 0 - print the channel data being prepared for FRAP-T every IPRINTth time steps of RELAP4.
11-20	F	TMIN	Initial problem time (sec). RELAP4 records at earlier times will be skipped.
21-30	F	TMAX	Final problem time (sec). If left blank or zero, processing will continue to the end of the RELAP4 tape.
26-35	F	TDEL	Minimum FRAP-T data interval (sec). RELAP4 records are skipped if not at least TDEL later than the last point processed. Normally, these columns are left blank.
Card 2	Plenum definition.		
Columns	Format	Name	
1-5	I	NLP	Lower plenum number - the RELAP4 number for the volume containing the core inlet coolant conditions.
6-10	I	NUP	Upper plenum number - the RELAP4 number for the volume containing the core outlet coolant conditions.
Cards 3-ff	One card for each RELAP volume which overlays fuel rod being analyzed. Number of cards must equal NZONE of card 5.1.		

TABLE E-I (continued)

Columns	Format	Name	
1-5	I	M	Volume in RELAP4 problem.
11-20	F	ZB	Distance from bottom of fuel rods to bottom of RELAP volume. M (ft). For contiguous coolant zones, ZB may be left blank, and the top of the previous zone will be used for ZB (zero for the first zone).
21-30	F	ZT	Distance from bottom of fuel rods to top of RELAP volume (ft).
31-40	F	AR	Coolant channel area (ft^2) in the RELAP4 problem - used to convert flow from lb/hr to lb/hr-ft^2 (same as flow area of RELAP volume M).

TABLE E-II

CONTROL CARDS FOR FCOOL AND STRIP4 SUBCODES

Job Card

Accounting Card

STAGE, TAPE3, PE, E, VSN = T9aaaa. (Stage in RELAP4 plot tape)

FILE, TAPE3, RT = U.

STAGE, TAPE8, E, PE, POST. (Post stage FRAP-T coolant condition tape)

FTN, R = 2, OPT = 2.

LGO.

7-8-9 punch in column 1

Source cards of FCOOL or STRIP4 subcodes

7-8-9 punch in column 1

Input data cards for conversion program

End of file card

573 346.

TABLE E-III

INPUT FOR STRIP4 SUBCODE

Card 1

Columns	Format	Name	Quantity
4-5	I	NSW	Insert "-1" in columns 4 and 5.

Card 2

Columns	Format	Name	Quantity
5	I	NTOT	Insert "1" in column 5.

Card 3

Columns	Format	Name	Quantity
1-5	I	IPRINT	Print control variable. The RELAP4 coolant conditions are printed every IPRINT-th RELAP4 time step.
6-10	I	NSLABS	Number of RELAP4 heat slabs in stack that represents fuel rod to be analyzed.
11-20	F	TMIN	Initial RELAP4 problem time (sec).
21-30	F	TMAX	Final problem time (sec). If left blank or zero processing will continue to the end of the RELAP4 tape.

Cards 4-ff

One card for each heat slab which overlays fuel rod being analyzed. Number of cards must equal NSLABS of Card 3. Also, NZONE of Card 5.1 must equal NSLABS.

Columns	Format	Name	Quantity
1-5	I	NV	RELAP4 thermal-hydraulic volume number which overlays heat slab number NH of column 6-10.
6-10	I	NH	RELAP4 heat slab number.

573 347

TABLE E-III (continued)

Columns	Format	Name	Quantity
11-20	F	ZB	Distance from bottom of fuel rod to bottom of heat slab #NH (ft).
21-30	F	ZT	Distance from bottom of fuel rod to top of heat slab #NH (ft).

Continue to input one card for each RELAP4 heat slab until NSLABS cards have been input for Card Group 4.

APPENDIX F

CONFIGURATION CONTROL PROCEDURE

APPENDIX F

CONFIGURATION CONTROL PROCEDURE

A Configuration Control Procedure (CCP) has been defined to maintain a traceability of results from developing computer codes. During the development process of a computer code, there are requirements for using the code for generating both checkout results and production results, depending on the stage of development.

The CCP consists of a method by which changes can be made to the code and traceability of results maintained. Any time a modification to the code is made, the following data are recorded in a log book:

(1) Version of code to which modification was made

(2) Reason for modification

(3) Results affected by modification

(4) Date of modification

(5) Person responsible for modification

(6) The change cards used to modify the original version of the code.

The Fuel Analysis Research and Development Branch at the Idaho National Engineering Laboratory is responsible for recording changes made to FRAP-T in the FRAP-T log book. A tape update routine is used to modify the code. This routine requires only those computer cards defining new statements or deleting old statements. These "change cards" are kept on file so any version of the code can be reproduced if necessary.

573 350

A new identification number is assigned to the modified version of the code, and this new number is programmed into the code where it will be listed at the top of each page of output and on each plot produced by the code.

APPENDIX G

NUMERICAL SOLUTION OF THE PLENUM ENERGY EQUATIONS

APPENDIX G

NUMERICAL SOLUTION OF THE PLENUM ENERGY EQUATIONS

The Crank-Nicolson finite difference form of the six energy equations presented in Section III-2.1 of the main text is

Plenum Gas:

$$\rho_g V_g C_g \frac{(T_g^{m+1} - T_g^m)}{\tau} = \frac{A_{ep} h_{ep}}{2} (T_{ep}^m - T_g^m - T_g^{m+1} + T_{ip}^{m+1}) + \frac{A_{cl} h_{cl}}{2} (T_{cli}^m - T_g^m + T_{cli}^{m+1} - T_g^{m+1}) + \frac{A_{ss} h_s}{2} (T_{ss}^m - T_g^m + T_{ss}^{m+1} - T_g^{m+1}) \quad \text{(G-1)}$$

Spring Center Node:

$$\rho_s V_{sc} C_s \frac{(T_{sc}^{m+1} - T_{sc}^m)}{\tau} = \bar{q}\cdots V_{sc} + \frac{A_{sc} K_s}{2 R_{ss}} (T_{ss}^m - T_{sc}^m + T_{ss}^{m+1} - T_{sc}^{m+1}) \quad \text{(G-2)}$$

Spring Surface Node:

$$\rho_s V_{ss} C_s \frac{(T_{ss}^{m+1} - T_{ss}^m)}{\tau} = \bar{q}\cdots V_{ss} + \frac{A_{sc} K_s}{2 R_{ss}} (T_{sc}^m - T_{ss}^m + T_{sc}^{m+1} - T_{ss}^{m+1}) + A_{ss} \frac{(h_{rads} + h_{conc})}{2} (T_{cli}^m - T_{ss}^m + T_{cli}^{m+1} - T_{ss}^{m+1}) + A_{ss} \frac{h_s}{2} (T_g^m - T_{ss}^m + T_g^{m+1} - T_{ss}^m) \quad \text{(G-3)}$$

Cladding Interior Node:

$$\rho_{cli} V_{cli} C_{cl} \frac{(T_{cli}^{m+1} - T_{cli}^m)}{\tau} = \bar{q}\cdots V_{cli} + \frac{(A_{cl} h_{radc} + A_{ss} h_{conc})}{2}$$

573 358

$$(T^m_{ss} - T^m_{cli} + T^{m+1}_{ss} - T^{m+1}_{cli}) + \frac{A_{cl}h_{cl}}{2}(T^m_g - T^m_{cli} + T^{m+1}_g - T^{m+1}_{cli})$$
$$+ \frac{A_{cl}K_{cl}}{2.\Delta r/2}(T^m_{clc} - T^m_{cli} + T^{m+1}_{clc} - T^{m+1}_{cli}) \qquad (G\text{-}4)$$

Cladding Center Node:

$$\rho_{cl}C_{cl}V_{clc}\frac{(T^{m+1}_{clc} - T^m_{clc})}{\tau} = \bar{q}\cdots V_{clc} + \frac{A_{cl}K_{cl}}{2.\Delta r/2}(T^m_{cli} - T^m_{clc} + T^{m+1}_{cli} - T^{m+1}_{clc})$$
$$+ \frac{A_{cl}K_{cl}}{2.\Delta r/2}(T^m_{clo} - T^m_{clc} + T^{m+1}_{clo} - T^{m+1}_{clc}) \qquad (G\text{-}5)$$

Cladding Exterior Node:

$$T^{m+1}_{clo} - T^{m+1}_{cool} \qquad (G\text{-}6)$$

The superscripts m and m+1 represent the values of quantities at the old (m) and new (m+1) time. The steady state finite difference equations are obtained by setting the left side of Equations (G-1) through (G-5) to zero, and by dropping the superscripts m and m+1. Equations (G-1) through (G-5) can be written in the following simplified form by combining constant coefficients and known temperatures (T^m_j):

Plenum Gas:

$$A_1T^{m+1}_g + B_1T^{m+1}_{cli} + C_1T^{m+1}_{ss} = I_1 \qquad (G\text{-}7)$$

Spring Center Node:

$$C_2T^{m+1}_{ss} + D_2T^{m+1}_{sc} = I_2 \qquad (G\text{-}8)$$

Spring Surface Node:

$$A_3 T_g^{m+1} + B_3 T_{cli}^{m+1} + C_3 T_{ss}^{m+1} + D_3 T_{sc}^{m+1} = I_3 \qquad \text{(G-9)}$$

Combining Equations (G-8) and (G-9):

$$A_3 T_g^{m+1} + B_3 T_{cli}^{m+1} + \bar{C}_3 T_{sc}^{m+1} = \bar{I}_3 \qquad \text{(G-10)}$$

where

$$\bar{C} = C_3 - \frac{D_3}{D_2} C_2$$

$$\bar{I} = I_3 - \frac{D_3}{D_2} I_2$$

Cladding Interior Node:

$$A_4 T_g^{m+1} + B_4 T_{cli}^{m+1} + C_4 T_{ss}^{m+1} + E_4 T_{clc}^{m+1} = I_4 \qquad \text{(G-11)}$$

Cladding Center Node:

$$B_5 T_{cli}^{m+1} + E_5 T_{clc}^{m+1} + F_3 T_{clo}^{m+1} = I_5 \qquad \text{(G-12)}$$

Equations (G-6) through (G-12) represent a set of six equations, with six unknowns.

In the above equations, all material properties and heat transfer coefficients (except convection to the coolant) are shown as constants. For the transient case, the temperature-dependent material properties and heat transfer coefficients are evaluated at the average of the temperatures (TBAR) at the start and end times of each time step. For the steady state calculation, TBAR represents an estimate of the true steady state temperature. Therefore, it is required that the steady state and transient solutions to Equations (G-7) through (G-12) be iterated to convergence on TBAR.

APPENDIX H

LIST OF INFORMATION IN ACTIVE LINK OF FRAP-T5 WITH THERMAL-HYDRAULIC CODE

APPENDIX H

LIST OF INFORMATION IN ACTIVE LINK OF FRAP-T5 WITH THERMAL-HYDRAULIC CODE

Two types of links are available for linking FRAP-T5 with a thermal-hydraulic computer code. In the first type of link, information is communicated between the two codes via a subroutine argument list. In the second type, information is communicated via a common block.

1. SUBROUTINE ARGUMENT LIST LINK

The communication of information occurs through the argument list of a subroutine named FRAP. A call to FRAP by the thermal-hydraulic code will link FRAP-T with the thermal-hydraulic code. The argument list of FRAP contains three categories of variables. The first category contains variables which control initialization, storage, and time span of calculations. The second category contains variables which specify the coolant conditions. The third category contains variables which specify the fuel rod conditions. The first two categories are in the subroutine input variables while the third category is the subroutine output variables. A list and a dictionary of the variables is shown below.

```
SUBROUTINE FRAP (NCARDS, NREST, NRODS, NCOOL,
# T1, T2, TIMC1, TIMC2, IMAXA, ZCA, PRESC1, PRESC2, TCOOL1, TCOOL2,
# HC1, HC2, GA1, GA2, HCIN1, HCIN2, HCOUT1, HCOUT2,
# TIMR1, TIMR2, KMAXR, ELVR, RODOD1, RODOD2, AA1, AA2, BB1, BB2,
# TSURF1, TSURF2, HFLUX1, HFLUX2, NDTAD, NBUGPR)

ARGUMENT LIST DICTIONARY

ARGUMENTS NCARDS THRU HC2 ARE ALWAYS INPUT

IF NCOOL = 6, ARGUMENTS GA1 THRU HCOUT2 ARE ADDITIONAL INPUT
```

TIMR1 THRU HFLUX2 ARE ALWAYS OUTPUT

INPUT VARIABLES (COOLANT CONDITIONS) ENDING IN 1 APPLY TO TIME TIMC1

INPUT VARIABLES ENDING IN 2 APPLY TO TIME TIMC2

OUTPUT VARIABLES (FUEL ROD CONDITIONS) ENDING IN 1 APPLY TO TIME TIMR1

OUTPUT VARIABLES ENDING IN 2 APPLY TO TIME TIMR2

FRAP CONTROLS TIME STEP SO THAT TIMR1=T1, TIMR2=T2

INDEX I DENOTES I-TH VERTICALLY STACKED REGION IN COOLANT CALCULATIONS

INDEX K DENOTES K-TH AXIAL NODE IN FUEL ROD CALCULATIONS

INDEX N DENOTES FUEL ROD NUMBER

NCARDS = CONTROL SWITCH ON INPUT CARD READ.
- 1 = READ INPUT CARDS THIS CALL (FIRST CALL FOR GIVEN ROD)
- 0 = DO NOT READ CARDS

NREST = CONTROL SWITCH ON RESTART
- 1 = SINGLE ROD CALCULATIONS. IF RESTARTING FROM PREVIOUS JOB, NREST MUST EQUAL 1 OR 3 ON FIRST CALL TO FRAP
- 2 = MULTI-ROD CALCULATIONS WITH LCM STORAGE
- 3 = MULTI-ROD CALCULATIONS WITH DISK STORAGE INSTEAD OF LCM STORAGE. IF NREST = 3,
  ARRAY AFRAP IN COMMON BLOCK/FRPSTO/NEEDS A
  LENGTH OF 32000 INDEPENDENT OF NUMBER OF FUEL RODS
  IF NREST = 3 AND RESTARTING JOB FROM PREVIOUS RUN,
  STAGE IN RESTART TAPE ON TAPE3

NRODS = NUMBER OF FUEL RODS

573 358

573 3

NCOOL = CONTROL SWITCH ON THERMAL/HYDRAULIC - FUEL ROD TYPE OF LINK.
5 = SUBROUTINE ARGUMENT LIST LINK WITH H.T.C. FROM THERMAL-HYDRAULIC CODE
6 = SUBROUTINE ARGUMENT LIST LINK WITH PRESSURE, ENTHALPY AND MASS FLUX FROM THERMAL-HYDRAULIC CODE

T1 = START TIME (SEC)
T2 = END TIME (SEC)

TIMC1 = TIME OF COOLANT CONDITIONS WITH NAME ENDING IN 1 (SEC)
TIMC2 = TIME OF COOLANT CONDITIONS WITH NAME ENDING IN 2 (SEC)

IMAXA(N) = NUMBER OF COOLANT REGIONS
IMAXA(N) ≤ 20

ZCA(I,N) = ELEVATION OF TOP OF COOLANT REGION I (FT)
ZCA(1,N) = 0. ASSUMED

PRESC1(I,N) = COOLANT PRESSURE (PSIA)

TCOOL1(I,N) = COOLANT TEMPERATURE (F)
IF NCOOL = 5, HC1(I,N)*(TSURF1(I,N)-TCOOL(I,N)) = HFLUX1(I,N)
IE > TCOOL1 = SATURATION TEMP IF BOILING
IF NCOOL = 5, HC1(I,N) = HEAT TRANSFER COEFFICIENT (BTU/FT2-F-HR)

IF NCOOL = 6, HC1(I,N) = COOLANT ENTHALPY (BTU/LB)

GA1(I,N) = COOLANT MASS FLUX (LB/HR-FT2)

HCIN1(N) = INLET ENTHALPY (BTU/LB)

HCOUT1(N) = OUTLET ENTHALPY (BTU/LB)

TIMR1 = TIME CORRESPONDING WITH VARIABLES WITH NAME ENDING IN 1 (SEC)
TIMR2 = TIME CORRESPONDING WITH FUEL ROD VARIABLES WITH NAME ENDING IN 2 (SEC)

KMAXR(N) = NUMBER OF AXIAL NODES IN FRAP CALCULATION OF ROD N
MAXIMUM NUMBER OF AXIAL NODES = 20

ELVR(K) = ELEVATION OF AXIAL NODE K, ROD N(FT)
BOTTOM OF FUEL ROD ASSUMED TO HAVE ELEVATION OF ZERO

RODOD1(K,N) = OUTER DIAMETER OF FUEL ROD (FT)

AA1, BB1 ARE COEFFICIENTS SUCH THAT >
AA1(K,N)*TSURF1(K,N) + BB1(K,N) = HFLUX1(K,N)

TSURF1(K,N) = CLADDING SURFACE TEMPERATURE (F)

HFLUX1(K,N) = CLADDING SURFACE HEAT FLUX (BTU/FT2-SEC)

NDTAD = SWITCH TO ADVANCE TIME OR PERFORM CALCULATIONS ONLY
AT TIME T1
= 0 = ADVANCE IN TIME (TRANSIENT CALCULATIONS)
= 1 = ONLY PERFORM CALCULATIONS AT TIME T1 (STEADY-STATE
INITIALIZATION)
NBUGPR = SWITCH TO TURN ON DEBUG PRINTOUT
= 0 = NO
= 1 = YES
THE VARIABLES IN THE SUBROUTINE ARGUMENT LIST ARE DIMENSIONED AND
STORED AS FOLLOWS:

```
DIMENSION  ZCA(20,3) , PRESC1(20,3) , PRESC2(20,3)
#TCOOL1(20,3), TCOOL2(20,3), HC1(20,3), HC2(20,3),
#GA1(20,3), GA2(20,3), HCIN1(3), HCIN2(3), HCOUT1(3),
# HCOUT2(3), IMAXA(3)
  LEVEL 2, ZCA, PRESC1, PRESC2, TCOOL1, TCOOL2, HC1, HC2, GA1,
# GA2, HCIN1, HCIN2, HCOUT1, HCOUT2, IMAXA
  DIMENSION     RODOD1(20,3), RODOD2(20,3), AA1(20,3),
# AA2(20,3), BB1(20,3), BB2(20,3), TSURF1(20,3), TSURF2(20,3),
# HFLUX1(20,3), HFLUX2(20,3), KMAXR(3), ELVR(20,3)
  LEVEL 2, RODOD1, RODOD2, AA1, AA2, BB1, BB2, TSURF1, TSURF2,
#HFLUX1, HFLUX2, KMAXR, ELVR
```


573 360

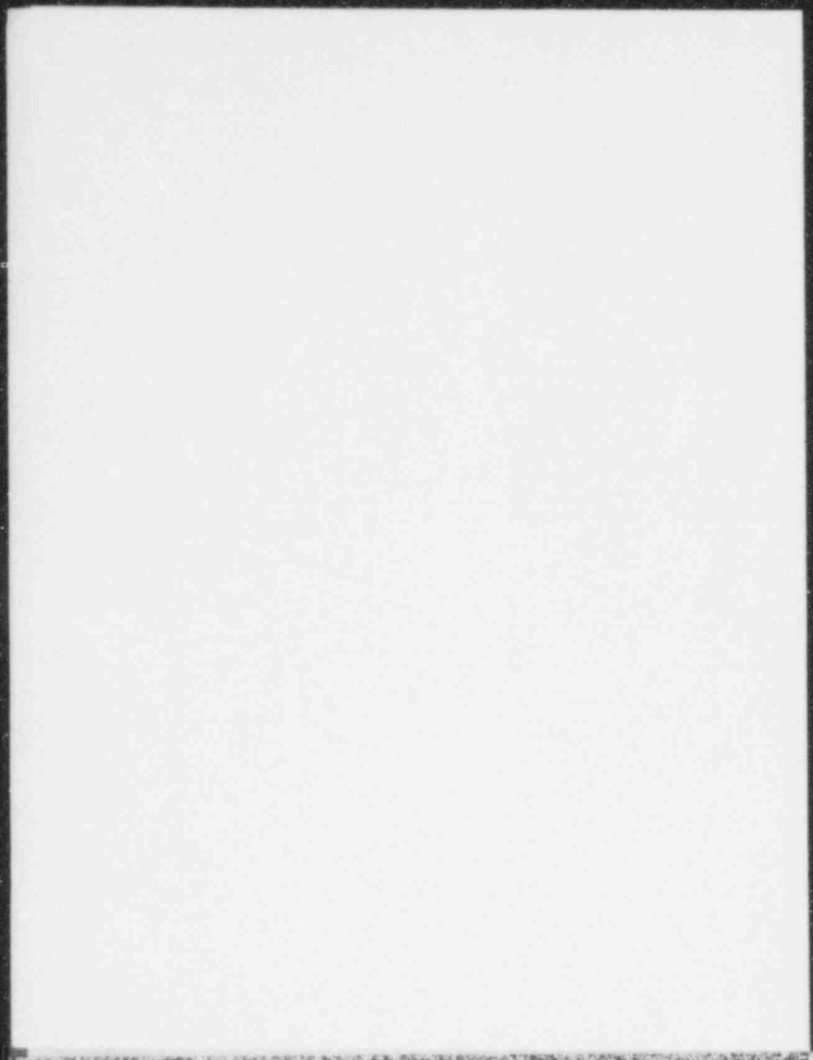

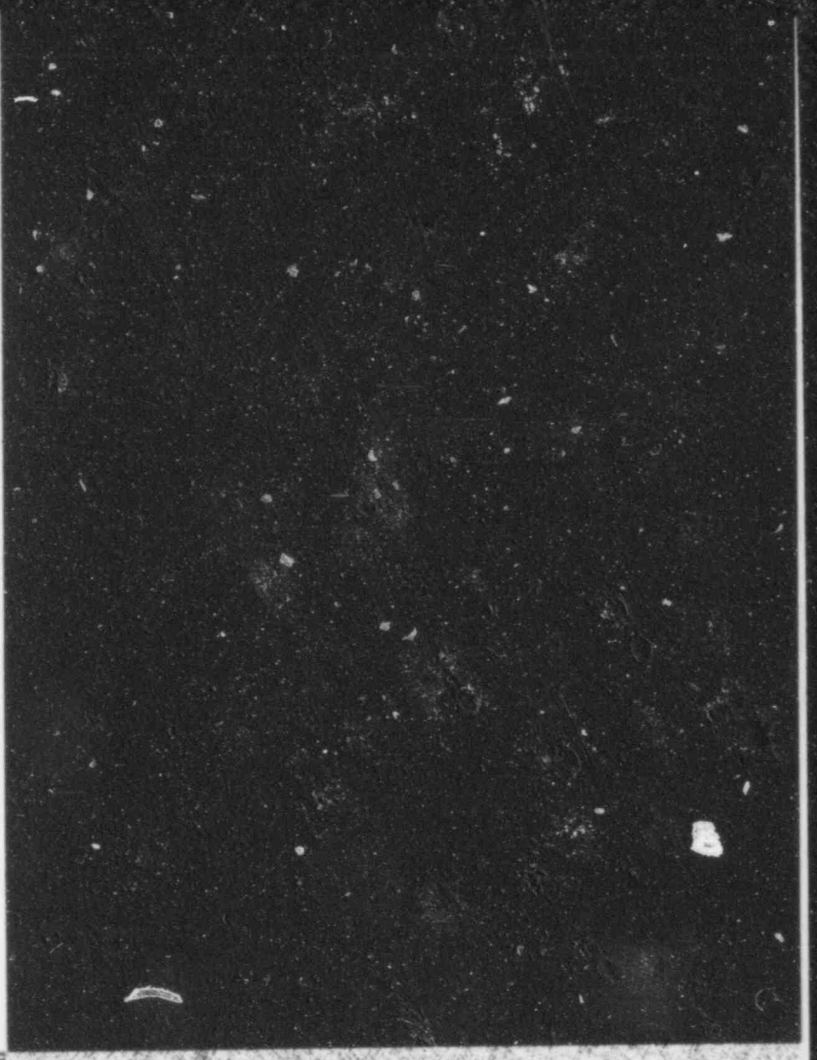

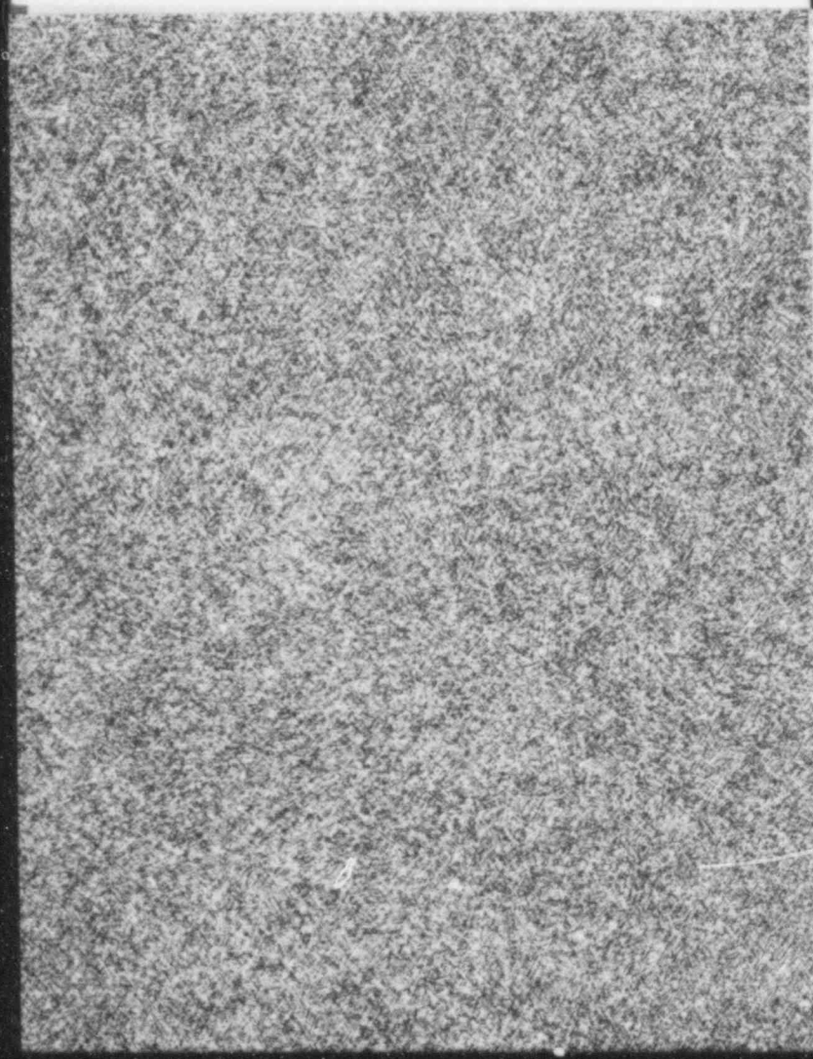

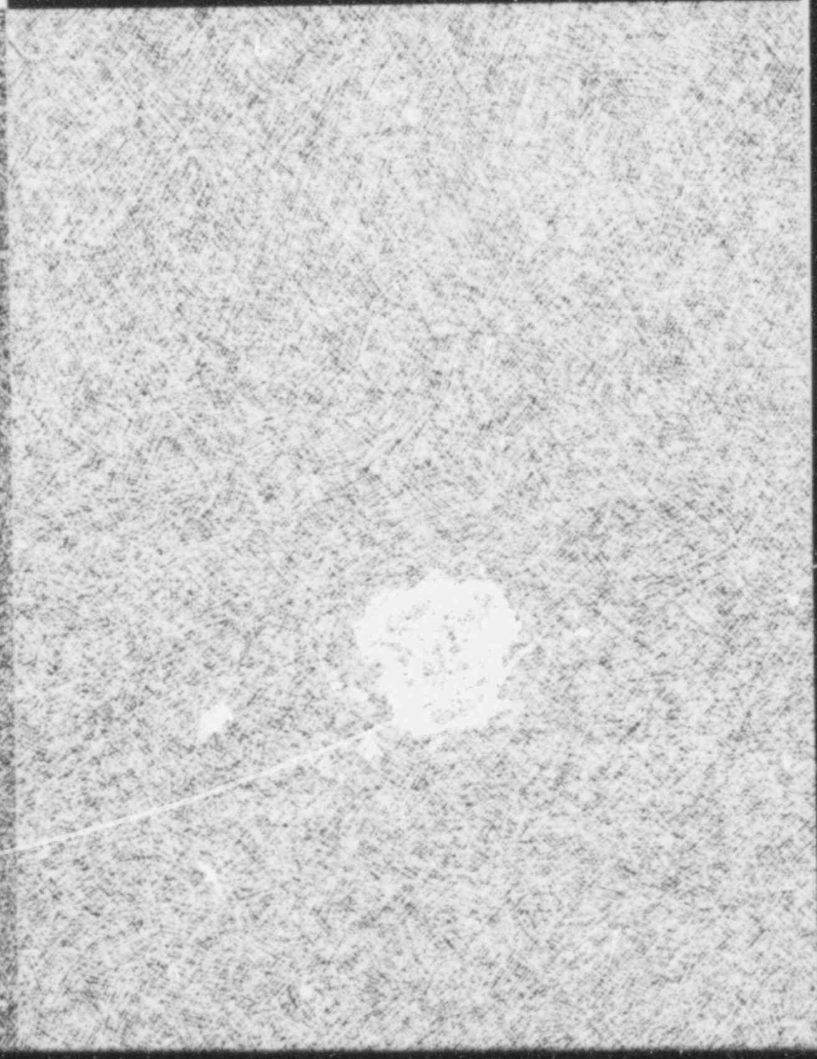

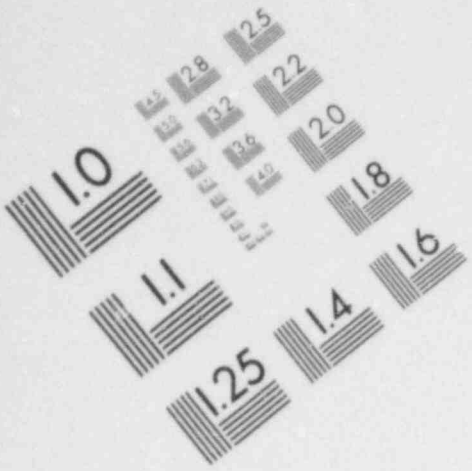

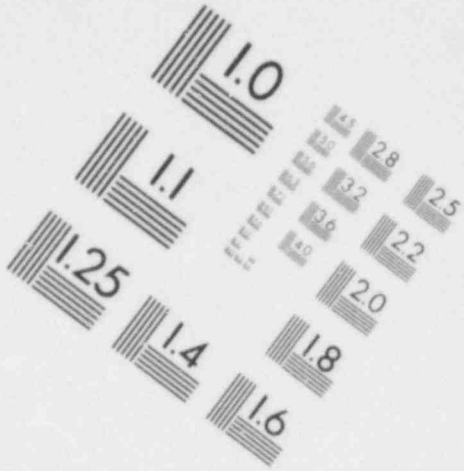

IMAGE EVALUATION TEST TARGET (MT-3)

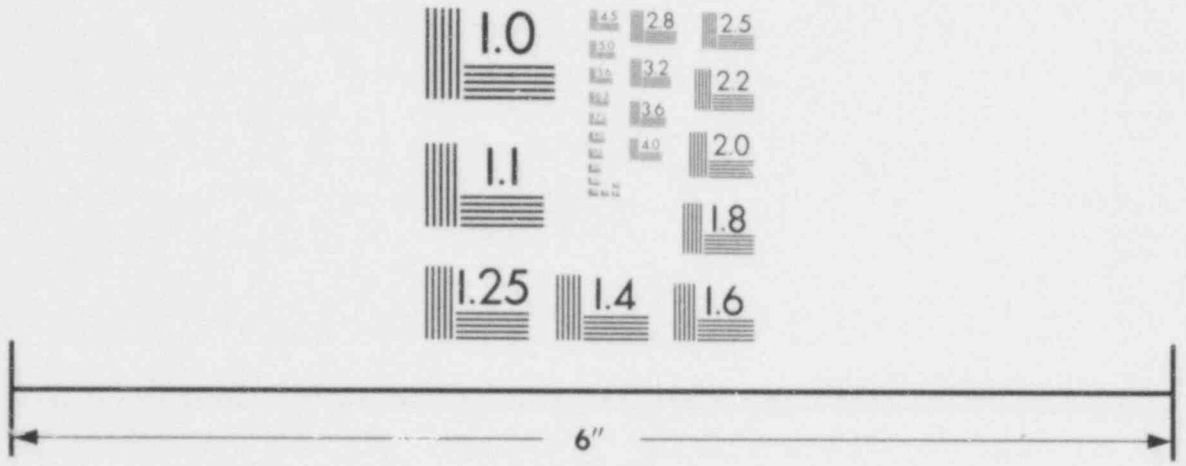

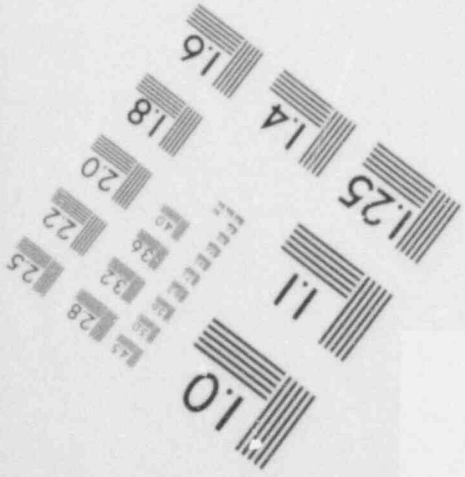

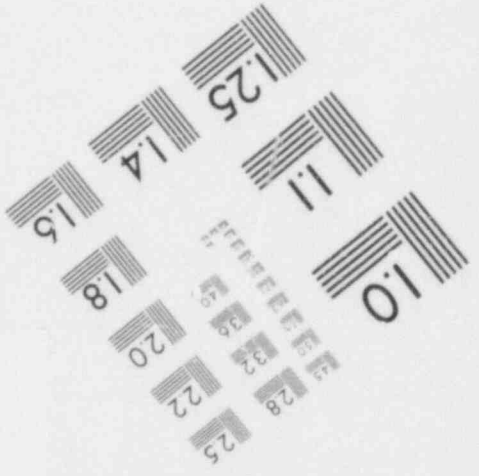

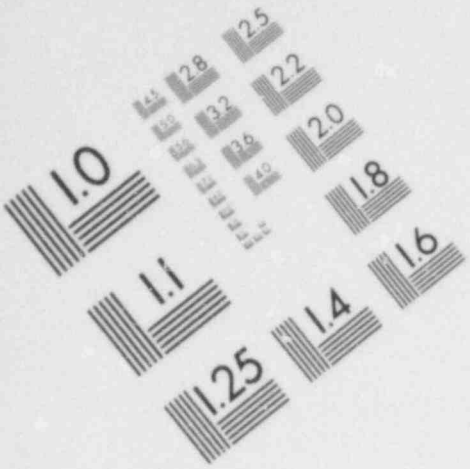

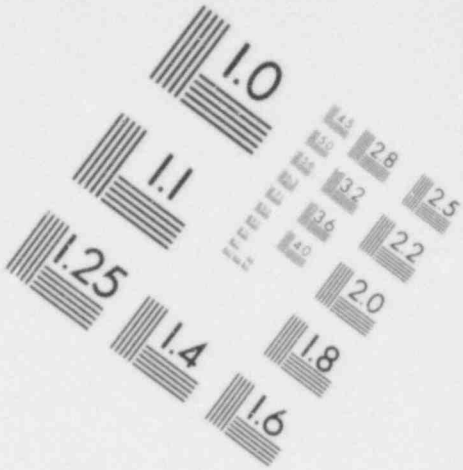

IMAGE EVALUATION TEST TARGET (MT-3)

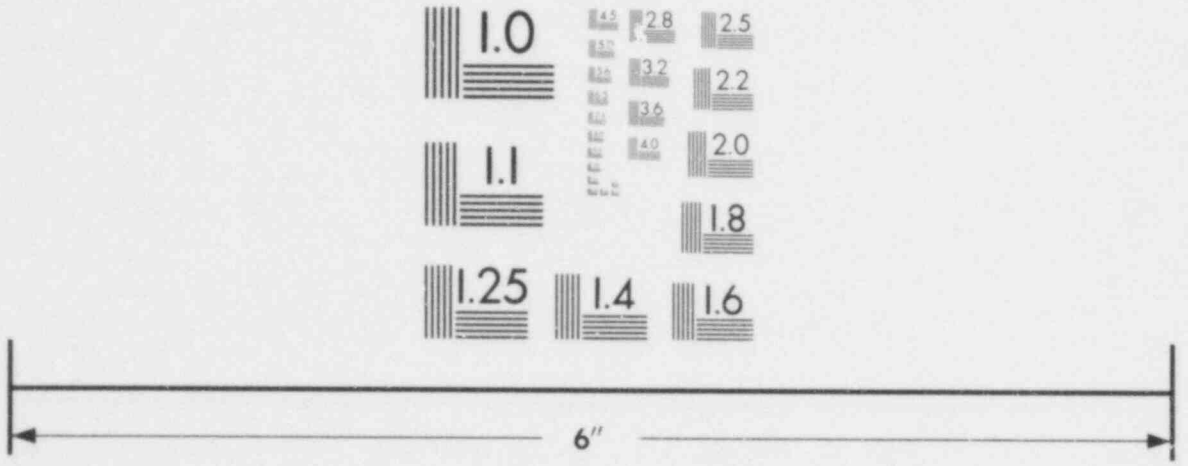

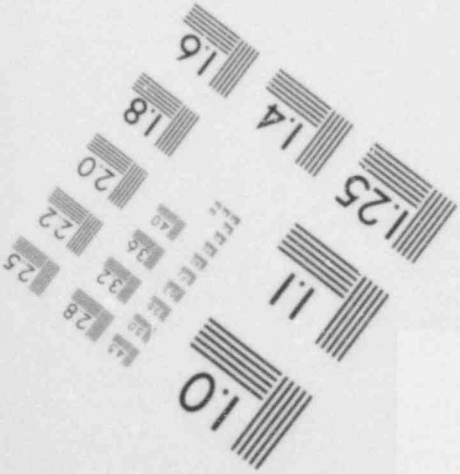

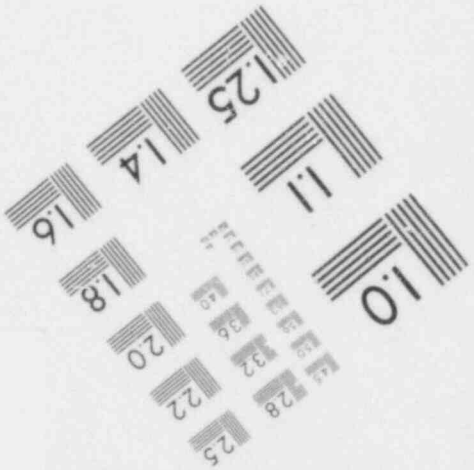

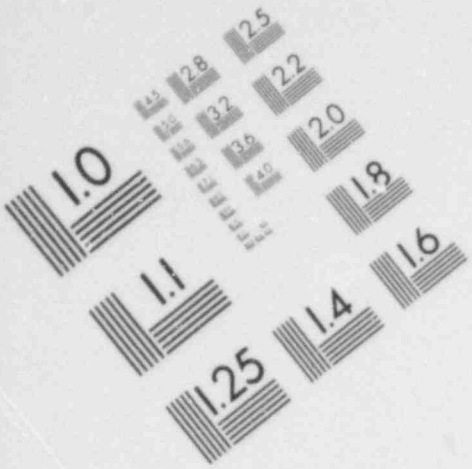

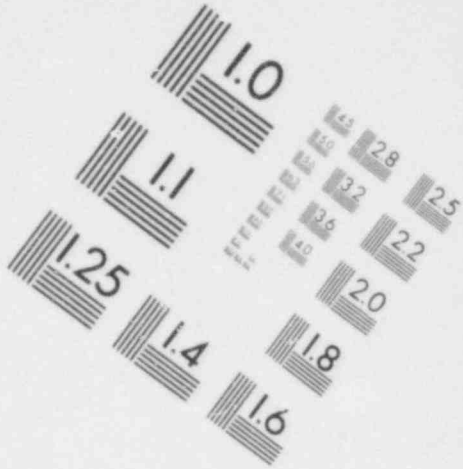

IMAGE EVALUATION TEST TARGET (MT-3)

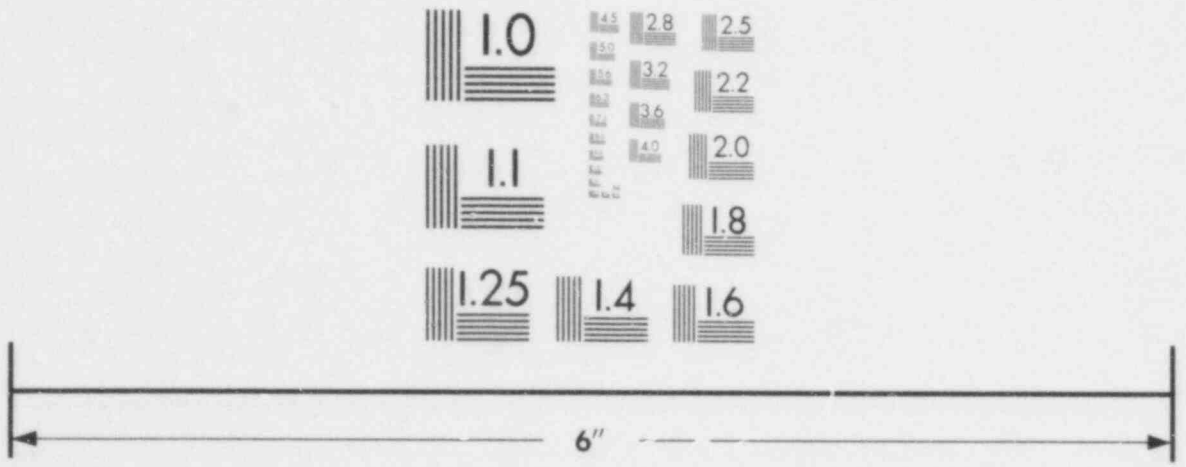

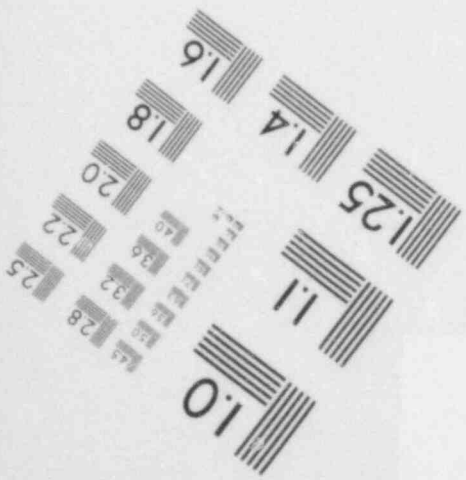

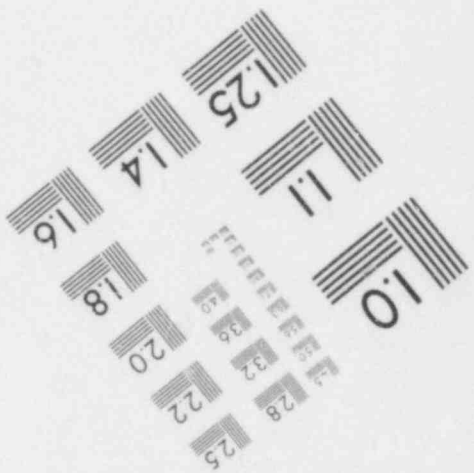

2. COMMON BLOCK LINK

In this type of link, the communication of information occurs through a common block named FRAPC. The common block contains three types of variables. The first type, positioned in the first part of the common block, are variables which control initialization, storage, and end time. The second type, positioned in the middle of the common block, are variables calculated by the thermal-hydraulic computer code and passed to FRAP-T. The third type, positioned in the last part of the common block, are variables calculated by FRAP-T5 and passed to the thermal-hydraulic code. This common block is used to link RELAP4/MOD7 and FRAP-T5. The variables calculated by the thermal-hydraulic code are noted in parantheses as being passed from RELAP4. The common block and dictionary of the variables in the common block are shown below.

```
COMMON/FRAPC/NCARD2, NREST2, NRODS2, NCOOL2, NDTADV, NBUGSH, T12,
# T22,        TMPRLP(20,24,12),RMRLP(20,12), TPRLP(12),
1          NFORLP(12),NCIRLP(12),NCORLP(12),PCLRLP(24,12),
2ELVRLP(24,12), KMXRLP(12),
3KMXFRP(12),ELVFRP(20,12),HGPFRP(20,12),
4              DRDFRP(20,12),IFFRP(20,12), VRLFRP(20,12),
5 PGPFRP(20,12), GSFRP(9,12), BUFRP(20,12), GSMFRP(12)
  LEVEL 2, NCARD2
```

DICTIONARY

NCARD2 = NCARDS, WHICH IS DEFINED BELOW (LEVEL 2 STORAGE)

NCARDS = CONTROL SWITCH ON INPUT CARD READ
- 1 = READ INPUT CARDS THIS CALL (FIRST CALL FOR GIVEN ROD)
- 0 = DO NOT READ CARDS

NREST2 = NREST, WHICH IS DEFINED BELOW

NREST = CONTROL SWITCH ON RESTART AND STORAGE
- ALWAYS SET NREST = 3

574 001

NRODS2 = NRODS, WHICH IS DEFINED BELOW

NRODS = NUMBER OF FUEL RODS

NCOOL2 = NCOOL, WHICH IS DEFINED BELOW
NCOOL = CONTROL SWITCH ON THERMAL/HYDRAULIC - FUEL ROD TYPE OF
LINK. ALWAYS SET NCOOL = 7

NDTADV = SWITCH TO ADVANCE IN TIME OR PERFORM CALCULATIONS ONLY
AT TIME T12
0 = ADVANCE IN TIME
1 = ONLY PERFORM CALCULATIONS AT TIME T12

NBUGSW = SWITCH TO TURN ON DEBUG PRINTOUT
0 = NO
1 = YES

T12 = START TIME FOR FRAP CALCULATIONS (SEC)
T22 = END TIME FOR FRAP CALCULATIONS (SEC)

FOR ALL ARRAYS, MAXIMUM VALUE OF L = 20, N = 12

FOR ARRAYS WITH NAME ENDING IN RLP, MAXIMUM VALUE OF K = 24
FOR ARRAYS WITH NAME ENDING IN FRP, MAXIMUM VALUE OF K = 20

L = RADIAL NODE, K = AXIAL NODE (HEAT SLAB), N = FUEL ROD NUMBER

TMPRLP(L,K,N) = RELAP COMPUTED TEMPERATURE (F)
RMRLP(L,N) = RADIAL COORDINATE (COLD STATE) (FT) (FROM RELAP)
RADIUS TO RADIAL NODE L OF FUEL ROD N
RMRLP(1,N) = 0 (FUEL CENTERLINE)
RMRLP(LMAX,N) = RADIUS OF CLADDING OUTSIDE SURFACE
TPRLP(N) = PLENUM GAS TEMPERATURE (F) (FROM RELAP)
NFORLP(N) = RADIAL NODE AT FUEL PELLET SURFACE (FROM RELAP)
NCIRLP(N) = RADIAL NODE AT CLADDING INSIDE SURFACE (RELAP)
NCORLP(N) = RADIAL NODE AT CLADDING OUTSIDE SURFACE (RELAP)

PCLRLP(K,N) = COOLANT PRESSURE (PSIA) (RELAP)
ELVRLP(K,N) = ELEVATION OF RELAP AXIAL NODE (HEAT SLAB) K, FT
KMXRLP(N) = NUMBER OF AXIAL NODES IN FUEL ROD N (RELAP)
KMXFRP(N) = NUMBER OF FRAP AXIAL NODES, ROD N (FRAP)
ELVFRP(K,N) = ELEVATION OF FRAP K-TH AXIAL NODE, FT (FRAP)
HGPFRP(K,N) = GAS GAP CONDUCTANCE (BTU/SEC-F-FT**2) (FRAP)
DRDFRP(K,N) = FUEL ROD OUTER DIAMETER (FT) (FRAP)
IFFRO(K,N) = CLADDING FAILURE INDICATOR, 0 = NO, 1 = YES (FRAP)
VRLFRP(K,N) = FUEL CRACK VOLUME GENERATED BY RELOCATION (FT**3/FT) (FRAP)
PGPFRP(K,N) = FUEL ROD INTERNAL GAS PRESSURE (PSIA) (FRAP)
GSFRP(J,N) = FRACTION OF J-TH GAS IN FUEL ROD N (FRAP)
BUFRP(K,N) = FUEL BURNUP (MW-SEC/KG) (FRAP)
GSMFRP(N) = GRAM-MOLES OF GAS

If the common block link is used, only a portion of the input data blocks, shown in Appendix A, are input. The input data blocks are blocks 1, 6, and 7. Also, only a portion of the cards in block 1 is input. These are cards 1.1 through 1.6 and 1.11 through 1.14. All of the input variables on these card that refer to the temperature solution are ignored.

574 003

DISTRIBUTION RECORD FOR NUREG/CR-0840
(TREE-1281)

Internal Distribution

1 - R. J. Beers, ID

2 - P. E. Litteneker, ID

3-5 - INEL Technical Library

6-50 - Special Internal

External Distribution

51-52 - Saul Levine, Director
Office of Nuclear Regulatory Research, NRC
Washington, D.C. 20555

53-347 - Distribution under R4, Water Reactor Safety Research - Analysis Development